

## **Final Report**

# **Observation-Based Analyses of the Sensitivity of Ozone Formation in the Lake Michigan Region to NO<sub>x</sub> and VOC Emissions**

prepared for

**Lake Michigan Air Directors Consortium (LADCO)  
9501 W. Devon Ave, Suite 701  
Rosemont, IL 60018**

submitted by

**Charles L. Blanchard  
526 Cornell Avenue  
Albany, CA 94706  
charles.ld.blanchard@gmail.com  
cbevair@pacbell.net  
(510) 525-6231**

**September 30, 2020**



# Contents

1. Summary .....	1
1.1 Generalized Additive Model (GAM).....	1
1.2 Ozone Sensitivity Indicators Using NO <sub>x</sub> and VOC Measurements.....	2
1.3 Implications.....	3
2. Introduction.....	5
2.1 Background.....	5
2.2 Past Progress in Reducing Emissions and Ozone Levels .....	5
2.3 Conceptual Model.....	7
2.4 Objectives .....	9
2.5 Scope.....	10
2.6 Approach.....	11
3. VOCs as Ozone Sensitivity Indicators.....	13
3.1 Background.....	13
3.2 Site Selection .....	13
3.3 Indicators Based on HCHO, NO <sub>2</sub> , and NO <sub>y</sub> .....	14
3.3.1 Methods.....	14
3.3.2 Results.....	16
3.4 Indicators Based on NMOC, NO <sub>x</sub> , and NO <sub>y</sub> .....	21
3.4.1 Methods.....	21
3.4.2 Results.....	21
3.5 Section Summary .....	24
4. NO <sub>y</sub> and NO <sub>z</sub> as Ozone Sensitivity Indicators.....	25
4.1 Background.....	25
4.1.1 Indicator Species and Ratios.....	25
4.1.2 Correlation of O <sub>3</sub> with NO <sub>y</sub> and NO <sub>z</sub> .....	25
4.1.3 The Weekend Effect .....	27
4.1.4 Observed O <sub>3</sub> Response.....	29
4.2 Site Selection .....	29
4.3 Methods.....	29
4.4 Results.....	29
4.5 Section Summary .....	33

5. Generalized Additive Model (GAM).....	34
5.1 Background .....	34
5.2 Site Selection .....	36
5.3 Input Data.....	36
5.4 Model Development and Testing.....	38
5.4.1 Model Fitting .....	38
5.4.2 Performance Evaluation.....	38
5.5 O <sub>3</sub> Sensitivity Results .....	46
5.5.1 Sensitivity of O <sub>3</sub> to Weather .....	46
5.5.2 Sensitivity of O <sub>3</sub> to Temporal Factors .....	53
5.5.3 Sensitivity of O <sub>3</sub> to Emissions and Precursors.....	59
5.6 GAM Predictions .....	71
5.7 Section Summary .....	86
6. Synthesis .....	89
6.1 HCHO/NO <sub>2</sub> and NMOC/NO <sub>x</sub> Ratios.....	89
6.2 O <sub>3</sub> /NO <sub>y</sub> Ratios.....	90
6.3 Generalized Additive Model (GAM).....	90
7. Conclusions.....	92
7.1 VOC and NO <sub>x</sub> Limitation, Spatial Patterns, and Temporal Changes .....	92
7.2 Implications for Emission Control Strategies .....	92
7.3 Implications for Monitoring Needs.....	92
8. References.....	94
9. Appendix.....	102
9.1 Data Sources .....	102
9.2 Data Availability .....	103
9.3 Data Evaluation.....	104
9.3.1 NO <sub>2</sub> and NO <sub>x</sub> .....	104
9.3.2 Sampling Duration.....	108
9.3.3 Indicator Transition Ranges.....	108
9.4 Data Summaries and Comparisons .....	118
9.4.1 Trends in Emissions and Ambient Concentrations.....	118
9.4.2 Surface Wind .....	126

9.4.3 Hourly Observations .....	126
9.4.4 Radiosonde Measurements .....	134
9.4.5 Isoprene .....	137
9.4.6 Day-of-Week Variations .....	140
9.4.7 VOC Reactivity .....	145
9.4.8 O <sub>3</sub> Trends .....	146
9.5 Supplemental GAM Model Performance and O <sub>3</sub> Sensitivity Graphs .....	150
9.6 Computer Programs .....	155
9.6.1 R Code for Reading JSON Format Files .....	155
9.6.2 Other Programs .....	156

## 1. Summary

The primary objective of this study is to evaluate the sensitivity of ozone ( $O_3$ ) formation along Wisconsin's Lake Michigan shoreline, in and near Chicago, and at shoreline locations in southwestern Michigan to changes in emissions and ambient concentrations of nitrogen oxides ( $NO_x = NO + NO_2$ ) and volatile organic compounds (VOCs). The principal focus is on current  $O_3$ - $NO_x$ -VOC sensitivity along the western shore of Lake Michigan, addressing the spatial and temporal variability of this sensitivity.  $O_3$  sensitivity between 2000 and 2019 is evaluated for 20 monitoring locations. All methods rely on existing data sets.

Three observation-based approaches are utilized to evaluate the sensitivity of  $O_3$  in the southern Lake Michigan area to changes in VOC and  $NO_x$  emissions. First, the report evaluates measurements of VOCs and various VOC-based ratios as ozone sensitivity indicators. Second, measurements of oxidized nitrogen species ( $NO_y$ ) and  $NO_z$  ( $NO_y - NO_x$ ) are compiled and evaluated as  $O_3$  sensitivity indicators. Finally, a generalized additive model (GAM) is used to investigate  $O_3$  responses at 20 locations to changes in regional emissions and ambient precursor concentrations.

Previous studies have suggested that  $O_3$  formation is generally VOC-responsive in and near the Chicago metropolitan area but transitions into  $NO_x$ -sensitive conditions at varying downwind distances on high- $O_3$  days. In this study, the GAM indicates that  $O_3$  formation is generally  $NO_x$ -inhibited in the Chicago metropolitan area, thereby supporting previous research. The GAM analyses also show that  $O_3$  formation at the majority of study locations in WI and MI was in a regime in which  $O_3$  was responsive to both VOC and  $NO_x$  on high- $O_3$  days ( $> 50$  ppbv) between 2015 and 2019.  $O_3$  sensitivity indicators, compiled from ambient VOC and  $NO_x$  measurements, qualitatively support the GAM results.

### 1.1 Generalized Additive Model (GAM)

The GAM was applied to model maximum daily 8-hour average (MDA8)  $O_3$  at 20 sites: 12 in WI, 5 in IL, and 3 in MI. Model performance was evaluated for each location. Predictor variables included multistate (IL, IN, WI) annual VOC and  $NO_x$  emissions, multisite mean concentrations of CO,  $NO_x$ , and  $SO_2$  ( $SO_2$  was not statistically significant), upper air (850 and 500 mb) meteorological variables, and surface weather variables (temperature, relative humidity, wind speed and direction).

NMOC measurements are limited spatially to a small number of sites and temporally to 24-hour samples collected once every six days. As a result, the data were not useful as inputs to the GAM. However, other predictor variables represented variations in total NMOC (CO) and isoprene (day of year and temperature).

By representing both meteorological and emission influences on  $O_3$ , the GAM was able to determine weather-adjusted sensitivities of  $O_3$  to emissions and ambient precursor concentrations.

Urban sites in Chicago (Cook and Lake counties) and in southern WI (Milwaukee and Kenosha) showed counterproductive predicted  $O_3$  increases of 1 to 6 ppbv in response to hypothetical 10%

and 40% reductions of the sum of multistate VOC and NO<sub>x</sub> emissions. Coupling hypothetical reductions in the sum of VOC and NO<sub>x</sub> emissions with different combinations of reductions in ambient concentrations of O<sub>3</sub> precursors yielded predicted O<sub>3</sub> decreases at locations outside the Chicago metropolitan area, but not at all Chicago sites.

The majority (9 of 12) of WI sites showed a higher predicted frequency of days (50 – 90%) for which hypothetical decreases in ambient NO<sub>x</sub> concentrations yielded a greater reduction in predicted MDA8 O<sub>3</sub> than hypothetical reductions in ambient CO did. The opposite was true for Chicago sites. However, the predicted O<sub>3</sub> responses to 10% CO and NO<sub>x</sub> reductions differed by less than 1 ppbv, which was smaller than the prediction uncertainties.

Ambient CO and NO<sub>x</sub> reductions of 10% relative to 2015 – 2019 concentrations were predicted to lower MDA8 O<sub>3</sub> by zero to 2 ppbv throughout the distribution of O<sub>3</sub> values exceeding 50 ppbv. Larger (40%) reductions of ambient CO and NO<sub>x</sub> were predicted to lower MDA8 O<sub>3</sub> by 2 to 6 ppbv.

GAM sensitivities of O<sub>3</sub> to CO and NO<sub>x</sub> showed increasingly NO<sub>x</sub>-responsive values between 2000 and 2019 as ambient NO<sub>x</sub> concentrations declined. Other indicators support both this result and the GAM predictions of VOC-sensitivity in the Chicago metropolitan area.

The GAM identified large and statistically significant sensitivities of MDA8 O<sub>3</sub> to multiple weather variables. The predicted MDA8 O<sub>3</sub> increased by ~20 – 30 ppbv as daily maximum temperature increased from 20 to over 30° C. Relative humidity, Lake Michigan surface temperature, and daily maximum solar radiation were each associated with ~5 – 20 ppbv nonlinear predicted changes in MDA8 O<sub>3</sub>. The lake breeze effect was evident in the sensitivities of MDA8 O<sub>3</sub> to mid-day and daily-average wind directions. Predicted MDA8 O<sub>3</sub> responses to 850 mb and 500 mb weather variables linked higher O<sub>3</sub> with synoptic-scale stagnation.

## **1.2 Ozone Sensitivity Indicators Using NO<sub>x</sub> and VOC Measurements**

Measurements of formaldehyde (HCHO), nitrogen dioxide (NO<sub>2</sub>), and oxidized nitrogen species (NO<sub>y</sub>) were available from four locations. Three of the four sites are urban: two are within the Chicago metropolitan area and one is in Milwaukee.

Sampling duration (3 or 24 hours for HCHO) and measurement bias (non-specific NO<sub>2</sub>) make the available measurements incommensurate with published transition values, i.e., the value above which HCHO/NO<sub>2</sub> indicates NO<sub>x</sub>-sensitivity. Biases lower the HCHO/NO<sub>2</sub> ratios obtained from ground-based monitors relative to ratios based on satellite measurements or model predictions, by a factor of two up to as much as three to four. Although the relationship of O<sub>3</sub> with HCHO/NO<sub>2</sub> varied depending on the averaging times of O<sub>3</sub> and HCHO/NO<sub>2</sub>, both maximum O<sub>3</sub> concentrations and the frequency of peak daily 8-hour O<sub>3</sub> values exceeding 50 ppbv occurred when mid-day and 24-hour ratios of HCHO/NO<sub>2</sub> were in the range 0.2 – 0.6.

Observed HCHO/NO<sub>2</sub> and HCHO/NO<sub>y</sub> are examined primarily in a relative sense rather than in relation to well-defined crossover values. HCHO/NO<sub>2</sub> ratios increased (1) from Chicago to Milwaukee to rural Horicon/Mayville and (2) as O<sub>3</sub> increased, indicating a tendency toward increasingly NO<sub>x</sub>-limited conditions from south-to-north, urban-to-rural, and low-to-high O<sub>3</sub>.

HCHO/NO<sub>2</sub> ratios were higher on average during summer months (June – August) than in other months. If observed 24-hour HCHO/NO<sub>2</sub> ratios > 1 indicate NO<sub>x</sub>-limitation, as suggested by the data, then O<sub>3</sub> formation was VOC-limited or transitional on most (~75% to >90%) summer days at the four study sites. Many or most of the high-O<sub>3</sub> (> 60 ppbv) days fall into an apparently transitional (or indeterminate) range of HCHO/NO<sub>2</sub> ratios of 0.3 – 1.

Measurements of NO<sub>y</sub> were made at two urban and two nonurban locations between 2000 and 2019 (an additional site reported data for 2000 and 2001). Measurements (non-specific NO<sub>2</sub>) bias NO<sub>x</sub> high and NO<sub>z</sub> low. Regression slopes for hourly O<sub>3</sub> vs. NO<sub>z</sub> were very steep (e.g., 15:1 – 35:1) and highly variable. Consequently, day-specific slopes of hourly O<sub>3</sub> vs. NO<sub>z</sub> regressions were not robust indicators of O<sub>3</sub> sensitivity.

Mid-day (11 a.m. – 2 p.m.) and daily average ratios of O<sub>3</sub>/NO<sub>x</sub>, O<sub>3</sub>/NO<sub>y</sub>, and O<sub>3</sub>/NO<sub>z</sub> were computed. The mid-day ratios are more consistent than daily averages with the theoretical rationale that supports using them as indicators of VOC or NO<sub>x</sub> sensitivity. Since measured NO<sub>x</sub> is biased high, observed O<sub>3</sub>/NO<sub>x</sub> ratios are lower than they would be for unbiased measurements. The data suggest site-specific ranges of transitions between VOC and NO<sub>x</sub> sensitivity: 7 – 12 for O<sub>3</sub>/NO<sub>y</sub> and 9 – 14 for O<sub>3</sub>/NO<sub>x</sub> at Milwaukee but ~10 – 14 for O<sub>3</sub>/NO<sub>y</sub> and 12 – 16 for O<sub>3</sub>/NO<sub>x</sub>, and more variable, at non-urban Manitowoc. If transition ranges are site-specific, the universality and applicability of O<sub>3</sub>/NO<sub>y</sub> as an indicator are unclear. The observed ranges are approximately consistent with published transition ranges of 8 – 9 for O<sub>3</sub>/NO<sub>y</sub> and ~15 for O<sub>3</sub>/NO<sub>x</sub>.

Mid-day ratios of O<sub>3</sub>/NO<sub>y</sub> are approximately one order of magnitude lower than corresponding ratios of O<sub>3</sub>/NO<sub>z</sub>. Mid-day ratios of O<sub>3</sub>/NO<sub>y</sub> show little correlation with ratios of HCHO/NO<sub>2</sub>. Different day-specific results would therefore be obtained from these two ratios, even if their sensitivity ranges were known exactly.

### **1.3 Implications**

Reductions of both VOC and NO<sub>x</sub> emissions are predicted to reduce MDA8 O<sub>3</sub> at sites in WI and MI. However, the results indicate that NO<sub>x</sub>-focused emission control strategies have had, and will continue to have, counterproductive effects at locations in the Chicago metropolitan area. This effect is also evident at some urban locations in southern WI (Milwaukee and Kenosha). The results highlight the need to evaluate emission-control strategies that are either geographically specific or that are crafted to achieve larger VOC than NO<sub>x</sub> reductions within urban Chicago and Milwaukee while also reducing NO<sub>x</sub> emissions sufficiently to benefit shoreline sites north of Milwaukee.

Further study of potential emission-control strategies is needed. Current understanding of O<sub>3</sub> could be enhanced by locating instruments for continuous measurement of NO, species-specific NO<sub>2</sub>, NO<sub>y</sub>, and total NMOC at each site where high O<sub>3</sub> values continue to occur.

WI recently (mid 2019) installed high-sensitivity (0.04 ppbv detection limit) species-specific NO<sub>2</sub> instruments at Milwaukee SER and Manitowoc. These two sites also have NO<sub>y</sub> monitors. Consideration should be given to placing high-sensitivity NO instruments at these locations. The

minimum detection limit of the current NO instruments (5 ppbv) is too high to allow reliable determination of NO<sub>z</sub> from the difference between NO<sub>y</sub> and NO<sub>x</sub>.

The present NMOC measurements are limited spatially to a small number of sites and temporally to 24-hour samples collected once every six days. As a result, the data are not useful for many kinds of data analyses, which often require continuous measurements. NMOC sampling is challenging due to cost and complexity.

## 2. Introduction

### 2.1 Background

Tropospheric ozone (O<sub>3</sub>) adversely affects people, vegetation, and materials (U.S. EPA, 2020a). O<sub>3</sub> is one of six pollutants for which the U.S. Environmental Protection Agency (EPA) sets ambient concentration criteria known as National Ambient Air Quality Standards (NAAQS). The 2015 primary (relating to public health) and secondary (relating to public welfare) O<sub>3</sub> NAAQS are each 0.070 parts per million by volume (ppmv), or 70 parts per billion (ppbv), applicable to the annual 4<sup>th</sup>-highest maximum daily average 8-hour O<sub>3</sub> concentration (4<sup>th</sup> MDA8) averaged over three consecutive years. The 2008 NAAQS (75 ppbv) also remains in effect.

O<sub>3</sub> formation is a complex, nonlinear function of sunlight, emissions of volatile organic compounds (VOC, also known in a measurement context as non-methane organic compounds, or NMOC<sup>1</sup>), and emissions of oxides of nitrogen (NO<sub>x</sub>, largely comprised of nitric oxide [NO] and nitrogen dioxide [NO<sub>2</sub>]). Many factors affect ambient O<sub>3</sub> concentrations<sup>2</sup>, including the rates of formation and removal of O<sub>3</sub>, the rates of dispersion of O<sub>3</sub> and its precursors, transport of urban plumes into downwind areas subject to fresh emissions, and meteorological factors such as temperature, ventilation, and solar intensity.

### 2.2 Past Progress in Reducing Emissions and Ozone Levels

U.S. air quality management programs have reduced O<sub>3</sub> concentrations across the country: the national average of the annual 4<sup>th</sup>-highest MDA8 decreased by 35% between 1980 and 2019 (or by 21% between 2000 and 2019) (U.S. EPA, 2020b). For the upper Midwest, the O<sub>3</sub> reduction averaged 18% between 2000 and 2019 and exhibited little trend between 2008 and 2018 (U.S. EPA, 2020b). High O<sub>3</sub> levels persist in many locations nationally and pose challenges for attaining the O<sub>3</sub> NAAQS (U.S. EPA, 2020c). In the area surrounding southern Lake Michigan, the monitoring sites that continue to experience O<sub>3</sub> concentrations exceeding 70 ppbv are situated near the shoreline (U.S. EPA, 2020d). O<sub>3</sub> exceedances persist despite reductions of emissions of O<sub>3</sub> precursors (NO<sub>x</sub> and VOCs) and related pollutants (carbon monoxide, CO, and sulfur dioxide, SO<sub>2</sub>) within the states of Wisconsin, Illinois, and Indiana, which declined by approximately half between 2000 and 2019 (Figure 1; Section 9.4.1). Improved understanding of how and when high O<sub>3</sub> concentrations occur over Lake Michigan, and their relationship to emission changes, will contribute to efforts to achieve the O<sub>3</sub> NAAQS in this region.

---

<sup>1</sup> The U.S. EPA uses “volatile organic compound” to refer to gas-phase organic compounds having one to 12 carbon atoms (C<sub>1</sub> – C<sub>12</sub>) and a vapor pressure greater than 0.15 mm Hg (U.S. EPA, 1996). The term is also used less restrictively to denote all reactive, gas-phase organic compounds, including hydrocarbons, aldehydes, ketones, organic acids, organic nitrates, and peroxides (National Research Council, 1991). Early measurement efforts focused on obtaining concentrations of low-molecular weight (C<sub>2</sub> - C<sub>12</sub>), gas-phase non-methane hydrocarbons (NMHC), defined as VOCs comprised of hydrogen and carbon atoms only, excluding methane. The most common approach to measuring total NMHC concentration was flame-ionization detection (FID), the response of which is proportional to the number of carbon atoms in a compound. Since carbon atoms bound to oxygen, nitrogen, or halogens also respond to FID, the method came to be considered as an organic carbon analyzer and the measurements are now usually described as non-methane organic compound (NMOC) concentrations (U.S. EPA, 1996).

<sup>2</sup> I adopt a common convention using “concentration” in place of the technically correct “mixing ratio”.

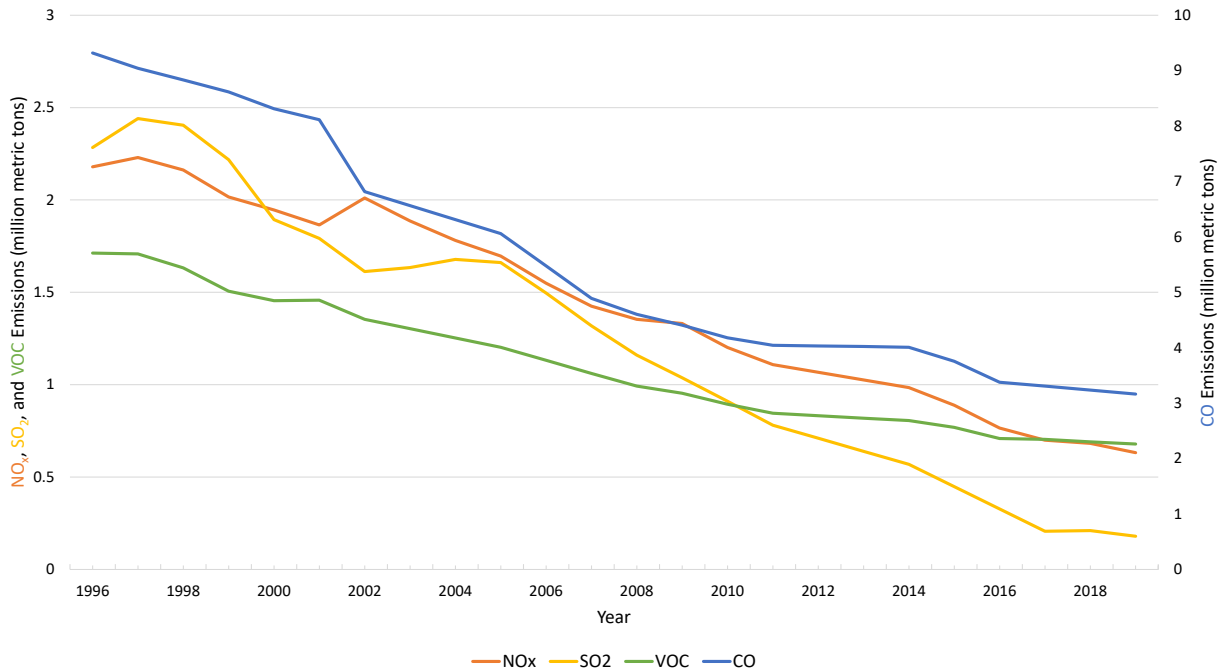


Figure 1. Annual anthropogenic emissions (including wildfires and other biomass burning sources) of CO, NO<sub>x</sub>, SO<sub>2</sub>, and VOCs in Illinois, Indiana, and Wisconsin. The shift between 2001 and 2002 is attributable to EPA’s revision of its emission model for on-road mobile sources (from MOBILE6 to MOVES). Data source: U.S. EPA (2020e).

U.S. EPA modeling projections found that 14 counties outside California, including Sheboygan County, Wisconsin, would continue to violate the 2015 O<sub>3</sub> NAAQS with design values exceeding 70 ppbv in 2025 even after implementing on-the-book rules and emission reductions necessary to achieve the 2008 O<sub>3</sub> NAAQS (U.S. EPA, 2016; 2018). Nine of 12 eastern counties that EPA modeling projected would fail to attain the NAAQS by 2025 are located on coastlines (Abdioskouei et al., 2019) near major metropolitan areas. Section 2.3 discusses coastal processes affecting O<sub>3</sub> at Wisconsin shoreline sites.

Hidy and Blanchard (2015) concluded that the EPA model predictions were likely more sensitive to emission changes than ambient observations indicated. Nearly all (75 of 89) core-based statistical areas (CBSAs) showed statistically significant ( $p < 0.05$ ) correlations ( $r^2 = 0.57$  to  $0.83$ ) between mean annual 4<sup>th</sup>-highest MDA8 and mean 98<sup>th</sup> percentiles of site daily 1-hour maximum NO<sub>2</sub> concentrations. The observed rates of change ranged from 0.6 to 1.6 ppbv O<sub>3</sub> (maximum-site 4<sup>th</sup>-highest MDA8) per ppbv change in mean annual daily 1-hr peak NO<sub>2</sub> concentration which, if continued, would yield smaller O<sub>3</sub> changes than predicted by EPA modeling (Hidy and Blanchard, 2015). The annual 4<sup>th</sup>-highest MDA8 in the Chicago and Milwaukee CBSAs declined by 1.29% and 1.20% per year, respectively, between 1990 and 2014.

## 2.3 Conceptual Model

Studies over the past 40 years have shown that regional high O<sub>3</sub> concentrations in the southern Lake Michigan area involve both long-range transport and local O<sub>3</sub> formation, typically occur over Lake Michigan, and are advected toward shoreline monitoring sites (e.g., Lyons and Cole, 1976; Dye et al., 1995; Pierce et al., 2017). The roles of synoptic-scale meteorology, pollutant transport, the Lake Michigan land-lake breeze, and local emissions on O<sub>3</sub> concentrations in the southern Lake Michigan area are described in the LMOS 2017 White Paper, which also summarizes the historical development of understanding of these processes (Pierce et al., 2017). In very general terms, early morning land breezes, driven by relatively warm temperatures over Lake Michigan and subsidence over land, carry pollutants emitted from coastal urban and industrial areas over the lake, where they form O<sub>3</sub> and other secondary species if sufficient sunlight is available (Abdioskouei et al., 2019). Mid-day heating of the land leads to lake breezes that transport O<sub>3</sub>-rich air from over the lake into coastal locales.

High-O<sub>3</sub> episodes are particularly associated with lake breezes that are reinforced by synoptic-scale southerly winds, which transport polluted air from upwind, high-emissions regions northward along the lakefront (Abdioskouei et al., 2019). Southerly synoptic-scale air mass movement generally occurs along the western side of high-pressure systems (Haney et al., 1989; Dye et al., 1995; Hanna and Chang, 1995; Pierce et al., 2017). During summer, such systems bring hot weather that is conducive to O<sub>3</sub> formation. The lake breeze and south-to-north synoptic-scale transport affect not only the magnitudes of MDA8 O<sub>3</sub> but also their times of occurrence (Figure 2). Wisconsin shoreline sites exhibit, on average, later starting times of the 1<sup>st</sup>-through-4<sup>th</sup> highest MDA8 O<sub>3</sub> than inland Wisconsin sites do. From south to north along the Wisconsin shoreline, the highest MDA8 begin later, except in Milwaukee (Figure 2). There is also a south-to-north progression of MDA8 starting times along the Michigan shoreline (during summer, Michigan and Wisconsin observe EDT and CDT, respectively). The earlier starting hours of the highest MDA8 in Chicago and Milwaukee likely reflect the influence of higher emission densities compared to non-urban locales, because afternoon emissions of NO<sub>x</sub> tend to reduce O<sub>3</sub> concentrations within urban areas. The association of later MDA8 with downwind locations therefore reflects not only transport, but also longer duration of high O<sub>3</sub> values. The shoreline distances shown in Figure 2 are too great (~600 km south-to-north) for air masses to traverse within the span of a few hours, so the temporal patterns do not imply simple movement of a compact, polluted air mass from the urbanized southern area toward the north.

Research activities continue to focus on elucidating the mechanisms that determine the spatial, temporal, and chemical dimensions of O<sub>3</sub>-rich air masses over Lake Michigan. Preliminary findings from the 2017 Lake Michigan Ozone Study (LMOS) are described in Abdioskouei et al. (2019). During the 2017 LMOS, airborne measurements and in situ profiling during O<sub>3</sub> events showed high O<sub>3</sub> and NO<sub>2</sub> concentrations and rapid O<sub>3</sub> formation within a ~50 to ~370 m boundary layer over Lake Michigan (Abdioskouei et al., 2019). Measurements made at the Sheboygan ground supersite during LMOS 2017 showed the influence of the lake breeze and indicated that O<sub>3</sub> formation was sometimes limited by NO<sub>x</sub> and sometimes limited by VOCs (Abdioskouei et al., 2019).

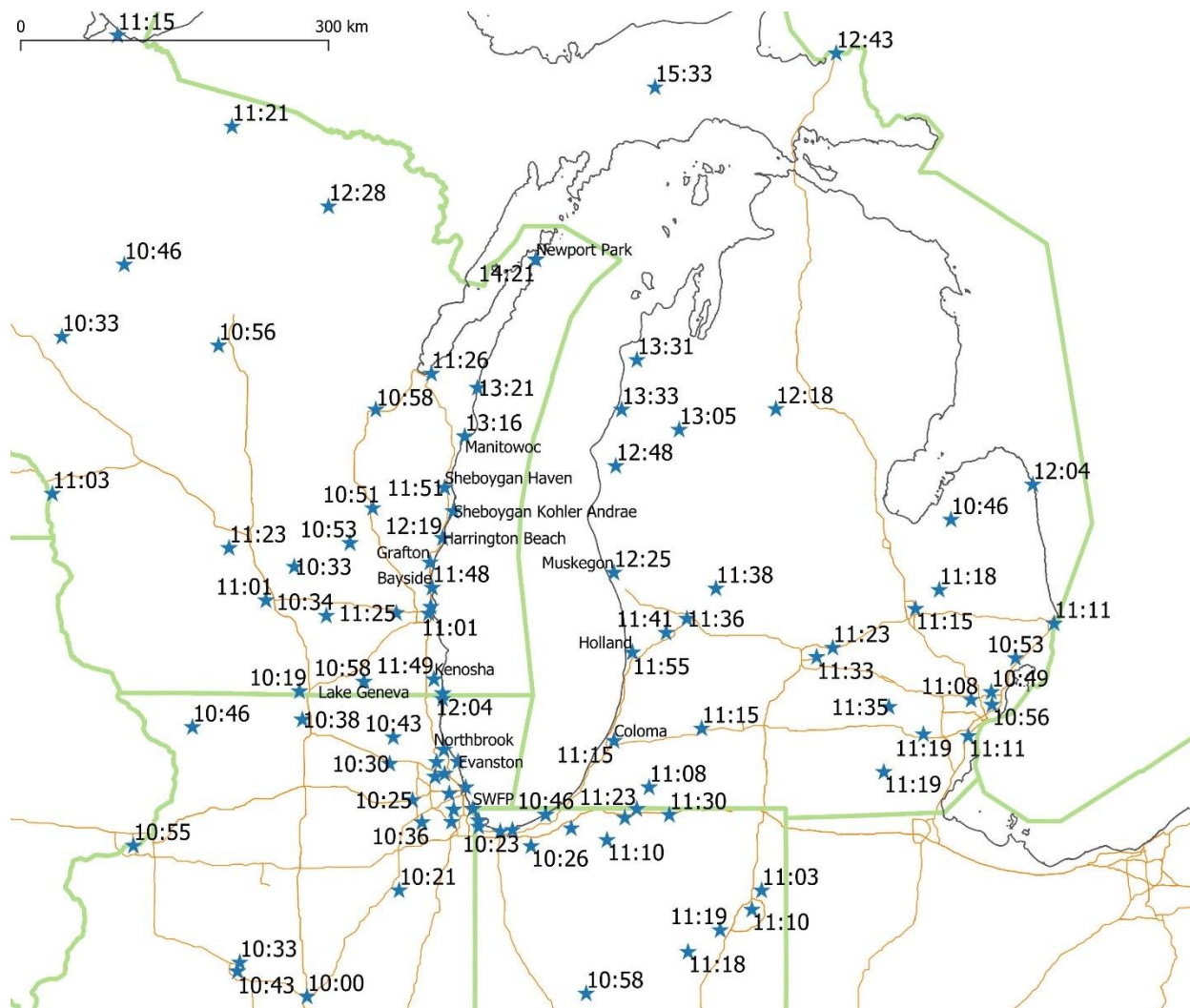


Figure 2. Average time of occurrence of 1<sup>st</sup>-through-4<sup>th</sup> highest MDA8 between 2010 and 2018 (MDA8 starting hour, LST).

Vermeuel et al. (2019) suggest that O<sub>3</sub> production over the urban Chicago source region was strongly VOC sensitive and progressed towards a more NO<sub>x</sub>-sensitive regime as the plume advected north along the Lake Michigan coastline on June 2, 2017, which was the 1<sup>st</sup>, 2<sup>nd</sup>, or 3<sup>rd</sup>-highest O<sub>3</sub> day at Wisconsin shoreline sites that year. Box-model isopleths indicated that O<sub>3</sub> in the arriving air parcel formed in a VOC-sensitive regime with measured  $\Delta O_3 = 51$  ppbv (their Figure 6). The Vermeuel et al. (2019) isopleths of O<sub>3</sub> production are qualitatively consistent with older isopleths showing predicted VOC-sensitive O<sub>3</sub> concentrations in the Chicago urban core (Reynolds et al., 2004). Modeling studies associated with the 1991 LMOS and with recent work have also indicated that VOC emission reductions lowered O<sub>3</sub> in and near Chicago more

effectively than NO<sub>x</sub> reductions did, but the opposite was true further downwind (e.g., Wisconsin shoreline) (Kaleel, 2015).

Past studies have used several terms somewhat interchangeably, variously describing O<sub>3</sub> formation as NO<sub>x</sub> (VOC) sensitive, NO<sub>x</sub> (VOC) responsive, or NO<sub>x</sub> (VOC) limited. Used in the narrowest sense, the terms “NO<sub>x</sub>-limited” and “VOC-limited” refer to the instantaneous sensitivity of O<sub>3</sub> production or concentrations at a specific place and time to small (nearly infinitesimal) changes in ambient concentrations or emissions of NO<sub>x</sub> or VOC. Instantaneous sensitivities vary spatially and temporally, for example, during the course of a day at a single location or in an advected air parcel (e.g., Vermeuel et al., 2019). Used less narrowly, “NO<sub>x</sub>-limited” and “VOC-limited” may refer to instantaneous rates of O<sub>3</sub> production (or concentrations) that have been integrated over the course of a day or more, again considering small perturbations in emissions or precursor concentrations.

If emissions or precursor changes are not small (e.g., 30% emission reduction), studies typically report the predicted (or actual) O<sub>3</sub> response, not instantaneous O<sub>3</sub> sensitivities. Usually, an O<sub>3</sub> response integrated over time is reported. From a regulatory perspective, instantaneous O<sub>3</sub> sensitivity is less relevant than how O<sub>3</sub> concentrations responded, or will respond, to larger (non-infinitesimal) NO<sub>x</sub> or VOC emission reductions. O<sub>3</sub> responses to larger (non-infinitesimal) perturbations in emissions or precursor concentrations are designated here as “O<sub>3</sub> responsiveness” (the term “non-instantaneous O<sub>3</sub> sensitivity” also appears in the literature). The well-known O<sub>3</sub> isopleth diagram (O<sub>3</sub> isopleths as a function of VOC and NO<sub>x</sub> emissions, e.g., National Research Council, 1991; Reynolds et al., 2004; Vermeuel et al., 2019) shows that even when O<sub>3</sub> formation is VOC-limited (an instantaneous sensitivity), O<sub>3</sub> could also be NO<sub>x</sub>-responsive if a sufficiently large reduction of NO<sub>x</sub> emissions were to occur and would ultimately lower peak O<sub>3</sub> concentrations. That is, O<sub>3</sub> may be VOC-limited initially before transitioning into NO<sub>x</sub> limitation. This report uses the terms “sensitivity,” “response,” and “limitation,” whose meanings are usually clear from context. More explicitly, “sensitivity” is used here as a general term to represent either “limitation” or “responsiveness.” “Limitation” is used more narrowly to reference instantaneous O<sub>3</sub> sensitivity.

The U.S. EPA (2019a) finds that summer daytime O<sub>3</sub> production typically increases as NO<sub>x</sub> concentrations increase over much of the U.S., which EPA describes as a “NO<sub>x</sub> limited” condition. In contrast, EPA finds that where NO<sub>x</sub> concentrations are higher or when meteorological conditions do not favor photochemical production, O<sub>3</sub> formation may be only weakly dependent on NO<sub>x</sub> emissions, or even inversely correlated; EPA describes these regimes in which O<sub>3</sub> increases as VOC concentrations increase as “VOC-limited.” These conclusions regarding instantaneous O<sub>3</sub> sensitivity (summer daytime O<sub>3</sub> production) suggest that high peak O<sub>3</sub> concentrations would generally be NO<sub>x</sub> responsive in most areas of the eastern U.S.

## **2.4 Objectives**

The primary objective of this study is to evaluate the sensitivity of O<sub>3</sub> formation along Wisconsin’s Lake Michigan shoreline, in and near Chicago, and at shoreline locations in southwestern Michigan to changes in emissions and ambient concentrations of NO<sub>x</sub> and VOCs.

The principal focus is on current O<sub>3</sub>-NO<sub>x</sub>-VOC sensitivity along the western shore of Lake Michigan, addressing the spatial and temporal variability of this sensitivity.

## 2.5 Scope

This report evaluates O<sub>3</sub> sensitivity at 20 key monitoring sites between 2000 and 2019 (Table 1 and Figure 3) using the approaches summarized in Section 2.6 and described in detail in Sections 3 through 5. All methods rely on existing data sets.

Table 1. Analyses carried out based on availability of air quality site data (Section 9, Table A1). The GAM input data consist of both regional and local measurements.

Monitor	VOC-Based Indicators	O <sub>3</sub> vs NO <sub>z</sub>	GAM
Newport Park WI			Yes
Manitowoc WI		High bias NO <sub>2</sub> , low bias NO <sub>z</sub>	Yes
Sheboygan Haven WI			Yes
Sheboygan Kohler WI			Yes
Harrington Beach WI			Yes
Horicon/Mayville WI	HCHO/ NO <sub>y</sub> (lacks NO <sub>2</sub> )	Lacks NO <sub>x</sub> but has NO <sub>y</sub>	Yes
Grafton WI			Yes
Bayside WI			Yes
Milwaukee DNR SER WI	HCHO/NO <sub>2</sub> ; NMOC/NO <sub>y</sub>	High bias NO <sub>2</sub> , low bias NO <sub>z</sub>	Yes
Milwaukee Health Ctr WI	HCHO (lacks NO <sub>2</sub> )		No
Kenosha Water Tower			Yes
Lake Geneva WI			Yes
Chiwaukee Prairie WI			Yes
Zion IL		2000 - 02 NO <sub>x</sub> (bias) and NO <sub>y</sub>	No
Northbrook IL	HCHO/NO <sub>2</sub> ; NMOC/NO <sub>y</sub>	High bias NO <sub>2</sub> , low bias NO <sub>z</sub>	Yes
Evanston IL			Yes
Schiller Park IL			Yes
Jardine IL			Yes
Cicero IL			No
Chicago Lawndale IL			No
S. Water Filtration Plant			Yes
Whiting-Center St/HS IN			No
Hammond IN			No
East Chicago-Marina IN			No
Gary-IITRI IN			No
Ogden Dunes IN			No
S Bend - Shields Dr IN			No
Coloma MI			Yes
Holland MI			Yes
Muskegon MI			Yes

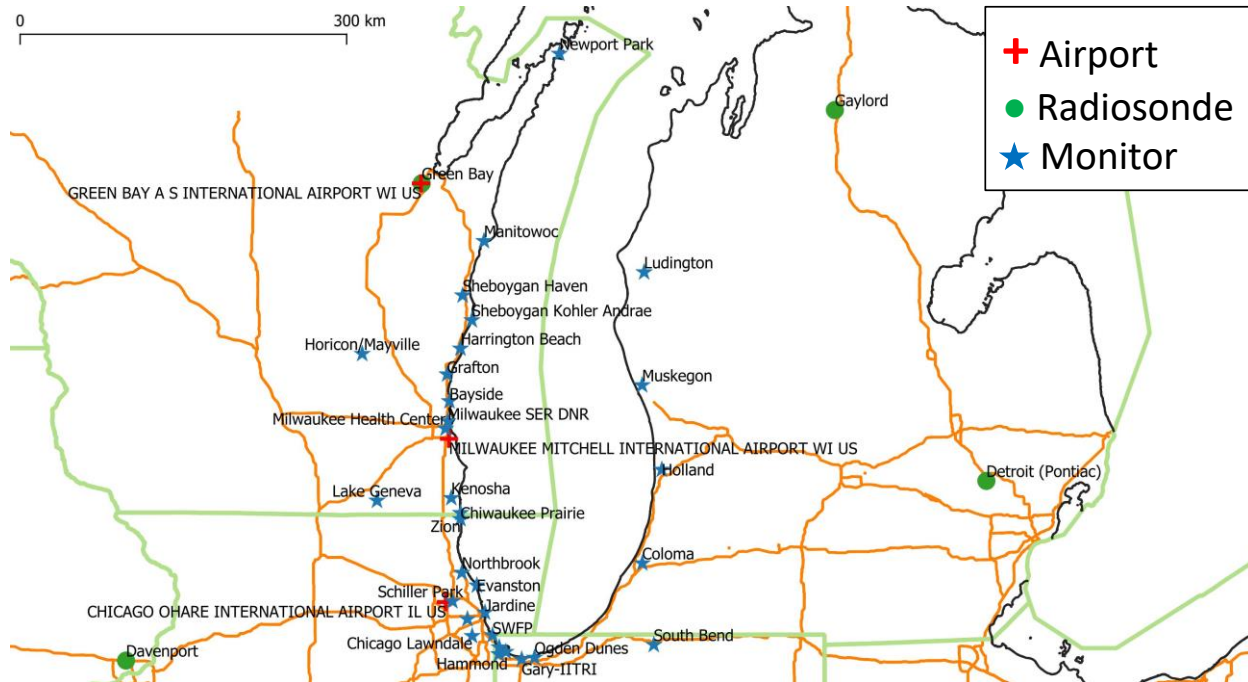


Figure 3. Locations of airports, radiosonde sites, and air-quality monitoring stations.

## 2.6 Approach

Grid-based air quality models account for a wide range of physical and chemical processes that affect  $O_3$  formation and are the state-of-the-art approach to evaluating emissions scenarios and projecting future conditions. However, modeling predictions are subject to uncertainties due to uncertainties in emission estimates and simplifications that limit the capacity of gridded models to accurately simulate complex atmospheric processes. In the Lake Michigan area, gridded models do not yet simulate observed high  $O_3$  events along the western shoreline as accurately as needed (Abdioskouei et al., 2019).

EPA guidance (U.S. EPA, 2007; 2018) recommends using model predictions in a relative, rather than an absolute, sense for State Implementation Plan (SIP) attainment demonstrations. This approach is known as the relative response factors (RRF) procedure and ties a modeling-based attainment demonstration to observations.<sup>3</sup> While the RRF approach helps address complications arising from discrepancies between base-case model predictions and observations, scaling observed design values by RRFs may not yield a correct answer. The most problematic cases are those in which model results are directionally wrong (Sillman et al., 1997).

<sup>3</sup> For the federal 8-hour ozone standard, the design value is calculated on a site-by-site basis as the three-year average of the annual 4<sup>th</sup>-highest daily peak 8-hour ozone concentration. EPA guidelines specify the treatment of missing data.

Corroborating analyses can provide important independent verification of key physical and chemical processes, such as changes in O<sub>3</sub> photochemical production rates in response to decreasing anthropogenic emissions of NO<sub>x</sub> and VOCs (Trainer et al., 2000). EPA guidance recommends the use of supplementary weight-of-evidence (WoE) analyses to complement modeling as part of an attainment demonstration. EPA (2018) notes that “ambient data and emissions trends become more important (and hence model results become less important) the closer in time the area is to its attainment date.” EPA has recognized the following types of weight-of-evidence analyses: (1) additional modeling (EPA, 2007; 2018), (2) analyses of trends in air quality and emissions (EPA, 2007; 2018), (3) observational models and diagnostic analyses (EPA, 2007), and (4) additional emission reductions (EPA, 2018). EPA (2007) identifies two classes of observational models relevant to weight-of-evidence assessments: (1) receptor models, such as chemical mass balance (CMB), that are used for source attribution, and (2) indicators that qualitatively describe the sensitivity of a secondary pollutant to changes in precursor species concentrations (sensitivity indicators). EPA (2018) states, “In addition to ambient data trends, further analysis of ambient data can provide information on ozone production efficiency, evidence of transport and assist in the quality assurance of emissions inputs.”

Many of the O<sub>3</sub> sensitivity indicator methods received significant attention during the 1990s (e.g., Hess et al., 1992; Trainer et al., 1993; Olszyna et al., 1994; Milford et al., 1994; Cardelino and Chameides, 1995; Chang and Suzio, 1995; Sillman, 1995; Blanchard et al., 1999; Kleinman, 2000; Trainer, 2000), but typically have not been incorporated into SIP attainment demonstrations. Their use has been limited because sensitivity indicators do not provide quantitative estimates of the magnitudes of emission control needed and because uncertainties remain about the accuracy of sensitivity indicators (e.g., Lu and Chang, 1998; Sillman and He, 2002; Liang et al., 2006) (Section 3). Nonetheless, observation-based approaches have potential as WoE methods, provided that supporting information is used to establish both the predictive power and the accuracy of indicator threshold values (“crossover points”).

This project utilizes three observation-based approaches to evaluating the sensitivity of O<sub>3</sub> in the southern Lake Michigan area to changes in VOC and NO<sub>x</sub> emissions. First, the report evaluates measurements of VOCs and various VOC-based ratios as ozone sensitivity indicators, including (1) HCHO (ratios to NO<sub>2</sub> or NO<sub>y</sub>) and (2) NMOC (ratios to NO<sub>x</sub> or NO<sub>y</sub>). Other indicator species or ratios (e.g., peroxide/nitric acid, H<sub>2</sub>O<sub>2</sub>/HNO<sub>3</sub>) are not evaluated because the necessary measurements were not made on a long-term basis at state and federal monitoring sites. Second, measurements of NO<sub>y</sub> and NO<sub>z</sub> are compiled and evaluated as O<sub>3</sub> sensitivity indicators. Measurement limitations are listed in Tables 1 and A1 and discussed in Section 9.3. Finally, a generalized additive model (GAM) is used to investigate O<sub>3</sub> responses at 20 locations to changes in regional emissions and ambient precursor concentrations.

The measurement locations for each approach are listed in Table 1 and the measurement availability for these and other sites is delineated in Table A1. Site locations are shown in Figure 3, which also includes the locations of meteorological data used in the GAM (Sections 5 and 9).

### 3. VOCs as Ozone Sensitivity Indicators

#### 3.1 Background

Sillman (1995) proposed that certain ratios of species could serve as indicators of the history of ozone formation, because the pollutant concentrations preserved a memory of the conditions under which ozone formed, e.g.,  $\text{NO}_x$ -rich or  $\text{NO}_x$ -limited. The species of use are those that are secondary, or principally secondary, in origin, i.e., reaction products. As proposed, the method represented  $\text{O}_3$  responsiveness (e.g., to 35% reductions of precursor emissions in model simulations) and was not intended to represent instantaneous  $\text{O}_3$  sensitivities.

The ratios  $\text{O}_3/\text{NO}_y$ ,  $\text{O}_3/\text{NO}_z$ ,  $\text{HCHO}/\text{NO}_y$ , and  $\text{H}_2\text{O}_2/\text{HNO}_3$  are indicators that can be derived from equations of atmospheric chemistry under reasonable assumptions. Except for the ratios involving  $\text{NO}_y$ , the species in these ratios are secondary pollutants, and so can be expected to reveal which atmospheric reactions predominated during the time course of air mass movement toward a given monitoring site. For ratios involving  $\text{NO}_y$ , both primary ( $\text{NO}_x = \text{NO} + \text{NO}_2$ ) and secondary ( $\text{NO}_z$ ) species are included in the denominator terms. The inclusion of primary species appears to stabilize the ratios. Similarly, the ratio  $\text{O}_3/\text{NO}_x$  mixes secondary and primary species, but appears to have desirable characteristics (Tonnesen and Dennis, 2000a; 2000b). The indicators  $\text{HCHO}/\text{NO}_2$  and  $\text{HCHO}/\text{NO}_y$  are subject to confounding effects if primary emissions of HCHO are large enough to contribute substantially to observed atmospheric concentrations.

Kleinman (2000) extended the indicator framework by distinguishing between instantaneous and integrated net ozone production. Kleinman et al. (2000, 2001, 2003, 2005) describe applications illustrating instantaneous sensitivity of  $\text{O}_3$  production. Methods that characterize the sensitivity of instantaneous *net ozone production* to emission changes are sometimes known as local methods. Methods that characterize the sensitivity of *ozone concentrations* to emission changes are known as non-local methods.

Lu and Chang (1998) argued that the transition values of indicator ratios are location specific. Blanchard and Stoeckenius (2001) found that the transitional ranges of sensitivity indicator values were relatively large, but the spatial scale over which the transition between VOC and  $\text{NO}_x$  sensitivity occurred was nonetheless typically less than ~10 km. Liang et al. (2006) concluded that sensitivity indicators were more capable of diagnosing where  $\text{NO}_x$  reductions were beneficial and where they were detrimental; sensitivity indicators were less capable of diagnosing where the benefits of VOC reductions were greater than the benefits of  $\text{NO}_x$  reductions and where they were smaller.

Sillman (2019) provides a review originally prepared as a draft report to EPA in 2002; his Table 2.2 lists proposed values of VOC-sensitive,  $\text{NO}_x$ -sensitive, and transitional regimes derived from models.

#### 3.2 Site Selection

The sites with necessary measurements of VOC and  $\text{NO}_{x/y}$  are (1) Horicon/Mayville, (2) Milwaukee DNR SER, and (3) Northbrook, IL (Tables 1 and A1). Measurement biases are an important consideration at each site.

### 3.3 Indicators Based on HCHO, NO<sub>2</sub>, and NO<sub>y</sub>

#### 3.3.1 Methods

Measurements of HCHO, NO<sub>2</sub>, and NO<sub>y</sub> are available (Tables 1 and A1). However, sampling duration (3 or 24 hours for HCHO) and measurement bias (non-specific NO<sub>2</sub>) make these measurements somewhat incommensurate with published values of crossover points, e.g., the value above which HCHO/NO<sub>2</sub> indicates NO<sub>x</sub>-sensitivity.

Previous work proposes the following crossover values for mid-day concentrations of ratios involving HCHO, NO<sub>2</sub>, and NO<sub>y</sub>:

1. Sillman (1995) identified HCHO/NO<sub>y</sub> < 0.3 as indicating VOC-responsive peak O<sub>3</sub> in modeling simulations (including simulations for Lake Michigan-area modeling). Simulations used a 35% emission reduction relative to 1980 emissions. The crossover was 0.20 – 0.23 for base-case VOC emissions lowered by 50% (which would be more comparable to current VOC emissions).
2. Tonnessen and Dennis (2000b) found HCHO/NO<sub>2</sub> more useful than HCHO/NO<sub>y</sub> as an indicator of VOC or NO<sub>x</sub>-limitation (approximated as model response to 15% emission changes) at 5 p.m. Modeling simulations used 1988 emissions. VOC-limitation was indicated for HCHO/NO<sub>2</sub> < 0.8, NO<sub>x</sub>-limitation was indicated for HCHO/NO<sub>2</sub> > 1.8, and intermediate values were transitional.
3. Duncan et al. (2010) derived a transition range of O<sub>3</sub> sensitivity based on satellite column ratios of HCHO/NO<sub>2</sub> between 1 and 2.
4. Schroeder et al. (2017) evaluated aircraft and satellite HCHO/NO<sub>2</sub>. They concluded that it was preferable to use observed HCHO/NO<sub>2</sub> in a relative sense rather than in relation to published crossover values. This conclusion was based upon results indicating that the transition (or ambiguous) range of sensitivity corresponded to a wide and spatially variable range of HCHO/NO<sub>2</sub>. The transition ranges were 0.9 – 1.8 for Colorado (2014), 0.7 – 2.0 for Houston (2013), and 1 – 2.3 for Maryland (2011).
5. Jin et al. (2020) used satellite column measurements of HCHO and NO<sub>2</sub> with ground-level O<sub>3</sub> to estimate a crossover value of 3.6 (3.2 to 4.1, 2σ uncertainty) applicable to 1 – 2 p.m. O<sub>3</sub>. Results for Chicago matched the overall values, but the uncertainty was higher (± 0.6 compared to ± 0.2). Sensitivity was defined based on observed frequencies of O<sub>3</sub> exceeding 70 ppbv between 2005 and 2016.

The values proposed by Jin et al. (2020) are the most recent and are derived entirely from observations, so are not subject to biases caused by inconsistencies between monitoring data and model-based grid-cell averages or by modeling inaccuracies. However, column measurements generally do not reflect ground-based concentrations (Schroeder et al., 2017) and the available surface data exhibit the following biases and characteristics that require consideration:

1. Ground-based HCHO/NO<sub>2</sub> is typically lower than satellite HCHO/NO<sub>2</sub>. Because NO<sub>2</sub> concentrations decrease above ~500 m, column HCHO/NO<sub>2</sub> usually exceeds ground-based HCHO/NO<sub>2</sub> (Schroeder et al., 2017).

2. Typical NO<sub>2</sub> measurements (thermal conversion to NO on a molybdenum oxide catalytic converter) are biased high by inclusion of other oxidized nitrogen species, thus leading to ratios of HCHO/NO<sub>2</sub> that are biased low. Vermeuel et al. (2020) reported a 12% difference between biased and unbiased NO<sub>2</sub> concentrations at Zion on June 2, 2017. Differences at other times and places are potentially much larger (Section 9.3.1).
3. 24-hour resolution HCHO/NO<sub>2</sub> is lower than mid-day HCHO/NO<sub>2</sub> due to lower HCHO and higher NO<sub>2</sub>. HCHO/NO<sub>2</sub> averaged over 24 hours is approximately a factor of two lower than HCHO/NO<sub>2</sub> averaged over three hours (11 a.m. – 2 p.m.) (Section 9.3.2).
4. If NO<sub>y</sub> data are available but NO<sub>2</sub> measurements are not (Table 1), ratios of HCHO/NO<sub>y</sub> < HCHO/NO<sub>2</sub>.

Each of the preceding factors acts to lower the HCHO/NO<sub>2</sub> ratios obtained from ground-based monitors relative to ratios based on satellite measurements or model predictions. It may be preferable to use observed HCHO/NO<sub>2</sub> and HCHO/NO<sub>y</sub> in a relative sense rather than in relation to published crossover values, as suggested by Schroeder et al. (2017). Given the quantified factor-of-two correction (item 3 above) and the unquantified biases (items 1 and 2), the crossover value reported in prior studies would need to be adjusted downward by greater than a factor of two and possibly by a factor of as much as three to four. If derived from the available measurements, therefore, an HCHO/NO<sub>2</sub> crossover value of approximately one (1) or lower would be expected. The expected uncertainty is at least ± 0.6 (Jin et al., 2020), which spans the width of most of the transition ranges reported by Tonnessen and Dennis (2000b) (range of 1), Duncan et al. (2010) (range of 1), and Schroeder et al. (2017) (ranges of 1 to 3). That is, the available ambient measurements are expected to show a transitional range for HCHO/NO<sub>2</sub> ratios of ~0.3 – 1.5. This expectation can be examined using the available data.

VOC limitation is likely to occur at urban sites on most days during spring, prior to higher rates of isoprene emissions. Isoprene concentrations increased seasonally at all VOC-monitoring sites in the study area beginning in mid-May (Section 9.4.3). The 90<sup>th</sup> percentiles of April HCHO/NO<sub>2</sub> ratios were 0.25 at Schiller, 0.18 at Northbrook, and 0.31 at Milwaukee SER DNR. Ambient 24-hour ground-level HCHO/NO<sub>2</sub> ratios < 0.3 are therefore plausibly indicative of VOC-limited O<sub>3</sub> formation.

NO<sub>x</sub> limitation is likely to occur at rural, inland sites on many, or most, days during June or July. At Horicon/Mayville, the 50<sup>th</sup> percentiles of July HCHO/NO<sub>y</sub> and HCHO/(NO<sub>y</sub> – NO) ratios were 0.77 and 0.80, respectively. No measurements of NO<sub>2</sub> (biased or unbiased) were made, however. If NO<sub>2</sub> concentrations averaged ~75% of NO<sub>y</sub> at this site, ambient 24-hour ground-level HCHO/NO<sub>2</sub> ratios > 1 would be plausibly indicative of NO<sub>x</sub>-limited O<sub>3</sub> formation. For comparison, at a rural site in New York State, the median (unbiased) NO<sub>2</sub> was 72% of NO<sub>y</sub> in July 2017 and 80% in July 2018 (Ninneman, et al., 2020).

The relationship of O<sub>3</sub> with HCHO/NO<sub>2</sub> varies depending on the averaging times of both O<sub>3</sub> and HCHO/NO<sub>2</sub> (Section 9.3.2). At Milwaukee SER DNR, maximum O<sub>3</sub> production appears to occur when mid-day HCHO/NO<sub>2</sub> is ~0.3 (~0.2 – 0.6). The highest MDA8 O<sub>3</sub> values also occurred for values of 24-hour HCHO/NO<sub>2</sub> in the range 0.2 – 0.6.

### 3.3.2 Results

Few days at any site exhibit HCHO/NO<sub>2</sub> ratios > 1 (Figure 4). If 24-hour HCHO/NO<sub>2</sub> ratios > 1 indicate NO<sub>x</sub>-limitation, then O<sub>3</sub> formation was VOC-limited or transitional on most dates at the sites shown. Three of the four sites are urban: two are within the Chicago metropolitan area and one is in Milwaukee. It is possible that O<sub>3</sub> formation was NO<sub>x</sub>-limited at shoreline sites north of Milwaukee, but HCHO data are not available for such sites.

Many or most of the high-O<sub>3</sub> (> 60 ppbv) days fall into a transitional (or indeterminate) range of HCHO/NO<sub>2</sub> ratios of 0.3 – 1. Most of the low-O<sub>3</sub> days exhibit HCHO/NO<sub>2</sub> ratios of ~0.1 (Figure 4). This result suggests that high MDA8 O<sub>3</sub> occurred when weather favored maximum O<sub>3</sub> production associated with an optimal VOC/NO<sub>x</sub> ratio.

HCHO/NO<sub>2</sub> ratios increase from (1) Chicago to Milwaukee to rural Horicon/Mayville (where NO<sub>2</sub> was not measured, but HCHO/NO<sub>2</sub> > HCHO/NO<sub>y</sub>) and (2) as O<sub>3</sub> increases (Figure 5). This result indicates a tendency toward increasingly NO<sub>x</sub>-limited conditions from south-to-north, urban-to-rural, and low-to-high O<sub>3</sub>. The last tendency implies that high O<sub>3</sub> days are typically more NO<sub>x</sub>-limited than other days, which could occur, for example, if higher O<sub>3</sub> production rates generated more O<sub>3</sub> and consumed more NO<sub>x</sub>. This scenario would imply that more NO<sub>x</sub> was converted to O<sub>3</sub>, and that higher O<sub>3</sub> days exhibit high O<sub>3</sub> concentrations because atmospheric reactions proceeded further toward maximum potential O<sub>3</sub> formation.

HCHO/NO<sub>2</sub> ratios also increase during summer months (Figure 6). At Horicon/Mayville, 23% of the summer (June – August) days exhibited HCHO/NO<sub>y</sub> > 1 (>25% in July), implying higher ratios of HCHO/NO<sub>y</sub> and suggesting some frequency of days when O<sub>3</sub> was NO<sub>x</sub>-limited. Ten of 67 (15%) summer days with MDA8 O<sub>3</sub> > 50 ppbv exhibited HCHO/NO<sub>y</sub> > 1; an additional 10 days exhibited HCHO/NO<sub>y</sub> between 0.9 and 1.

HCHO/NO<sub>2</sub> ratios increased after 2008 at Schiller Park and Northbrook, but not at the two Wisconsin sites (Figure 7). Average NO<sub>2</sub> concentrations declined by 0.8 and 0.5 ppbv y<sup>-1</sup>, respectively, at Schiller Park and Northbrook.

Table 2 summarizes results for days with MDA8 O<sub>3</sub> > 50 ppbv.

Table 2. Summary of HCHO/NO<sub>2</sub> ratios for days with MDA8 O<sub>3</sub> > 50 ppbv.

Site	Number of Days <sup>1</sup>	HCHO/NO <sub>2</sub> < 0.3 (% Days)	HCHO/NO <sub>2</sub> 0.3 – 1 (% Days)	HCHO/NO <sub>2</sub> ≥ 1 (% Days)
Schiller Park	31	61	39	0
Northbrook	172	86	13	1
Milwaukee SER	84	50	50	0
Horicon <sup>2</sup>	178	7	75	18

<sup>1</sup>Data records are 2000 – 2019 for Schiller Park, 2000 – 2016 for Northbrook, 2004 – 2016 for Milwaukee, and 2007 – 2019 for Horicon/Mayville

<sup>2</sup>HCHO/NO<sub>y</sub> ratios: < 0.2, 0.2 – 0.8, ≥ 0.8

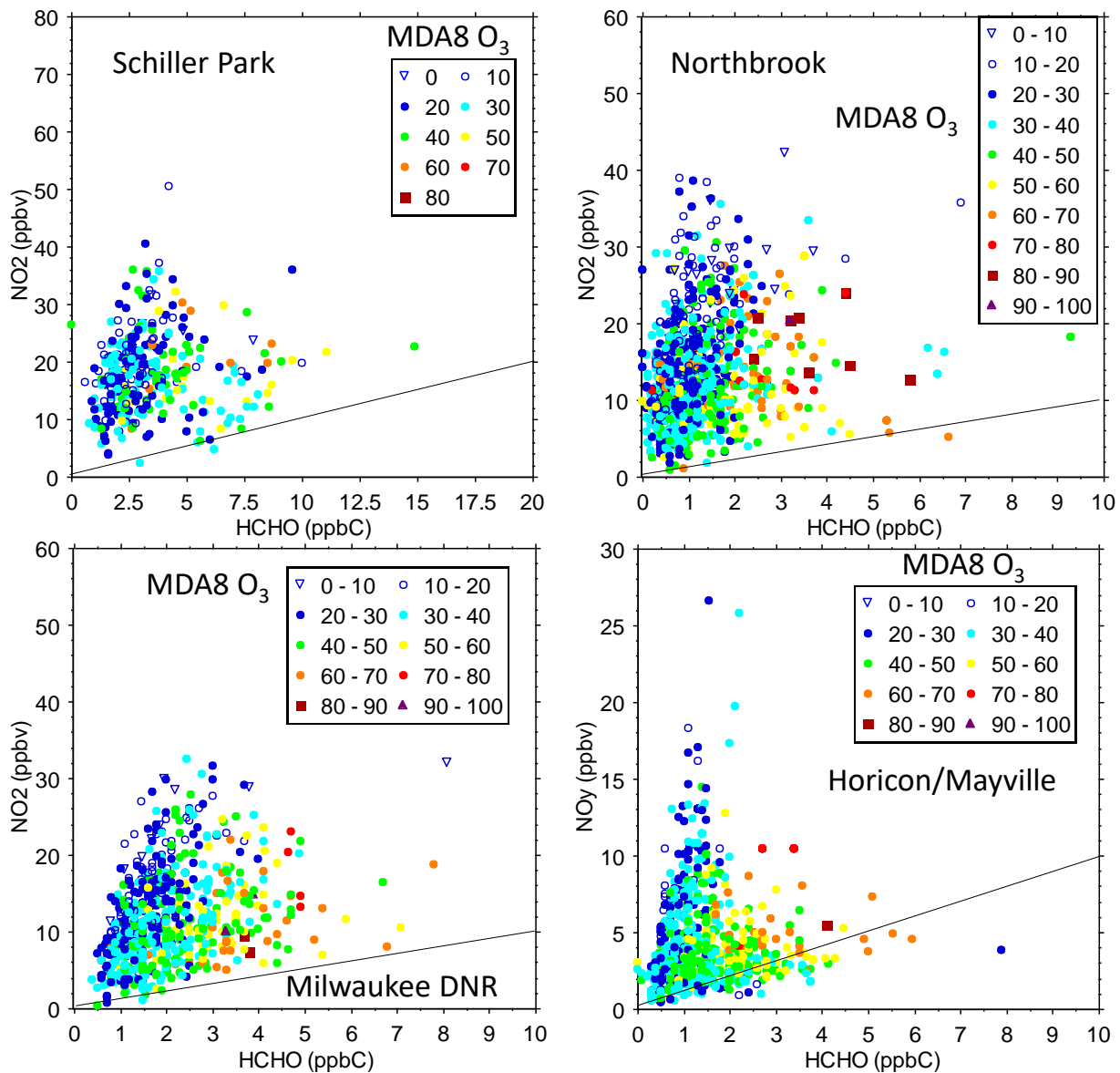


Figure 4. Daily-average NO<sub>2</sub> vs HCHO stratified by MDA8 O<sub>3</sub>. 1:1 lines are shown.

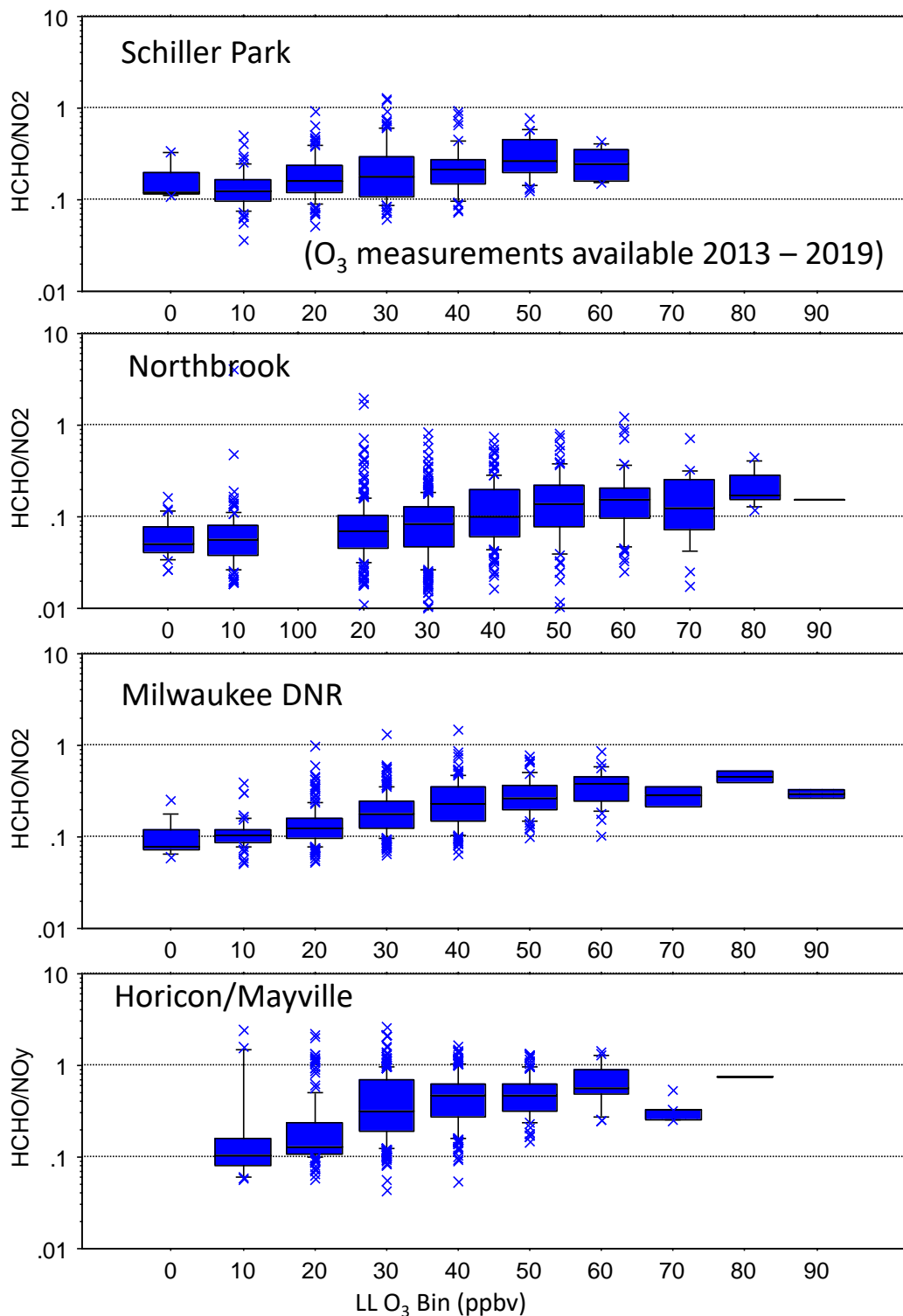


Figure 5. Statistical distributions (10<sup>th</sup>, 25<sup>th</sup>, 50<sup>th</sup>, 75<sup>th</sup>, 90<sup>th</sup> percentiles) of HCHO/NO<sub>2</sub> (or HCHO/NO<sub>y</sub>) versus lower limit (LL) of 10-ppbv width O<sub>3</sub> bins. Dashed horizontal lines are shown at 0.1 and 1 for reference. Data records are 2000 – 2019 for Schiller Park, 2000 – 2016 for Northbrook, 2004 – 2016 for Milwaukee, and 2007 – 2019 for Horicon/Mayville.

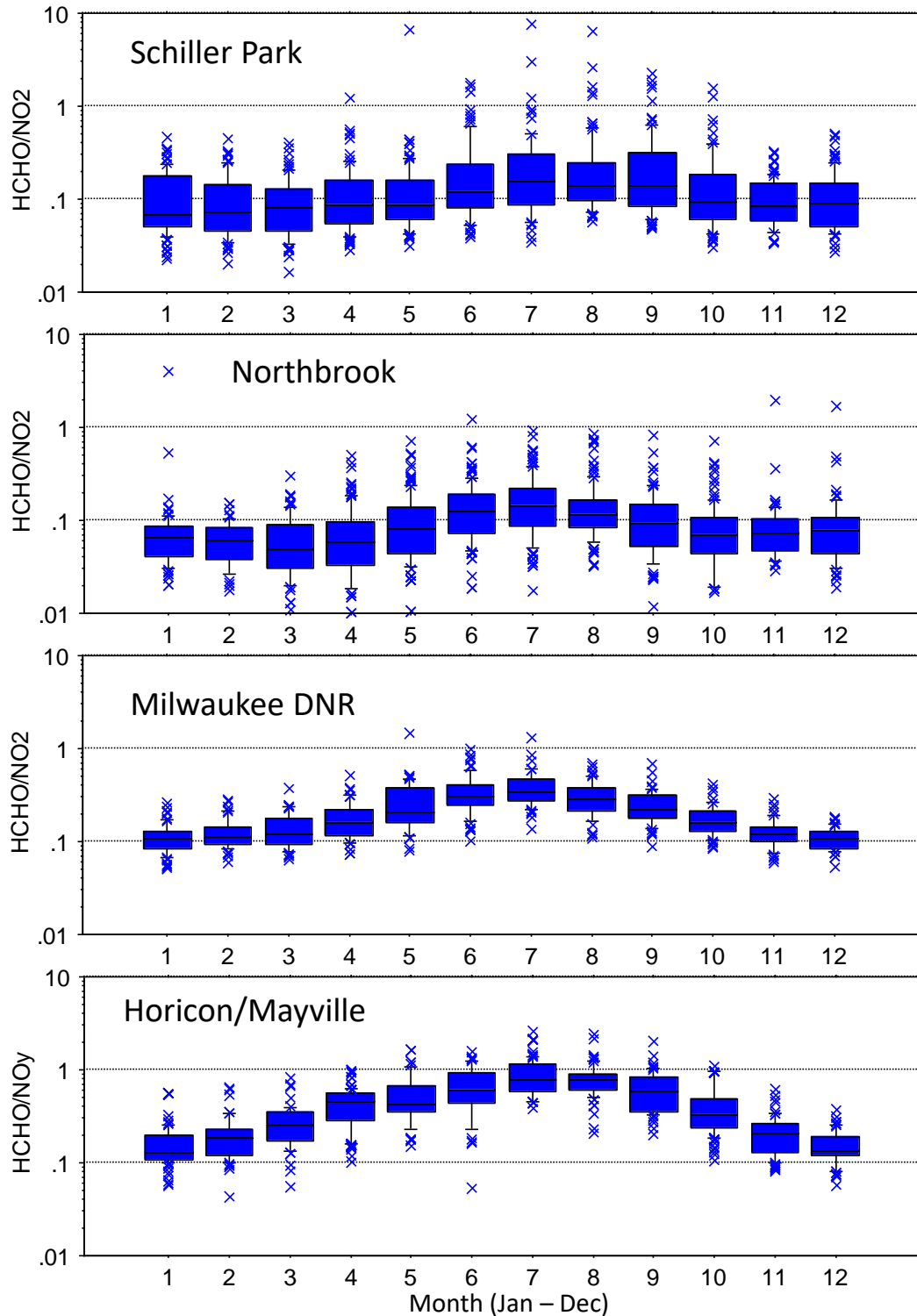


Figure 6. Statistical distributions (10<sup>th</sup>, 25<sup>th</sup>, 50<sup>th</sup>, 75<sup>th</sup>, 90<sup>th</sup> percentiles) of HCHO/NO<sub>2</sub> (or HCHO/NO<sub>y</sub>) versus month. Dashed horizontal lines are shown at 0.1 and 1 for reference. Data records are 2000 – 2019 for Schiller Park, 2000 – 2016 for Northbrook, 2004 – 2016 for Milwaukee, and 2007 – 2019 for Horicon/Mayville.

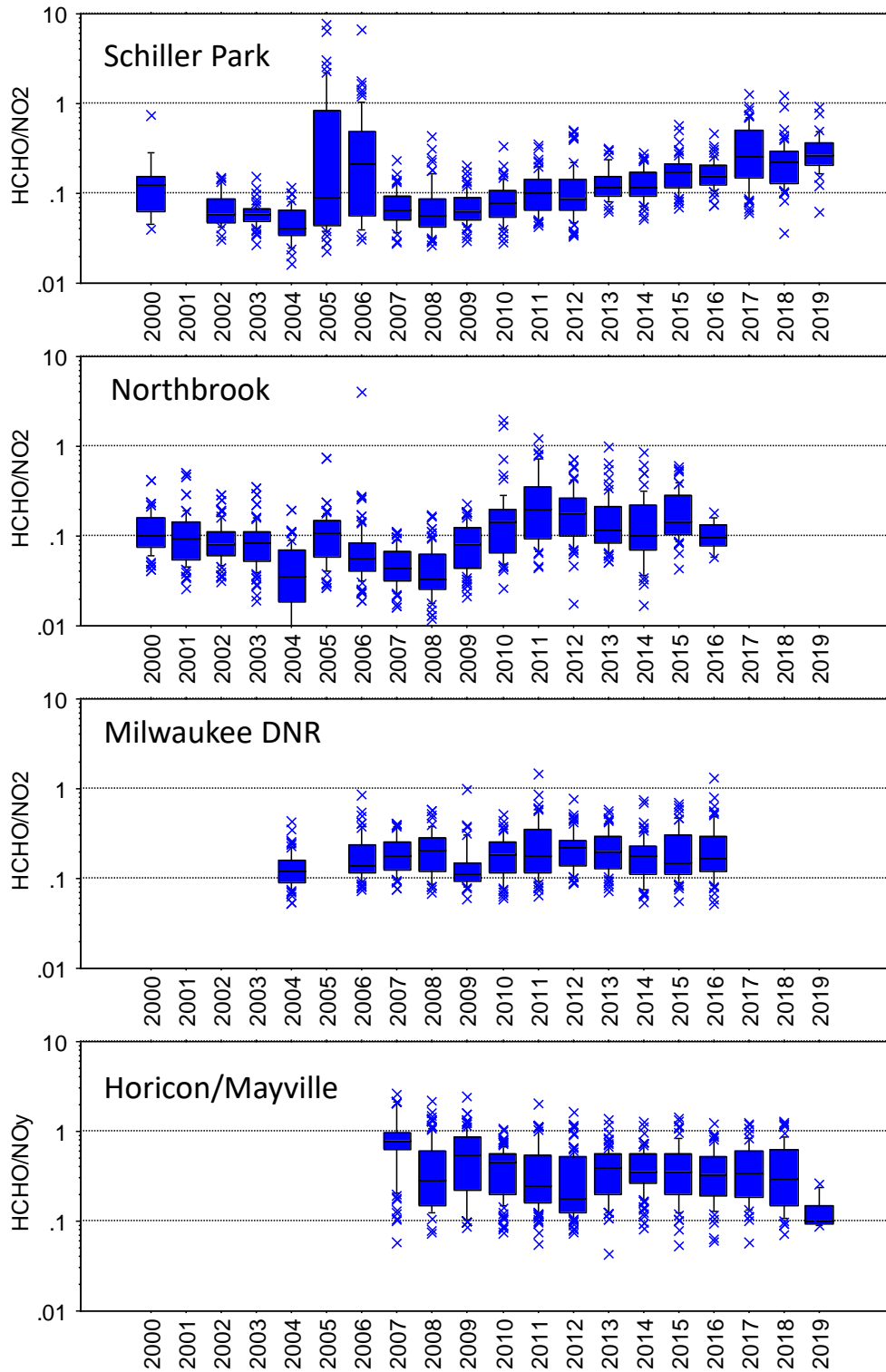


Figure 7. Statistical distributions (10<sup>th</sup>, 25<sup>th</sup>, 50<sup>th</sup>, 75<sup>th</sup>, 90<sup>th</sup> percentiles) of HCHO/NO<sub>2</sub> (or HCHO/NO<sub>y</sub>) versus year. Dashed horizontal lines are shown at 0.1 and 1 for reference.

### **3.4 Indicators Based on NMOC, NO<sub>x</sub>, and NO<sub>y</sub>**

#### **3.4.1 Methods**

Measurements of NMOC, NO<sub>x</sub>, and NO<sub>y</sub> are available for two locations, Milwaukee SER DNR and Northbrook, IL (Tables 1 and A1). The data suggest that O<sub>3</sub> formation is most efficient in these locations when the ambient NMOC/NO<sub>y</sub> ratios are ~3:1 – 10:1 ppbC ppbv<sup>-1</sup> (Section 9.3.3). At Milwaukee SER DNR, the ratio of NMOC and NO<sub>y</sub> values appears to represent emission ratios (Section 9.3.3). Greater scatter occurs for Northbrook. The observed NMOC/NO<sub>y</sub> ratios are considered here in their historical context (e.g., EKMA) as qualitative predictors of O<sub>3</sub> response, rather than as indicators of the chemical evolution of air masses. The ratios are used to characterize spatial and temporal patterns in relative terms.

VOC OH reactivities were computed for sites that reported NMOC species concentrations (Section 9.4.7). Reactivity has not been used as an O<sub>3</sub> sensitivity indicator but provides additional insight into O<sub>3</sub> formation.

#### **3.4.2 Results**

NMOC/NO<sub>x</sub> ratios exhibit higher average values on weekends, during summer, and (less clearly) in more recent years (Figures 8 and 9). Qualitatively, the result is consistent with the expectation of increasingly NO<sub>x</sub>-limited O<sub>3</sub> formation as NO<sub>x</sub> emissions and ambient NO<sub>x</sub> concentrations decline. More definitive conclusions are difficult to substantiate.

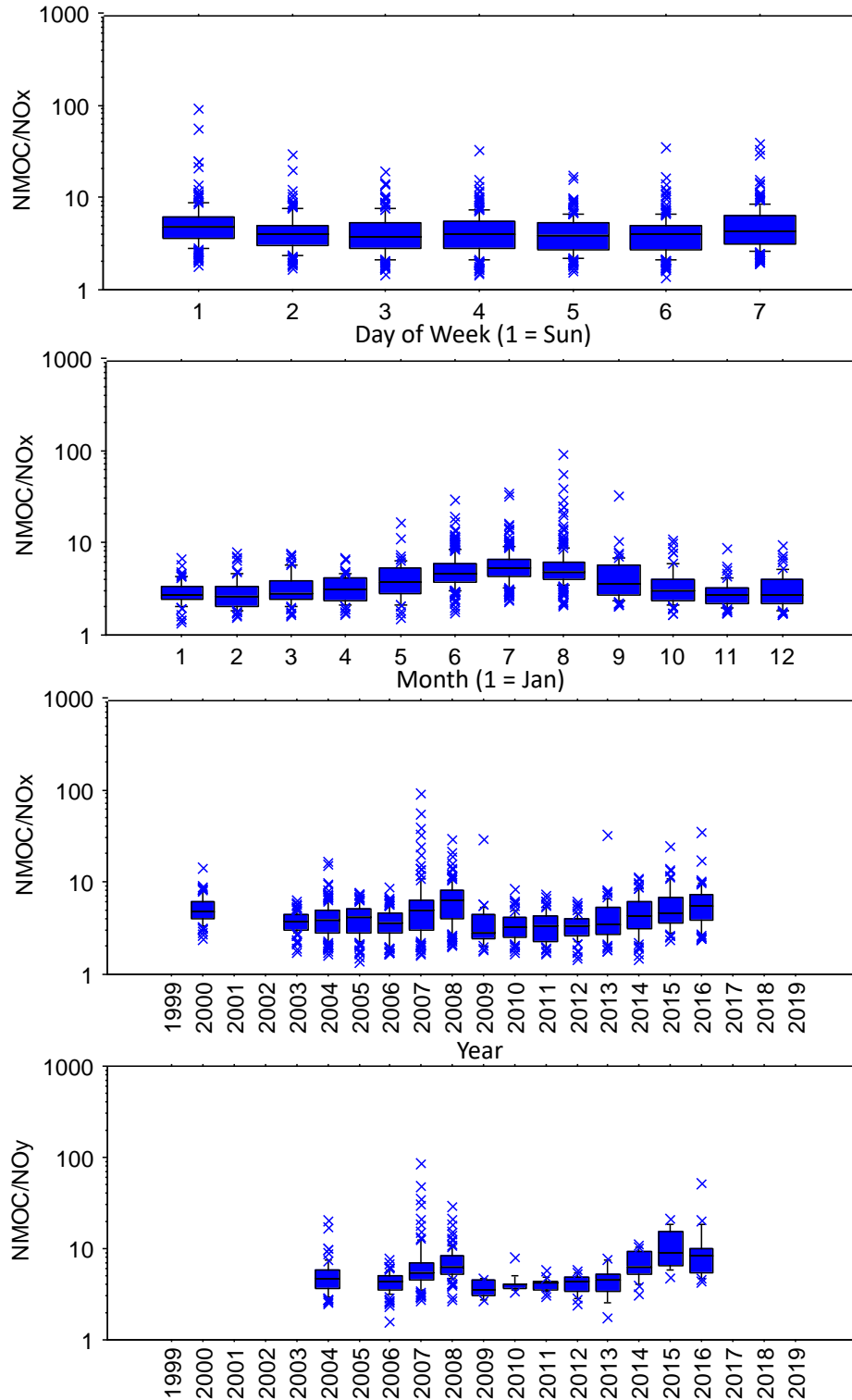


Figure 8. Statistical distributions (10<sup>th</sup>, 25<sup>th</sup>, 50<sup>th</sup>, 75<sup>th</sup>, 90<sup>th</sup> percentiles) of NMOC/NO<sub>x</sub> or NMOC/NO<sub>y</sub> versus day of week, month, and year at Milwaukee SER DNR. NMOC measurements were not made after 2016.

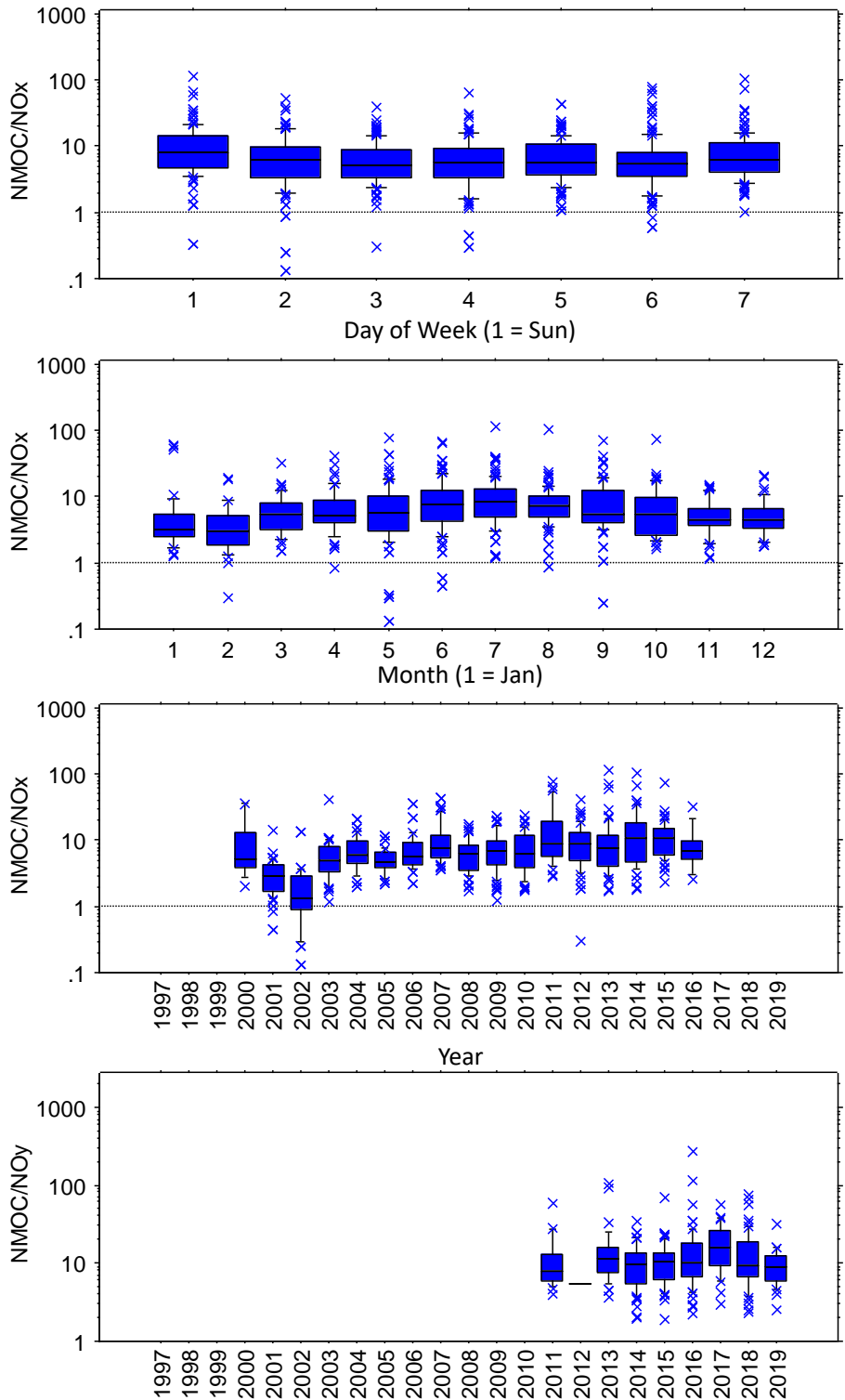


Figure 9. Statistical distributions (10<sup>th</sup>, 25<sup>th</sup>, 50<sup>th</sup>, 75<sup>th</sup>, 90<sup>th</sup> percentiles) of NMOC/NO<sub>x</sub> or NMOC/NO<sub>y</sub> versus day of week, month, and year at Northbrook IL.

### 3.5 Section Summary

In this section, four indicators of O<sub>3</sub> sensitivity were examined: HCHO/NO<sub>2</sub>, NMOC/NO<sub>y</sub>, O<sub>3</sub>/NO<sub>y</sub>, and regression of O<sub>3</sub> versus NO<sub>z</sub>. Additional discussion of VOC OH reactivity is presented in Section 9.4.7.

The utility of each of the individual indicators is limited by measurement accuracy or availability and by methodological uncertainties.

HCHO/NO<sub>2</sub> ratios were determined for three urban sites (Schiller Park, Northbrook, and Milwaukee SER DNR) and one non-urban site (Horicon/Mayville). The 24-hour surface measurements are not commensurate with mid-day satellite data or modeling predictions that have been used previously to delineate ranges of HCHO/NO<sub>2</sub> ratios indicative of VOC, NO<sub>x</sub>, or transitional O<sub>3</sub> sensitivity. Subject to day-to-day variability and uncertainty, the data are consistent with VOC sensitivity typically occurring at low (<0.3) HCHO/NO<sub>2</sub> ratios, a transition between 0.3 and 1, and NO<sub>x</sub> sensitivity at ratios exceeding one (1).

Most (50 – 86%) high-O<sub>3</sub> (> 50 ppbv) days show low (<0.3) HCHO/NO<sub>2</sub> ratios at urban sites or fall into a transitional (or indeterminate) range of HCHO/NO<sub>2</sub> ratios of 0.3 – 1 at nonurban Horicon/Mayville (75%). On average, HCHO/NO<sub>2</sub> ratios increase from (1) Chicago to Milwaukee to rural Horicon/Mayville. These patterns indicate a tendency toward increasingly NO<sub>x</sub>-limited conditions from south-to-north, urban-to-rural, and low-to-high O<sub>3</sub>. The results suggest that high O<sub>3</sub> days are typically more NO<sub>x</sub>-limited than other days, which could occur, for example, when higher O<sub>3</sub> production rates generated more O<sub>3</sub> and consumed more NO<sub>x</sub>. This scenario would imply that more NO<sub>x</sub> was converted to O<sub>3</sub>, and that higher O<sub>3</sub> days exhibit high O<sub>3</sub> concentrations because atmospheric reactions proceeded further toward maximum potential O<sub>3</sub> formation.

NMOC/NO<sub>x</sub> ratios were determined for two sites (Milwaukee SER DNR and Northbrook); they exhibit higher average values on weekends, during summer, and to some extent in more recent years. The patterns are qualitatively consistent with the expectation of increasingly NO<sub>x</sub>-limited O<sub>3</sub> formation as NO<sub>x</sub> emissions and ambient NO<sub>x</sub> concentrations decline.

## 4. NO<sub>y</sub> and NO<sub>z</sub> as Ozone Sensitivity Indicators

### 4.1 Background

Four types of indicators are discussed: (1) ratios (O<sub>3</sub>/NO<sub>y</sub> or O<sub>3</sub>/NO<sub>z</sub>), (2) correlations between high time-resolution O<sub>3</sub> and NO<sub>z</sub>, (3) contrasts between weekday and weekend O<sub>3</sub> and NO<sub>x</sub>, and (4) historical O<sub>3</sub> and NO<sub>x</sub> trends.

#### 4.1.1 Indicator Species and Ratios

The ratio O<sub>3</sub>/NO<sub>z</sub> has been studied not only as an indicator of O<sub>3</sub>-NO<sub>x</sub>-VOC sensitivity but also as an indicator of NO<sub>x</sub> lifetime and its relationship to O<sub>3</sub> production. O<sub>3</sub>-NO<sub>x</sub>-VOC sensitivity is related to NO<sub>x</sub> lifetime.

Correlations between O<sub>3</sub> and various oxidized nitrogen species provide evidence for the responsiveness of O<sub>3</sub> to changes in NO<sub>x</sub> emissions (Sillman, 2019). Sillman (1995) identified O<sub>3</sub>/NO<sub>z</sub> < 8 as indicating VOC-responsive peak O<sub>3</sub> in modeling simulations (including simulations for Lake Michigan-area modeling). The transition range was 8 – 9. Simulations used a 35% emission reduction relative to 1980 emissions.

Tonnessen and Dennis (2000b) found O<sub>3</sub>/NO<sub>x</sub> more useful than O<sub>3</sub>/NO<sub>y</sub> than O<sub>3</sub>/NO<sub>z</sub> as an indicator of VOC or NO<sub>x</sub>-limitation (approximated as model response to 15% emission changes). Modeling simulations used 1988 emissions. VOC-limitation was indicated for O<sub>3</sub>/NO<sub>x</sub> < 15.

#### 4.1.2 Correlation of O<sub>3</sub> with NO<sub>y</sub> and NO<sub>z</sub>

Trainer et al. (1993) described the correlation of O<sub>3</sub> with NO<sub>y</sub> in photochemically aged air. They noted that field studies and modeling indicated the existence of linear relationships between O<sub>3</sub> and NO<sub>x</sub> oxidation products (NO<sub>z</sub> = NO<sub>x</sub> - NO<sub>y</sub>) in rural and urban environments, in which the amount of O<sub>3</sub> formed per unit NO<sub>x</sub> was greater in rural environments. This difference is potentially an indicator of VOC and NO<sub>x</sub> sensitivity.

Various modeling and field studies have shown that the rate of photochemical production of O<sub>3</sub> in many locations depends on the rate of oxidation of NO<sub>x</sub> (Trainer et al., 2000). This relationship can be described in terms of the efficiency of O<sub>3</sub> production. Ozone production efficiency (OPE) with respect to NO<sub>x</sub> is the average number of O<sub>3</sub> molecules that are formed from each NO<sub>x</sub> molecule before the NO<sub>x</sub> molecule is irreversibly removed from the atmosphere (Liu et al., 1987; Trainer et al., 2000; Zaveri et al., 2003). In general, as NO<sub>x</sub> emissions are reduced, OPE tends to increase (e.g., Lin et al., 1988; Kleinman, 2000; NARSTO, 2000; Pollack et al., 2013). Below a certain NO<sub>2</sub> or NO<sub>y</sub> concentration the efficiency declines to zero (e.g., Lin et al., 1988; Thornton et al., 2002). The regime where O<sub>3</sub> production decreases is believed to be <1 ppbv NO<sub>2</sub>.

The O<sub>3</sub> response to changes in NO<sub>x</sub> emissions depends on the magnitudes of both the ambient NO<sub>x</sub> change and the change in OPE. An increase in OPE acts counter to a decrease in NO<sub>x</sub>, potentially reducing the effectiveness of the NO<sub>x</sub> emission decline. However, as OPE increases, each subsequent unit reduction of NO<sub>x</sub> can lead to larger O<sub>3</sub> reductions until ambient NO<sub>x</sub> concentrations become too low to sustain O<sub>3</sub> production. Whether ongoing NO<sub>x</sub> emission reductions lead to stronger or weaker O<sub>3</sub> trends becomes an empirical question. Various approaches have been used to study this question.

Empirically, the slope of a linear fit of afternoon  $O_3$  (or  $O_x = O_3 + NO_2$ ) versus  $NO_z$  ( $NO_z =$  sum of  $NO_2$  reaction products) has been used to estimate OPE (e.g., Trainer et al., 1993; Pollack et al., 2013). This estimate, especially for ground-level data, tends to yield an upper bound for OPE because it does not explicitly account for rapid loss of  $HNO_3$  (primarily through dry deposition, but also through gas-to-particle conversion) (Trainer et al., 2000) and regeneration of  $NO_2$  from peroxyacetylnitrates (PAN) and other species. Data from field studies have nonetheless been used since the 1990s to determine upper bounds for OPE and the results have continued to appear in the literature as an indicator of relevance to  $O_3$  chemistry (e.g., Trainer et al., 1995; Zaveri et al., 2003; Berkowitz et al., 2005; Neuman et al., 2009; Kim et al., 2016; Travis et al., 2016). Because field measurements reveal the net of production and loss, they potentially overestimate actual OPE by factors of 3 to 6 due to rapid chemical and deposition losses of  $HNO_3$  and other  $NO_z$  species (e.g., Trainer et al., 2000).

Net OPE (the number of  $O_3$  molecules present in a plume or air parcel for each  $NO_x$  molecule originally emitted) is more readily determined from ambient measurements than is the photochemical OPE (the number of  $O_3$  molecules formed for each  $NO_x$  molecule emitted, which can be calculated in a model simulation) (Trainer et al., 2000). Net OPE is useful for interpreting both trends in  $O_3$  formation and differences between  $O_3$  formation in urban compared with rural areas. Where measurements are inadequate for determining  $NO_z$  or where a correction for the loss of  $O_3$  or  $NO_z$  species to deposition is needed, an alternate approach combines measurements with emission estimates. The slope of the correlation of  $O_3$  with carbon monoxide (CO), multiplied by the ratio of  $NO_x$  to CO emissions, has been used to estimate net OPE (Trainer et al., 2000). Hirsch et al. (1996) applied this approach to measurements made at Harvard Forest, MA.

Ryerson et al. (1998) determined net OPE using both a mass balance approach and a concentration ratio approach in plume transects. A key finding from this study of three power plant plumes was that a nine-fold difference in  $NO_x$  emission rates between the plumes from two facilities led to a three-fold difference in net OPE, i.e., net OPE was  $\sim 1:1 - 2:1$  in the plume with higher  $NO_x$  emissions and  $\sim 3:1 - 7:1$  in the plume with lower  $NO_x$  emissions. Although this study was of short duration (1 day), comparison across locations permitted consideration of the potential effects on  $O_3$  of lowering the higher  $NO_x$  emissions associated with one facility to the lower values of the second plant. In this case, a reasonable interpretation of the one-day study would be that  $O_3$  production would be reduced by lowering  $NO_x$  by a factor of nine but the factor-of-three increase in net OPE resulted in a factor-of-three upper bound on  $O_3$  reduction (the actual reduction would be less than three-fold due to the presence of unmanageable background  $O_3$ ).

Ninneman et al. (2017) reported consistently high observed OPE for measurements made at a rural site (Pinnacle State Park) in New York State during the summer (June – September) of 2016: the observed OPE ranged from  $\sim 10$  at mean  $NO_x$  mixing ratios of  $\sim 0.3 - 0.4$  ppbv and increased  $10 - 14:1$  to  $17:1$  at mean  $NO_x$  mixing ratios of  $\sim 0.1 - 0.3$  ppbv. Observed OPE did not exhibit a maximum at intermediate  $NO_x$  mixing ratios. In comparison, model-predicted OPE

ranged from ~5:1 to 11:1, possibly lower than the observed OPE because the model predicted higher ambient NO<sub>x</sub> mixing ratios than were observed (Ninneman et al., 2017).

Blanchard et al. (2018) reported increases over time in the slopes of regressions relating O<sub>3</sub> to NO<sub>z</sub> in various locations in the Southeast between 1992 and 2014. The observed relationships of O<sub>3</sub> to NO<sub>z</sub> supported past model predictions of increases in cycling of NO and increasing responsiveness of O<sub>3</sub> to NO<sub>x</sub> (Blanchard et al., 2018). Increasing rates of O<sub>3</sub> reduction during the second half of the study period suggested increasing effectiveness of NO<sub>x</sub> emission controls. Blanchard et al. (2018) concluded that long-term documentation and analysis of trends in O<sub>3</sub> mixing ratios in relation to NO<sub>x</sub> emission reductions and decreases in ambient reactive nitrogen concentrations yields opportunities for obtaining insights about ambient O<sub>3</sub> reductions that complement and corroborate air quality modeling predictions.

Few data sets can support a meaningful analysis of net OPE. Ground-level and aircraft data from short-term field campaigns have been used (e.g., Frost et al., 1998; Ryerson et al., 1998; Trainer et al., 1995; Zaveri et al., 2003; Berkowitz et al., 2005; Neuman et al., 2009; Kim et al., 2016; Travis et al., 2016). Previous studies have also utilized specialized long-term ground-level research data from Los Angeles (Pollack et al., 2013), Pinnacle State Park in New York State (Ninneman et al., 2017), and the Southeastern Aerosol Research and Characterization (SEARCH) study (Blanchard et al., 2018).

#### **4.1.3 The Weekend Effect**

Weekends potentially provide an opportunity to examine how O<sub>3</sub> and other secondary species respond to large reductions in precursor emissions that occur on weekends relative to weekdays. In some U.S. metropolitan areas, peak O<sub>3</sub> concentrations are as high, or higher, on weekends than on weekdays, despite large weekend reductions in the ambient concentrations of O<sub>3</sub> precursors.

Originally observed in air quality data from the mid-1960s and early 1970s, the weekend effect in California has been studied at length. Fujita et al. (2003) and Lawson (2003) concluded that weekend reductions of NO emissions are the most important factor leading to higher weekend ozone, allowing O<sub>3</sub> to accumulate earlier in the day and to reach higher concentrations compared with weekdays, and further concluded that proposed alternative hypotheses are not supported by ambient data and do not explain the weekend effect in southern California. In contrast, Croes et al. (2003) considered the available air quality data and photochemical models inadequate to conclusively determine the causes of the weekend ozone effect in southern California due to the lack of air quality data aloft and the complex spatial, temporal, and source contribution changes that occur in emissions during the transition from weekday to weekend. The regulatory relevance of the O<sub>3</sub> weekend effect has also been questioned because the magnitude of the weekend effect is different for high-O<sub>3</sub> days that exceed national ambient air quality standards than for other ozone-season days (Croes et al., 2003).

Marr and Harley (2002a; 2002b) show that weekend reductions of diesel truck traffic volumes cause lower weekend emissions of NO<sub>x</sub> relative to VOC emissions compared with weekdays. Pollack et al. (2012) showed that weekends exhibited more extensive photochemical processing

and higher OPE compared to weekdays during a special study in southern California in May and June of 2010.

During the 2017 LMOS, NO<sub>2</sub> column values were larger on weekdays than on weekends at Schiller Park, Zion, and Milwaukee, but exhibited little day-of-week variation at Grafton and Sheboygan (Abdioskouei et al., 2019). Many shoreline areas are tourist destinations and some are influenced by base-load power plants, suggesting that day-of-week emission profiles in shoreline areas may differ from those in urban areas (Abdioskouei et al., 2019). Analyses by WI DNR staff also show that day-of-week variations in ground-level NO<sub>x</sub> concentrations are less pronounced at Manitowoc than at Milwaukee SER DNR (WI DNR, 2017). At both locations, the amplitude of the day-of-week NO<sub>x</sub> variations diminished between 2000 – 05 and 2011 – 16. During the same periods, the amplitudes of day-of-week variations in 95<sup>th</sup>-percentile O<sub>3</sub> also decreased at all WI shoreline sites and at Cook County, IL monitors. However, weekend O<sub>3</sub> concentrations tend to be higher than on weekdays even in recent years, despite lower ambient NO<sub>x</sub> concentrations at many locations.

One measure of the significance of the weekend effect is the number of high O<sub>3</sub> days occurring on Fridays, Saturdays, or Sundays (Table 3). If the four highest O<sub>3</sub> days were evenly distributed across days of the week, each site would exhibit 1.7 combined Friday, Saturday, and Sunday 1<sup>st</sup> through 4<sup>th</sup> MDA8 O<sub>3</sub> days each year ( $3/7 \times 4$ ), or 8.6 combined Fridays, Saturdays, and Sundays over five years. All sites exhibited a disproportionately high number (10 – 12) of 1<sup>st</sup> through 4<sup>th</sup> highest O<sub>3</sub> days occurring on Fridays, Saturdays, and Sundays), despite lower weekend NO<sub>x</sub> concentrations in upwind urban areas. In 2019, fewer 1<sup>st</sup> through 4<sup>th</sup> highest O<sub>3</sub> days occurred on Fridays, Saturdays, and Sundays than during any of the preceding years (1 day at 5 of the 6 sites). In 2019, annual 4<sup>th</sup> highest MDA8 O<sub>3</sub> were distinctly lower (66 – 68 ppbv at each of the selected sites, except 59 ppbv at Sheboygan Haven) than in previous years.

Table 3. Number of occurrences of annual 1<sup>st</sup> through 4<sup>th</sup> highest MDA8 O<sub>3</sub> on Fridays, Saturdays, or Sundays at selected WI shoreline sites, by year.

<b>Site</b>	<b>2015</b>	<b>2016</b>	<b>2017</b>	<b>2018</b>	<b>2019</b>	<b>Sum</b>
Manitowoc	3	1	3	4	1	12
Sheboygan Haven	1	3	3	3	2	12
Sheboygan Kohler	3	1	3	4	1	12
Harrington Beach	2	2	3	4	1	12
Grafton	2	3	3	3	1	12
Chiwaukee Prairie	2	1	2	4	1	10

#### 4.1.4 Observed O<sub>3</sub> Response

The historical monitoring record provides opportunities for examining the observed response of O<sub>3</sub> to emission reductions. Unlike weekday/weekend comparisons, long-term trends are directly relevant to actual emission rules and provide possible insight into their effectiveness. Unlike modeling, the accuracy of the model is not in question. However, distinguishing effects of emission rules and emission reductions from other perturbations, such as meteorological variations, is challenging. Coupled with other approaches, trend analyses offer the possibility of identifying actual O<sub>3</sub> responses, plausibly attributing them to emission changes, and drawing conclusions of relevance to air quality management. From analyses of 50 years of data from southern California, Pollack et al. (2013) demonstrated that faster rates of decrease in VOC than NO<sub>x</sub> emissions resulted in lower VOC/NO<sub>x</sub> ratios and reductions in concentrations of O<sub>3</sub> and other secondary species concentrations. Blanchard and Hidy (2018) and Blanchard et al. (2013) discuss O<sub>3</sub> responses to emission reductions in the southeastern U.S. based on long-term trends. Blanchard et al. (2019) discuss emission influences on trends in air pollutant concentrations in New York State.

The generalized additive model (GAM, Section 5) is a tool for separating meteorological and emission effects.

#### 4.2 Site Selection

The sites with measurements of NO<sub>x/y</sub> are (1) Manitowoc, (2) Horicon/Mayville, (3) Milwaukee DNR SER, (4) Zion, IL, and (5) Northbrook, IL (Tables 1 and A1). Measurement biases are an important consideration at each site (Section 9.3.1).

#### 4.3 Methods

Mid-day (11 a.m. – 2 p.m.) and daily average ratios of O<sub>3</sub>/NO<sub>x</sub>, O<sub>3</sub>/NO<sub>y</sub>, and O<sub>3</sub>/NO<sub>z</sub> were computed and compared using data from Milwaukee SER DNR (Section 9.3.3) The mid-day ratios are more consistent than daily averages with the theoretical rationale that supports using them as indicators of VOC or NO<sub>x</sub> sensitivity.

Day-specific slopes of hourly O<sub>3</sub> vs. NO<sub>z</sub> regressions were computed but were not robust indicators of O<sub>3</sub> sensitivity (Section 9.4.3). New species-specific NO<sub>2</sub> measurements made at Milwaukee SER DNR and Manitowoc beginning June 1, 2019 may provide more robust results (Section 9.3.1).

#### 4.4 Results

The data suggest a transition range of 7 – 12 for O<sub>3</sub>/NO<sub>y</sub> and 9 – 14 for O<sub>3</sub>/NO<sub>x</sub> at Milwaukee but higher (~10 – 14 for O<sub>3</sub>/NO<sub>y</sub> and 12 – 16 for O<sub>3</sub>/NO<sub>x</sub>), and more variable, at Manitowoc (Section 9.3.3). If transition ranges are site-specific, the universality and applicability of O<sub>3</sub>/NO<sub>y</sub> as an indicator are unclear. The observed ranges are approximately consistent with published transition ranges of 8 – 9 for O<sub>3</sub>/NO<sub>y</sub> (Sillman, 1995) and ~15 for O<sub>3</sub>/NO<sub>x</sub> (Tonnessen and Dennis, 2000b). Since measured NO<sub>x</sub> is biased high, observed O<sub>3</sub>/NO<sub>x</sub> ratios are lower than they would be for unbiased measurements.

Mid-day ratios of  $O_3/NO_y$  are approximately one order of magnitude lower than corresponding ratios of  $O_3/NO_z$  (Section 9.3.3). Since  $NO_z$  is biased low, ratios of  $O_3/NO_y$  may be more reliable than ratios of  $O_3/NO_z$ . The same measurement issue (high bias in  $NO_2$  and  $NO_x$ ) yields similar ratios of  $O_3/NO_y$  and  $O_3/NO_x$ , especially for MDA8  $O_3$  exceeding 60 ppbv. In contrast, mid-day ratios of  $O_3/NO_y$  show little relation to ratios of  $HCHO/NO_2$  (Section 9.3.3). The lack of correlation indicates that different results would be obtained from these two indicator ratios even if their sensitivity ranges for  $O_3/NO_y$  were known exactly (i.e., fully corrected for observed differences from literature values).

Statistical distributions of Milwaukee SER DNR mid-day  $O_3/NO_y$  are shown in Figure 10. Nearly half of weekend mid-day  $O_3/NO_y$  values exceed 10, whereas over 75% of weekday mid-day  $O_3/NO_y$  values are less than 10. If the transition into  $NO_x$ -limitation occurs at Milwaukee at ratios exceeding ~12, then MDA8  $O_3$  is  $NO_x$ -sensitive more often when  $NO_x$  levels are lower, as they are on weekends. These statistics are roughly reversed for VOC sensitivity: nearly half of weekday mid-day  $O_3/NO_y$  values are less than 7, whereas less than 25% of weekend mid-day  $O_3/NO_y$  values are less than 7. A clear progression over time occurred: fewer than 10% of the mid-day  $O_3/NO_y$  values exceeded 10 in 2004, whereas nearly half did by 2019. As  $NO_x$  emissions and ambient concentrations declined, therefore, the frequency of  $NO_x$ -sensitive MDA8  $O_3$  increased.

Statistical distributions of Manitowoc mid-day  $O_3/NO_y$  are shown in Figure 11. Values of  $O_3/NO_y$  are distinctly higher than at Milwaukee SER DNR, reflecting differences in  $NO_y$  concentrations (midday  $NO_y$  means = 7.3 ppbv at Milwaukee SER DNR and 2.4 ppbv at Manitowoc). For Manitowoc, 75 – 90% of the midday  $O_3/NO_y$  ratios exceeded 10, varying by day of week, month, and year (Figure 11). It is plausible that Manitowoc  $O_3$  is more frequently  $NO_x$ -limited than Milwaukee  $O_3$ ; however, the transition ranges at Manitowoc appear to be higher than at Milwaukee SER DNR (Section 9.3.3).

Overall, the percentages of high- $O_3$  (>50 ppbv) days at Milwaukee SER DNR with low (<7), transitional (7 – 12), and high ( $\geq 12$ ) mid-day  $O_3/NO_y$  ratios were 41, 40, and 19%, respectively (380 days, 2004 – 2019). For 2015 – 2019 (113 days), the corresponding percentages were 22, 47, and 31%, respectively.

For Manitowoc, the percentages of high- $O_3$  (>50 ppbv) days with low (<9), transitional (9 – 14), and high ( $\geq 14$ ) mid-day  $O_3/NO_y$  ratios were 13, 24, and 63%, respectively (393 days, 2004 – 2019). For 2015 – 2019 (93 days), the corresponding percentages were 10, 11, and 79%, respectively.

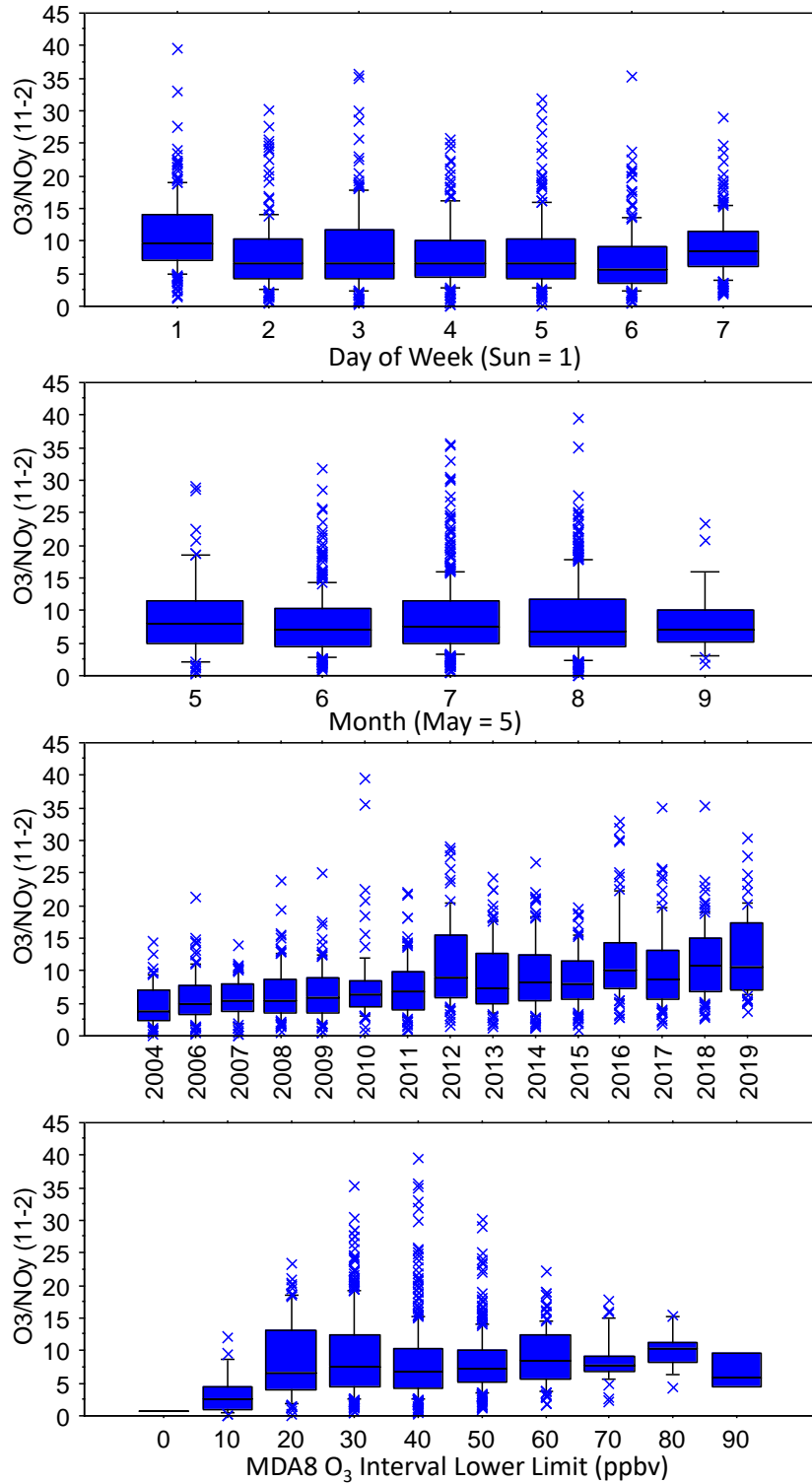


Figure 10. Statistical distributions (10<sup>th</sup>, 25<sup>th</sup>, 50<sup>th</sup>, 75<sup>th</sup>, 90<sup>th</sup> percentiles) of mid-day  $O_3/NO_y$  versus day of week, month, year, and MDA8  $O_3$  at Milwaukee SER DNR. Data are restricted to observations with  $NO_y > 1$  ppbv (N = 1222 of 1266 observations). The data suggest that VOC-sensitive, transitional, and  $NO_x$ -sensitive  $O_3/NO_y$  ranges are  $<7$ ,  $7 - 12$ , and  $\geq 12$ , respectively.

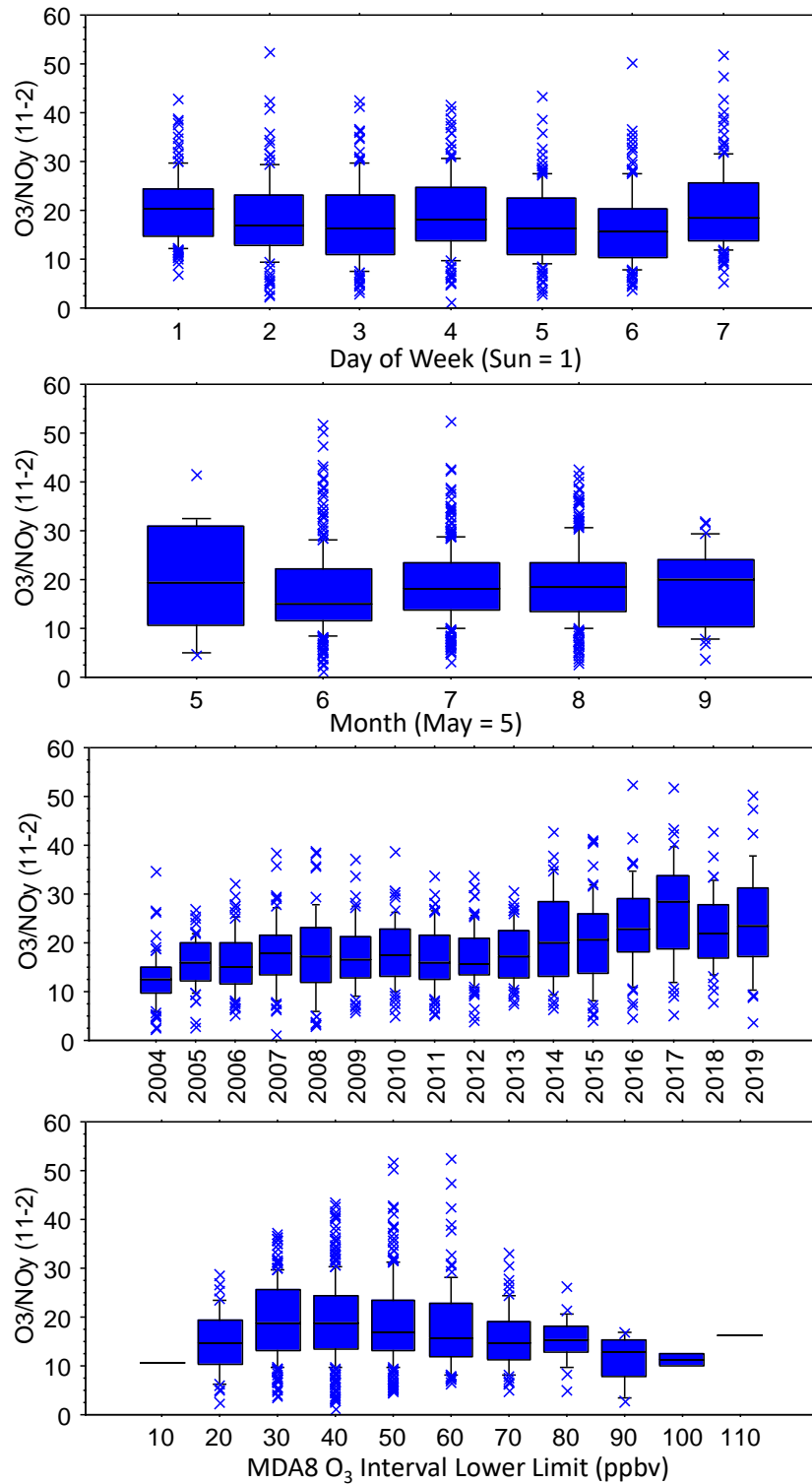


Figure 11. Statistical distributions (10<sup>th</sup>, 25<sup>th</sup>, 50<sup>th</sup>, 75<sup>th</sup>, 90<sup>th</sup> percentiles) of mid-day O<sub>3</sub>/NO<sub>y</sub> versus day of week, month, year, and MDA8 O<sub>3</sub> at Manitowoc. Data are restricted to observations with NO<sub>y</sub> > 1 ppbv (N = 902 of 1239 observations). The data suggest that VOC-sensitive, transitional, and NO<sub>x</sub>-sensitive O<sub>3</sub>/NO<sub>y</sub> ranges are <10, 10 – 14, and ≥14, respectively.

#### 4.5 Section Summary

Day-specific slopes of hourly  $O_3$  vs.  $NO_z$  regressions were computed but were not robust indicators of  $O_3$  sensitivity due to measurement biases (non-specific  $NO_2$ , Section 9.4.3). New species-specific  $NO_2$  measurements made at Milwaukee SER DNR and Manitowoc beginning June 1, 2019 may provide more robust results.

The universality and applicability of  $O_3/NO_y$  as an indicator are unclear because the transition ranges appear to be site-specific. The data suggest a transition range of 7 – 12 for  $O_3/NO_y$  and 9 – 14 for  $O_3/NO_x$  at Milwaukee but higher (~10 – 14 for  $O_3/NO_y$  and 12 – 16 for  $O_3/NO_x$ ), and more variable, at Manitowoc (Section 9.3.3). The observed ranges are approximately consistent with published transition ranges of 8 – 9 for  $O_3/NO_y$  (Sillman, 1995) and ~15 for  $O_3/NO_x$  (Tonnessen and Dennis, 2000b).

Mid-day (11 a.m. – 2 p.m.) ratios of  $O_3/NO_y$  show little relation to ratios of  $HCHO/NO_2$  (Section 9.3.3). This lack of correlation indicates that different results would be obtained from these two indicator ratios for individual days even if the sensitivity ranges for  $O_3/NO_y$  could be fully corrected for observed differences from literature values.

Overall, the percentages of high- $O_3$  (>50 ppbv) days at Milwaukee SER DNR with low (<7), transitional (7 – 12), and high ( $\geq 12$ ) mid-day  $O_3/NO_y$  ratios were 41, 40, and 19%, respectively (380 days, 2004 – 2019). For 2015 – 2019 (113 days), the corresponding percentages were 22, 47, and 31%, respectively.

For Manitowoc, the percentages of high- $O_3$  (>50 ppbv) days with low (<9), transitional (9 – 14), and high ( $\geq 14$ ) mid-day  $O_3/NO_y$  ratios were 13, 24, and 63%, respectively (393 days, 2004 – 2019). For 2015 – 2019 (93 days), the corresponding percentages were 10, 11, and 79%, respectively.

## 5. Generalized Additive Model (GAM)

### 5.1 Background

Camalier et al., 2007 developed a generalized additive model (GAM) that is used by EPA for determining O<sub>3</sub> trends adjusted for variations in weather (U.S. EPA, 2020h). This method is cited by EPA (2018) for use as part of weight-of-evidence (WoE) analysis for O<sub>3</sub> attainment demonstrations. Accounting for year-to-year variations in meteorological conditions reveals a downward trend in mean May – September daily peak 8-hour O<sub>3</sub> in the east-north-central region of the U.S. and at individual monitoring sites in the Lake Michigan area between 2000 and 2010 (Figure 12, U.S. EPA, 2020h). This model also indicates that meteorologically-adjusted May – September average MDA8 changed minimally between 2010 and 2019; the observed decline between 2018 and 2019 is attributed to weather.

Gong et al. (2017) used a GAM to quantify the influence of wildfires on O<sub>3</sub> in cities in the western U.S. Gong et al. (2018) applied a GAM to identify the influence of meteorological factors on O<sub>3</sub> in 16 cities in China. Jaffe (2020) adapted and applied the Gong et al. (2017, 2018) GAM to the Los Angeles area to study the influences of weather, emissions, and smoke.

In this report, we develop and extend the EPA GAM to describe the relative influences of weather, VOCs, and NO<sub>x</sub> on O<sub>3</sub> in the southern Lake Michigan area. We summarize the EPA GAM in this section. Site selection and input data are discussed in Sections 5.2 and 5.3, respectively, model development is described in Section 5.4, and the computer program is provided in Section 9.4.

The EPA GAM uses natural splines (Hastie and Tibshirani, 1990) to model nonlinear dependence of O<sub>3</sub> on predictor variables. Trends need not be linear or monotonic. Camalier et al. (2007) discuss model accuracy. An advantage of the GAM is that it distinguishes the observed sensitivities of O<sub>3</sub> to different weather variables. Camalier et al. (2007) use the GAM to predict area (e.g., air basin, statistical area, etc.) maximum (across all monitoring sites) peak daily 8-hour O<sub>3</sub> over a long time period (> 10 years) for many areas nationwide.

Camalier et al. (2007) found that the most consistently significant predictors of peak daily 8-hour O<sub>3</sub> in the 39 eastern U.S. metropolitan areas studied were: (1) daily maximum surface temperature (T), (2) mid-day (10 a.m. to 4 p.m.) relative humidity (RH), (3) morning (7 a.m. to 10 a.m.) average wind speed (WS), (4) afternoon (1 p.m. to 4 p.m.) average wind speed, (5) morning (~1200 UTC) difference between 925 mb T and surface T, (6) deviation of morning (~1200 UTC) 850 mb T from 10-year monthly average, (7) air mass transport direction and distance (determined from back trajectories), (8) occurrence of rain (as number of hours), (9) julian day, (10) day of week, and (11) year. Blanchard et al. (2014; 2019) added sea-level pressure gradients and solar radiation as predictors. Blanchard et al. (2019) supplemented monitoring site data with upper-air (radiosonde) measurements from Albany, NY, and substituted 850 mb T for 925 mb T in computing the difference between 1200 UTC (7 a.m. EST) upper-air T and surface T. Whereas Camalier et al. (2007) and Blanchard et al. (2014) used HYSPLIT back trajectories, Blanchard et al (2019) used the 850 mb WS and wind direction (WD) as indicators of transport distance and direction.

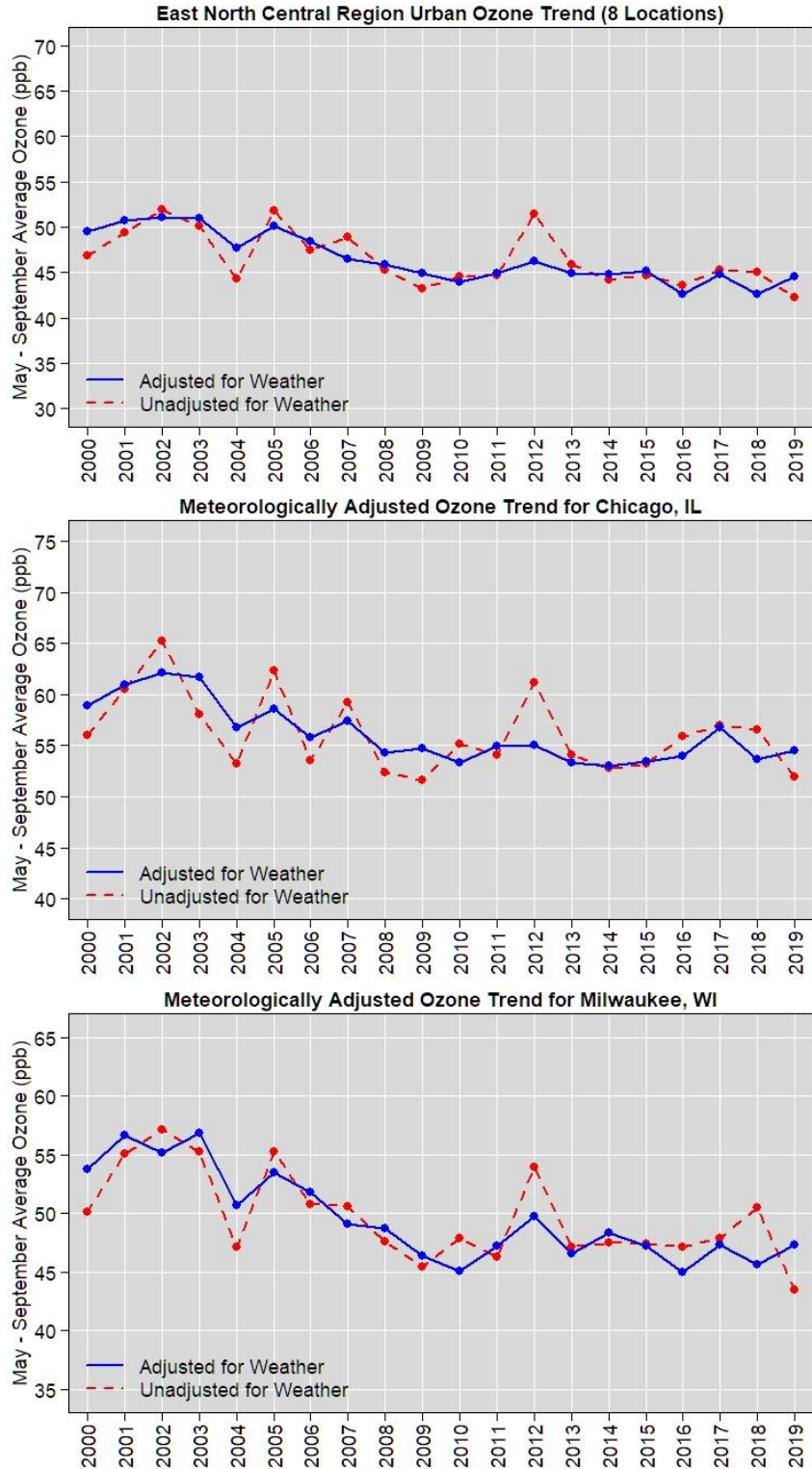


Figure 12. Composite trends in mean May – September daily peak 8-hour O<sub>3</sub> at (top) eight locations in Michigan, Wisconsin, Minnesota, and Iowa, (middle) in Chicago, and (bottom) in Milwaukee, with and without adjusting for year-to-year variations in weather. Source: U.S. EPA 2020h.

The GAM is expressed as:

$$l(O_3)_i = \mu + f_1(x_1)_i + \dots + f_m(x_m)_i + g_1(y_1)_i + \dots + g_n(y_n)_i + h_1(z_1) + \dots + h_p(z_p) + e_i \quad (1)$$

Following Camalier et al. (2007),  $l(O_3)_i$  is the logarithm of the peak 8-hour  $O_3$  on day “i” but either a different  $O_3$  metric or a function other than the logarithm could be used. The terms  $f_1(x_1)_i$  through  $f_m(x_m)_i$  parameterize the associations of meteorological variables on peak 8-hour  $O_3$ , and  $g_1(y_1)_i$  through  $g_n(y_n)_i$  parameterize associations of ambient concentrations of  $O_3$  precursors on  $O_3$ . For consistency with  $l(O_3)_i$ , the variables  $y_1$  through  $y_n$  are logarithms of air quality measurements. The terms  $h_1(z_1)$  through  $h_p(z_p)$  represent temporal variables, including “day of week” and “year”. The last term,  $e_i$ , is the difference between observed and predicted  $O_3$  (error). Each term parameterizes the response of daily peak 8-hour  $O_3$  as a deviation from the long-term mean, “ $\mu$ ” (logarithm of peak 8-hour  $O_3$  averaged over all days). Since  $\mu$  is the observed long-term average  $O_3$ , its value is independent of the choice of parameters in the model. “Day of week” and “year” are categorical variables and are used to represent weekly cycles and trend, respectively.

Camalier et al. (2007) demonstrated that their GAM could show empirical sensitivities of  $O_3$  to meteorological variables. Blanchard et al. (2012; 2014; 2019) adapted the EPA model to relate daily peak 8-hour  $O_3$  to weather and to ambient concentrations of  $O_3$  precursors ( $NO$  and  $NO_2$ ) and to  $NO_x$  reaction products ( $NO_z$ , determined here as  $NO_y - NO_x$ ). Blanchard et al. (2014) applied the model to data from the SEARCH network to show that daily peak 8-hour  $O_3$  increased as morning  $NO_2$  and afternoon  $NO_z$  concentrations increased but decreased as daily maximum  $NO$  increased. The results indicate that the model was able to delineate empirical sensitivities of  $O_3$  to different components of  $NO_y$ , while also accounting for day-to-day variations in weather. Blanchard et al. (2019) used the GAM to identify empirical sensitivities of daily peak  $O_3$ , separating the contributions of meteorological and precursor changes to observed trends in daily peak  $O_3$ .

## 5.2 Site Selection

Twenty sites were selected, focusing on WI shoreline locations with additional IL and MI sites (Table 1). The WI sites are Newport Park, Manitowoc, Sheboygan Kohler Andrae, Sheboygan Haven, Harrington Beach, Grafton, Horicon/Mayville, Bayside, Milwaukee DNR SER, Lake Geneva, Kenosha, and Chiwaukee Prairie (Figure 3). IL sites are Northbrook, Evanston, Schiller Park, Jardine, and South Water Filtration Plant (Chicago). MI sites are Coloma, Holland, and Muskegon.

## 5.3 Input Data

Input data sets were developed for each of the 20 locations. In each case, the dependent variable was the site MDA8  $O_3$ . For most sites, EPA reported MDA8  $O_3$  for days during the  $O_3$  season (mid-April to mid-October). Some sites (e.g., Horicon/Mayville) reported MDA8  $O_3$  for all days of the year. The starting time of each MDA8  $O_3$  was included as a predictor variable.

Annual-average multistate (IL, IN, WI) emissions of VOCs and  $NO_x$  were used as inputs to account for long-term emission trends (Section 9.4.1). In addition, multisite daily-average

concentrations of CO, NO<sub>x</sub>, and SO<sub>2</sub> (primarily sites in Chicago and Milwaukee) were used to represent day-to-day variations of O<sub>3</sub> precursors in the urban upwind area (Section 9.4.1). Because daily NMOC measurements were not available, CO data were substituted for the purpose of representing mobile-source VOC emissions (Sections 9.2, 9.4.1, and 9.4.4). Site-specific precursor concentrations were not used as inputs because (1) few sites had measurements of both O<sub>3</sub> and precursors (Table A1) and (2) missing data were common.

Upper-air measurements were acquired from NOAA (<https://ruc.noaa.gov/raobs/>) for seven sites: Minneapolis MN, Davenport IO, Lincoln IL, Wilmington OH, Green Bay WI, Gaylord MI, and Detroit (Pontiac) MI (Figure 3). Multisite averages and pressure gradients were determined using data from the four sites that most closely surrounded southern Lake Michigan: Lincoln IL, Green Bay WI, Gaylord MI, and Detroit (Pontiac) MI. Section 9.4.3 describes these data. Soundings are made twice each day, at midnight and noon universal coordinated time (UTC). The noon sounding was used because it represents the beginning of each day (i.e., 6 a.m. CST, 7 a.m. EST). The radiosonde sites also provided surface-level barometric pressure (BP).

Surface weather observations were obtained for airport locations (Green Bay, Milwaukee, and Chicago) (Figure 3). These data included daily maximum temperature (T<sub>max</sub>), precipitation, daily-average wind speed (WS), and the direction of the fastest 2-min wind gust (Section 9.4.2). The airport data were complete (no missing values).

Surface weather measurements were also obtained for air-quality monitoring sites (Table A1). These data were typically incomplete. They were used to develop location-specific measures of daily-average and hourly WS and wind direction (WD).

Surface measurements from air-quality monitoring sites were also used to generate five multisite time series of average daily relative humidity (RH). Of the WI sites, only Horicon data were found in the EPA RH data sets. Although Horicon is an inland site, Horicon RH data were used to ensure representation from a WI site. Some differences were apparent between sites whose data were combined (e.g., between Zion and Horicon), but the daily average RH measurements were correlated among all sites ( $r^2 = 0.5 - 0.9$ , varying with distance). The combinations of site measurements were: (1) Zion (2000 – 2009) and Horicon (2010 – 2019), N = 5961 days combined, (2) Zion (2000 – 2009) and Northbrook (2010 – 2019), N = 5055 days combined, (3) Jardine (2000 – 2010) and Northbrook (2010 – 2019), N = 5620 days combined, (4) Gary (2000 – 2019), N = 7179 days, and Hammond (2008 – 2019), N = 4007 days, and (5) Holland MI (2000 – 2016) and Grand Rapids MI (2017 – 2019), N = 7087 days combined. To make each RH series complete (N = 7305 days), missing values were replaced with measurements from the closest location, followed by the second and third nearest locations if necessary. The multisite RH values were complete, whereas RH data were incomplete for all individual sites.

Solar radiation measurements were obtained from EPA for WI sites. The data record began in 2001 and the data were not complete. They were supplemented with measurements and modeled values from NREL (<https://www.nrel.gov/docs/fy12osti/54824.pdf>). The NREL solar radiation model uses solar zenith, length of day, and airport measurements of visibility and cloud cover to predict daily average and maximum solar radiation.

Lake Michigan surface water temperatures were obtained from NOAA (<https://coastwatch.glerl.noaa.gov/statistic/>). NOAA prepared this data series using data from multiple locations around the lake.

## **5.4 Model Development and Testing**

### **5.4.1 Model Fitting**

Models were fit using all available days of data, 2000 – 2019, for each site. Additional model fits were developed for selected test sites (e.g., Sheboygan Kohler Andrae) using only the 30 highest MDA8 O<sub>3</sub> each year (Top 30). For selected sites, model fits were examined for both log-transformed O<sub>3</sub> and untransformed concentrations. Because the distributions of the MDA8 O<sub>3</sub> were more nearly log-normal than normal, and because the model fits were not very sensitive to the variable transformation, reported results are based on the fits for log-transformed O<sub>3</sub>. The results were transformed back to concentration units for presentation.

Many of the candidate input variables were highly correlated (e.g.,  $r^2 \sim 0.8$ ). Predictor variables that are highly correlated typically have unstable coefficients, i.e., removing one of two correlated variables changes the coefficients of the other. Both the correlations among predictor variables and the stability of model coefficients were examined. In general, only one predictor variable from among a group of correlated predictors was retained. For example, Milwaukee daily maximum temperature correlated highly with the multisite 7 a.m. CST (UTC 1200) 850 and 500 mb temperatures ( $r^2 = 0.88$  and  $0.76$ , respectively), so only the maximum surface temperature was retained.

A stepwise approach was followed to account for the most important predictor variables and to obtain a more parsimonious model by further removing variables that were not statistically significant at most sites (using the criterion  $p < 0.05$ ). The removed variables included multisite mean SO<sub>2</sub> concentration, the hour of the maximum solar radiation, the hour of maximum local relative humidity (RH), and 500 and 850 mb RH.

Because daily NMOC measurements were not available, CO data were included for the purpose of representing mobile-source VOC emissions (Sections 9.2, 9.4.1, and 9.4.4). Isoprene, like other total NMOC and other NMOC species, was measured on samples collected once every six days. This sampling frequency limits the utility of isoprene as an input variable, though it was tested. Testing was carried out (1) for days with isoprene measurements, and (2) for all days by interpolating isoprene concentrations. Neither actual nor interpolated isoprene concentrations were statistically significant in the GAM. Since the GAM included a suite of variables (day of year, Tmax, wind speed and direction) that account for much of the variability in isoprene concentrations (Section 9.4.4), the isoprene concentrations may have been statistically redundant even if isoprene itself is a source of VOC reactivity (Section 9.4.7).

### **5.4.2 Performance Evaluation**

Multiple methods and metrics were used to evaluate the quality of the model fits. Graphs were prepared to show predicted and observed MDA8 O<sub>3</sub>. Scatter plots and time series graphs were examined. Graphs of residuals (predicted minus observed) versus various predictor and non-

predictor variables were examined to reveal biases and to identify possible relationships to predictors that had not been included in the model.

Performance statistics were compiled for fit ( $R^2$ ), percent of model predictions correctly above or below an MDA8 O<sub>3</sub> threshold of 70 ppbv (PC, percent correct), false alarm rate (FAR = incorrect predictions > threshold divided by total predictions > threshold), probability of detection (PoD = correct predictions > threshold divided by total observations > threshold), and consolidated success index (which combines FAR and PoD). The Akaike information criterion (AIC) was also determined. AIC is a relative score that is useful for comparing models (it increases with the number of parameters and decreases with improved fit).

Root-mean square error (RMSE) was computed for each site's full model and for reduced models (dropping each term while keeping all others).

Table 4 summarizes model performance for each of the 20 sites. RMSE ranged from 6 to 8 ppbv, tending to be proportional to concentration. RMSE errors were generally highest during earlier years (2000 – 2004) and lowest during recent years (2015 – 2019). For Sheboygan Kohler Andrae, for example, the 2000 – 2004 RMSE was 9.5 ppbv, the 2015 – 2019 RMSE was 7.4 ppbv, and the overall RMSE was 8.1 ppbv.

The RMSE that results from dropping each individual model term (dropterm RMSE), while retaining all others, provides one measure of the relative importance of each predictor variable. Two predictors with consistently high dropterm RMSE values are the daily maximum temperature (Tmax) and the starting hour of the MDA8 O<sub>3</sub>. Surface RH also is an important predictor. The modeled relationships between MDA8 O<sub>3</sub> and each of these and other variables are discussed in Section 5.5. Some terms were often not statistically significant (e.g., 500 mb WD, significant at 6 of 20 sites). Such variables exercise little influence on the model fits. Selected graphs are shown in Section 9.5.

The correlations between observed and predicted MDA8 O<sub>3</sub> ( $R^2$ ) are ~0.7 (0.64 – 0.78). Scatterplots indicate reasonable fits across a range of O<sub>3</sub> concentrations (Figure 13). Time-series graphs demonstrate model skill in predicting day-to-day variations (Figure 14). As non-significant or redundant predictor variables were removed in fitting the model,  $R^2$  values tended to decrease by small amounts (0.01 – 0.02 units) while other metrics, including RMSE and percent correct, frequently improved. Maximizing  $R^2$  is known to lead to overfitting and the final models are reasonably parsimonious. Because sample sizes were large (1203 – 6405 days), the models have ample degrees of freedom despite using 23 predictor variables (with additional parameter estimates required by the natural splines). The GAM tended to underpredict some of the very highest MDA8 O<sub>3</sub>, most of which occurred between 2000 and 2004. Although the probability of correctly predicting exceedances of 70 ppbv exceeded 50% for only one location (Sheboygan Kohler Andrae), the probability of detection was affected by the low number of observed MDA8 O<sub>3</sub> values exceeding 70 ppbv (Figure 14). The GAM typically predicted observed values of 60 – 80 ppbv within the RMSE (e.g., Figure 13). Mean bias was small (-0.03 – 0.06 ppbv).

Table 4. GAM performance summary (continued on following pages). Dropterm RMSE results from dropping each individual model term while retaining all others, which provides one measure of the relative importance of each predictor variable. Asterisk (\*) denotes a variable that was not statistically significant at  $p < 0.05$ . Percent correct, false alarm rate, and probability of detection are relative to a threshold value of 70 ppbv.

<b>Metric</b>	<b>Newport Park</b>	<b>Manitowoc</b>	<b>Sheboygan Haven</b>	<b>Kohler Andrae</b>	<b>Horicon</b>
Period	2000-19	2000-19	2014-19	2000-19	2000-19
N Days	3559	3607	1203	3559	6581
R <sup>2</sup>	0.695	0.695	0.694	0.725	0.716
Bias (ppbv)	-0.033	-0.019	0.004	-0.031	0.000
Akaike information criterion	25070	25320	7957	25130	43658
Percent correct (70 ppbv criterion)	96.85	96.81	99.00	95.62	98.57
False alarm rate (70 ppbv)	23.36	24.75	25.00	20.63	25.93
Probability of detection (70 ppbv)	48.52	45.78	21.43	56.12	18.69
Consolidated success index	42.27	39.79	20.00	49.02	17.54
RMSE (ppbv)	8.00	7.90	6.16	8.06	6.59
Tmax Milwaukee	8.37	8.32	6.40	8.62	6.87
Tmin Milwaukee	8.01	7.92	6.19	8.08	6.60
Lake Michigan surface T	8.01	7.92	6.17	8.07*	6.67
RH (local and near-local)	8.03	7.96	6.28	8.14	6.72
SR max Milwaukee	8.04	8.04	6.30	8.21	6.73
BP (mean 4 sonde sites)	8.04	7.94	6.17	8.11	6.60
WS (local daily)	8.06	7.96	6.16*	8.09	6.59*
WD (local daily)	8.06	7.94	6.19	8.09	6.63
WD midday (nearest site)	8.08	7.97	6.25	8.14	6.59
850 mb WD (mean 4 sites)	8.06	7.94	6.21	8.12	6.59
500 mb WD (mean 4 sites)	8.01	7.91*	6.17*	8.07	6.59*
850 mb WS (mean 4 sites)	8.02	7.92	6.17	8.08	6.60
500 mb WS (mean 4 sites)	8.14	8.01	6.25	8.16	6.67
850 mb height (mean 4 sites)	8.03	7.94	6.23	8.10	6.61
500 mb height (mean 4 sites)	8.00*	7.91	6.17	8.07*	6.60
Pressure Green Bay - Lincoln	8.02	7.92	6.18	8.11	6.60
Pressure Green Bay - Detroit	8.08	7.95	6.18	8.12	6.60
Day of year	8.09	7.96	6.21	8.13	6.78
MDA8 O <sub>3</sub> start hour	8.43	8.27	6.40	8.47	6.73
Day of week	8.04	7.95	6.18	8.13	6.61
VOC + NO <sub>x</sub> emissions	8.01	7.90*	6.16	8.07*	6.59
NO <sub>x</sub> (mean 5 sites)	8.08	8.01	6.23	8.18	6.70
CO (mean 8 sites)	8.01	7.94	6.36	8.11	6.62

<b>Metric</b>	<b>Harrington Beach</b>	<b>Grafton</b>	<b>Bayside</b>	<b>Milwaukee SER</b>	<b>Lake Geneva</b>
Period	2000-19	2000-19	2000-19	2000-19	2000-18
N Days	3601	3544	3502	6019	3413
R <sup>2</sup>	0.704	0.701	0.708	0.727	0.691
Bias (ppbv)	-0.025	-0.021	-0.022	0.010	0.002
Akaike information criterion	25168	24680	24380	41210	23280
Percent correct (70 ppbv criterion)	96.47	96.61	96.52	98.54	96.57
False alarm rate (70 ppbv)	29.70	27.08	22.43	28.95	38.78
Probability of detection (70 ppbv)	42.26	42.68	45.86	25.96	23.44
Consolidated success index	35.86	36.84	40.49	23.48	20.41
RMSE (ppbv)	7.78	7.69	7.67	7.32	7.15
Tmax Milwaukee	8.36	8.18	8.20	7.72	7.37
Tmin Milwaukee	7.79	7.69*	7.68*	7.32	7.15*
Lake Michigan surface T	7.82	7.71	7.68	7.35	7.21
RH (local and near-local)	7.88	7.81	7.77	7.36	7.29
SR max Milwaukee	7.92	7.92	7.88	7.51	7.48
BP (mean 4 sonde sites)	7.82	7.71	7.71	7.33	7.17
WS (local daily)	7.79*	7.69*	7.68*	7.33	7.16
WD (local daily)	7.82	7.78	7.73	7.40	7.25
WD midday (nearest site)	7.85	7.75	7.70	7.34	7.15*
850 mb WD (mean 4 sites)	7.83	7.73	7.71	7.33	7.15*
500 mb WD (mean 4 sites)	7.79*	7.70*	7.68*	7.32*	7.18
850 mb WS (mean 4 sites)	7.81	7.71	7.69	7.33	7.16
500 mb WS (mean 4 sites)	7.87	7.76	7.74	7.39	7.23
850 mb height (mean 4 sites)	7.83	7.72	7.72	7.34	7.18
500 mb height (mean 4 sites)	7.79*	7.69*	7.69	7.35	7.16
Pressure Green Bay - Lincoln	7.80	7.70	7.69	7.35	7.17
Pressure Green Bay - Detroit	7.84	7.74	7.74	7.33	7.20
Day of year	7.80	7.70*	7.71	7.50	7.21
MDA8 O <sub>3</sub> start hour	8.12	8.00	7.94	7.58	7.35
Day of week	7.82	7.75	7.71	7.43	7.16
VOC + NO <sub>x</sub> emissions	7.79	7.69*	7.68*	7.37	7.17
NO <sub>x</sub> (mean 5 sites)	7.86	7.79	7.75	7.48	7.24
CO (mean 8 sites)	7.82	7.74	7.71	7.38	7.16

<b>Metric</b>	<b>Kenosha</b>	<b>Chiwaukee</b>	<b>Northbrook</b>	<b>Evanston</b>	<b>Schiller Park</b>
Period	2013-19	2000-19	2000-19	2000-19	2013-19
N Days	1475	3861	6405	5780	2085
R <sup>2</sup>	0.742	0.715	0.757	0.744	0.781
Bias (ppbv)	0.002	-0.016	0.060	0.053	0.024
Akaike information criterion	9711	27110	44210	40570	13580
Percent correct (70 ppbv criterion)	98.37	95.21	97.81	97.70	99.86
False alarm rate (70 ppbv)	40.00	30.39	54.55	40.63	0.00
Probability of detection (70 ppbv)	23.08	49.22	22.39	26.21	25.00
Consolidated success index	20.00	40.51	17.65	22.22	25.00
RMSE (ppbv)	6.14	7.92	7.53	7.97	6.02
Tmax Milwaukee	6.36	8.42	7.88	8.37	6.16
Tmin Milwaukee	6.20	7.93*	7.54	7.99	6.04
Lake Michigan surface T	6.19	7.94	7.56	8.04	6.15
RH (local and near-local)	6.31	8.07	7.66	8.05	6.20
SR max Milwaukee	6.42	8.07	7.64	8.05	6.15
BP (mean 4 sonde sites)	6.15*	7.93	7.54	7.99	6.07
WS (local daily)	6.17	7.94	7.55	7.98	6.05
WD (local daily)	6.19	8.00	7.55	8.02	6.05
WD midday (nearest site)	6.15*	7.92*	7.55	8.02	6.06
850 mb WD (mean 4 sites)	6.18	7.98	7.54	7.99	6.03*
500 mb WD (mean 4 sites)	6.16*	7.94	7.53*	7.97*	6.05
850 mb WS (mean 4 sites)	6.16*	7.93*	7.54	7.98*	6.06
500 mb WS (mean 4 sites)	6.20	7.98	7.59	8.03	6.07
850 mb height (mean 4 sites)	6.16*	7.94	7.55	8.00	6.06
500 mb height (mean 4 sites)	6.15*	7.93	7.56	8.01	6.05
Pressure Green Bay - Lincoln	6.15*	7.94	7.55	7.99	6.05
Pressure Green Bay - Detroit	6.17	7.95	7.54	8.00	6.05
Day of year	6.17	8.01	7.74	8.32	6.21
MDA8 O <sub>3</sub> start hour	6.35	8.14	7.76	8.25	6.20
Day of week	6.16*	7.95	7.57	8.01	6.20
VOC + NO <sub>x</sub> emissions	6.20	7.92*	7.63	8.01	6.08
NO <sub>x</sub> (mean 5 sites)	6.24	8.01	7.67	8.06	6.13
CO (mean 8 sites)	6.39	7.99	7.56	8.02	6.05

<b>Metric</b>	<b>Jardine</b>	<b>SWFP</b>	<b>Coloma</b>	<b>Holland</b>	<b>Muskegon</b>
Period	2000-12	2000-19	2000-19	2000-19	2000-19
N Days	2592	3994	3582	3575	3577
R <sup>2</sup>	0.639	0.668	0.688	0.725	0.746
Bias (ppbv)	0.009	0.008	-0.006	-0.004	-0.001
Akaike information criterion	18641	28318	25052	25105	24680
Percent correct (70 ppbv criterion)	97.03	96.54	94.92	94.66	95.89
False alarm rate (70 ppbv)	38.71	33.80	32.24	29.06	27.22
Probability of detection (70 ppbv)	22.62	29.19	43.64	52.17	54.91
Consolidated success index	19.79	25.41	36.14	42.99	45.56
RMSE (ppbv)	8.53	8.21	7.80	7.91	7.44
Tmax Milwaukee	8.80	8.39	8.01	8.17	7.91
Tmin Milwaukee	8.55*	8.21*	7.82	7.95	7.45*
Lake Michigan surface T	8.56	8.21*	7.81*	7.92	7.45
RH (local and near-local)	8.68	8.53	8.09	8.26	7.87
SR max Milwaukee	8.71	8.33	7.87	7.99	7.54
BP (mean 4 sonde sites)	8.59	8.26	7.90	8.02	7.52
WS (local daily)	8.54*	8.21*	7.83	7.93	7.45*
WD (local daily)	8.57	8.25	7.82	7.94	7.49
WD midday (nearest site)	8.61	8.25	7.81*	7.92	7.47
850 mb WD (mean 4 sites)	8.56	8.22	7.83	7.94	7.46
500 mb WD (mean 4 sites)	8.55*	8.21	7.81*	7.91*	7.45*
850 mb WS (mean 4 sites)	8.54*	8.22	7.82	7.92*	7.45*
500 mb WS (mean 4 sites)	8.58	8.24	7.87	7.98	7.53
850 mb height (mean 4 sites)	8.62	8.26	7.90	8.01	7.51
500 mb height (mean 4 sites)	8.58	8.21	7.82*	7.94	7.45
Pressure Green Bay - Lincoln	8.55	8.22	7.81*	7.92	7.46
Pressure Green Bay - Detroit	8.55	8.24	7.85	7.97	7.49
Day of year	8.63	8.31	7.85	7.94	7.49
MDA8 O <sub>3</sub> start hour	8.91	8.46	7.96	8.09	7.58
Day of week	8.55*	8.23	7.82	7.93*	7.46
VOC + NO <sub>x</sub> emissions	8.55	8.23	7.84	7.96	7.47
NO <sub>x</sub> (mean 5 sites)	8.56	8.27	7.84	7.95	7.49
CO (mean 8 sites)	8.55	8.29	7.90	8.01	7.54

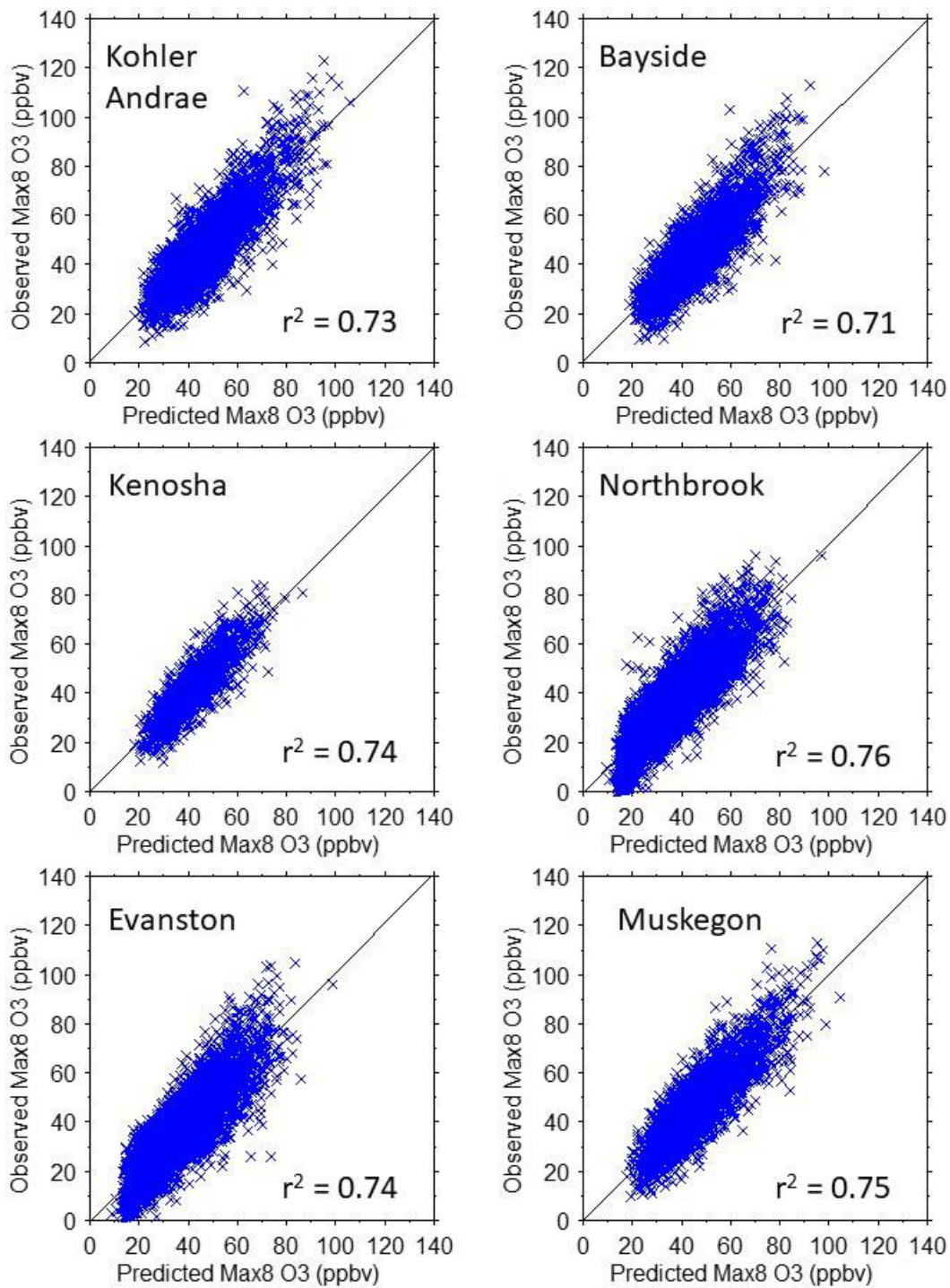


Figure 13. Example scatter plots of observed vs predicted MDA8 O<sub>3</sub>. Sampling records are 2000 – 2019 except at Kenosha, 2013 – 2019.

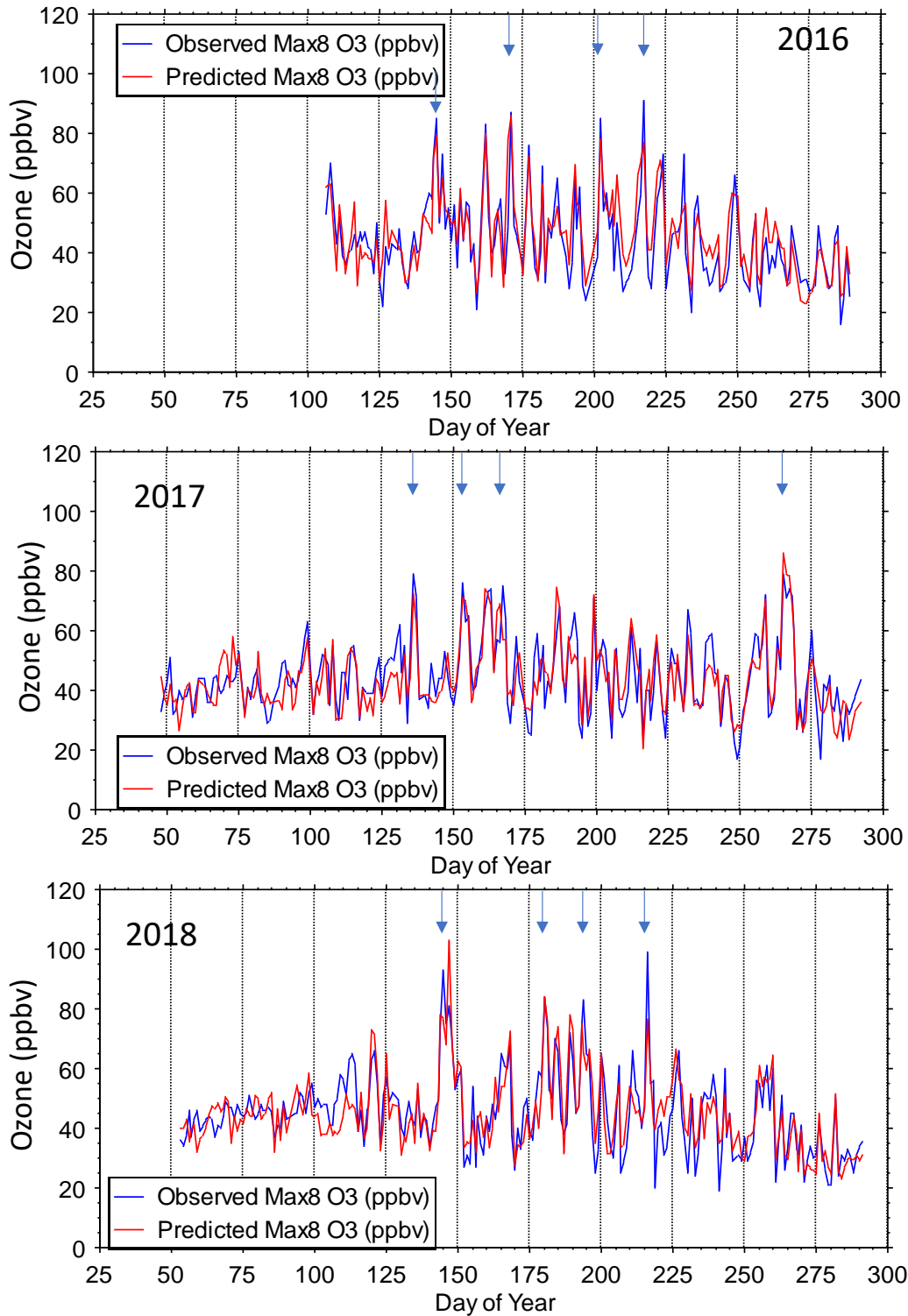


Figure 14. Example time series of Sheboygan Kohler Andrae observed and predicted MDA8 O<sub>3</sub>. Arrows mark the dates of the 1<sup>st</sup> through 4<sup>th</sup> highest MDA8 O<sub>3</sub> each year.

## 5.5 O<sub>3</sub> Sensitivity Results

The GAM predicts O<sub>3</sub> (logarithm MDA8 O<sub>3</sub>) as an additive function of nonlinear variables. The relationships between O<sub>3</sub> and the predictor variables are depicted here as sensitivity plots. The GAM constructs these relationships as deviations from a site's overall mean MDA8 O<sub>3</sub>, so the plots show modeled O<sub>3</sub> deviations versus predictor values. The sensitivity curves are smooth, because they are model-predicted values. Times series or scatter plots are useful for demonstrating day-to-day variations in the contributions of each predictor variable.

### 5.5.1 Sensitivity of O<sub>3</sub> to Weather

Figures 15 through 20 show MDA8 O<sub>3</sub> sensitivities to six key weather variables: Tmax, RH, Lake Michigan surface water temperature, mid-day (1800 UTC) wind direction, daily maximum solar radiation, and 500 mb WS. Plots are shown for various sites to illustrate similarities and differences among sites. Different sites have been used to illustrate the various sensitivities to provide examples from a larger number of sites (rather than using the same set of sites for each weather variable). The sensitivities are nonlinear and exhibit qualitative consistency among sites.

Ozone-season MDA8 O<sub>3</sub> is associated with Tmax exceeding ~10° C. The predicted effect of increasing Tmax is to increase MDA8 O<sub>3</sub> by ~20 – 30 ppbv as Tmax increases from 20 to over 30° C (Figure 15). Surface Tmax is strongly associated with other variables, such as the 850 and 500 mb temperatures. The strong associations of MDA8 O<sub>3</sub> with Tmax potentially represent multiple causal factors, including photochemical processing (many reactions are temperature dependent) and air mass stagnation.

The predicted effects of RH, Lake Michigan surface temperature, and SRmax are associated with ~5 – 20 ppbv ranges of MDA8 O<sub>3</sub> deviations (Figures 16 – 18). MDA8 O<sub>3</sub> deviations increases with decreasing RH, decreasing Lake Michigan surface water temperature, and increasing SRmax. These relationships are consistent with known principles. Lower Lake Michigan surface water temperatures, for example, potentially increase the strength of the lake breeze because they can set up a stronger lake-land pressure gradient. The relationship to SRmax represents photochemical processing.

The effect of the lake breeze is explicitly captured in the sensitivities of MDA8 O<sub>3</sub> deviations to mid-day (1800 UTC) WD (Figure 19), which show maxima in the directions of Lake Michigan relative to each site (map, Figure 3). The magnitude of the effect is not as large as some of the other weather effects. The mid-day WD does not represent the full diurnal dynamics of the lake breeze (e.g., Sections 9.4.2 and 9.4.3). However, many of the highest MDA8 O<sub>3</sub> days exhibit daytime consistency of WD, which is then represented by the mid-day WD. In addition, the daily-average WD was statistically significant (Table 3).

The upper-air variables together represent MDA8 O<sub>3</sub> sensitivity to synoptic-scale weather. For example, MDA8 O<sub>3</sub> increases with decreasing 500 mb WS (Figure 20). Nearly all MDA8 O<sub>3</sub> values exceeding 50 ppbv occur with 500 mb WS below 20 m s<sup>-1</sup>. The GAM therefore associates higher O<sub>3</sub> with synoptic-scale air mass stagnation.

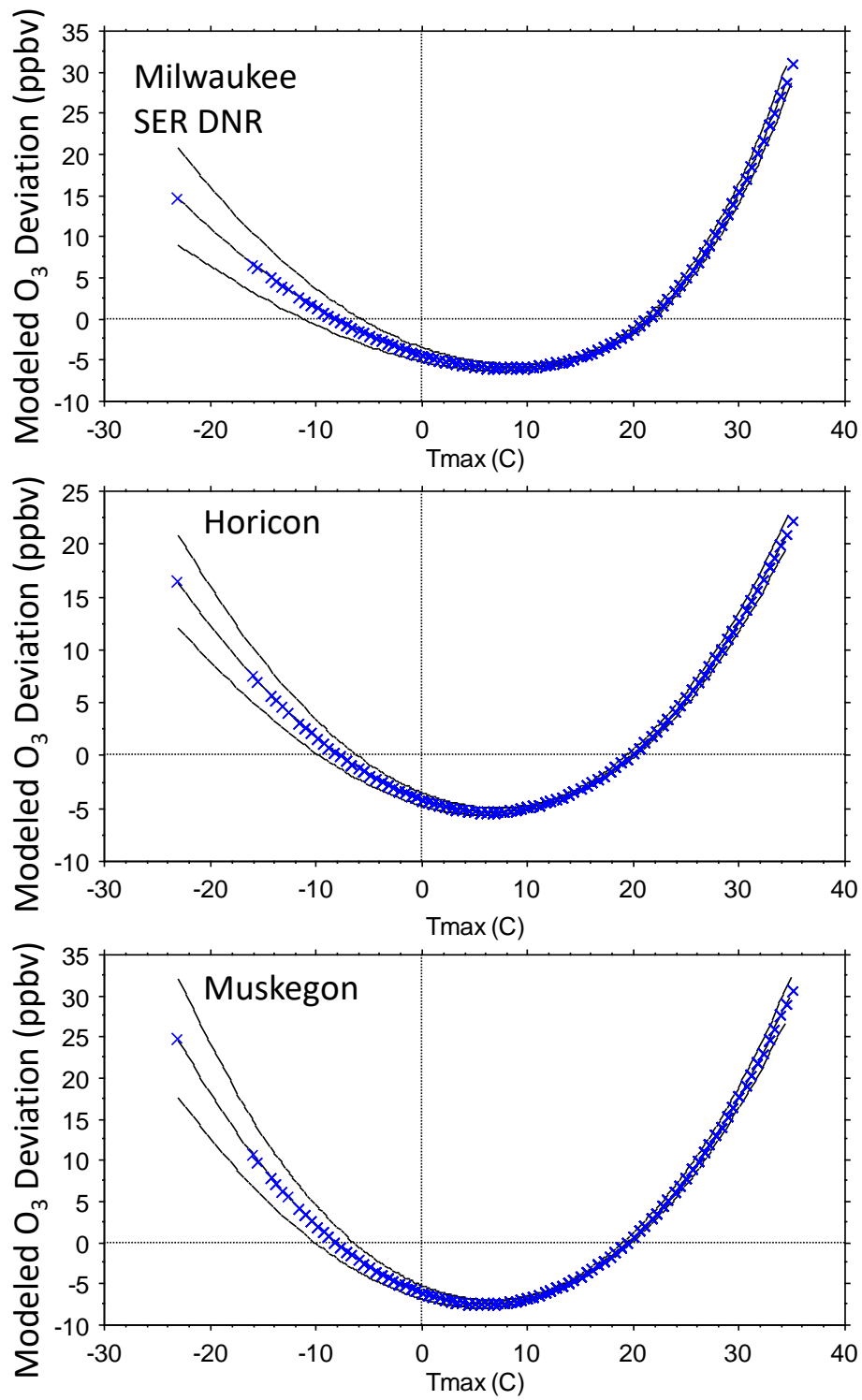


Figure 15. Modeled O<sub>3</sub> sensitivity ( $\pm 1$  SE) to Tmax.

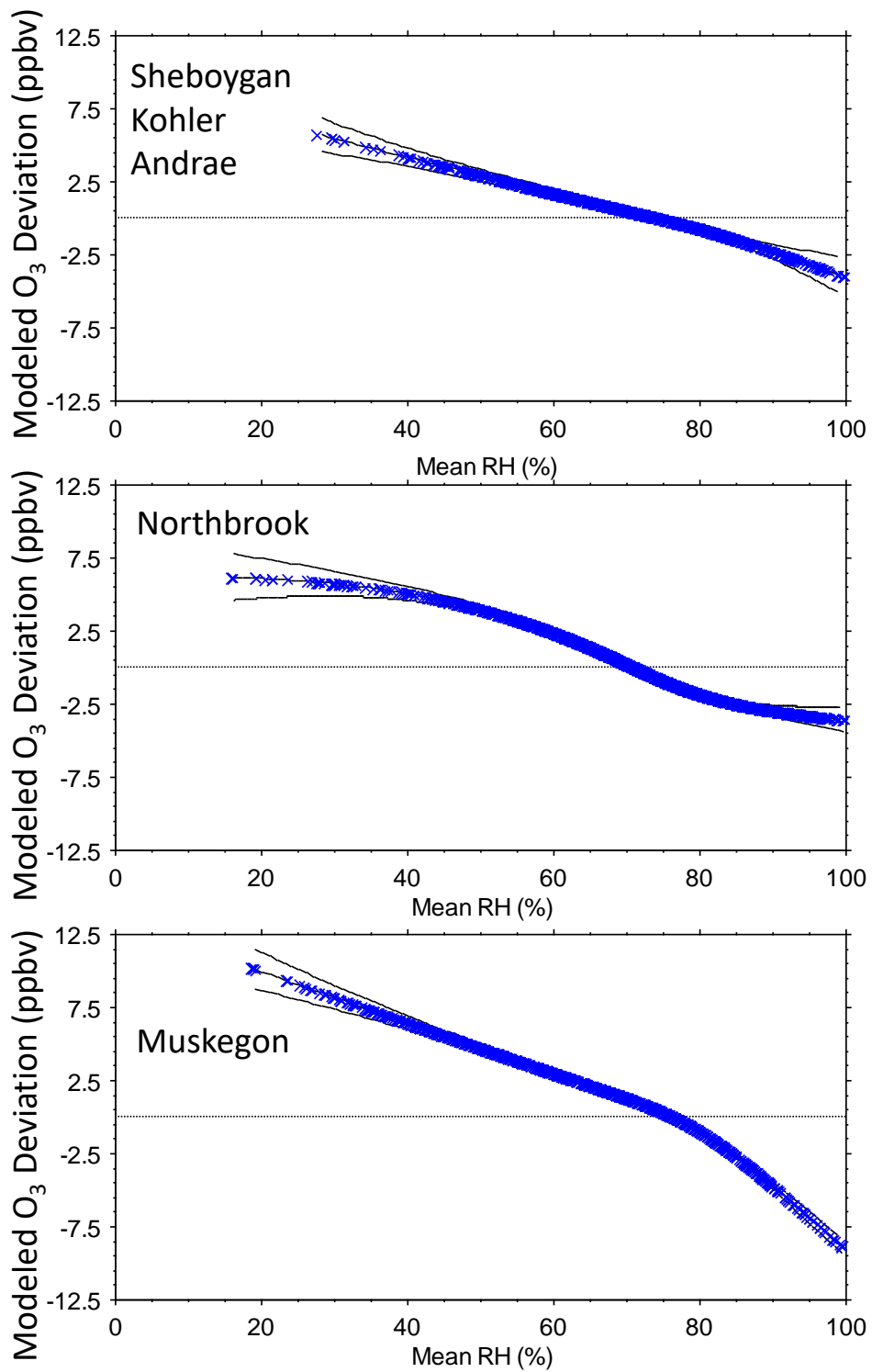


Figure 16. Modeled O<sub>3</sub> sensitivity ( $\pm 1$  SE) to RH.

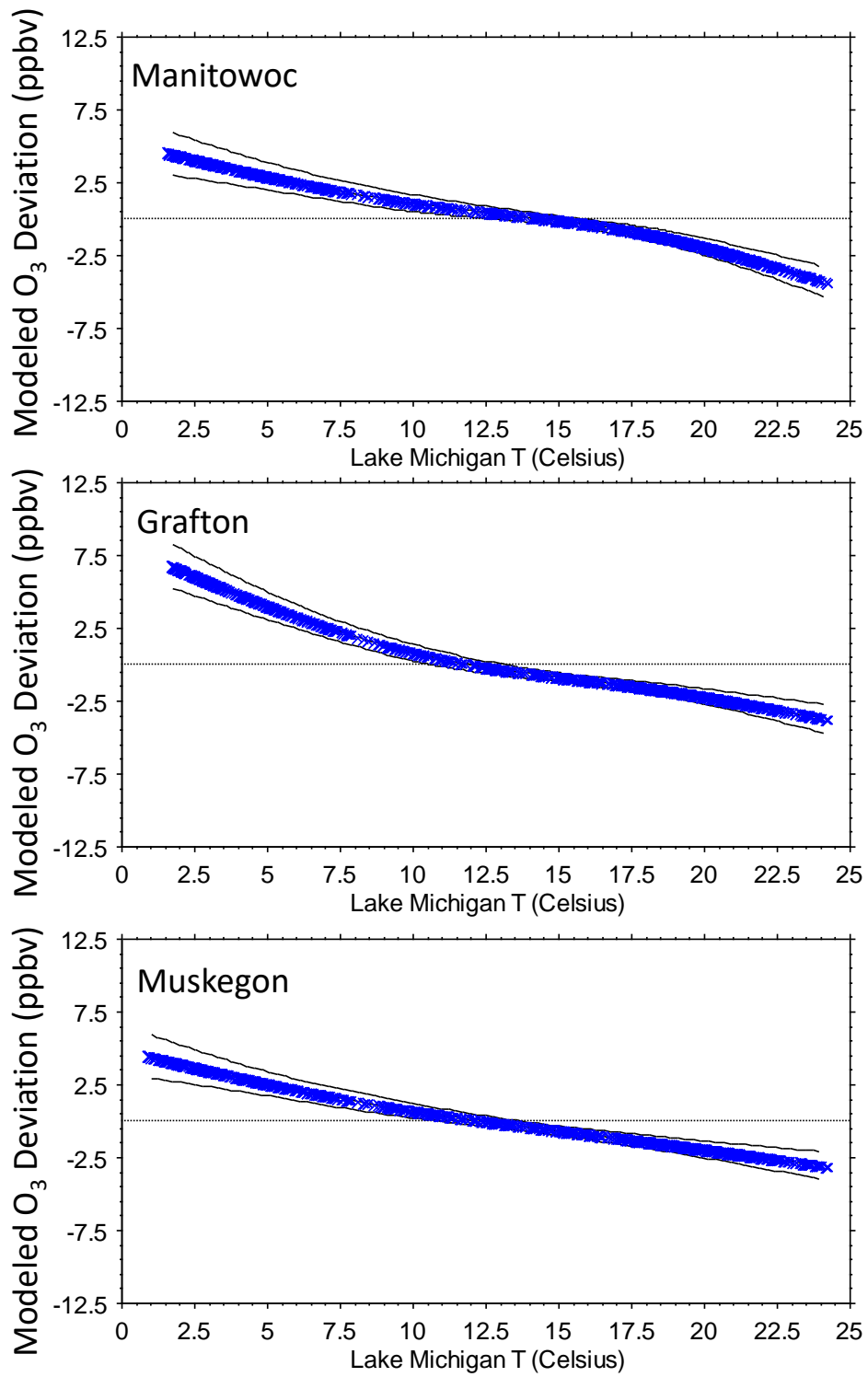


Figure 17. Modeled O<sub>3</sub> sensitivity ( $\pm 1$  SE) to Lake Michigan surface temperature.

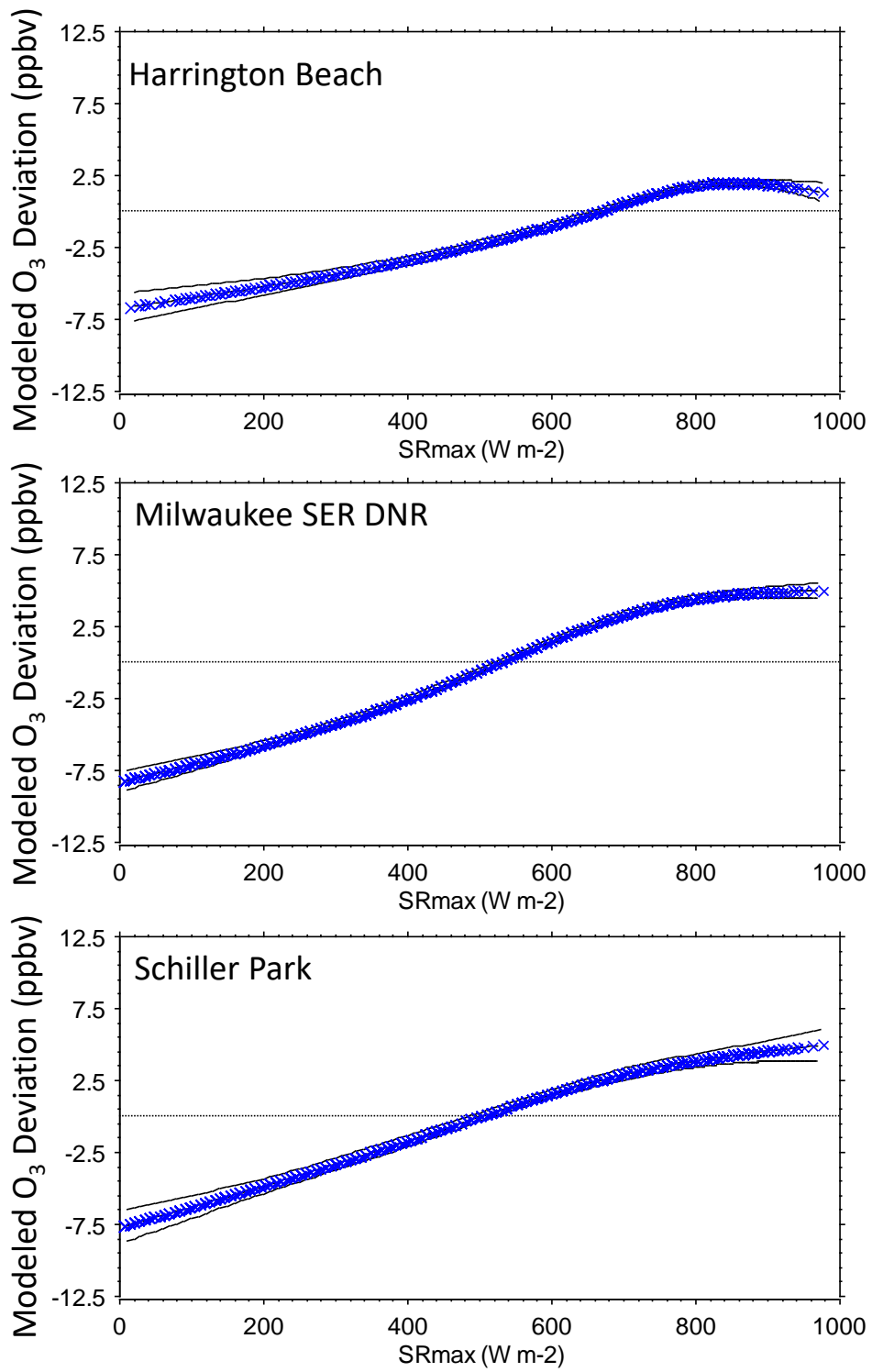


Figure 18. Modeled O<sub>3</sub> sensitivity ( $\pm 1$  SE) to daily maximum solar radiation.

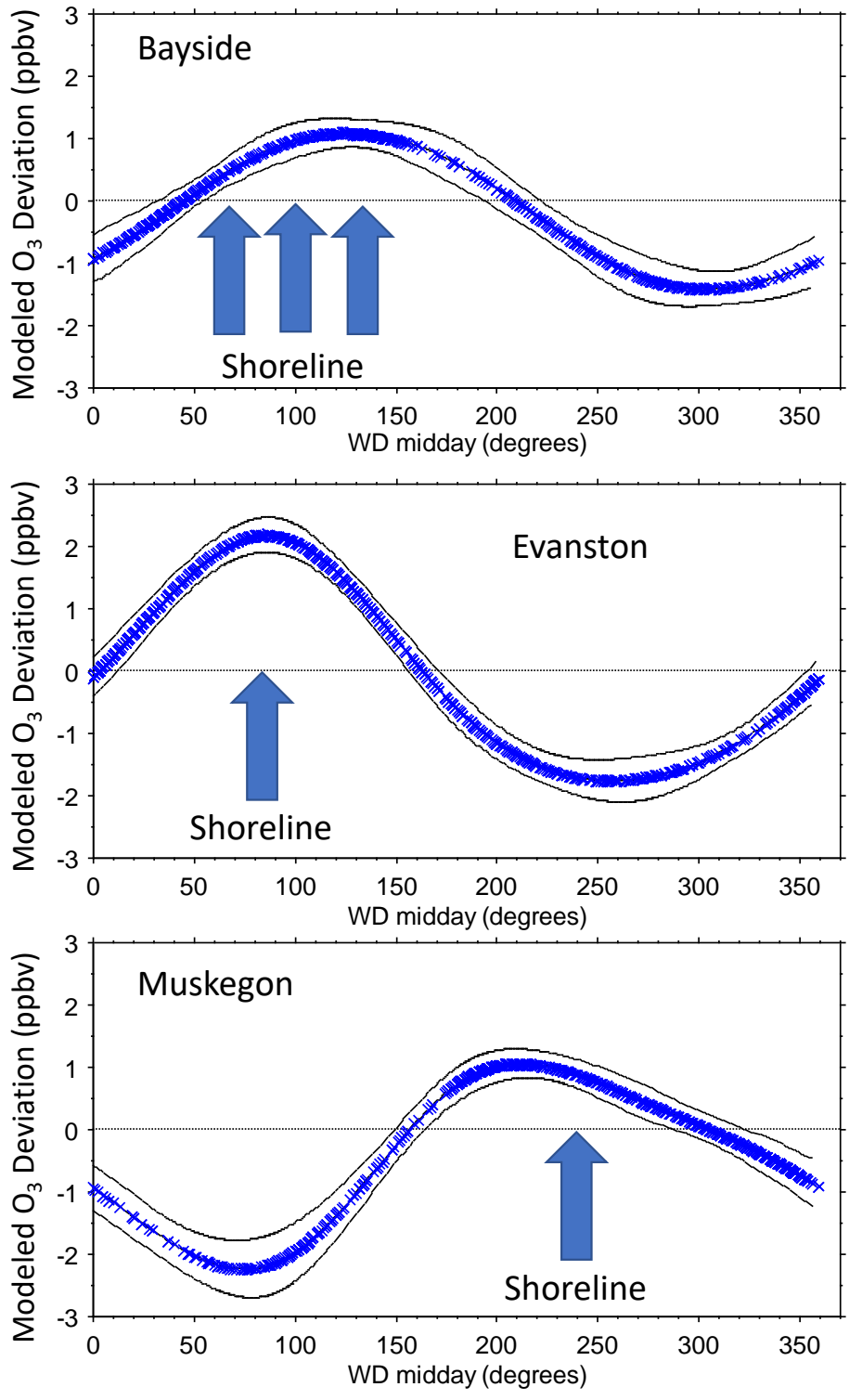


Figure 19. Modeled O<sub>3</sub> sensitivity ( $\pm 1$  SE) to mid-day WD.

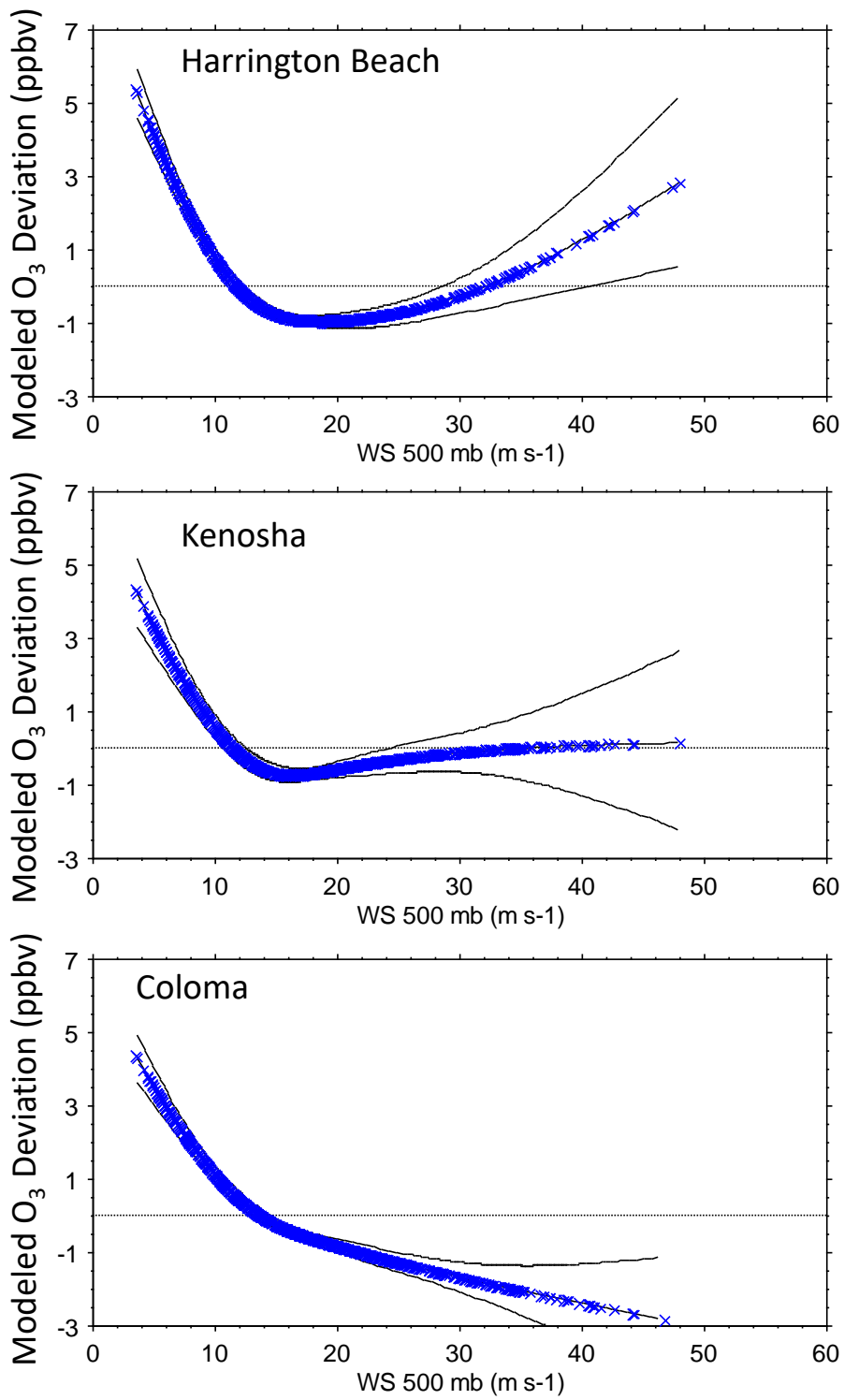


Figure 20. Modeled O<sub>3</sub> sensitivity ( $\pm 1$  SE) to 500 mb WS.

### 5.5.2 Sensitivity of O<sub>3</sub> to Temporal Factors

Temporal factors in the GAM represent phenomena that are not otherwise explicitly included among the predictor variables or whose complexities are incompletely represented by the predictors. The temporal factors are the day of the year, the day of the week, and the starting hour of the MDA8 O<sub>3</sub>. Examples of each are provided and discussed here.

The day of year was statistically significant at 19 of 20 sites (Table 4). A seasonal pattern exists in which higher predicted MDA8 O<sub>3</sub> peaks sometime between days 100 and 200 (Figure 21). Where the day-of-year factor is most prominent, it peaks on or about day 160. Although this seasonality could be related to seasonal weather variations, various weather variables provide explicit representations of meteorological seasonality. It is plausible that the seasonality that is represented by the day of the year is related to seasonal emissions variations, likely VOC variations because model inputs include daily ambient concentrations of CO and NO<sub>x</sub>. Seasonal VOC variations could include, for example, evaporative emissions (which are temperature sensitive), fuels composition, and biogenic emissions. Isoprene concentrations exhibit a seasonal pattern resembling those shown in Figure 21 (Section 9.4.5).

The seasonal patterns in the predicted effects of the day of year, Lake Michigan surface temperature, daily Tmax, and daily SR max are shown in Figure 22 for one site and year. These effects peak at different times of the year and exhibit differing degrees of day-to-day variability. The Lake Michigan surface temperature acts to increase MDA8 O<sub>3</sub> earlier in the year (approximately prior to day 125). The effect varies little from day-to-day because surface water temperature changes slowly. In contrast, Tmax and the effects of Tmax vary substantially from day-to-day, and indeed drive day-to-day variability in MDA8 O<sub>3</sub>. Seasonally, Tmax lags other variables, such as solar radiation. Higher MDA8 O<sub>3</sub> due to high Tmax tends to occur near or after day 150 (i.e., beginning late May). Solar radiation peaks at the summer solstice, but exhibits low daily SRmax on cloudy days. The seasonal peak is broad because SRmax changes slowly from day to day near the solstices.

GAM models that exclude the day-of-year input variable shift the Tmax and SRmax sensitivities without changing the RMSE much (Table 4). Day of year was retained because it was statistically significant and because seasonal variations occur that are not otherwise represented in the model input data. As discussed in Section 9.4.5, isoprene was measured only once every six days and was not statistically significant as a predictor.

The day of week was statistically significant at 17 of 20 sites (Table 4). Typical patterns are shown in Figure 23. GAM inputs include daily averages of CO and NO<sub>x</sub>, so the higher predicted O<sub>3</sub> on weekends implies that either other emissions (e.g., evaporative VOCs) were higher on weekends or the formation of O<sub>3</sub> was more efficient on weekends than on weekdays (potentially due to more favorable VOC/NO<sub>x</sub> ratios). Day-of-week variations in species concentrations and ratios are depicted in Section 9.4.6. The GAM day-of-week sensitivities imply that MDA8 O<sub>3</sub> concentrations were higher on weekends than on weekdays when both types of days had the same concentrations of CO and the same concentrations of NO<sub>x</sub>.

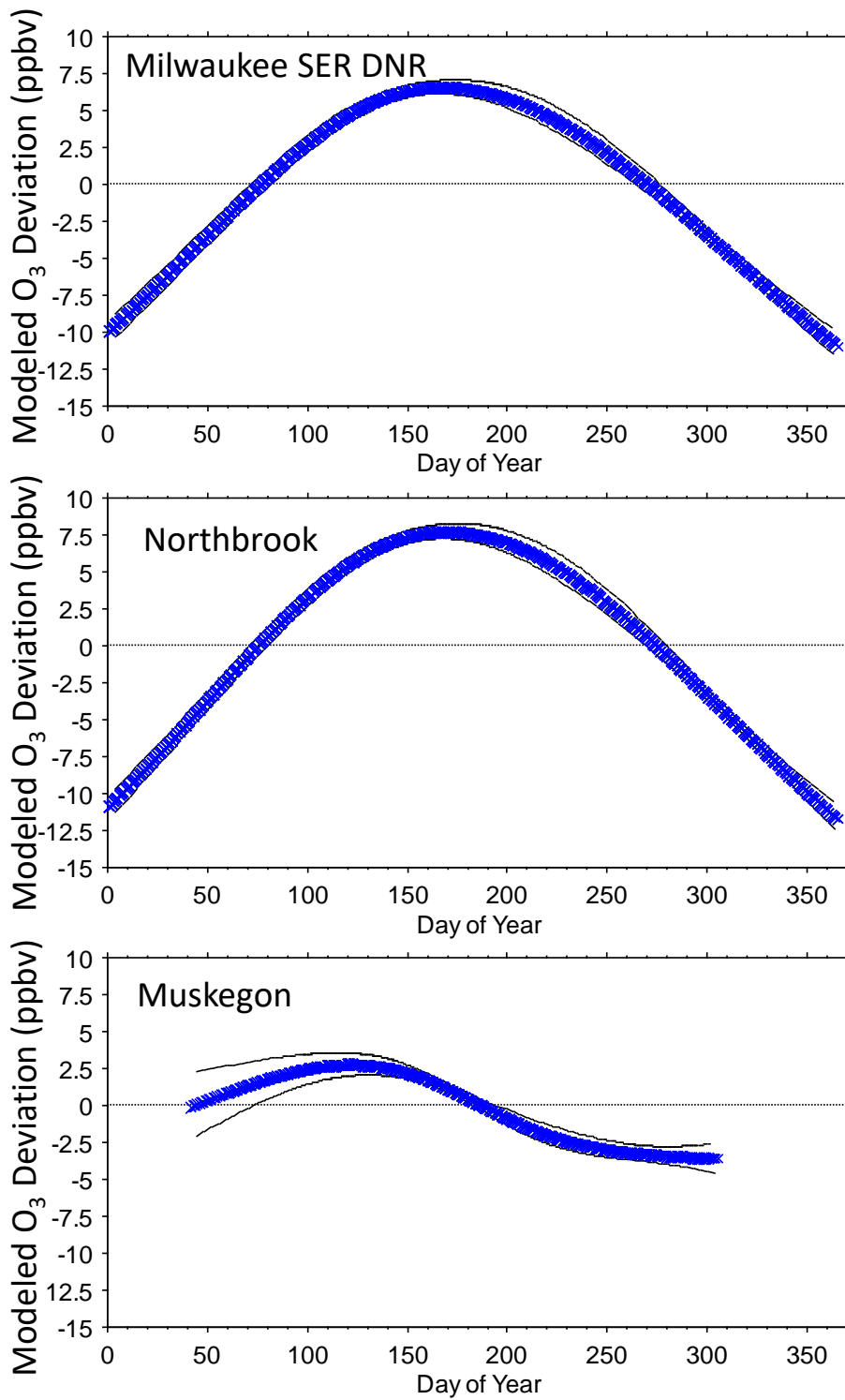


Figure 21. Modeled O<sub>3</sub> sensitivity ( $\pm 1$  SE) to day of year.

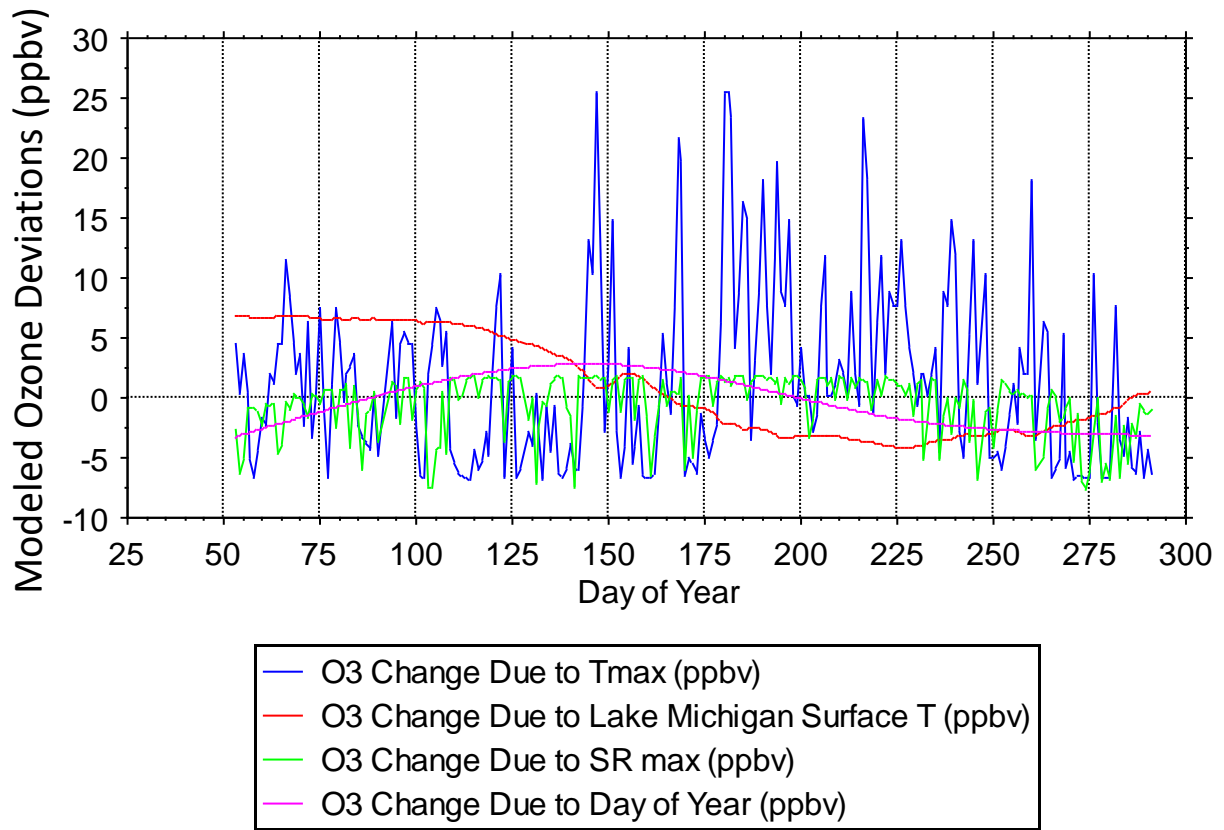


Figure 22. Sheboygan Kohler Andrae 2018 modeled O<sub>3</sub> sensitivity ( $\pm 1$  SE) to day of year, SRmax, Tmax, and Lake Michigan surface temperature.

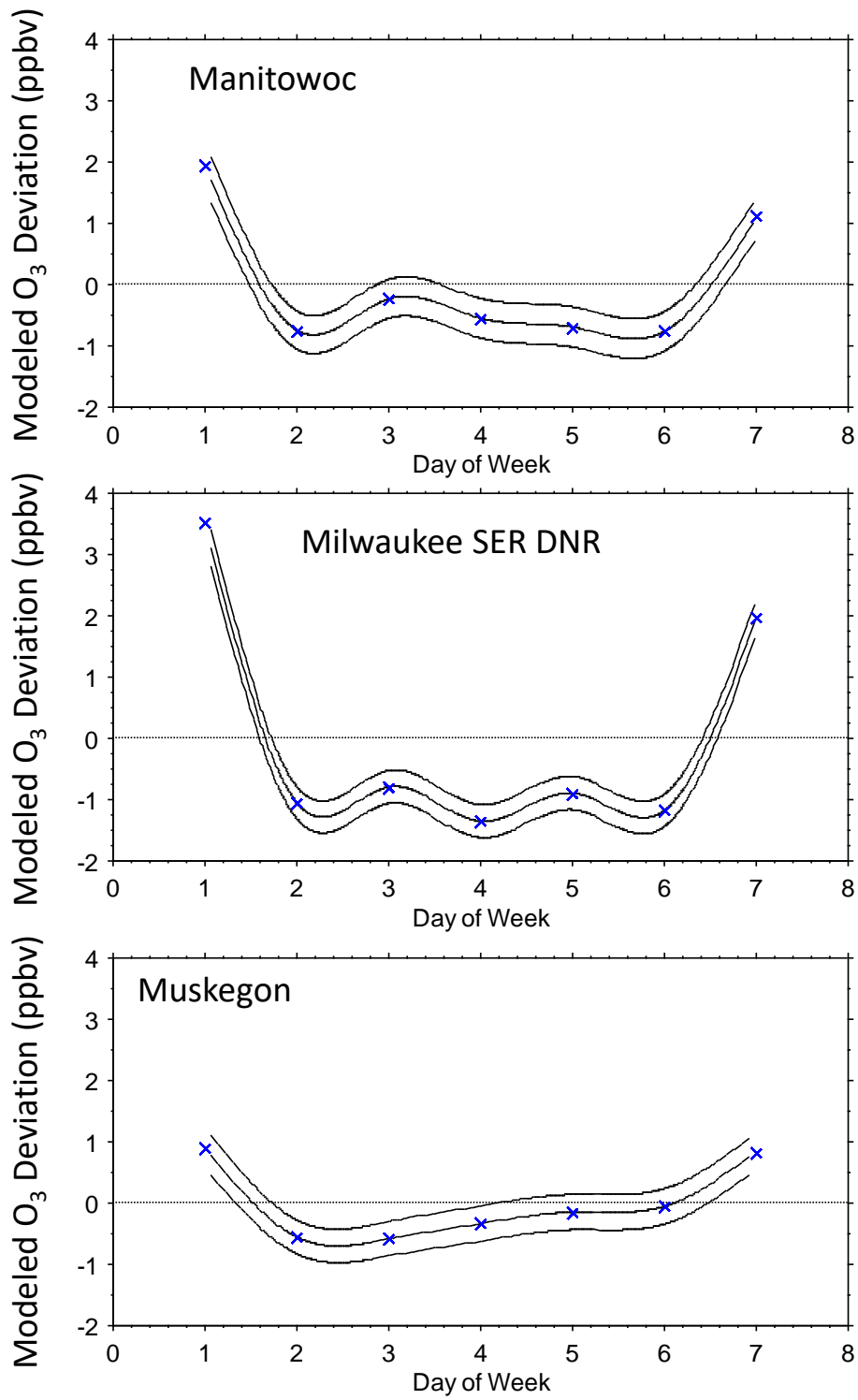


Figure 23. Modeled O<sub>3</sub> sensitivity ( $\pm 1$  SE) to day of week.

Example sensitivities of MDA8 O<sub>3</sub> to the starting hour of the highest 8-hour average are shown in Figure 24. This variable was a consistently important predictor of the concentration of the MDA8 O<sub>3</sub>. When the highest MDA8 O<sub>3</sub> occurred beginning between about noon and 6 p.m., it was higher than when the starting hours were earlier or later. This sensitivity could represent more than one phenomenon. One possible phenomenon would be lower MDA8 O<sub>3</sub> occurring when O<sub>3</sub> formation was cut off by early afternoon, for example by cloud cover, precipitation, or fresh NO emissions. On such days, O<sub>3</sub> would not reach its maximum potential level and the MDA8 O<sub>3</sub> starting hour would be in the early morning. MDA8 O<sub>3</sub> starting hours later than 6 p.m. could occur for multiple reasons. One reason would be that O<sub>3</sub> formation began later in the day, for reasons such as those already mentioned. Another plausible association is with O<sub>3</sub> transport to downwind locations, where longer transport times could be associated with greater dilution and dispersion (see Figure 2).

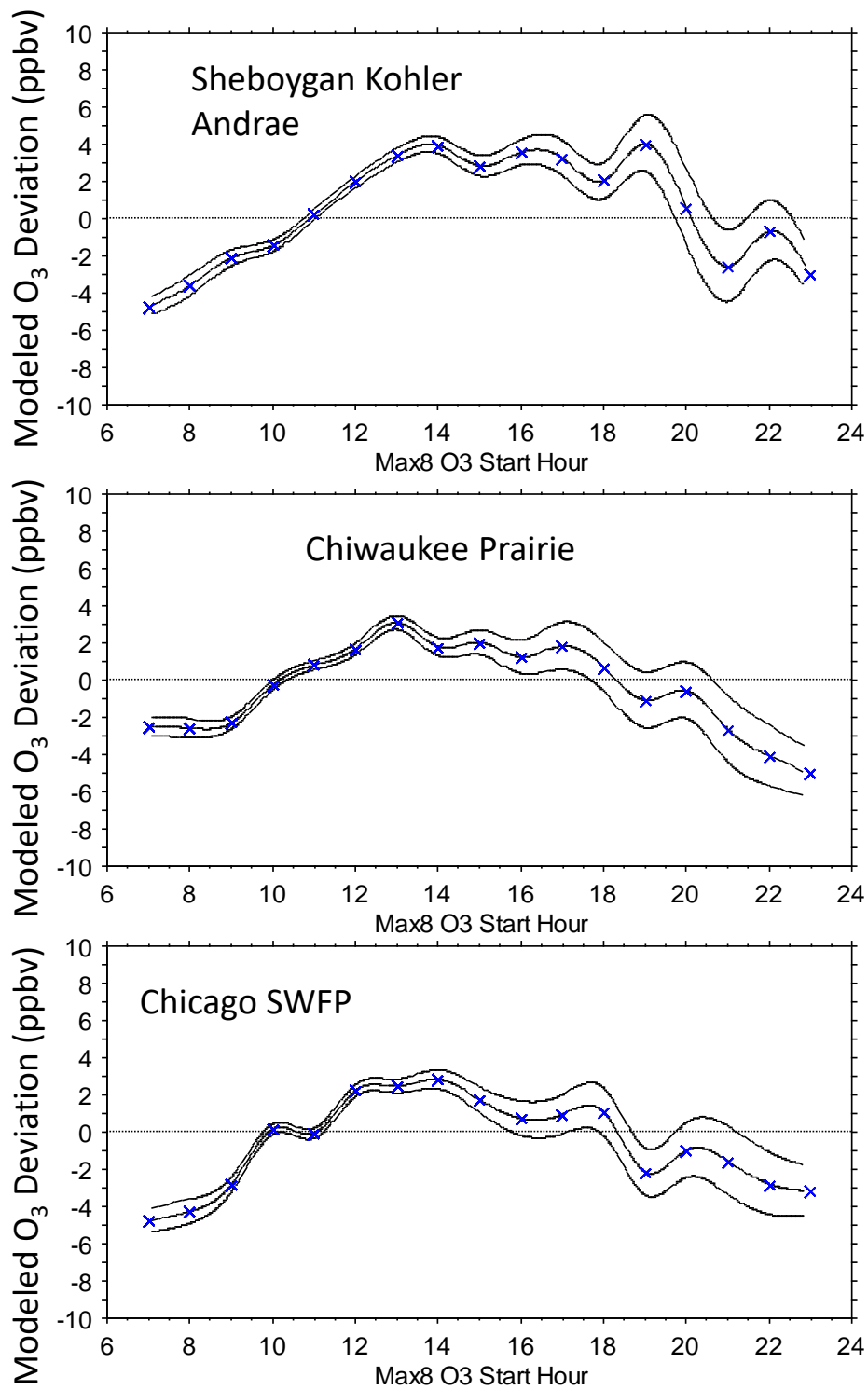


Figure 24. Modeled O<sub>3</sub> sensitivity ( $\pm 1$  SE) to MDA8 O<sub>3</sub> starting hour.

### 5.5.3 Sensitivity of O<sub>3</sub> to Emissions and Precursors

The sensitivities of O<sub>3</sub> to variations in emissions and ambient precursor concentrations are modeled in the GAM using three types of input variables: (1) annual-average multistate (IN, IL, WI) VOC and NO<sub>x</sub> emissions (Figure 1 and Section 9.4.1), (2) daily-average multisite concentrations of CO and NO<sub>x</sub> (Section 9.4.1, Table A3), and (3) day of week. The day of week variation was discussed in the previous section.

The annual emissions term was statistically significant at 15 of 20 sites (Table 4). At an annual-average, multistate scale, VOC and NO<sub>x</sub> emissions were highly correlated (Figure 1 and Section 9.4.1). As a result, they could not be incorporated as individual predictor variables. Instead, the model input was the sum of VOC and NO<sub>x</sub> emissions. The predicted O<sub>3</sub> sensitivities therefore represent the effects of regional-scale combined VOC and NO<sub>x</sub> emissions. Daily-average concentrations of CO and NO<sub>x</sub> were included as predictor variables to help represent day-to-day variations in emissions levels and composition. The long-term O<sub>3</sub> response to emission changes is represented by trends in both emissions and ambient precursor concentrations.

Because emissions were provided on an annual-average timescale, the GAM tended to match the emissions trend to long-term trends, if any, in the ozone-season average MDA8 O<sub>3</sub> (Figure 25). The latter trends were downward at some sites, upward at others, and negligible at some. Long-term trends in MDA8 O<sub>3</sub> extrema (>90<sup>th</sup> percentile) were downward except at some Chicago sites but upward trends were common in the 50<sup>th</sup> and 75<sup>th</sup> percentiles (Section 9.4.8).

The associations between emissions and O<sub>3</sub> trends do not capture the year-to-year variability in average MDA8 O<sub>3</sub>, nor do they exactly reproduce the trends in average MDA8 O<sub>3</sub>, because other predictor variables also contribute to long-term trend. Ambient precursor concentrations, though input to the GAM as daily concentrations, also exhibited long-term downward trends (Section 9.4.1, Figures A8 and A13). The trends in precursor concentrations therefore yielded trends in O<sub>3</sub> associated with those precursors (Table 5). The sensitivities of MDA8 O<sub>3</sub> to daily CO and NO<sub>x</sub> concentrations, which are discussed next, account for the CO- and NO<sub>x</sub>-related O<sub>3</sub> trends shown in Table 5.

The GAM emission-trend effects are consistent with simple univariate regressions of annual average MDA8 O<sub>3</sub> vs. emissions (Table 5). Differences between GAM and univariate emission-related O<sub>3</sub> trends exist for some sites with short (6 – 13 years) records, but the differences are smaller than the statistical uncertainties. The standard errors of the trends are smaller for the GAM fit than for univariate regression, because the GAM also accounts for other sources of variation.

The interpretation of the emission associations is that emission changes have tended to affect mid-range O<sub>3</sub> differently than O<sub>3</sub> extrema (Section 9.4.8). The effects are spatially variable. At locations where NO<sub>x</sub> concentrations are relatively high due to higher emission densities, lower NO<sub>x</sub> in recent years has led to less suppression of O<sub>3</sub> by reaction with fresh NO emissions. In such locations, ozone-season average MDA8 O<sub>3</sub> may be increasing.

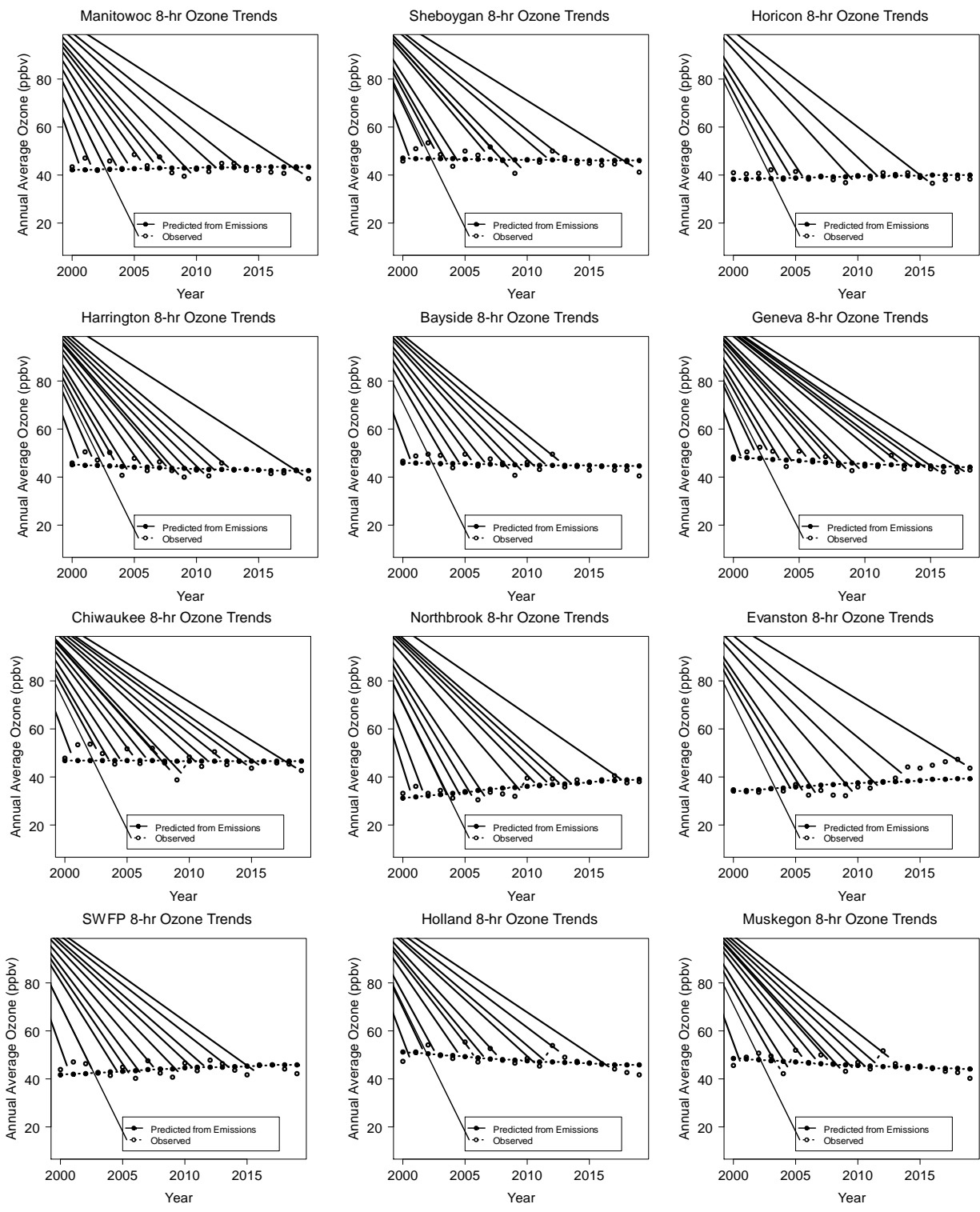


Figure 25. Observed ozone season average MDA8 O<sub>3</sub> and GAM predicted emission-related trends in MDA8 O<sub>3</sub>.

Table 5. GAM components that account for long-term O<sub>3</sub> trends compared with simple univariate regression of annual average MDA8 O<sub>3</sub> vs. emissions. Negative values are O<sub>3</sub> decreases with respect to time (O<sub>3</sub> decreases in response to decreasing emissions or ambient concentrations). Trends were determined by regressing annual averages against year, expressed as ppbv decade<sup>-1</sup> ± 1 SE. For GAM-predicted values, the SE terms were determined through propagation of errors: (1) prediction uncertainties for O<sub>3</sub> deviations due to emissions (annual) or precursors (daily CO and NO<sub>x</sub>), and (2) predictor trend versus time.

<b>Site</b>	<b>Univariate Regression Annual Average MDA8 O<sub>3</sub> vs. Year (ppbv decade<sup>-1</sup> ± 1 SE<sup>2</sup>)</b>	<b>GAM MDA8 O<sub>3</sub> Emissions Response Trend (ppbv decade<sup>-1</sup> ± 1 SE<sup>3</sup>)</b>	<b>GAM MDA8 O<sub>3</sub> CO Response Trend (ppbv decade<sup>-1</sup> ± 1 SE<sup>3</sup>)</b>	<b>GAM MDA8 O<sub>3</sub> NO<sub>x</sub> Response Trend (ppbv decade<sup>-1</sup> ± 1 SE<sup>3</sup>)</b>
Newport Park WI	-4.01 ± 0.91	-1.67 ± 0.52	-0.40 ± 0.25	-2.55 ± 0.60
Manitowoc WI	-2.39 ± 0.90	0.75 ± 0.46	-0.86 ± 0.24	-2.40 ± 0.62
Sheboygan Haven WI <sup>1</sup>	-4.90 ± 5.98	-0.68 ± 1.52	-4.23 ± 1.07	0.15 ± 0.05
Sheboygan Kohler WI	-3.08 ± 1.11	-0.51 ± 0.49	-0.80 ± 0.22	-2.62 ± 0.64
Horicon/Mayville WI	-1.29 ± 0.55	0.98 ± 0.30	-1.17 ± 0.28	-1.52 ± 0.47
Harrington Beach WI	-3.58 ± 0.99	-1.34 ± 0.49	-1.13 ± 0.39	-1.95 ± 0.60
Grafton WI	-1.97 ± 0.96	0.74 ± 0.47	-1.52 ± 0.37	-2.01 ± 0.57
Bayside WI	-3.23 ± 0.87	-0.70 ± 0.50	-1.11 ± 0.28	-1.85 ± 0.60
Milwaukee SER WI	-2.22 ± 1.29	3.19 ± 0.36	-1.09 ± 0.22	-0.81 ± 0.21
Lake Geneva WI	-4.39 ± 0.95	-2.33 ± 0.47	-0.30 ± 0.11	-2.38 ± 0.61
Kenosha Wtr Twr WI <sup>1</sup>	-0.47 ± 1.96	5.76 ± 1.14	-2.27 ± 0.52	0.21 ± 0.01
Chiwaukee Prairie WI	-3.53 ± 1.26	-0.06 ± 0.42	-1.94 ± 0.42	-1.46 ± 0.46
Northbrook IL	3.63 ± 0.84	4.16 ± 0.35	-1.52 ± 0.38	0.50 ± 0.13
Evanston IL	7.30 ± 1.10	2.81 ± 0.39	-2.11 ± 0.57	-0.16 ± 0.05
Schiller Park IL <sup>1</sup>	8.67 ± 5.30	5.09 ± 0.84	-0.21 ± 0.12	0.34 ± 0.12
Jardine IL <sup>1</sup>	1.71 ± 2.78	2.59 ± 0.96	-2.67 ± 1.29	1.30 ± 0.49
S Water Filtr Plant IL	0.007 ± 0.95	2.25 ± 0.47	-2.81 ± 0.62	-0.55 ± 0.62
Coloma MI	-4.15 ± 1.12	-2.99 ± 0.54	-1.95 ± 0.45	-1.03 ± 0.45
Holland MI	-3.96 ± 1.15	-2.99 ± 0.48	-2.42 ± 0.52	-0.75 ± 0.52
Muskegon MI	-3.16 ± 1.10	-2.35 ± 0.44	-1.87 ± 0.38	-1.16 ± 0.38

<sup>1</sup>Partial records: Sheboygan Haven (2014-19), Kenosha (2013-19), Schiller Park (2013-19), Jardine (2000-12).

<sup>2</sup>Standard error of regression slope.

<sup>3</sup>Propagated from SE of GAM coefficient for O<sub>3</sub> deviations due to predictor combined with SE of slope of GAM predictor versus time.

Examples of GAM-predicted sensitivities of daily MDA8 O<sub>3</sub> to daily-average CO and NO<sub>x</sub> concentrations are shown in Figures 26 through 30. MDA8 O<sub>3</sub> shows a positive response to daily-average CO over the range of CO concentrations occurring between 2000 and 2019 (Figure 26), but this response is flattest for mid-range CO values (300 – 600 ppbv). Many days with MDA8 O<sub>3</sub> exceeding 70 ppbv between 2015 and 2019 were in this flat-response region (Figure 27). MDA8 O<sub>3</sub> shows both positive and inverse responses to daily-average NO<sub>x</sub> over the range of NO<sub>x</sub> concentrations occurring between 2000 and 2019 (Figure 28). Thus, most sites exhibited both NO<sub>x</sub>-limited and NO<sub>x</sub>-inhibited days with MDA8 O<sub>3</sub> exceeding 70 ppbv (Figure 28). However, when the data are restricted to recent years (2015 – 2019), only Chicago sites clearly showed NO<sub>x</sub>-inhibited days with MDA8 O<sub>3</sub> exceeding 70 ppbv (Figures 29 and 30).

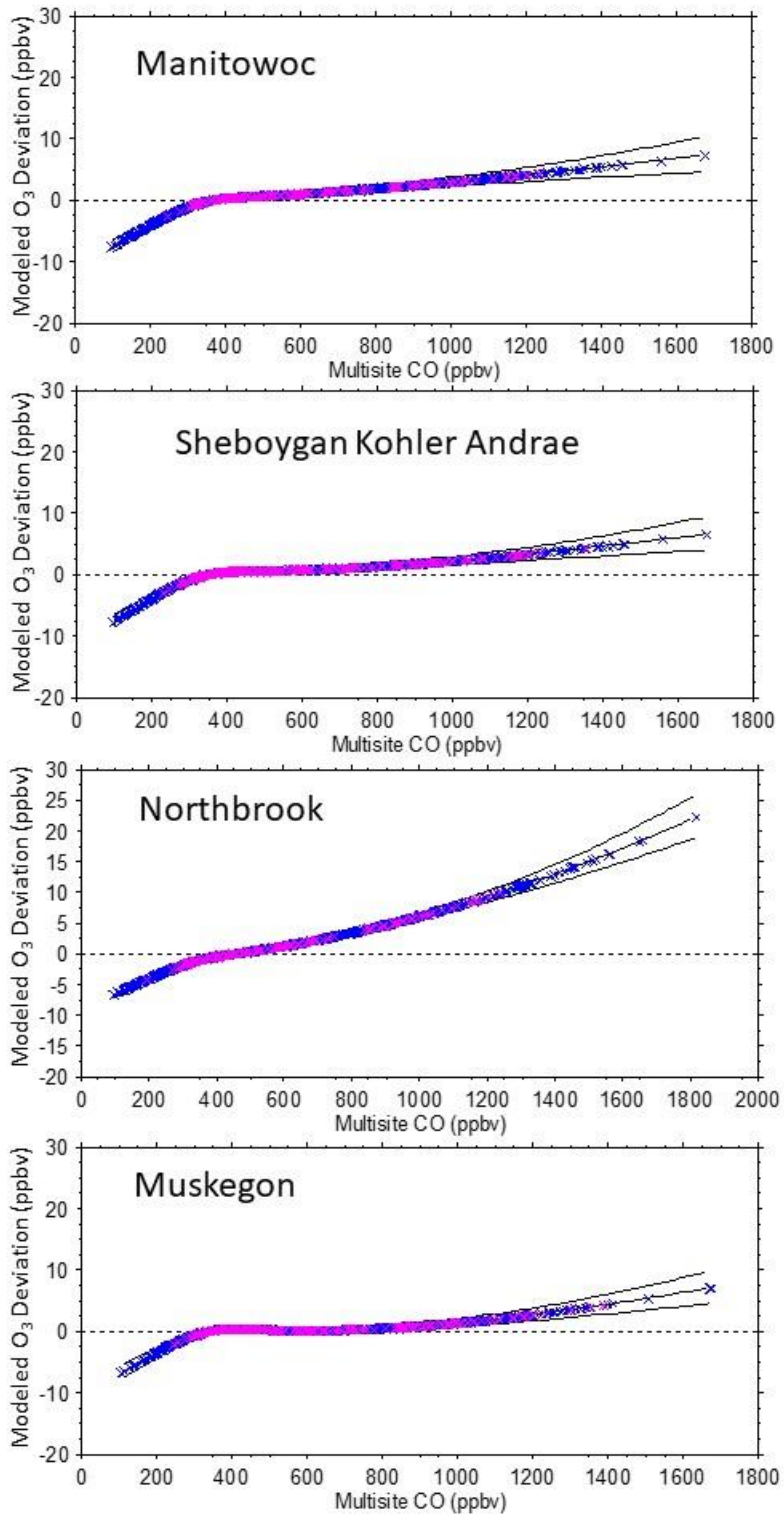


Figure 26. Modeled O<sub>3</sub> sensitivity ( $\pm 1$  SE) to multisite daily-average CO, 2000 - 2019. MDA8 O<sub>3</sub> values exceeding 70 ppbv are color-coded lavender.

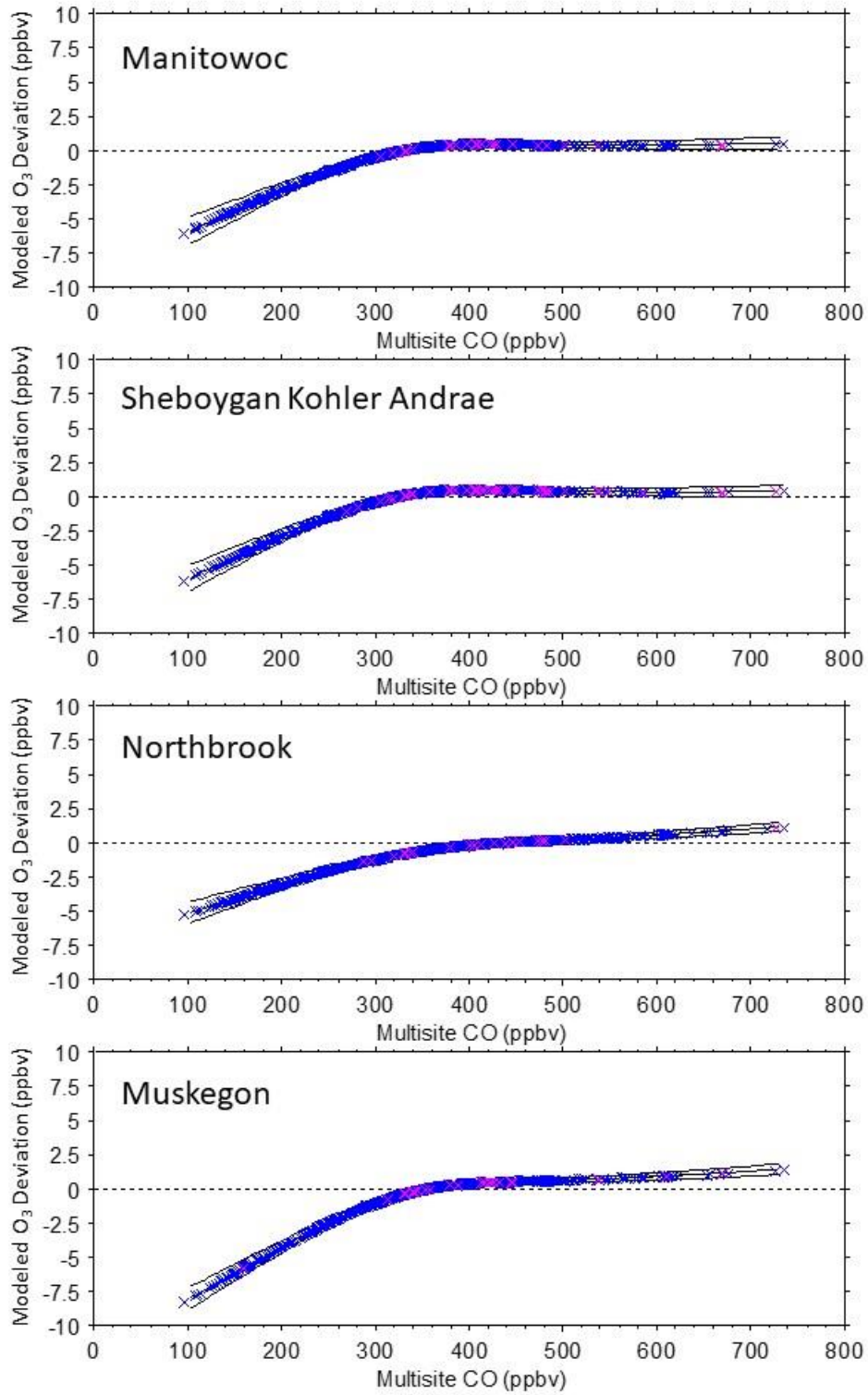


Figure 27. Modeled O<sub>3</sub> sensitivity ( $\pm 1$  SE) to multisite daily-average CO, 2015 - 2019. MDA8 O<sub>3</sub> values exceeding 70 ppbv are color-coded lavender.

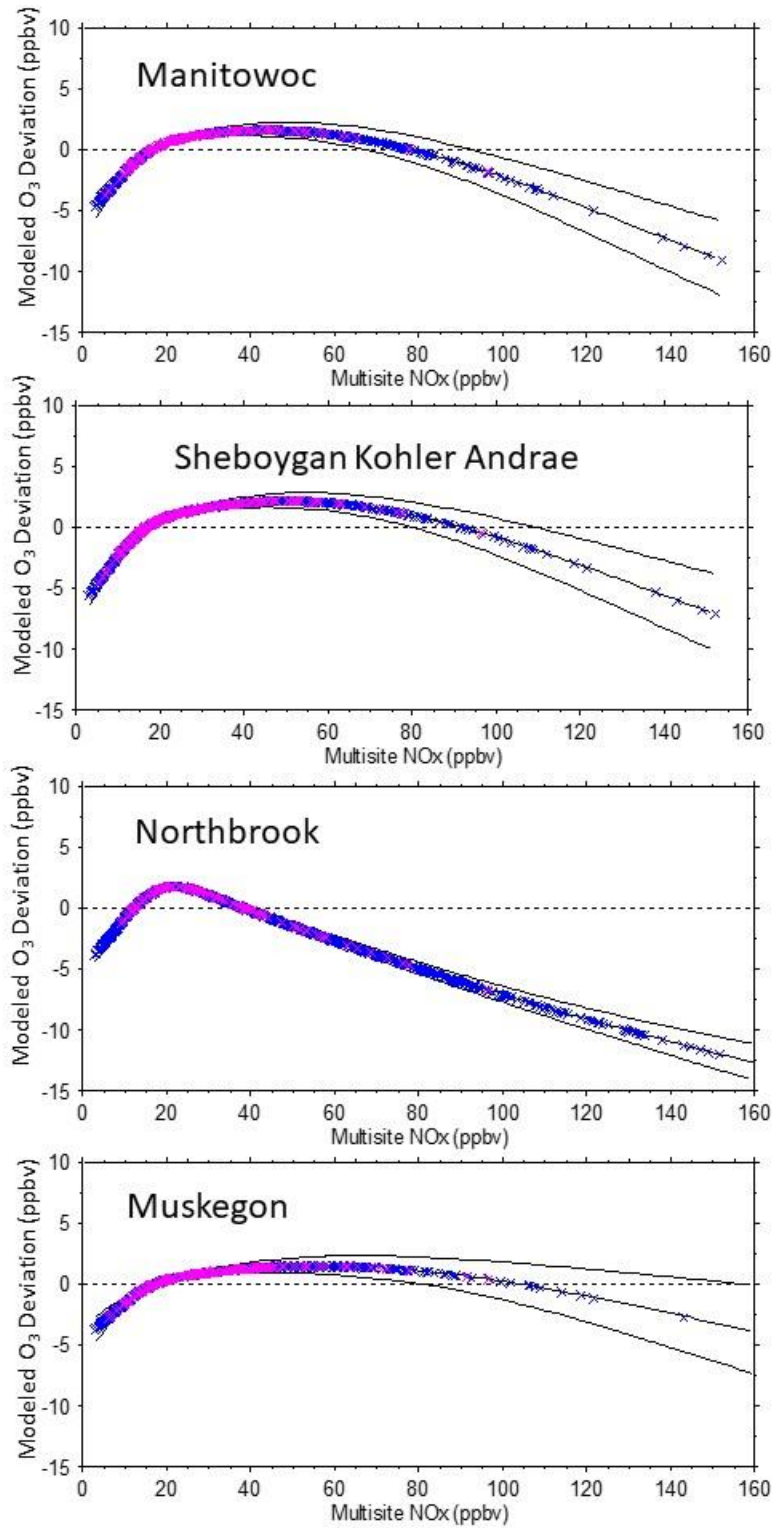


Figure 28. Modeled O<sub>3</sub> sensitivity ( $\pm 1$  SE) to multisite daily-average NO<sub>x</sub>, 2000 - 2019. MDA8 O<sub>3</sub> values exceeding 70 ppbv are color-coded lavender.

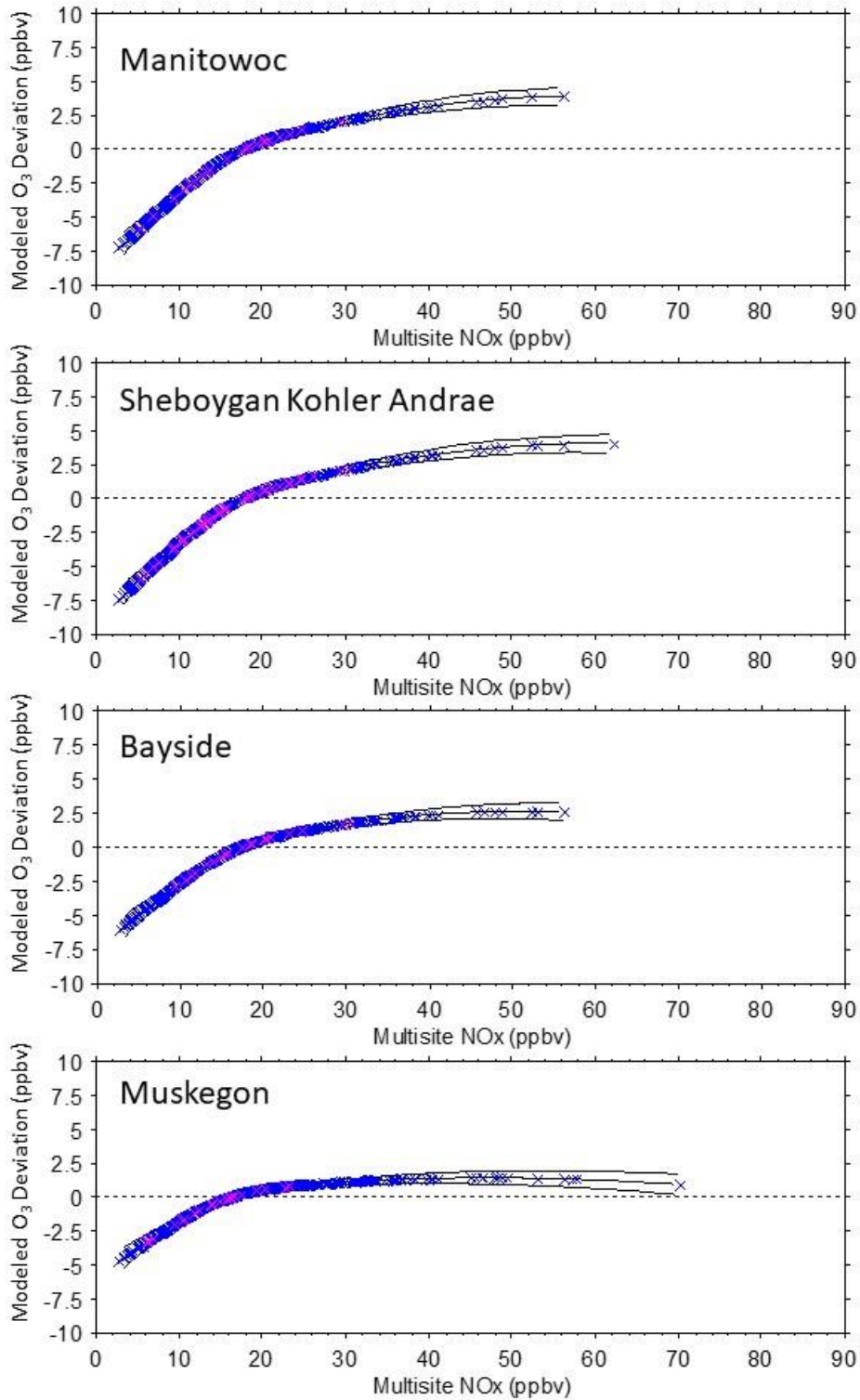


Figure 29. Modeled O<sub>3</sub> sensitivity ( $\pm 1$  SE) to multisite daily-average NO<sub>x</sub>, 2015 – 2019. MDA8 O<sub>3</sub> values exceeding 70 ppbv are color-coded lavender.

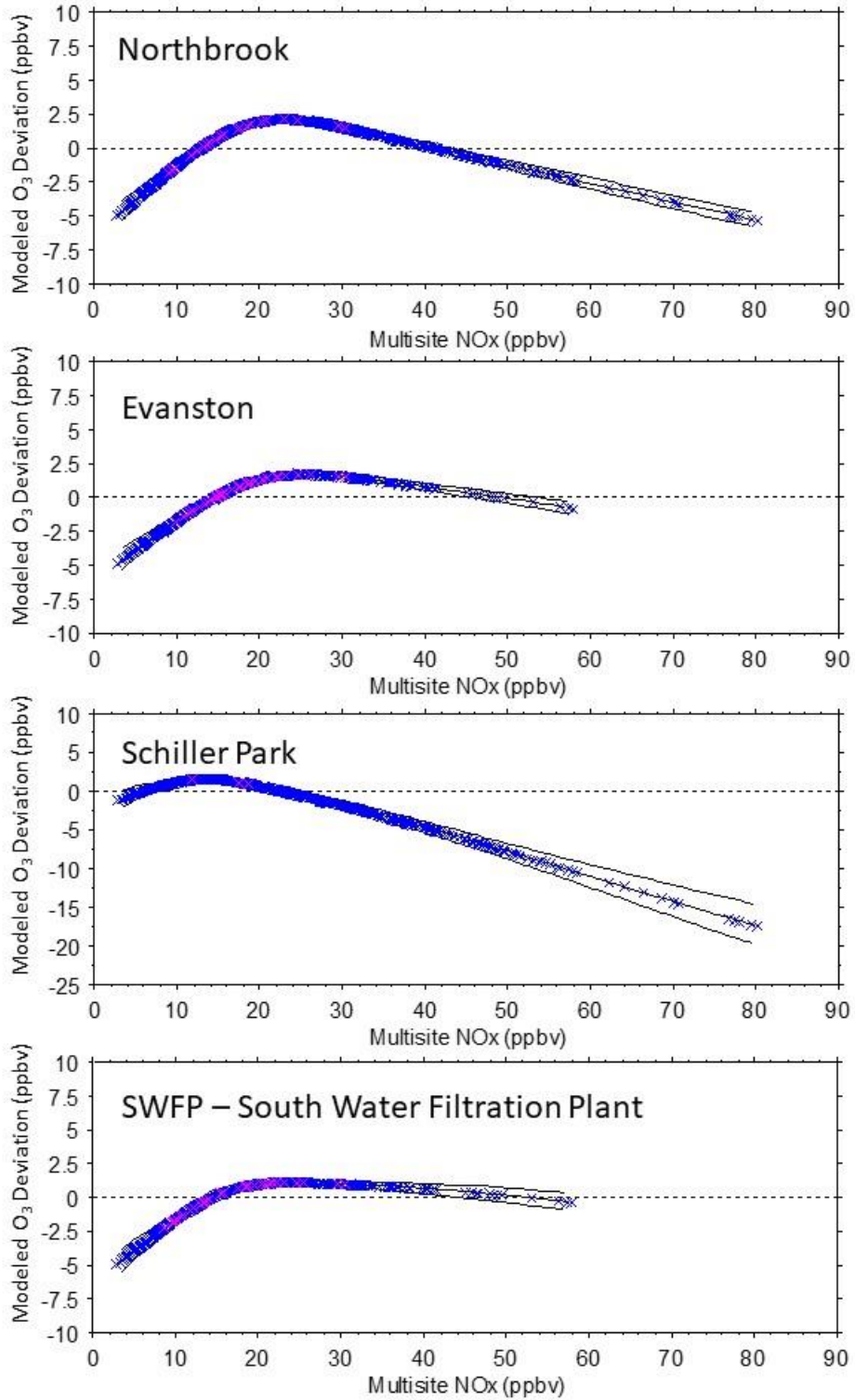


Figure 30. Modeled O<sub>3</sub> sensitivity ( $\pm 1$  SE) to multisite daily-average NO<sub>x</sub>, 2015 – 2019, Chicago sites. MDA8 O<sub>3</sub> values exceeding 70 ppbv are color-coded lavender.

Figures 31 and 32 combine the individual O<sub>3</sub> sensitivities to CO and NO<sub>x</sub> to generate O<sub>3</sub> response surfaces for Sheboygan Kohler Andrae and Northbrook. The response surfaces are nonlinear and reveal a ridgeline for each site. It is possible to define the ridgeline using various criteria. To illustrate, two lines are shown in each graph. First, as an approximation of the vertical tangent to each bin-range isopleth (i.e., CO is fixed and  $\Delta O_3/\Delta NO_x = 0$ ), the minimum CO concentration was found for each O<sub>3</sub> bin having positive O<sub>3</sub> deviations. Then, the NO<sub>x</sub> concentrations associated with each CO minimum were identified. The solid lines were then determined by regressing the NO<sub>x</sub> values associated with each CO minimum against the corresponding CO concentrations. For fixed CO, O<sub>3</sub> decreases as NO<sub>x</sub> concentrations either increase or decrease from the points on the solid lines. The solid lines therefore define the CO/NO<sub>x</sub> ratios where O<sub>3</sub> formation is maximal.

The dashed lines show equal CO – NO<sub>x</sub> responsiveness, which is a second possible criterion for identifying a ridgeline. For each day, the GAM fit determines O<sub>3</sub> deviations due to CO and to NO<sub>x</sub>. The set of points where these deviations are equal indicates the CO/NO<sub>x</sub> ratios having equal CO – NO<sub>x</sub> responsiveness.

Kohler Andrae MDA8 O<sub>3</sub> values exceeding 70 ppbv tend to fall within regions having the highest O<sub>3</sub> for given values of CO and NO<sub>x</sub> (Figure 31). Most of the Kohler Andrae annual 4<sup>th</sup>-highest MDA8 O<sub>3</sub> values are close to the dashed lines that show equal CO – NO<sub>x</sub> responsiveness.

Consistent with Figures 29 and 30, Northbrook shows a higher fraction of NO<sub>x</sub>-inhibited days, i.e., days falling above the solid lines in Figures 31 and 32. However, the placement of these lines is uncertain at low CO and NO<sub>x</sub> concentrations (<300 ppbv and <30 ppbv, respectively), characteristic of more recent years, due to the uneven distribution of data points. Because the isopleths have a sharp bend (strong NO<sub>x</sub> inhibition at higher NO<sub>x</sub> concentrations), the dashed lines that show equal CO – NO<sub>x</sub> responsiveness are short. They do not extend above the solid lines, where higher CO yields higher O<sub>3</sub> but higher NO<sub>x</sub> yields lower O<sub>3</sub>.

This section has shown the GAM-determined sensitivities to CO and NO<sub>x</sub> concentrations graphically for selected sites. In the next section, the GAM is used in a predictive mode to quantify the effects of hypothetical changes in emissions and precursor concentrations at all sites.

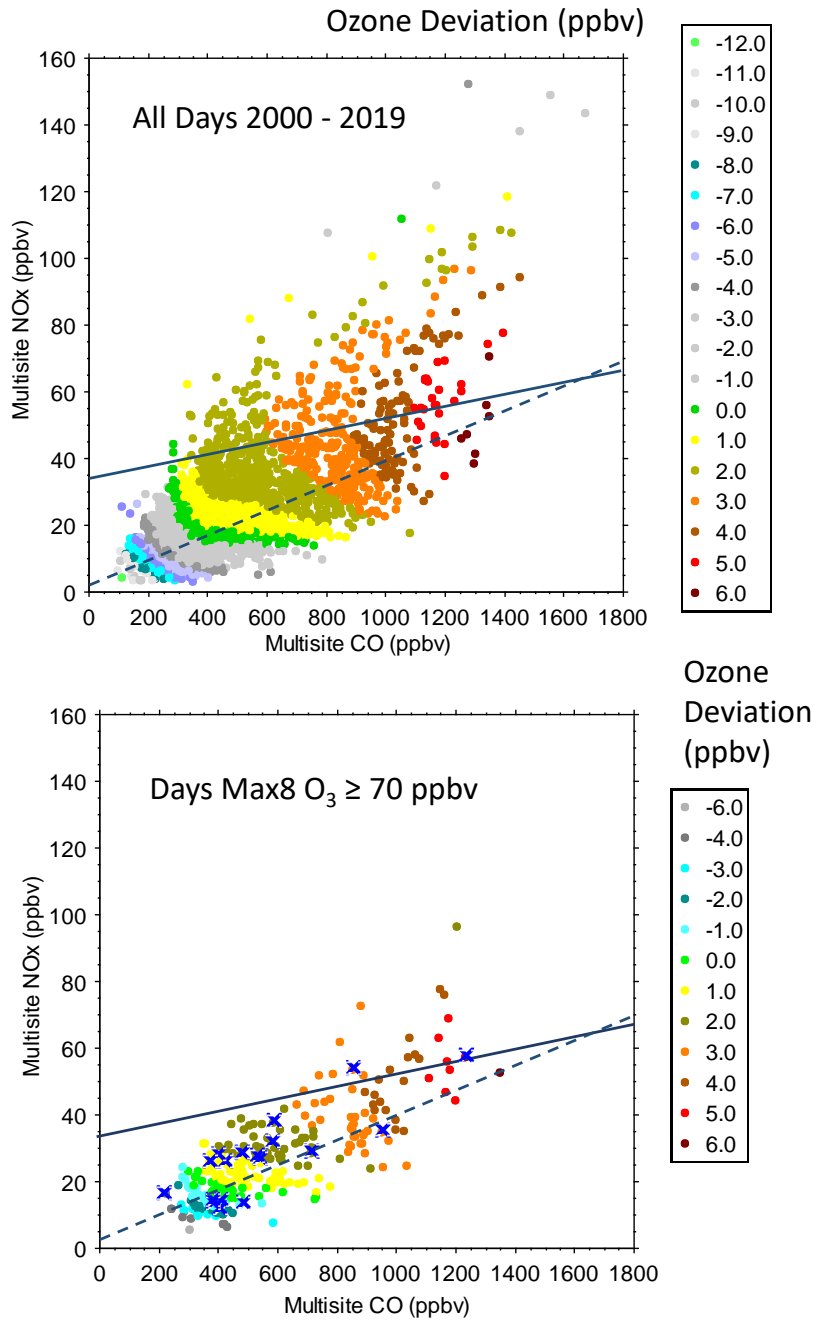


Figure 31. Sheboygan Kohler Andrae modeled O<sub>3</sub> sensitivity to multisite daily-average CO and NO<sub>x</sub>, 2000 – 2019, all days (top) and days with MDA8 O<sub>3</sub> values exceeding 70 ppbv (bottom). Annual 4<sup>th</sup>-highest MDA8 O<sub>3</sub> values are marked by “x” in the lower panel. As an approximation of  $\Delta O_3 / \Delta NO_x = 0$ , solid lines connect the NO<sub>x</sub> concentrations associated with minimum CO in each O<sub>3</sub> bin having positive O<sub>3</sub> deviations. Dashed lines show equal CO – NO<sub>x</sub> responsiveness.

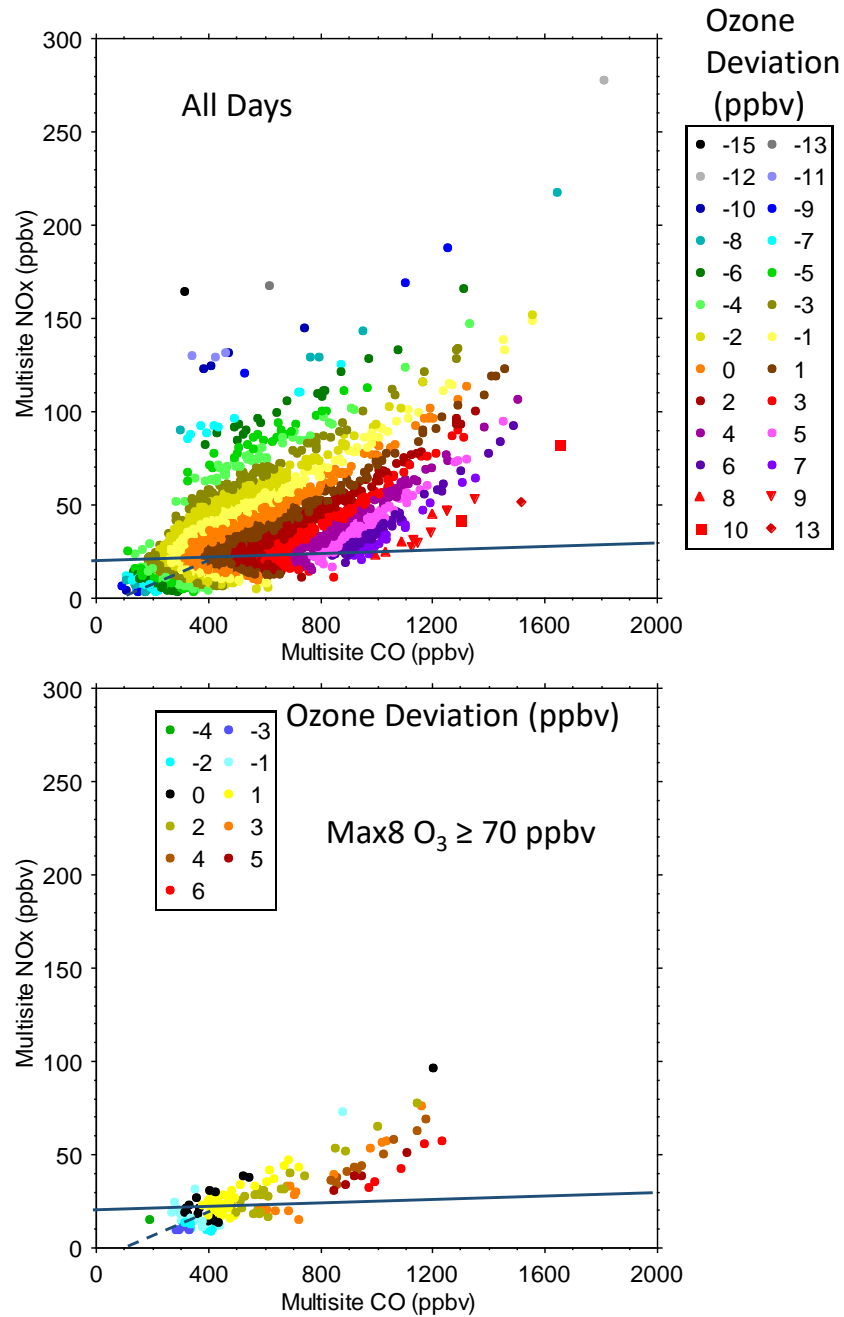


Figure 32. Northbrook modeled O<sub>3</sub> sensitivity to multisite daily-average CO and NO<sub>x</sub>, 2000 – 2019, all days (top) and days with MDA8 O<sub>3</sub> values exceeding 70 ppbv (bottom). As an approximation of  $\Delta O_3 / \Delta NO_x = 0$ , solid lines connect the NO<sub>x</sub> concentrations associated with the minimum CO in each O<sub>3</sub> bin having positive O<sub>3</sub> deviations. Dashed lines show equal CO – NO<sub>x</sub> responsiveness.

## 5.6 GAM Predictions

The GAM was used to predict the response of MDA8 O<sub>3</sub> at each site to hypothetical reductions in emissions and ambient precursor concentrations. All predicted responses are relative to base-case days during 2015 through 2019. Predictions were accomplished by applying the fitted site models to base-case input data that were modified in three alternate ways: (1) by reducing the sum of VOC and NO<sub>x</sub> emissions but leaving ambient concentrations of precursors unchanged, (2) by reducing the sum of VOC and NO<sub>x</sub> emissions and coupling these hypothetical emissions with various scenarios for ambient concentration reductions, or (3) by leaving emissions unchanged but reducing ambient precursor concentrations.

As discussed in Section 5.5.3, the GAM links O<sub>3</sub> trends to trends in both emissions and ambient precursor concentrations. Since multisite mean concentrations of CO, NO<sub>x</sub>, and NMOC tracked annual emissions (Section 9.4.1), some hypothetical scenarios are illustrative rather than expected, specifically (1) emission reductions without ambient concentration changes and (2) reductions in ambient concentrations without emission changes. Such scenarios serve to separate predicted O<sub>3</sub> responses to annual emissions from responses to daily precursor concentrations. This separation potentially distinguishes larger from smaller spatial and temporal scales. It is also useful for understanding the predicted O<sub>3</sub> responses at sites where mean O<sub>3</sub> has been increasing (i.e., Chicago sites) compared with other locations (Section 5.5.3).

Two levels of emission reduction were tested: 10% and 40%. The 10% emission reduction represents a relatively small departure from the base case, thus providing insight into current O<sub>3</sub> sensitivity. The 40% emission reduction is sufficiently large to represent O<sub>3</sub> responsiveness to a hypothetical decadal trend. For comparison, the sum of VOC and NO<sub>x</sub> emissions declined by 42% between 2009 and 2019 (Figure 1).

The ambient concentration reductions were 0%, 10%, 20%, and 40%. Historically, VOC and NO<sub>x</sub> emissions declined together, though at different rates (Section 9.4.1). Between 2009 and 2019, NO<sub>x</sub> emissions declined by 53% and VOC emissions declined by 29%. The historical emission reduction was therefore more strongly NO<sub>x</sub>-focused. The GAM predictions for the emission reduction scenarios implicitly represent a continuation of the historical balance of VOC and NO<sub>x</sub> emission reductions. Coupling the hypothetical 10% and 40% emission decreases with differing magnitudes of ambient reductions (including 0%) allows the GAM to depart from the historical VOC/NO<sub>x</sub> emission ratio. The 40% reduction scenarios were chosen to obtain a larger O<sub>3</sub> response given the predicted sensitivities to precursor concentrations (Section 5.5.3).

Scenarios are summarized in Table 6. Summary results were compiled from the predicted daily changes in MDA8 O<sub>3</sub> at each site relative to the 2015 – 2019 base case. Jardine was excluded because sampling there ended in 2012. The comparisons reported here focus on higher O<sub>3</sub> days (MDA8 O<sub>3</sub> > 50 ppbv).

Table 6. Summary of prediction scenarios. X = base case, 10% emission reduction, and 40% emission reduction, all without ambient reductions. Y = scenarios with and without 10% emission reduction. Z = scenarios with and without 40% emission reduction.

Ambient NO <sub>x</sub> (% of 2015 – 29)	Ambient CO (% of 2015 – 2019)			
	60	80	90	100
100	Z		Y	X
90			Y	Y
80		Z		
60				Z

The predicted O<sub>3</sub> responses to 10% reductions of emissions and ambient concentrations throughout the distributions of high-O<sub>3</sub> (> 50 ppbv) days are shown in Figures 33a through 33e. Key points are:

- O<sub>3</sub> changes are consistent throughout the distributions in the sense that their magnitudes vary by less than 1 ppbv from the 5<sup>th</sup> to 95<sup>th</sup> percentile and the relative efficacy of the four scenarios is the same or nearly the same across percentiles at any given site.
- Ambient CO and NO<sub>x</sub> reductions are predicted to lower MDA8 O<sub>3</sub> throughout the distribution of values exceeding 50 ppbv. The magnitudes of the predicted reductions vary among sites from zero to 2 ppbv.
- For any single site, the O<sub>3</sub> differences between CO and NO<sub>x</sub> scenarios are less than 1 ppbv, which is smaller than the prediction uncertainties (1 SE = 0.3 – 0.7 ppbv for each of CO and NO<sub>x</sub> predictions, Figures 26 through 30).
- Although the CO and NO<sub>x</sub> 10% reduction scenarios did not show statistically significant differences at any individual site, NO<sub>x</sub> reductions yielded greater predicted O<sub>3</sub> decreases at 9 of 12 WI sites. The opposite was true at Sheboygan Haven, Kenosha, and Schiller Park. For Chiwaukee Prairie and the other three Chicago-area sites, 10% CO and NO<sub>x</sub> reductions yielded comparable predicted O<sub>3</sub> decreases. For MI sites, CO reductions were slightly (<0.5 ppbv) more effective than NO<sub>x</sub> reductions with respect to lowering predicted O<sub>3</sub>.
- Consistent with historical trends, combined VOC and NO<sub>x</sub> emission reductions increased predicted O<sub>3</sub> at Chicago sites, Kenosha, and Milwaukee. Increases were 0.5 to 1.5 ppbv.
- Combined reductions of emissions and ambient precursor concentrations reduced predicted O<sub>3</sub> except at Schiller Park (all percentiles) and Northbrook (80<sup>th</sup> percentile). The combined reductions lowered the predicted O<sub>3</sub> by 0.5 to 1.5 ppbv except at the lowest percentile (5<sup>th</sup>) at Milwaukee SER DNR.

Overall, the predictions indicate a geographical mosaic of O<sub>3</sub> sensitivity. They imply greater sensitivity to NO<sub>x</sub> along the WI shoreline north of Milwaukee and slightly greater sensitivity to CO (VOCs) at MI sites. NO<sub>x</sub>-inhibited O<sub>3</sub> is evident at Chicago-area sites and Kenosha.

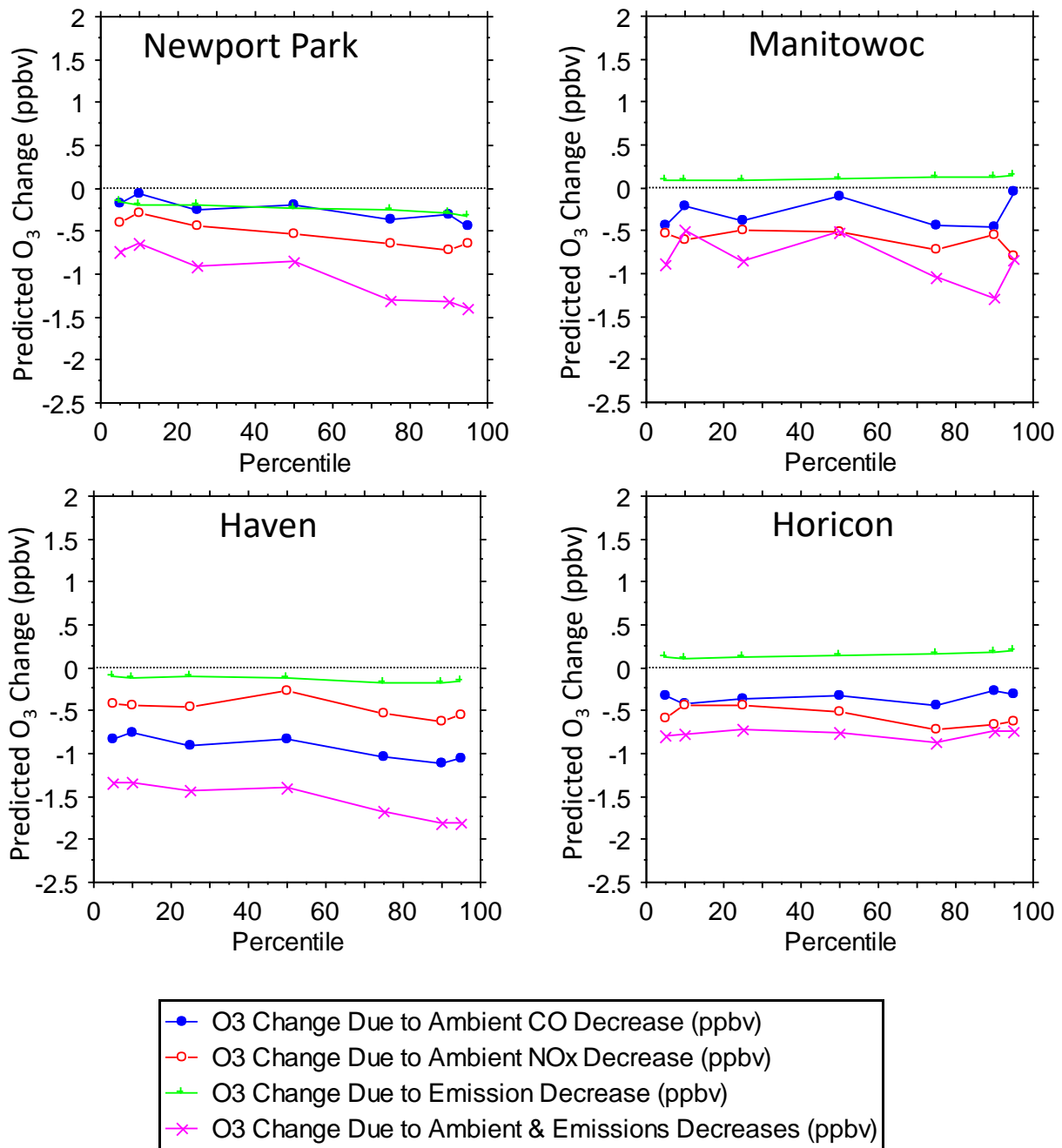


Figure 33a. Predicted O<sub>3</sub> changes at northern WI sites following 10% reductions of emissions or ambient precursor concentrations relative to 2015 – 2019 base cases versus percentile of the distributions of MDA8 O<sub>3</sub> (>50 ppbv).

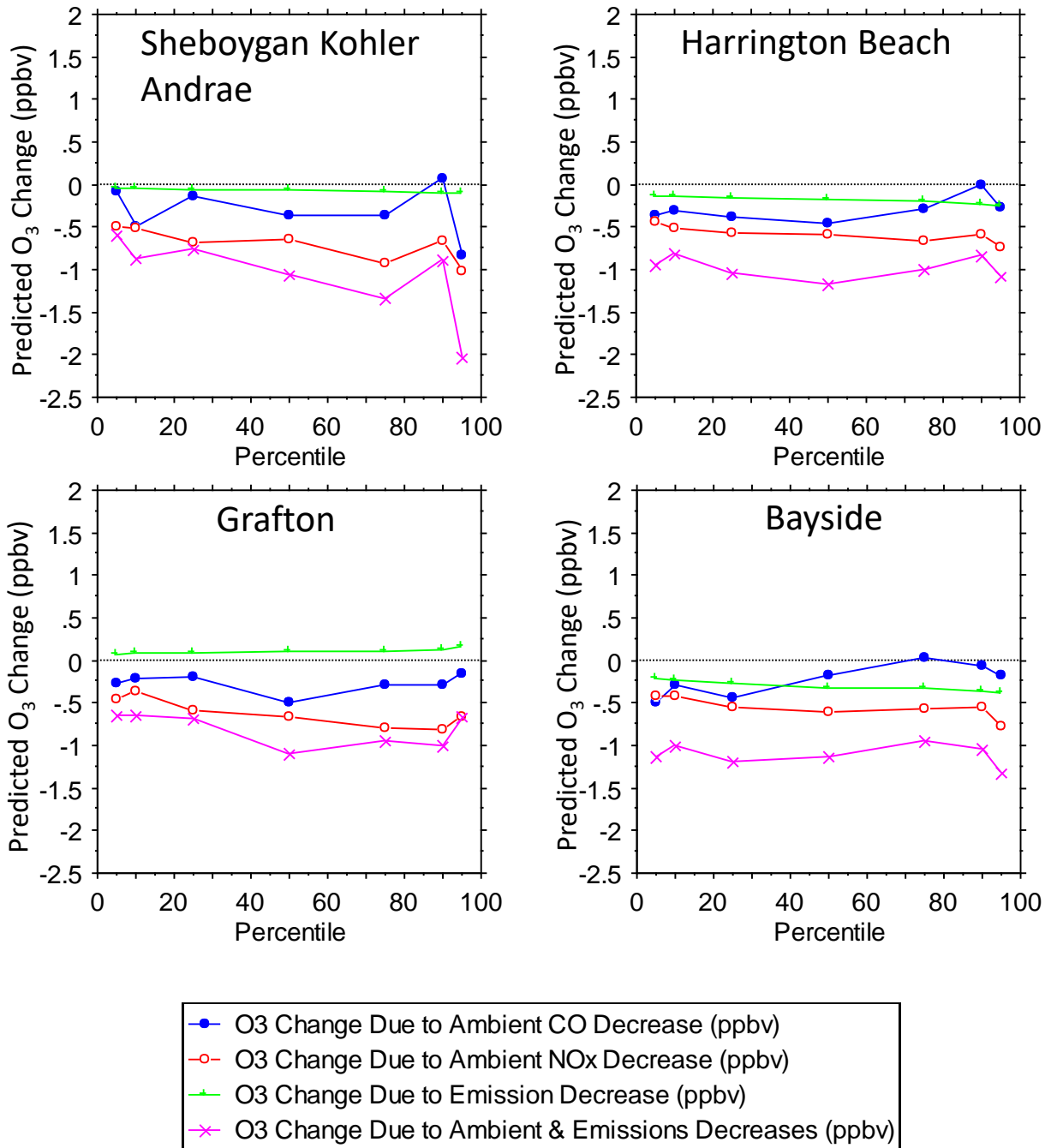


Figure 33b. Predicted O<sub>3</sub> changes at central shoreline WI sites following 10% reductions of emissions or ambient precursor concentrations relative to 2015 – 2019 base cases versus percentile of the distributions of MDA8 O<sub>3</sub> (>50 ppbv).

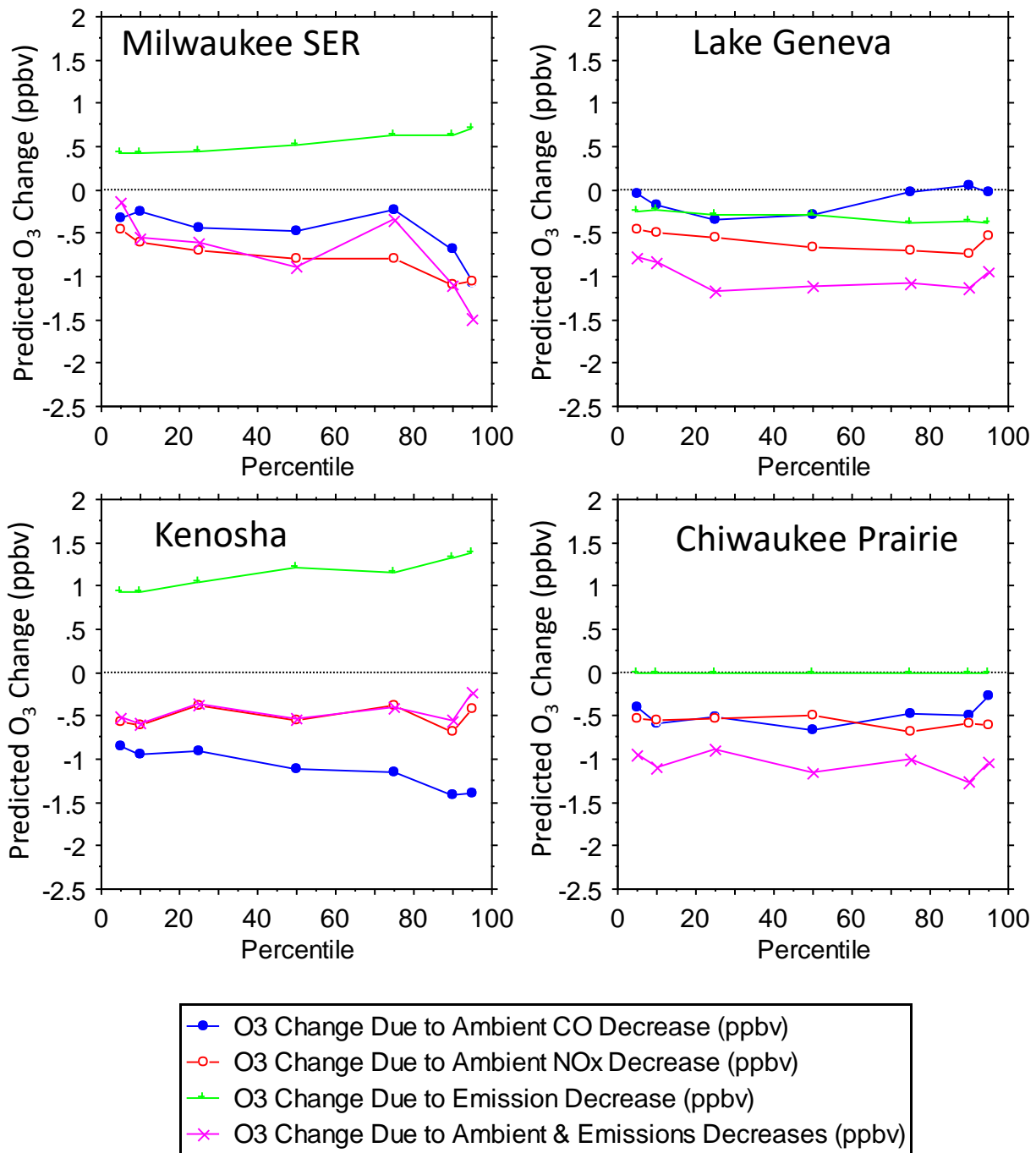


Figure 33c. Predicted O<sub>3</sub> changes at southern WI sites following 10% reductions of emissions or ambient precursor concentrations relative to 2015 – 2019 base cases versus percentile of the distributions of MDA8 O<sub>3</sub> (>50 ppbv).

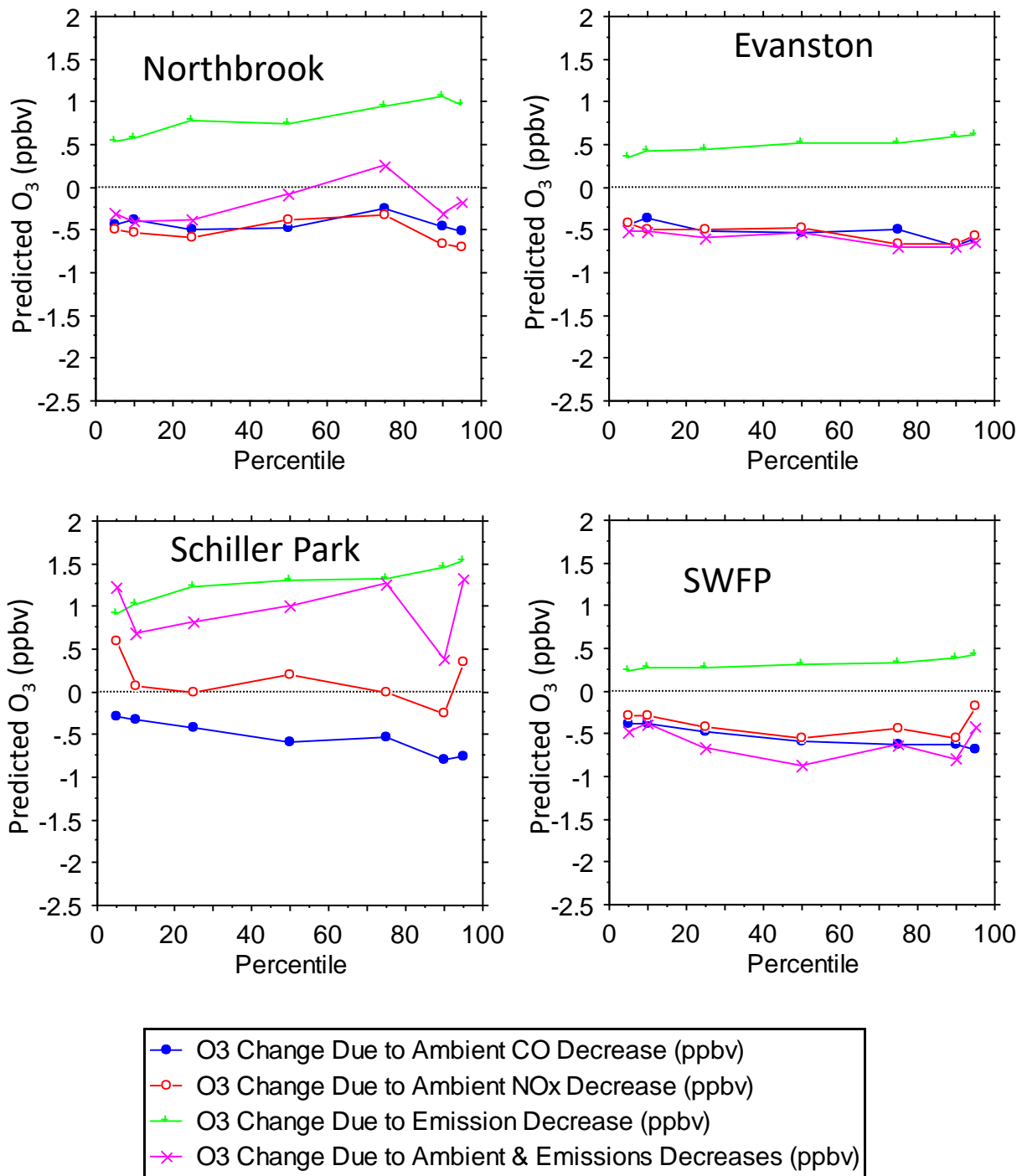


Figure 33d. Predicted O<sub>3</sub> changes at Chicago-area sites following 10% reductions of emissions or ambient precursor concentrations relative to 2015 – 2019 base cases versus percentile of the distributions of MDA8 O<sub>3</sub> (>50 ppbv).

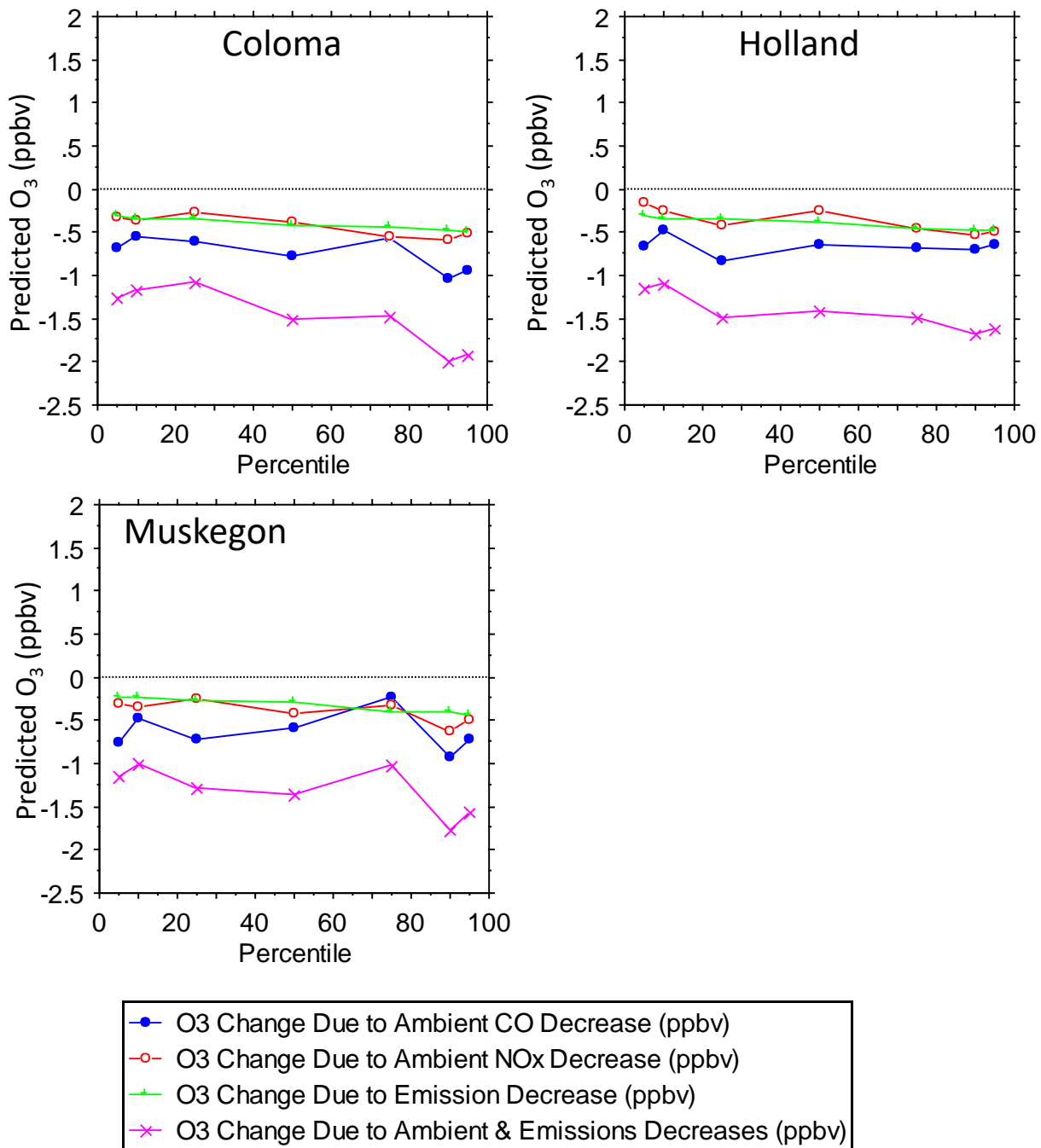


Figure 33e. Predicted O<sub>3</sub> changes at MI sites following 10% reductions of emissions or ambient precursor concentrations relative to 2015 – 2019 base cases versus percentile of the distributions of MDA8 O<sub>3</sub> (>50 ppbv).

The preceding results for 10% reductions of emissions and ambient concentrations were next compared to larger (20% or 40%) reductions as specified in Table 6. Figures 34a through 34d summarize the results for the 90<sup>th</sup> percentile of MDA8 O<sub>3</sub> values exceeding 50 ppbv. As previously noted, the predicted O<sub>3</sub> changes were consistent across percentiles of the 10% reduction scenarios, so the comparison of 10% to 40% reductions is simplified here by considering only the 90<sup>th</sup> percentiles. The 90<sup>th</sup> percentile is relevant to regulatory issues because it focuses on days close to the annual 4<sup>th</sup>-highest MDA8 O<sub>3</sub>. As an example, Sheboygan Kohler Andrae experienced 260 days with MDA8 O<sub>3</sub> > 50 ppbv between 2015 and 2019 (52 days per year, on average). The 90<sup>th</sup> percentile would therefore correspond to the average annual 5<sup>th</sup>-highest MDA8 O<sub>3</sub> (lower or higher depending on the year). For other sites, the 90<sup>th</sup> percentiles generally represent values comparable to the average annual 2<sup>nd</sup> through 6<sup>th</sup> highest MDA8 O<sub>3</sub>. The observed 90<sup>th</sup> percentiles are close to 70 ppbv at most sites (Figures 34a through 34d).

Larger (40%) reductions yielded larger predicted O<sub>3</sub> changes (up or down) than smaller (10%) reductions did. A larger O<sub>3</sub> reduction was predicted for some 40% precursor reductions than would be suggested by relatively small differences between the base case and 10% reductions. Examples include responses to CO reductions at Sheboygan Kohler Andrae, Grafton, Harrington Beach, and Bayside (Figures 34a and 34b). This type of nonlinearity is evident in the GAM sensitivity curves (Figure 27).

Table 7 provides a numerical tabulation of the results shown in Figures 34a through 34d. For all sites, both NO<sub>x</sub> and CO reductions led to lower predicted MDA8 O<sub>3</sub> (Table 6). For 11 sites, the combined precursor reduction (20% CO + 20% NO<sub>x</sub>) yielded less O<sub>3</sub> reduction than either of the single-precursor 40% reductions did. This result might occur if O<sub>3</sub> was more sensitive to one precursor than the other; a 40% reduction of the more limiting precursor would then yield a greater reduction than 20% reductions of each precursor. Alternatively or additionally, the result would be expected if the combined reduction kept conditions within a regime of highly efficient O<sub>3</sub> production (Figures 31 and 32), whereas single-pollutant reductions shifted O<sub>3</sub> production from more efficient VOC/NO<sub>x</sub> ratios to less efficient ratios.

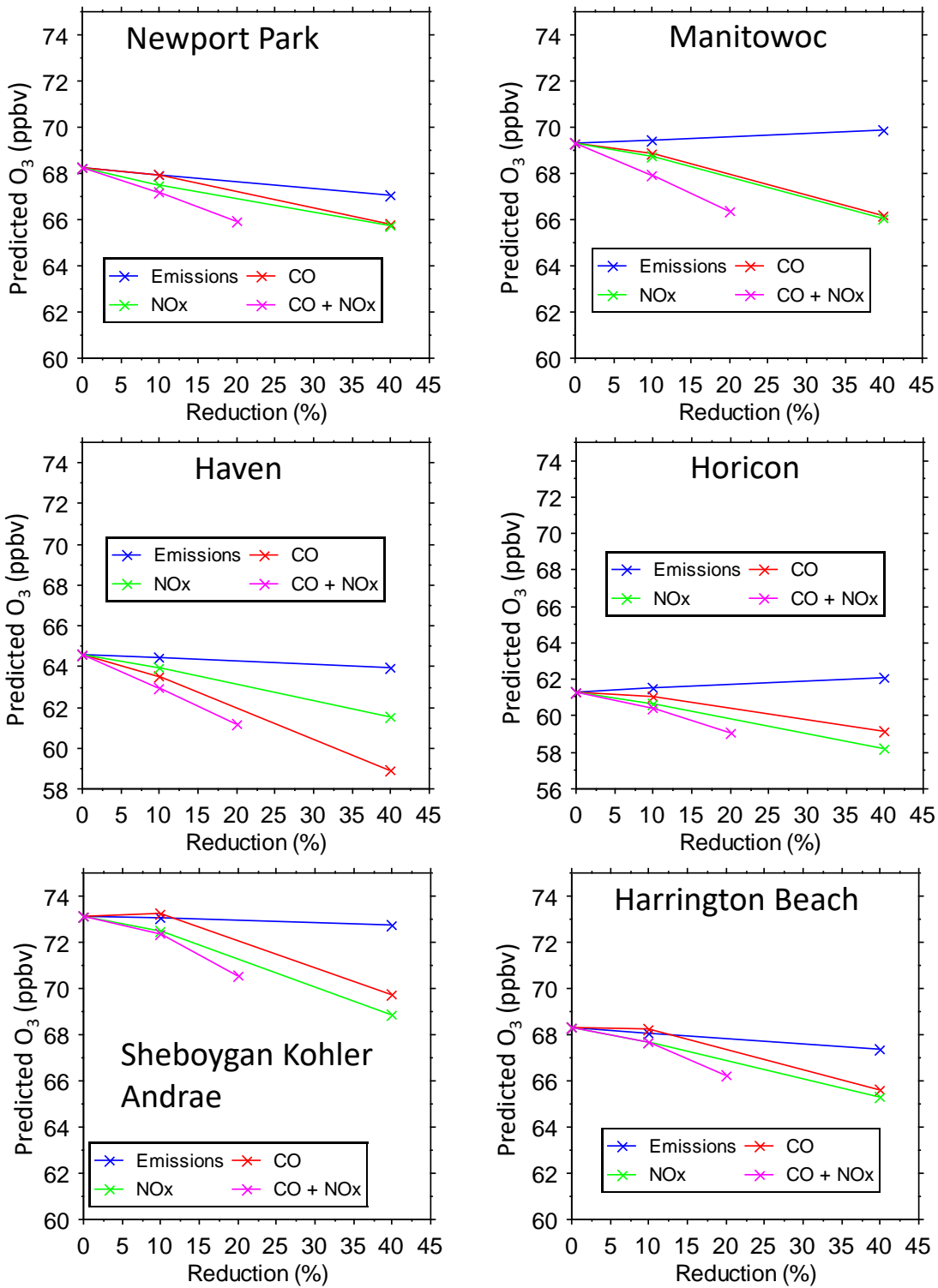


Figure 34a. Predicted 90<sup>th</sup> percentile (> 50 ppbv) O<sub>3</sub> at northern WI sites vs. magnitude of reductions of emissions or ambient precursor concentrations.

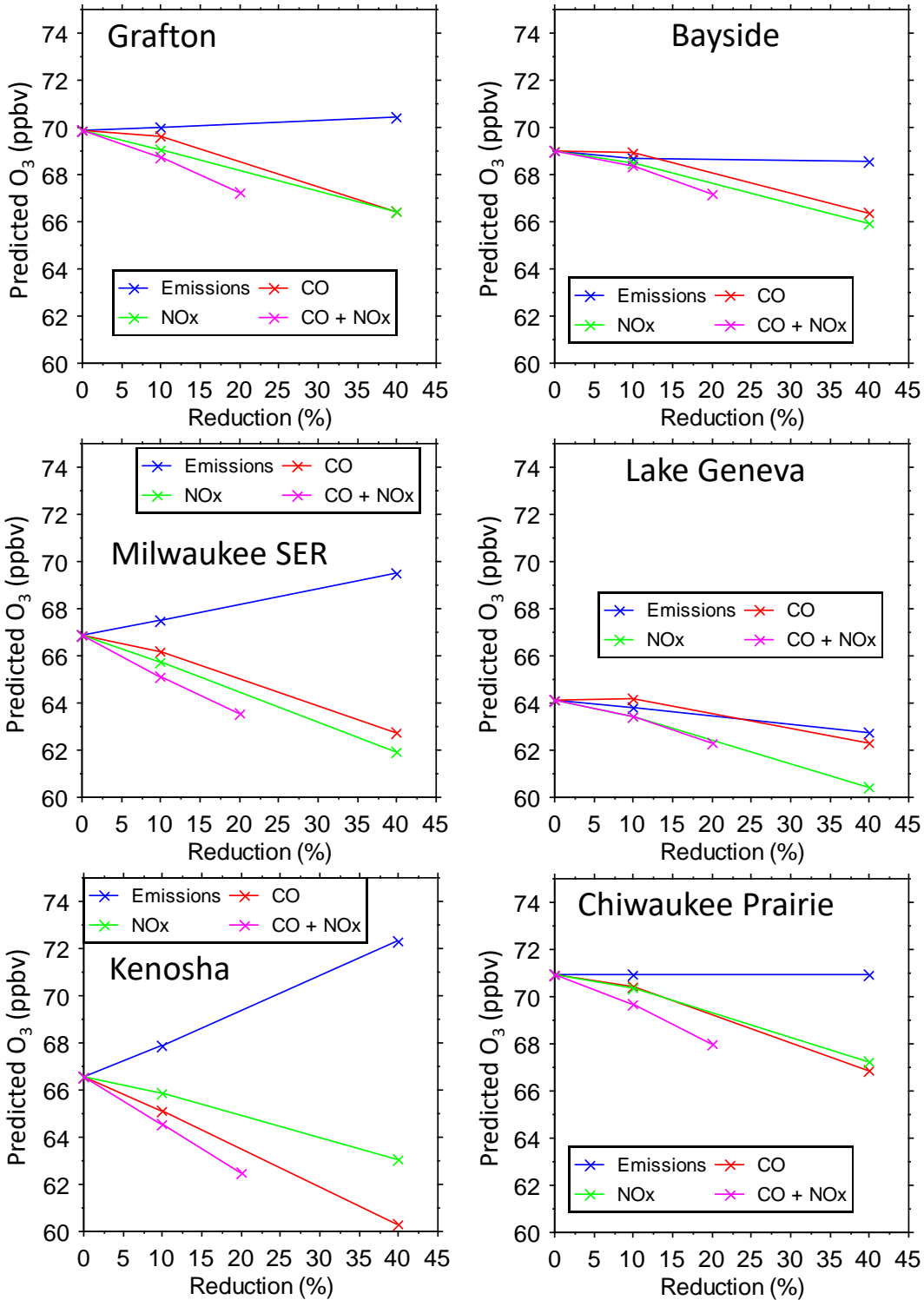


Figure 34b. Predicted 90<sup>th</sup> percentile (> 50 ppbv) O<sub>3</sub> at southern WI sites vs. magnitude of reductions of emissions or ambient precursor concentrations.

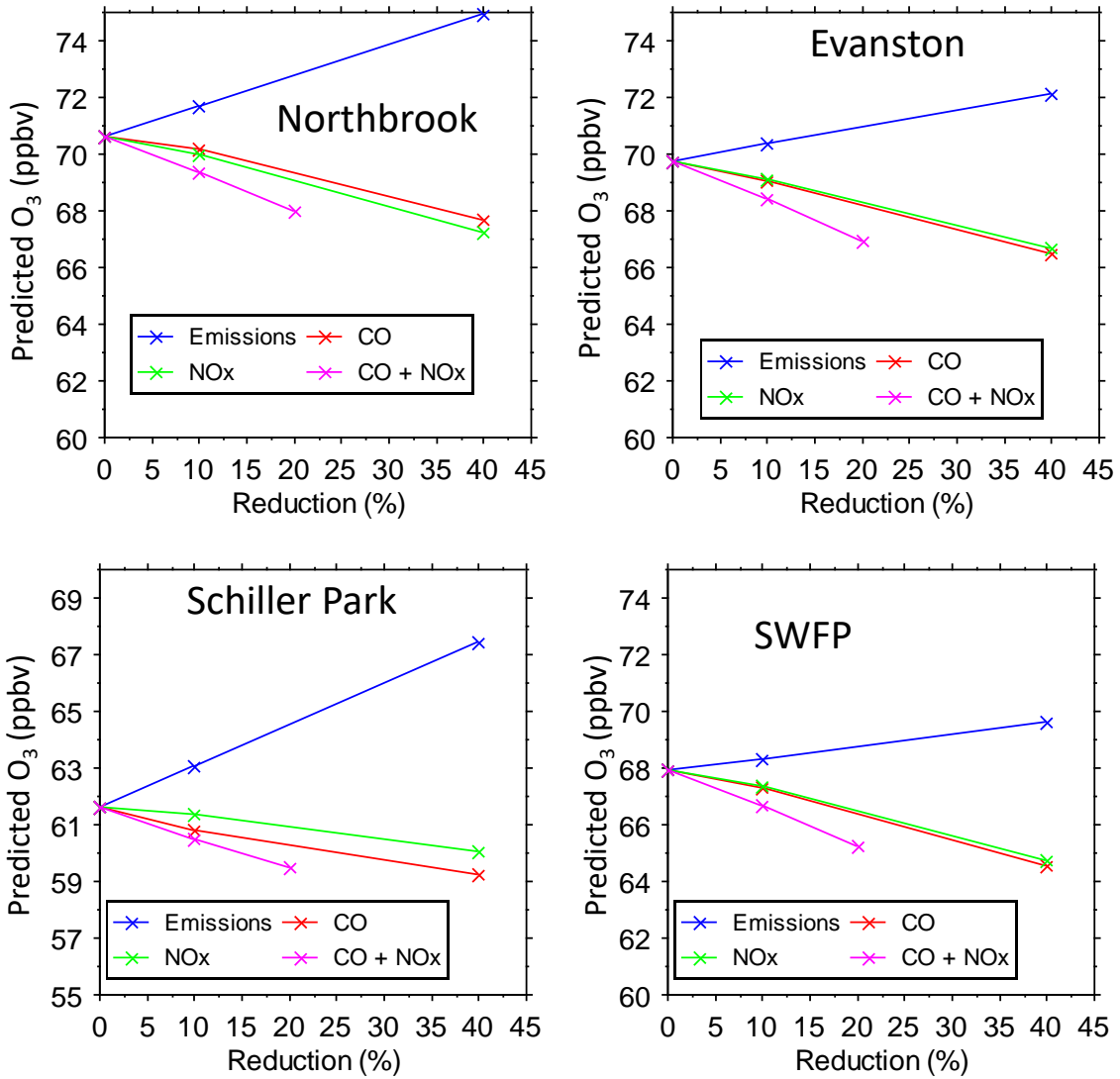


Figure 34c. Predicted 90<sup>th</sup> percentile (> 50 ppbv) O<sub>3</sub> at Chicago-area sites vs. magnitude of reductions of emissions or ambient precursor concentrations.

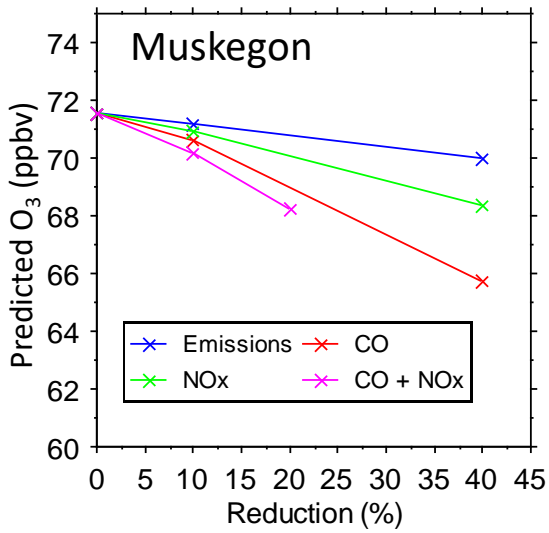
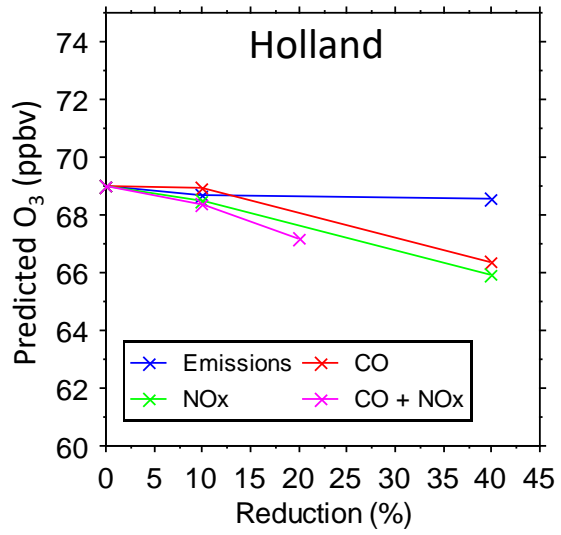
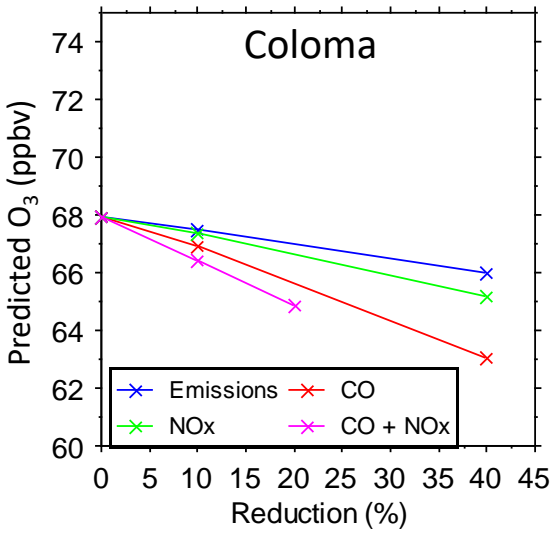


Figure 34d. Predicted 90<sup>th</sup> percentile (> 50 ppbv) O<sub>3</sub> at MI sites vs. magnitude of reductions of emissions or ambient precursor concentrations.

Table 7. Observed and predicted 90<sup>th</sup> percentiles of MDA8 O<sub>3</sub> exceeding 50 ppbv during 2015 through 2019. Differences between base-case predictions and predictions of MDA8 O<sub>3</sub> following reductions of ambient precursor concentrations are also shown. Wisconsin and Illinois sites are listed from north to south. Michigan sites are listed from south to north. Prediction uncertainties are ~1 ppbv (2 sigma).

Location	Days	Obs. MDA8 O <sub>3</sub>	Pred. MDA8 O <sub>3</sub>	Pred. O <sub>3</sub> after 40% Emission Decrease	Pred. O <sub>3</sub> after 40% CO Decrease	Pred. O <sub>3</sub> after Combined Decrease (20% CO, 20% NO <sub>x</sub> )	Pred. O <sub>3</sub> after 40% NO <sub>x</sub> Decrease	O <sub>3</sub> Decrease after 40% CO Decrease	O <sub>3</sub> Decrease after 20% CO and 20% NO <sub>x</sub> Decrease	O <sub>3</sub> Decrease after 40% NO <sub>x</sub> Decrease
All Sites	4480	70.0	68.6	69.6	65.0	65.8	65.4	3.6	2.8	3.2
Newport Pk	166	72.9	68.6	67.1	65.8	65.9	65.7	2.9	2.7	2.9
Manitowoc	191	71.4	69.6	69.8	66.2	66.4	66.1	3.4	3.2	3.6
SheboyganKA	260	73.0	73.3	72.7	69.8	70.6	68.9	3.5	2.7	4.4
Sheboy.Haven	177	68.8	64.6	63.9	58.9	61.2	61.5	5.7	3.4	3.1
Horicon	205	64.0	61.5	62.1	59.2	59.1	58.2	2.3	2.4	3.3
HarringtonBch	201	71.0	68.4	67.4	65.6	66.3	65.3	2.8	2.1	3.1
Grafton	215	71.0	70.3	70.4	66.5	67.2	66.4	3.9	3.1	3.9
Bayside	227	69.0	69.1	68.6	66.4	67.2	65.9	2.8	2.0	3.2
Milwaukee	197	67.8	67.1	69.5	62.7	63.5	62.0	4.4	3.6	5.2
Lake Geneva	163	67.0	64.2	62.7	62.3	62.3	60.5	1.9	1.9	3.8
Kenosha	273	69.0	66.6	72.3	60.3	62.5	63.1	6.3	4.1	3.5
Chiwaukee P	317	72.8	71.0	70.9	66.9	68.0	67.3	4.1	3.0	3.7
Northbrook	301	69.0	70.7	74.9	67.7	68.0	67.3	3.1	2.7	3.5
Evanston	320	70.5	69.8	72.1	66.5	66.9	66.7	3.3	2.8	3.1
Schiller Pk	132	65.3	61.7	67.4	59.2	59.5	60.0	2.4	2.1	1.6
SWFP	291	71.0	68.0	69.6	64.5	65.2	64.8	3.4	2.7	3.2
Coloma	298	69.0	68.0	66.0	63.1	64.9	65.2	4.9	3.1	2.8
Holland	295	69.0	70.1	68.3	65.7	67.3	67.4	4.4	2.9	2.7
Muskegon	251	69.0	71.6	70.0	65.7	68.2	68.4	5.9	3.4	3.2

A different way to consider the results is shown in Figure 35. NO<sub>x</sub>-reduction preference was greater for 10% reductions than for 40% reductions. The majority (9 of 12) of WI sites show a higher frequency of days when the decreases in ambient NO<sub>x</sub> concentrations yielded a greater reduction in MDA8 O<sub>3</sub> than the reductions in ambient CO did. The opposite was true for Chicago sites. For the three MI sites, the ambient NO<sub>x</sub> reductions yielded a larger O<sub>3</sub> reduction than CO did on only 2 to 32% of the days, depending on the magnitude of the reductions.

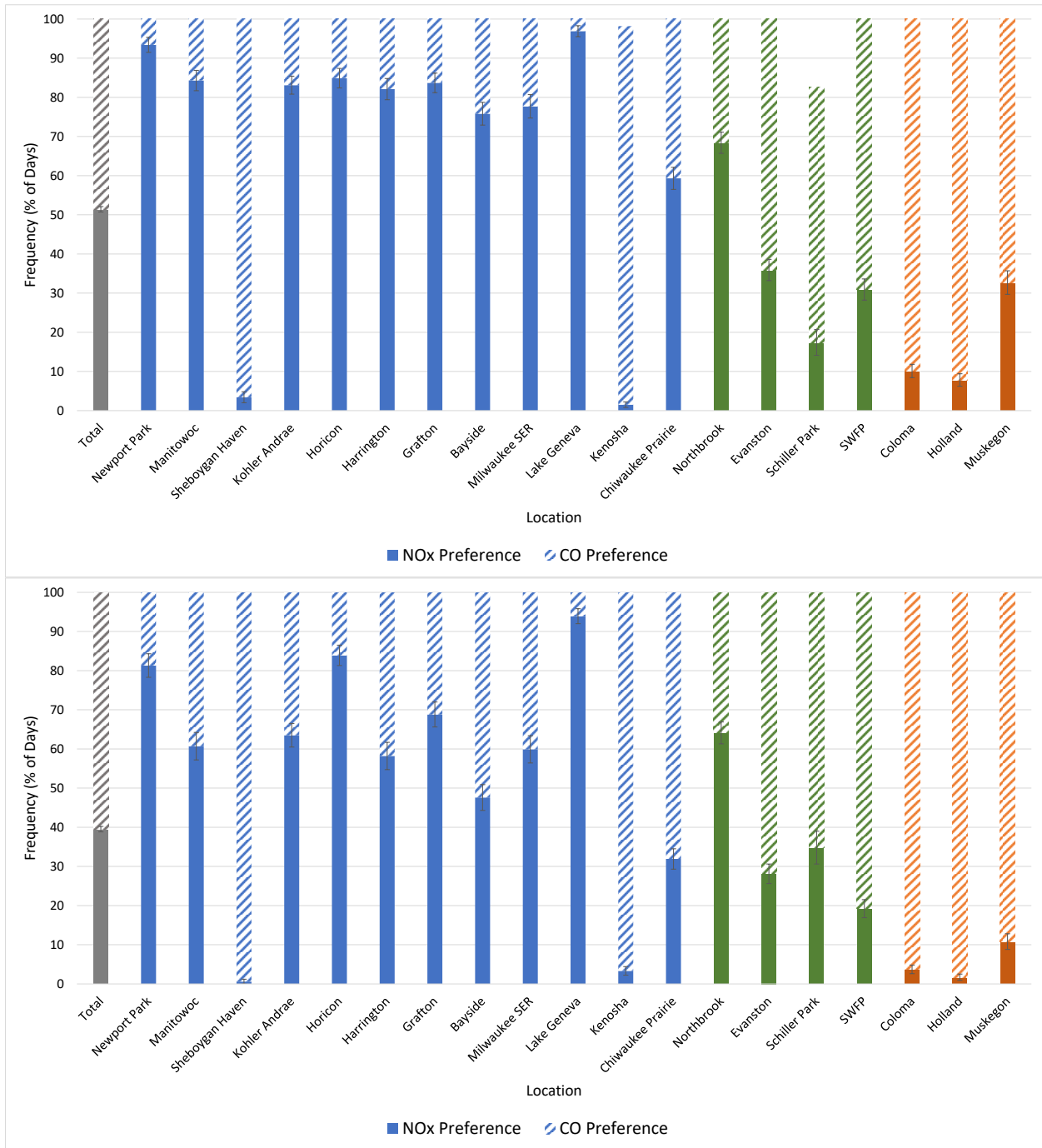


Figure 35. Frequencies of GAM predicted O<sub>3</sub> reductions (90<sup>th</sup> percentile of MDA8 O<sub>3</sub> > 50 ppbv) that were larger for reductions of ambient NO<sub>x</sub> (solid) or CO (hatched): (top) 10% reductions. (bottom) 40% reductions. Scenarios without emission reductions yielded indistinguishable results. Uncertainties are one standard error of the frequencies. Gray = all sites combined, blue = WI, green = IL, orange = MI.

## 5.7 Section Summary

A generalized additive model (GAM) was developed to predict MDA8 O<sub>3</sub> at twenty air-quality monitoring sites, focusing on WI shoreline locations along with additional IL and MI sites (Table 1, Figure 3). The WI sites are Newport Park, Manitowoc, Sheboygan Kohler Andrae, Sheboygan Haven, Harrington Beach, Grafton, Horicon/Mayville, Bayside, Milwaukee DNR SER, Lake Geneva, Kenosha, and Chiwaukee Prairie. IL sites are Northbrook, Evanston, Schiller Park, Jardine, and South Water Filtration Plant (Chicago). MI sites are Coloma, Holland, and Muskegon. Predictor variables included surface and upper-air weather data, temporal variables (day of week, day of year, starting hour of MDA8 O<sub>3</sub>), annual multistate (IN, IL, WI) VOC and NO<sub>x</sub> emissions, and multisite daily-average CO and NO<sub>x</sub> concentrations.

Performance statistics were compiled for multiple metrics. Statistical fit ( $R^2$ ) ranged from 0.64 to 0.78. Root-mean square error (RMSE) was computed for each site's full model and for reduced models (dropping each term while keeping all others). RMSE for the full models ranged from 6 to 8 ppbv. Additional forecasting metrics included percent of model predictions correctly above or below an MDA8 O<sub>3</sub> threshold of 70 ppbv, false alarm rate (incorrect predictions > threshold divided by total predictions > threshold), and probability of detection (correct predictions > threshold divided by total observations > threshold).

The GAM identified statistically-significant ( $p < 0.05$ ) sensitivities of MDA8 O<sub>3</sub> to multiple weather variables. Ozone-season MDA8 O<sub>3</sub> varied with daily maximum surface temperature (Tmax) exceeding ~10° C, other factors remaining constant. The predicted MDA8 O<sub>3</sub> increased by ~20 – 30 ppbv as Tmax increased from 20 to over 30° C. RH, Lake Michigan surface temperature, and daily maximum solar radiation (SRmax) were each associated with ~5 – 20 ppbv nonlinear predicted changes in MDA8 O<sub>3</sub>. Consistent with known principles, MDA8 O<sub>3</sub> increased with (1) decreasing RH, (2) decreasing Lake Michigan surface water temperature, and (3) increasing SRmax. The positive relationship of O<sub>3</sub> with SRmax is consistent with photochemical processing. Lower Lake Michigan surface water temperatures potentially increase the strength of the lake breeze because they can set up a stronger lake-land pressure gradient. The lake breeze effect was explicitly captured in the sensitivities of MDA8 O<sub>3</sub> to mid-day (1800 UTC) wind direction (WD), which showed predicted maxima in the directions from each site toward Lake Michigan. In addition, the daily-average WD was statistically significant. The sensitivities to upper-air variables together represent MDA8 O<sub>3</sub> responses to synoptic-scale weather. MDA8 O<sub>3</sub> increased with decreasing 500 mb WS, therefore associating higher O<sub>3</sub> with synoptic-scale air mass stagnation.

The day of year was statistically significant at 19 of 20 sites, with higher predicted MDA8 O<sub>3</sub> between days 100 and 200 often peaking on or about day 160. Since other weather variables explicitly represented meteorological seasonality, the day of the year is likely related to seasonal emissions variations. Seasonal VOC variations potentially include evaporative emissions (which are temperature sensitive), fuels composition, and biogenic emissions.

When the highest MDA8 O<sub>3</sub> occurred beginning between about noon and 6 p.m., it was higher than when starting hours were earlier or later. This sensitivity is consistent with lower MDA8 O<sub>3</sub> occurring when O<sub>3</sub> formation was cut off in the early afternoon, for example by cloud cover,

precipitation, or fresh NO emissions, so that O<sub>3</sub> could not reach its maximum potential level. Lower predicted MDA8 O<sub>3</sub> also occurred for starting hours later than 6 p.m., potentially associated with O<sub>3</sub> formation that began later in the day or when air masses were transported to downwind locations and experienced greater dilution and dispersion.

The GAM found sensitivities of O<sub>3</sub> to variations in three types of variables related to emissions and ambient precursor concentrations: (1) annual-average multistate (IN, IL, WI) VOC and NO<sub>x</sub> emissions, (2) daily-average multisite concentrations of CO and NO<sub>x</sub>, and (3) day of week. The annual emissions term was statistically significant at 15 of 20 sites (6 downward, 8 upward, 5 not significant). The GAM associated the annual emissions trend with trends in the ozone-season average MDA8 O<sub>3</sub>, which were downward at 15 sites and upward at Chicago-area locations. Differences between GAM-predicted emission-related O<sub>3</sub> trends and trends in ozone-season average MDA8 O<sub>3</sub> were smaller than the statistical uncertainties.

Long-term trends in MDA8 O<sub>3</sub> extrema (>90<sup>th</sup> percentile) were downward except at some Chicago sites, but upward trends were common in the 50<sup>th</sup> and 75<sup>th</sup> percentiles. Ambient precursor concentrations also exhibited long-term downward trends, though they were input to the GAM as daily concentrations.

The day of week was statistically significant at 17 of 20 sites. Since GAM inputs included daily averages of CO and NO<sub>x</sub> concentrations, the GAM predicted that O<sub>3</sub> on weekends was 1 – 4 ppbv higher than on weekdays even when both types of days had the same concentrations of CO and the same concentrations of NO<sub>x</sub>. The result implies that other emissions (e.g., evaporative VOCs) were higher on weekends or O<sub>3</sub> formation was more efficient on weekends than on weekdays (potentially due to more favorable VOC/NO<sub>x</sub> ratios).

GAM-predicted sensitivities of daily MDA8 O<sub>3</sub> to daily-average CO and NO<sub>x</sub> concentrations showed (1) a nonlinear positive response to daily-average CO and (2) both positive and negative responses to daily-average NO<sub>x</sub>. Most sites exhibited both NO<sub>x</sub>-limited and NO<sub>x</sub>-inhibited days for MDA8 O<sub>3</sub> exceeding 70 ppbv. When the data were restricted to recent years (2015 – 2019), only Chicago-area sites clearly showed NO<sub>x</sub>-inhibited days with MDA8 O<sub>3</sub> exceeding 70 ppbv.

The GAM was used to predict O<sub>3</sub> responses to 10% reductions of emissions or ambient precursor concentrations, which indicated that:

- The magnitudes of the predicted O<sub>3</sub> changes varied by less than 1 ppbv across the 5<sup>th</sup> to 95<sup>th</sup> percentiles of the distributions of daily O<sub>3</sub> exceeding 50 ppbv.
- Ambient CO and NO<sub>x</sub> reductions were predicted to lower MDA8 O<sub>3</sub> by zero to 2 ppbv throughout the distribution of values exceeding 50 ppbv.
- The predicted O<sub>3</sub> for CO and NO<sub>x</sub> reductions differed by less than 1 ppbv, which was smaller than the prediction uncertainties (1 SE = 0.3 – 0.7 ppbv for CO and NO<sub>x</sub> predictions).
- Although the CO and NO<sub>x</sub> 10% reduction scenarios did not show statistically significant differences at any individual site, NO<sub>x</sub> reductions yielded greater predicted O<sub>3</sub> decreases at 9 of 12 WI sites. The opposite was true at Sheboygan Haven, Kenosha, and Schiller Park.
- Consistent with historical trends, combined VOC and NO<sub>x</sub> emission reductions increased predicted O<sub>3</sub> at Chicago sites, Kenosha, and Milwaukee. Increases were 0.5 to 1.5 ppbv.

- Combined reductions of emissions and ambient precursor concentrations reduced predicted O<sub>3</sub> except at Schiller Park and Northbrook (80<sup>th</sup> percentile only) by 0.5 to 1.5 ppbv.

Larger (40%) reductions yielded larger predicted O<sub>3</sub> changes (up or down) than smaller (10%) reductions did. The predicted O<sub>3</sub> reduction was larger for some 40% precursor reductions than would be suggested by linear scaling of the 10% reductions. NO<sub>x</sub>-reduction preference was greater for 10% reductions than for 40% reductions of emissions and precursors.

Overall, the predictions indicate a geographical mosaic of O<sub>3</sub> sensitivity. They imply greater sensitivity to NO<sub>x</sub> along the WI shoreline north of Milwaukee and slightly greater sensitivity to CO (VOCs) at MI sites. NO<sub>x</sub>-inhibited O<sub>3</sub> is evident at Chicago-area sites and Kenosha.

## 6. Synthesis

Previous studies indicate that O<sub>3</sub> formation is generally VOC-responsive in and near the Chicago metropolitan area but transitions into NO<sub>x</sub>-sensitive conditions at varying downwind distances on high-O<sub>3</sub> days:

- Modeling studies associated with the 1991 LMOS and with recent work indicated that VOC emission reductions lowered O<sub>3</sub> in and near Chicago more effectively than NO<sub>x</sub> reductions did, but the opposite was true further downwind (e.g., Wisconsin shoreline) (Kaleel, 2015).
- O<sub>3</sub> isopleths from modeling based on 1996 emissions showed predicted VOC-sensitive O<sub>3</sub> concentrations in the Chicago urban core (Reynolds et al., 2004).
- Vermeuel et al. (2019) suggest that O<sub>3</sub> production over the urban Chicago source region was strongly VOC sensitive and progressed towards a more NO<sub>x</sub>-sensitive regime as the plume advected north along the Lake Michigan coastline on June 2, 2017, which was the 1<sup>st</sup>, 2<sup>nd</sup>, or 3<sup>rd</sup>-highest O<sub>3</sub> day at Wisconsin shoreline sites that year.
- Measurements made at the Sheboygan ground supersite during LMOS 2017 showed the influence of the lake breeze and indicated that O<sub>3</sub> formation was sometimes limited by NO<sub>x</sub> and sometimes limited by VOCs (Abdioskouei et al., 2019).
- Jin et al. (2020) used column measurements of HCHO and NO<sub>2</sub> with ground-level O<sub>3</sub> to infer that O<sub>3</sub> transitioned between VOC-sensitive and NO<sub>x</sub>-sensitive chemistry at 120 to 130 km from central Chicago in 1996 – 2000 and 30 to 60 km in 2013 – 2016.

The results reported here are consistent with the preceding findings and provide additional insights.

### 6.1 HCHO/NO<sub>2</sub> and NMOC/NO<sub>x</sub> Ratios

HCHO/NO<sub>2</sub> ratios were determined for three urban sites (Schiller Park, Northbrook, and Milwaukee SER DNR) and one non-urban site (Horicon/Mayville). Subject to day-to-day variability and uncertainty, the data are consistent with VOC sensitivity typically occurring at low (<0.3) HCHO/NO<sub>2</sub> ratios of 24-hour surface concentrations, a transition between 0.3 and 1, and NO<sub>x</sub> sensitivity at ratios exceeding one (1).

Most (50 – 86%) high-O<sub>3</sub> (> 50 ppbv) days showed low (<0.3) HCHO/NO<sub>2</sub> ratios at urban sites or fell into a transitional (or indeterminate) range of HCHO/NO<sub>2</sub> ratios of 0.3 – 1 at nonurban Horicon/Mayville (75%). On average, HCHO/NO<sub>2</sub> ratios increased from (1) Chicago to Milwaukee to rural Horicon/Mayville. These patterns indicate a tendency toward increasingly NO<sub>x</sub>-limited conditions from south-to-north, urban-to-rural, and low-to-high O<sub>3</sub>.

NMOC/NO<sub>x</sub> ratios were determined for two sites (Milwaukee SER DNR and Northbrook); they exhibit higher average values on weekends, during summer, and to some extent in more recent years. The patterns are qualitatively consistent with the expectation of increasingly NO<sub>x</sub>-limited O<sub>3</sub> formation as NO<sub>x</sub> emissions and ambient NO<sub>x</sub> concentrations decline.

## 6.2 O<sub>3</sub>/NO<sub>y</sub> Ratios

Day-specific slopes of hourly O<sub>3</sub> vs. NO<sub>z</sub> regressions were computed for four sites but were not robust indicators of O<sub>3</sub> sensitivity due to non-specific NO<sub>2</sub> measurements. Species-specific NO<sub>2</sub> measurements were made at Milwaukee SER DNR and Manitowoc beginning June 1, 2019.

Mid-day ratios of O<sub>3</sub>/NO<sub>y</sub> showed little correlation with ratios of HCHO/NO<sub>2</sub>. Different results were therefore obtained from these two indicator ratios for individual days.

The apparent transition ranges of mid-day (11 a.m. – 2 p.m.) O<sub>3</sub>/NO<sub>y</sub> ratios were specific to two study sites (Milwaukee SER DNR and Manitowoc) and largely qualitative. The percentages of high-O<sub>3</sub> (>50 ppbv) days at Milwaukee SER DNR with low (<7), transitional (7 – 12), and high (≥12) mid-day O<sub>3</sub>/NO<sub>y</sub> ratios were 22, 47, and 31%, respectively, between 2015 and 2019 (113 days). For Manitowoc, the percentages of high-O<sub>3</sub> (>50 ppbv) days with low (<9), transitional (9 – 14), and high (≥14) mid-day O<sub>3</sub>/NO<sub>y</sub> ratios were 10, 11, and 79%, respectively, between 2015 – 2019 (93 days).

Overall, the results indicate prevailing frequencies of transitional days at Milwaukee SER DNR and NO<sub>x</sub>-limited O<sub>3</sub> at Manitowoc. Compared with HCHO/NO<sub>2</sub> ratios, these results suggest a higher proportion of transitional compared with VOC-limited days at Milwaukee and a higher proportion of NO<sub>x</sub>-limited days at Manitowoc.

## 6.3 Generalized Additive Model (GAM)

A generalized additive model (GAM) was developed to predict MDA8 O<sub>3</sub> at twenty air-quality monitoring sites, focusing on WI shoreline locations along with additional IL and MI sites (Table 1, Figure 3). Predictor variables included surface and upper-air weather data, temporal variables (day of week, day of year, starting hour of MDA8 O<sub>3</sub>), annual multistate (IN, IL, WI) VOC and NO<sub>x</sub> emissions, and multisite daily-average CO and NO<sub>x</sub> concentrations.

Overall, the predictions indicated a geographical mosaic of O<sub>3</sub> sensitivity. They imply greater sensitivity to NO<sub>x</sub> along the WI shoreline north of Milwaukee and slightly greater sensitivity to CO (VOCs) at MI sites. NO<sub>x</sub>-inhibited O<sub>3</sub> was evident at Chicago-area sites and Kenosha.

The GAM identified statistically-significant ( $p < 0.05$ ) sensitivities of MDA8 O<sub>3</sub> to multiple weather variables. Ozone-season MDA8 O<sub>3</sub> varied with daily maximum surface temperature (T<sub>max</sub>) exceeding ~10° C, other factors remaining constant. The predicted MDA8 O<sub>3</sub> increased by ~20 – 30 ppbv as T<sub>max</sub> increased from 20 to over 30° C. RH, Lake Michigan surface temperature, and daily maximum solar radiation (SR<sub>max</sub>) were each associated with ~5 – 20 ppbv nonlinear predicted changes in MDA8 O<sub>3</sub>. Consistent with known principles, MDA8 O<sub>3</sub> increased with (1) decreasing RH, (2) decreasing Lake Michigan surface water temperature, and (3) increasing SR<sub>max</sub>. The positive relationship of O<sub>3</sub> with SR<sub>max</sub> is consistent with photochemical processing. Lower Lake Michigan surface water temperatures potentially increase the strength of the lake breeze because they can set up a stronger lake-land pressure gradient. The lake breeze effect was explicitly captured in the sensitivities of MDA8 O<sub>3</sub> to mid-day (1800 UTC) wind direction (WD), which showed predicted maxima in the directions from each site toward Lake Michigan. In addition, the daily-average WD was statistically significant. The

sensitivities to upper-air variables together represent MDA8 O<sub>3</sub> responses to synoptic-scale weather. MDA8 O<sub>3</sub> increased with decreasing 500 mb WS, therefore associating higher O<sub>3</sub> with synoptic-scale air mass stagnation.

The GAM found significant ( $p < 0.05$ ) sensitivities of O<sub>3</sub> to annual-average multistate (IN, IL, WI) VOC and NO<sub>x</sub> emissions at 15 of 20 sites. The GAM associated the annual emissions trend with trends in the ozone-season average MDA8 O<sub>3</sub>, which were downward at 15 sites and upward at Chicago-area locations. Differences between GAM-predicted emission-related O<sub>3</sub> trends and trends in ozone-season average MDA8 O<sub>3</sub> were smaller than the statistical uncertainties. Long-term trends in MDA8 O<sub>3</sub> extrema (>90<sup>th</sup> percentile) were downward except at some Chicago sites, but upward trends were common in the 20 sites' 50<sup>th</sup> and 75<sup>th</sup> percentiles.

The day of week was statistically significant at 17 of 20 sites. The GAM predicted that O<sub>3</sub> on weekends was 1 – 4 ppbv higher than on weekdays even when both types of days had the same concentrations of CO and the same concentrations of NO<sub>x</sub>. The result implies that other emissions (e.g., evaporative VOCs) were higher on weekends or O<sub>3</sub> formation was more efficient on weekends than on weekdays (potentially due to more favorable VOC/NO<sub>x</sub> ratios).

GAM-predicted sensitivities of daily MDA8 O<sub>3</sub> to daily-average CO and NO<sub>x</sub> concentrations showed (1) a nonlinear positive response to daily-average CO and (2) both positive and negative responses to daily-average NO<sub>x</sub>. Most sites exhibited both NO<sub>x</sub>-limited and NO<sub>x</sub>-inhibited days for MDA8 O<sub>3</sub> exceeding 70 ppbv. When the data were restricted to recent years (2015 – 2019), only Chicago-area sites clearly showed NO<sub>x</sub>-inhibited days with MDA8 O<sub>3</sub> exceeding 70 ppbv.

The GAM was used to predict O<sub>3</sub> responses to 10% reductions of emissions or ambient precursor concentrations, which indicated that:

- The magnitudes of the predicted O<sub>3</sub> changes varied by less than 1 ppbv across the 5<sup>th</sup> to 95<sup>th</sup> percentiles of the distributions of daily O<sub>3</sub> exceeding 50 ppbv.
- Ambient CO and NO<sub>x</sub> 10% reductions were predicted to lower MDA8 O<sub>3</sub> by zero to 2 ppbv throughout the distribution of values exceeding 50 ppbv.
- For any single site, the predicted O<sub>3</sub> for 10% CO and NO<sub>x</sub> reductions differed by less than 1 ppbv, which was smaller than the prediction uncertainties (1 SE = 0.3 – 0.7 ppbv).
- Although the CO and NO<sub>x</sub> 10% reduction scenarios did not show statistically significant differences at any individual site, NO<sub>x</sub> reductions yielded greater predicted O<sub>3</sub> decreases at 9 of 12 WI sites. The opposite was true at Sheboygan Haven, Kenosha, and Schiller Park.
- Consistent with historical trends, combined VOC and NO<sub>x</sub> emission reductions increased predicted O<sub>3</sub> at Chicago sites, Kenosha, and Milwaukee. Increases were 0.5 to 1.5 ppbv.
- Combined reductions of emissions and ambient precursor concentrations reduced predicted O<sub>3</sub> except at Schiller Park and Northbrook (80<sup>th</sup> percentile only) by 0.5 to 1.5 ppbv.

Larger (40%) emission and precursor reductions yielded larger predicted O<sub>3</sub> changes (up or down) than the 10% reductions did. For some 40% precursor reductions, the predicted O<sub>3</sub> reduction was larger than linear scaling of the 10% reductions would suggest. NO<sub>x</sub>-reduction preference was greater for 10% reductions than for 40% reductions of emissions and precursors.

## 7. Conclusions

### 7.1 VOC and NO<sub>x</sub> Limitation, Spatial Patterns, and Temporal Changes

Previous studies and this study all conclude that O<sub>3</sub> formation is generally VOC-responsive in and near the Chicago metropolitan area but transitions into NO<sub>x</sub>-sensitive conditions at varying downwind distances on high-O<sub>3</sub> days. The GAM indicates that O<sub>3</sub> formation is generally NO<sub>x</sub>-inhibited at Chicago-area monitoring sites. The GAM analyses also show that O<sub>3</sub> formation at the majority of study locations in WI and MI was in a regime in which O<sub>3</sub> was responsive to both VOC and NO<sub>x</sub> on high-O<sub>3</sub> days (> 50 ppbv) between 2015 and 2019. The majority (9 of 12) of WI sites showed a higher frequency of days when a hypothetical decrease in ambient NO<sub>x</sub> concentrations yielded a greater reduction in predicted MDA8 O<sub>3</sub> than a hypothetical reduction in ambient CO did. The opposite was true for Chicago-area sites. However, for any single site, the predicted O<sub>3</sub> responses to 10% CO and NO<sub>x</sub> reductions differed by less than 1 ppbv, which was smaller than the prediction uncertainties (1 SE = 0.3 – 0.7 ppbv). Ambient CO and NO<sub>x</sub> reductions of 10% relative to 2015 – 2019 concentrations were predicted to lower MDA8 O<sub>3</sub> by zero to 2 ppbv throughout the distribution of O<sub>3</sub> values exceeding 50 ppbv. Larger (40%) reductions of ambient CO and NO<sub>x</sub> were predicted to lower MDA8 O<sub>3</sub> by 2 to 6 ppbv.

Chicago sites showed counterproductive predicted O<sub>3</sub> increases of 1 to 6 ppbv in response to hypothetical multistate emission reductions ranging from 10% to 40% relative to 2015 – 2019 emissions.

GAM sensitivities of O<sub>3</sub> to CO and NO<sub>x</sub> showed increasingly NO<sub>x</sub>-responsive values between 2000 and 2019 as ambient NO<sub>x</sub> concentrations declined. Sensitivity indicators support this result.

The GAM identified large and statistically significant sensitivities of MDA8 O<sub>3</sub> to multiple weather variables. The predicted MDA8 O<sub>3</sub> increased by ~20 – 30 ppbv as daily maximum temperature increased from 20 to over 30° C. RH, Lake Michigan surface temperature, and daily maximum solar radiation (SRmax) were each associated with ~5 – 20 ppbv nonlinear predicted changes in MDA8 O<sub>3</sub>. The lake breeze effect was evident in the sensitivities of MDA8 O<sub>3</sub> to mid-day (1800 UTC) and daily-average wind directions. Predicted MDA8 O<sub>3</sub> responses to 850 mb and 500 mb weather variables associated higher O<sub>3</sub> with synoptic-scale stagnation.

### 7.2 Implications for Emission Control Strategies

Reductions of both VOC and NO<sub>x</sub> emissions are predicted to benefit sites in WI and MI. However, the results indicate that NO<sub>x</sub>-focused emission control strategies have had, and will continue to have, counterproductive effects at locations in the Chicago metropolitan area. Large (40%) reductions of both emissions and ambient precursor concentrations minimized the modeled counterproductive effect at three of four Chicago locations, but yielded only small (-0.5 – 1.8 ppbv) changes in predicted MDA8 O<sub>3</sub>. Further study of potential emission-control strategies would be informative.

### 7.3 Implications for Monitoring Needs

WI recently (mid 2019) installed high-sensitivity (0.04 ppbv detection limit) species-specific NO<sub>2</sub> instruments at Milwaukee SER and Manitowoc. These two sites also have NO<sub>y</sub> monitors.

Consideration should be given to placing high-sensitivity NO instruments at these locations. The minimum detection limit (MDL) of the current NO instruments (5 ppbv) is too high to allow reliable determination of NO<sub>z</sub> from the difference between NO<sub>y</sub> and NO<sub>x</sub>.

The present NMOC measurements are limited spatially to a small number of sites and temporally to 24-hour samples collected once every six days. As a result, the data are not useful for many kinds of data analyses, which often require continuous measurements. NMOC sampling is challenging due to cost and complexity.

Current understanding of O<sub>3</sub> could be enhanced by locating instruments for continuous measurement of NO, true NO<sub>2</sub>, NO<sub>y</sub>, and total NMOC at each site where high O<sub>3</sub> values continue to occur.

## 8. References

- Abdioskouei, M., Z. Adelman, J. Al-Saadi, T. Bertram, G. Carmichael, M. Christiansen, P. Cleary, A. Czarnetski, A. Dickens, M. Fuoco, M. Harkey, L. Judd, D. Kenski, D. Millet, B. Pierce, C. Stanier, B. Stone, J. Szykman, L. Valin, and T. Wagner. 2019. 2017 Lake Michigan Ozone Study (LMOS) Preliminary Finding Report. [https://www.ladco.org/wp-content/uploads/Research/LMOS2017/LMOS\\_LADCO\\_report\\_revision\\_apr2019\\_final.pdf](https://www.ladco.org/wp-content/uploads/Research/LMOS2017/LMOS_LADCO_report_revision_apr2019_final.pdf) (last access, July 27, 2020).
- Berkowitz, C. M., Jobson, T., Jiang, G., Spicer, C. W., and Doskey, P. V. 2004. Chemical and meteorological characteristics associated with rapid increases of O<sub>3</sub> in Houston, Texas. *J. Geophys. Res.* 109 (D10307). <https://doi.org/10.1029/2003JD004141>.
- Blanchard, C. L., S. L. Shaw, E. S. Edgerton, and J. J. Schwab. 2019. Emission influences on air pollutant concentrations in New York State : I. ozone. *Atmos. Environ. X*. <https://doi.org/10.1016/j.aeoa.2019.100033>.
- Blanchard, C. L. and G. M. Hidy. 2018. Ozone response to emission reductions in the southeastern United States. *Atmos. Chem. Phys.* 18 : 8183–8202. <https://doi.org/10.5194/acp-18-8183-2018>.
- Blanchard, C. L., G. M. Hidy, and S. Tanenbaum. 2014. Ozone in the southeastern United States: an observation-based model using measurements from the SEARCH network. *Atmos. Environ.* 88: 192-200. <http://dx.doi.org/10.1016/j.atmosenv.2014.02.006>.
- Blanchard, C. L., G. M. Hidy, S. Tanenbaum, E. Edgerton, and B. Hartsell. 2013. The Southeastern Aerosol Research and Characterization (SEARCH) study: temporal trends in gas and PM concentrations and composition, 1999-2010. *J. Air Waste Manage. Assoc.* 63: 247-259. doi: 10.1080/10962247.2012.748523.
- Blanchard, C. L., S. Tanenbaum, and J. Wilkinson. 2012. Corroborative and Weight-of-Evidence Development and Analyses. Final report prepared for San Joaquin Valleywide Air Pollution Study Agency, Central California Ozone Study.
- Blanchard, C. L., S. Tanenbaum, E. Fujita, J. Wilkinson, and D. Campbell. Effects of VOC and NO<sub>x</sub> emission changes on ozone and precursor concentrations in central California from 1990 to 2004. In: Steyn, D. G. and Rao, S. T. Air Pollution Modeling and Its Application XX. Proceedings of the 30<sup>th</sup> NATO/SPS International Technical Meeting on Air Pollution Modeling and its Application, San Francisco, California, U.S.A. 18-22 May 2009. pp. 587-590. Springer, The Netherlands, 2010.
- Blanchard, C. L., G. M. Hidy, S. Tanenbaum, R. Rasmussen, R. Watkins, and E. S. Edgerton. 2010b. NMOC, ozone, and organic aerosol in the southeastern United States, 1999-2007: 1. Spatial and temporal variations of NMOC concentrations and composition in Atlanta, Georgia. *Atmos. Environ.* 44: 4827 – 4839. doi:10.1016/j.atmosenv.2010.08.036.
- Blanchard, C. L., S. Tanenbaum, E. Fujita, D. Campbell, and J. Wilkinson. 2008. Understanding Relationships Between Changes in Ambient Ozone and Precursor Concentrations and Changes in VOC and NO<sub>x</sub> Emissions from 1990 to 2004 in Central California. Final Report, Contract No.

05-6CCOS, August 31, 2008. <https://www.arb.ca.gov/airways/ccos/ccos.htm> (last access, December 10, 2018).

Blanchard, C. L., S. Tanenbaum, and D. R. Lawson. 2008. Differences between weekday and weekend air pollutant levels in Atlanta; Baltimore; Chicago; Dallas–Fort Worth; Denver; Houston; New York; Phoenix; Washington, DC; and surrounding areas. *J. Air Waste Manage. Assoc.* 58: 1598–1615.

Blanchard, C. L., S. Tanenbaum, and G. M. Hidy. 2007. Effects of SO<sub>2</sub> and NO<sub>x</sub> emission reductions on PM<sub>2.5</sub> mass concentrations: regional comparisons. *J. Air Waste Manage. Assoc.* 57: 1337–1350.

Blanchard, C. L. and S. J. Tanenbaum. 2006. Weekday/weekend differences in ambient air pollutant concentrations in Atlanta and the southeastern U.S. *J. Air Waste Manage. Assoc.* 56: 271–284.

Blanchard, C. L. and D. Fairley. 2001. Spatial mapping of VOC and NO<sub>x</sub> limitation of ozone formation in central California. *Atmos. Environ.* 35: 3861–3873.

Blanchard, C. L. and T. Stoeckenius. 2001. Ozone response to precursor controls: comparison of data analysis methods with the predictions of photochemical air quality simulation models. *Atmos. Environ.* 35: 1203–1215.

Blanchard, C. L., P. M. Roth, S. J. Tanenbaum, S. D. Ziman, and J. H. Seinfeld. 2000. The use of ambient measurements to identify which precursor species limit aerosol nitrate formation. *J. Air Waste Manage. Assoc.* 50: 2073–2084.

Blanchard, C. L. 2000. Ozone process insights from field experiments - Part III: Extent of reaction and ozone formation. *Atmos. Environ.* 34: 2035–2043.

Blanchard, C. L., Frederick W. Lurmann, Philip M. Roth, Harvey E. Jeffries, and Marcelo Korc. 1999. The use of ambient data to corroborate analyses of ozone control strategies. *Atmos. Environ.* 33: 369–381.

Camalier, L., W. Cox, and P. Dolwick. 2007. The effects of meteorology and their use in assessing ozone trends. *Atmos. Environ.* 41: 7127–7137.

Cardelino, C. A. and W. L. Chameides. 1995. An observation-based model for analyzing ozone precursor relationships in the urban atmosphere. *J. Air Waste Manage. Assoc.* 45: 161–180.

Chang, T. Y. and M. J. Suzio. 1995. Assessing ozone-precursor relationships based on a smog production model and ambient data. *J. Air Waste Manage. Assoc.* 45: 20–28.

Croes, B. E., L. J. Dolislager, L. Larsen, and J. N. Pitts. 2003. Forum – the O<sub>3</sub> “weekend effect” and NO<sub>x</sub> control strategies – scientific and public health findings and their regulatory implications. *EM*. July: 27–35.

Duncan, B. N., Y. Yoshida, J. R. Olson, S. Sillman, R. V. Martin, L. Lamsal, Y. Hu, K. E. Pickering, C. Retscher, D. J. Allen, J. H. Crawford. 2010. Application of OMI observations to a space-based indicator of NO<sub>x</sub> and VOC controls on surface ozone formation. *Atmos. Environ.* 44(18): 2213–2223. doi:10.1016/j.atmosenv.2010.03.010.

- Dye, T. S., P. T. Roberts, and M. E. Korc, 1995: Observations of transport processes for ozone and ozone precursors during the 1991 Lake Michigan Ozone Study. *J. Appl. Meteor.* 34, 1877–1889.
- Foley, T., E. A. Betterton, P. E. R. Jacko, and J. Hillery. Lake Michigan air quality: The 1994–2003 LADCO Aircraft Project (LAP). *Atmos. Environ.* 45: 3192–3202.  
<https://doi.org/10.1016/j.atmosenv.2011.02.033> (last access, November 30, 2019).
- Frost, G. J., M. Trainer, G. Allwine, M.P. Buhr, J. G. Calvert, C. A. Cantrell, F. C. Fehsenfeld, P. D. Goldan, J. Herwehe, G. Hübler, W. C. Kuster, R. Martin, R. T. McMillen, S. A. Montzka, R. B. Norton, D. D. Parrish, B. A. Ridley, R. E. Shetter, J. G. Walega, B. A. Watkins, H. H. Westberg, and E. J. Williams. 1998. Photochemical ozone production in the rural southeastern United States during the 1990 Rural Oxidants in the Southern Environment (ROSE) program. *J. Geophys. Res.* 103 (D17) : 22,491–22,508.
- Fujita, E. M., W. R. Stockwell, D. E. Campbell, R. E. Keislar, and D. R. Lawson. 2003. Evolution of the magnitude and spatial extent of the weekend ozone effect in California’s South Coast Air Basin. *J. Air Waste Manage. Assoc.* 53: 802–815.
- Gong, X., A. Kaulfus, U. Nair, and D.A. Jaffe. 2017. Quantifying O<sub>3</sub> impacts in urban areas due to wildfires using a Generalized Additive Model. *Envir. Sci. Tech.* doi:10.1021/acs.est.7b03130.
- Gong, X., S. Hong, and D.A Jaffe. 2018. Ozone in China: Spatial distribution and leading meteorological factors controlling O<sub>3</sub> in 16 Chinese cities. *Aer. Air Qual. Res.* doi:10.4209/aaqr.2017.10.0368.
- Haney, J.L., S.G. Douglas, L.R. Chinkin, D.R. Souten, C.S. Burton, and P.T. Roberts. 1989. Ozone Air Quality Scoping Study for the Lower Lake Michigan Air Quality Region, SAI report #SYSAPP-89/101, prepared for US EPA, August, 197 pp.
- Hanna, S.R. and J.C. Chang. 1995. Relations between meteorology and ozone in the Lake Michigan 2010 region. *J. Applied Meteorology*, 34: 670–678.
- Hess, G. D., F. Carnovale, M. E. Cope, and G. M. Johnson, 1992. The evaluation of some photochemical smog reaction mechanisms - I. Temperature and initial composition effects. *Atmos. Environ.* 26A: 625–641.
- Hidy, G. M. and C. L. Blanchard. 2015. Precursor reductions and ground-level ozone in the continental U.S. *J. Air Waste Manage. Assoc.* 65: 1261–1282. doi: 10.1080/10962247.2015.1079564.
- Hirsch, A. I., J. W. Munger, D. J. Jacob, L. W. Horowitz, and A. H. Goldstein. 1996. Seasonal variation of the ozone production efficiency per unit NO<sub>x</sub> at Harvard Forest, Massachusetts. *J. Geophys. Res.: Atmos.* 101(D7): 12659–12666, doi:10.1029/96JD00557.
- Jaffe, D. 2020. Role of meteorology, emissions and smoke on O<sub>3</sub> in the South Coast air basins CRC Project A-118. <https://crcao.org/published-reports-full/> (last access, May 27, 2020).
- Kaleel, R. 2015. Photochemical grid modeling in the Midwest: a retrospective. *EM*. January 2015: 14–19. <http://pubs.awma.org/flip/EM-Jan-2015/kaleel.pdf>

- Kim, H. S., Y. H. Kim, K. M. Han, J. Kim, and C. H. Song. 2016. Ozone production efficiency of a ship-plume: ITCT 2K2 case study. *Chemosphere* 143: 17-23.
- Kleinman, L. 2000. Ozone process insights from field experiments—Part II. Observation-based analysis for ozone production. *Atmos. Environ.* 34:2023–34. doi:10.1016/S1352-2310(99)00457-4.
- Kleinman, L. I., Daum, P. H., Lee, Y-N., Nunnermacker, L. J., Springston, S. R., Newman, L., Weinstein-Lloyd, J., and Rudolph, J.: a comparative study of ozone production in five U.S. metropolitan areas. 2005. *J. Geophys. Res.* 110, D02301, doi:10.1029/2004JD005096.
- Kleinman, L. I., P. H. Daum, Y-N. Lee, L. J. Nunnermacker, S. R. Springston, J. Weinstein-Lloyd, P. Hyde, P. Doskey, J. Rudolf, J. Fast and C. Berkowitz. 2003. Photochemical age determinations in the Phoenix metropolitan area. *J. Geophys. Res.*, 10.1029/2002JD002621.
- Kleinman, L. H., P. H. Daum, Y-N. Lee, L. J. Nunnermacker, S. R. Springston, J. Weinstein-Lloyd, and Jochen Rudolph. 2001. Sensitivity of ozone production rate to ozone precursors. *Geophys. Res. Lett.* 28, 2903-2906, 2001.
- Kleinman, L. I., P. H. Daum, D. G. Imre, J. H. Lee, Y-N. Lee, L. J. Nunnermacker, S. R. Springston, J. Weinstein-Lloyd, and L. Newman, 2000. Ozone production in the New York City urban plume. *J. Geophys. Res.*, 105, 14495-14511.
- Lawson, D. R. 2003. Forum – the weekend ozone effect – the weekly ambient emissions control experiment. *EM*. July: 17-25.
- Lin, X., M. Trainer, and S. C. Liu. 1988. On the nonlinearity of the tropospheric ozone production. *J. Geophys. Res. Atmos.* 93(D12):15879–88. doi:10.1029/JD093iD12p15879.
- Liu, S. C., M. Trainer, F. C. Fehsenfeld, D. D. Parrish, E. J. Williams, D. W. Fahey, G. Hubler, and P. C. Murphy. 1987. Ozone production in the rural troposphere and the implications for regional and global ozone distributions, *J. Geophys. Res.*, 92(D4), 4191-4207.
- Liang, J., B. Jackson, and A. Kaduwela. 2006. Evaluation of the ability of indicator species ratios to determine the sensitivity of ozone to reductions in emissions of volatile organic compounds and oxides of nitrogen in northern California. *Atmos. Environ.* 40: 5156-5166.
- Lu, C. H. and J. S. Chang, 1998. On the indicator-based approach to assess ozone sensitivities and emissions features. *J. Geophys. Res.* 103(D3): 3453-3462.
- Lyons, W.A. and H.S. Cole. 1976. Photochemical oxidant transport: mesoscale lake breeze and synoptic-scale aspects. *J. Appl. Meteor.* 15: 733 – 743.
- Marr, L. C. and R. A. Harley. 2002a. Spectral analysis of weekday–weekend differences in ambient ozone, nitrogen oxide, and non-methane hydrocarbon time series in California. *Atmos. Environ.* 26: 2327-2335.
- Marr, L. C. and R. A. Harley. 2002b. Modeling the effect of weekday–weekend differences in motor vehicle emissions on photochemical air pollution in central California. *Environ. Sci. Technol.* 36: 4099-4106.

- Milford, J. B., D. Gao, S. Sillman, P. Blossey, and A. G. Russell. 1994. Total reactive nitrogen ( $\text{NO}_y$ ) as an indicator for the sensitivity of ozone to  $\text{NO}_x$  and hydrocarbons. *J. Geophys. Res.* 99(D2): 3533-3542.
- National Research Council. Rethinking the Ozone Problem in Urban and Regional Air Pollution. National Academy Press, Washington, DC, 1991. 489 pp.
- NARSTO. 2000. An assessment of tropospheric ozone pollution: A North American perspective. NARSTO Report 1000040. Palo Alto, CA: Electric Power Research Institute.
- Neuman, J. A., J. B. Nowak, W. Zheng, F. Flocke, T. B. Ryerson, M. Trainer, J. S. Holloway, D. D. Parrish, G. J. Frost, J. Peischl, E. L. Atlas, R. Bahreini, A. G. Wollny, and F. C. Fehsenfeld. 2009. Relationship between photochemical ozone production and  $\text{NO}_x$  oxidation in Houston, Texas. *J. Geophys. Res. Atmos.* 114, D00F08, doi:10.1029/2008JD011688.
- Ninneman, M., S. Lu, P. Lee, J. McQueen, J. Huang, K. Demerjian, and J. Schwab. 2017. Observed and model-derived ozone production efficiency over urban and rural New York State. *Atmosphere* 8: 126 – 140. doi:10.3390/atmos8070126.
- Ninneman, M., J. Marto, S. Shaw, E. Edgerton, C. Blanchard, and J. Schwab. 2020. Reactive oxidized nitrogen speciation and partitioning in urban and rural New York State. *Submitted to J. Air Waste Manage. Assoc.*
- Olszyna, K. J., E. M. Bailey, R. Simonaitis, and J. F. Meagher. 1994.  $\text{O}_3$  and  $\text{NO}_y$  relationships at a rural site. *J. Geophys. Res.* 99: 14557-14563.
- Pierce, B., R. Kaleel, A. Dickens, T. Bertram, C. Stanier, and D. Kenski. 2017. White Paper: Lake Michigan Ozone Study 2017 (LMOS 2017). [https://www-air.larc.nasa.gov/missions/lmos/docs/Great\\_Lakes\\_Ozone\\_Study\\_White\\_Paper\\_Draft\\_v6.pdf](https://www-air.larc.nasa.gov/missions/lmos/docs/Great_Lakes_Ozone_Study_White_Paper_Draft_v6.pdf). (last access November 30, 2019).
- Pollack, I., T. Ryerson, M. Trainer, J. Neuman, J. Roberts, and D. Parrish. 2013. Trends in ozone its precursors and related secondary oxidation products in Los Angeles, California: A synthesis of measurements from 1960–2010. *J. Geophys. Res. Atmos.* 118:5891–911. doi:10.1002/jgrd.50472.
- Pollack, I. B., et al. 2012. Airborne and ground-based observations of a weekend effect in ozone, precursors, and oxidation products in the California South Coast Air Basin. *J. Geophys. Res.* 117, D00V05, doi:10.1029/2011jd016772.
- Pusede, S. E. and R. C. Cohen. 2012. On the observed response of ozone to  $\text{NO}_x$  and VOC reactivity reductions in San Joaquin Valley California 1995–present. *Atmos. Chem. Phys.* 12: 8323–8339. doi:10.5194/acp-12-8323-2012.
- Qian, Y., L. R. F. Henneman, J. A. Mulholland, and A. G. Russell. 2019. Empirical development of ozone isopleths: applications to Los Angeles. *Environ. Sci. Technol. Lett.* 6 (5): 292-299. <https://doi.org/10.1021/acs.estlett.9b00160>.

Reynolds, S. D., C. L. Blanchard, and S. D. Ziman. 2004. Understanding the effectiveness of precursor reductions in lowering 8-hr ozone concentrations-Part II. The eastern United States. *J. Air Waste Manage. Assoc.* 54: 1452-1470.

Roberts, P. T., P. M. Roth, C. L. Blanchard, M. E. Korc, and F. W. Lurmann. 1993. Characteristics of VOC-Limited and NO<sub>x</sub>-Limited Areas Within the Lake Michigan Air Quality Region. Prepared for Lake Michigan Air Directors Consortium, Des Plaines, IL. Technical Memorandum STI-92322-1504-TM, Sonoma Technology, Inc, Santa Rosa, CA.

Ryerson, T. B., M.P. Buhr, G. J. Frost, P. D. Goldan, J. S. Holloway, G. Hübler, B. T. Jobson, W. C. Kuster, S. A. McKeen, D. D. Parrish, J. M. Roberts, D. T. Sueper, M. Trainer, J. Williams, and F. C. Fehsenfeld. 1998. Emissions lifetimes and ozone formation in power plant plumes. *J. Geophys. Res.* 103 (D17): 22,569-22,583.

Schroeder, J. R., J. H. Crawford, A. Fried, J. Walega, A. Weinheimer, A. Wisthaler, M. Müller, T. Mikoviny, G. Chen, M. Shook, D. R. Blake, and G. S. Tonnesen. 2017. New insights into the column CH<sub>2</sub>O/NO<sub>2</sub> ratio as an indicator of near-surface ozone sensitivity. *J. Geophys. Res.* 122: 8885-8907. doi:10.1002/2017JD026781.

Sillman, S. 2019. <http://www-personal.umich.edu/~sillman/obm.htm>

Sillman, S., D. He, C. Cardelino, and R. E. Imhoff. 1997. The use of photochemical indicators to evaluate ozone-NO<sub>x</sub>-hydrocarbon sensitivity: case studies from Atlanta, New York, and Los Angeles. *J. Air Waste Manage. Assoc.* 47: 1030-1040.

Sillman, S. 1995. The use of NO<sub>y</sub>, H<sub>2</sub>O<sub>2</sub>, and HNO<sub>3</sub> as indicators for ozone-NO<sub>x</sub>-hydrocarbon sensitivity in urban locations. *J. Geophys. Res.* 100(D7): 14175-14188.

Thornton, J., P. Wooldridge, R. Cohen, M. Martinez, H. Harder, W. Brune, E. Williams, J. Roberts, F. Fehsenfeld, F. Hall, S. Shetter, B. Wert, and A. Fried. 2002. Ozone production rates as a function of NO<sub>x</sub> abundances and HO<sub>x</sub> production rates in the Nashville urban plume. *J. Geophys. Res.* 107:4146, doi:10.1029/2001JD000932

Tonnesen, G.S. and Dennis, R.L. 2000a. Analysis of radical propagation efficiency to assess ozone sensitivity to hydrocarbons and NO<sub>x</sub>. Part 1: Local indicators of odd oxygen production sensitivity. *J. Geophys. Res.* 105: 9213–9225.

Tonnesen, G.S. and Dennis, R.L. 2000b. Analysis of radical propagation efficiency to assess ozone sensitivity to hydrocarbons and NO<sub>x</sub>. Part 2: Long-lived species as indicators of ozone concentration sensitivity. *J. Geophys. Res.* 105: 9227–9241.

Trainer, M., Parrish, D. D., Buhr, M. P., Norton, R. B., Fehsenfeld, F. D., Anlauf, K. G., Bottenheim, J. W., Tang, Y. Z., Wiebe, H. A., Roberts, J. M., Tanner, R. L., Newman, L., Bowersox, V. C., Meagher, J. F., Olszyna, K. J., Rodgers, M. O., Wang, T., Berresheim, H., Demerjian, K. L., Roychowdhury, U. K. 1993. Correlation of ozone with NO<sub>y</sub> in photochemically aged air. *J. Geophys. Res.* 98: 2917-2926.

Trainer, M., B. A. Ridley, M. P. Buhr, G. Kok, J. Walega, G. Hübler, D. D. Parrish, and F. C. Fehsenfeld: Regional ozone and urban plumes in the southeastern United States: Birmingham, A case study. 1995. *J. Geophys. Res. Atmos.*, 100(D9), 18823- 18834, doi:10.1029/95JD01641.

Trainer, M., D. Parrish, P. Goldan, P., J. Roberts, and F. Fehsenfeld. 2000. Review of observation-based analysis of regional factors influencing ozone concentration, *Atmos. Environ.*, 34, 2045-2062.

Travis, K. R., D. J. Jacob, J. A. Fisher, P. S. Kim, E. A. Marais, L. Zhu, K. Yu, C. C. Miller, R. M. Yantosca, M. P. Sulprizio, A. M. Thompson, P. O. Wennberg, J. D. Crouse, J. M. St. Clair, R. C. Cohen, J. L. Laughner, J. E. Dibb, S. R. Hall, K. Ullmann, G. M. Wolfe, I. B. Pollack, J. Peischl, J. A. Neuman, and X. Zhou. 2016. Why do models overestimate surface ozone in the Southeast United States? *Atmos. Chem. Phys.* doi:10.5194/acp-16-13561-2016.

U.S. Environmental Protection Agency. 1996. Air Quality Criteria for Ozone and Other Photochemical Oxidants. EPA/600/P-93/004aF. Office of Health and Environmental Assessment, Environmental Criteria Office, Research Triangle Park, N.C. NTIS, Springfield, VA. <http://www.epa.gov/nscep/> (last access November 30, 2019).

U.S. Environmental Protection Agency. 2007. Guidance on the Use of Models and Other Analyses for Demonstrating Attainment of Air Quality Goals for Ozone, PM<sub>2.5</sub>, and Regional Haze. EPA -454/B-07-002. <http://www.epa.gov/nscep/> (last access November 30, 2019).

U.S. EPA. 2015. Regulatory Impact Analysis of the Final Revisions to the National Ambient Air Quality Standards for Ground-Level Ozone. EPA-452/R-15-007. <https://www.epa.gov/naaqs/regulatory-impact-analysis-final-revisions-national-ambient-air-quality-standards-ground-level> (last access, November 30, 2019).

U.S. EPA. 2016. <https://www.epa.gov/sites/production/files/2016-03/documents/20151001datatable2025.pdf> (last access, November 30, 2019).

U.S. EPA. 2018. Modeling Guidance for Demonstrating Air Quality Goals for Ozone, PM<sub>2.5</sub>, and Regional Haze. EPA 454/R-18-009. [https://www3.epa.gov/ttn/scram/guidance/guide/O3-PM-RH-Modeling\\_Guidance-2018.pdf](https://www3.epa.gov/ttn/scram/guidance/guide/O3-PM-RH-Modeling_Guidance-2018.pdf) (last access, December 6, 2019).

U.S. EPA. 2020a. Integrated Science Assessment (ISA) for Ozone and Related Photochemical Oxidants. U.S. Environmental Protection Agency, Washington, DC, EPA/600/R-20/012, 2020. <https://www.epa.gov/isa/integrated-science-assessment-isa-ozone-and-related-photochemical-oxidants> (last access, July 24, 2020).

U.S. EPA. 2020b. Ozone Trends. <https://www.epa.gov/air-trends/ozone-trends> (last access, July 26, 2020).

U.S. EPA. 2020c. Air Quality Designations for Ozone. <https://www.epa.gov/ozone-designations> (last access, July 24, 2020).

U.S. EPA, 2020d. Ozone Designations Mapping Tool V1. <https://epa.maps.arcgis.com/apps/webappviewer/index.html?id=6a89e7170dd147b1852ec11ccb3880e8> (last access July 24, 2020).

U.S. EPA. 2020e. Air Pollutant Emissions Trends Data. <https://www.epa.gov/air-emissions-inventories/air-pollutant-emissions-trends-data> (last access July 24, 2020).

U.S. EPA. 2020f. Pre-Generated Data Files.

[https://aqs.epa.gov/aqsweb/airdata/download\\_files.html](https://aqs.epa.gov/aqsweb/airdata/download_files.html) (last access, August 10, 2020).

U.S. EPA. 2020g. Air Quality System (AQS) API.

[https://aqs.epa.gov/aqsweb/documents/data\\_api.html](https://aqs.epa.gov/aqsweb/documents/data_api.html) (last access, August 10, 2020).

U.S. EPA. 2020h. Trends in Ozone Adjusted for Weather Conditions. <https://www.epa.gov/air-trends/trends-ozone-adjusted-weather-conditions> (last access, July 27, 2020).

Vermeuel, M. P., G. A. Novak, H. D. Alwe, D. D. Hughes, R. Kaleel, A. F. Dickens, D. Kenski, A. Czarnetzki, E. A. Stone, C. O. Stanier, R. B. Pierce, D. B. Millet, and T. H. Bertram. 2019. Sensitivity of ozone production to NO<sub>x</sub> and VOC along the Lake Michigan coastline. *J. Geophys. Res. Atmos.* 124(20): 10989 – 11006. doi 10.1029/2019jd030842.

Wisconsin Department of Natural Resources (DNR). 2017. Attainment Plan for the Sheboygan County, Wisconsin 2008 8-Hour Ozone Nonattainment Area.

<https://dnr.wi.gov/topic/AirQuality/documents/SheboyganAttainmentPlan.pdf> (last access, July 30, 2020).

Zaveri, R. A., C. M. Berkowitz, L. I. Kleinman, S. R. Springston, P. V. Doskey, W. A. Lonneman, and C. W. Spicer. 2003. Ozone production efficiency and NO<sub>x</sub> depletion in an urban plume: Interpretation of field observations and implications for evaluating O<sub>3</sub>-NO<sub>x</sub>-VOC sensitivity, *J. Geophys. Res. Atmos.*, 108 (D14), doi:10.1029/2002JD003144.

## 9. Appendix

### 9.1 Data Sources

Annual state emissions were obtained from EPA (<https://www.epa.gov/chief>; <https://ampd.epa.gov/ampd/>)

O<sub>3</sub>, CO, NO, NO<sub>2</sub>, NO<sub>x</sub>, NO<sub>y</sub>, and speciated NMOC measurements were obtained from the EPA air quality system (AQS) as precompiled files or by means of API data queries for ([https://aqs.epa.gov/aqsweb/airdata/download\\_files.html](https://aqs.epa.gov/aqsweb/airdata/download_files.html) and [https://aqs.epa.gov/aqsweb/documents/data\\_api.html](https://aqs.epa.gov/aqsweb/documents/data_api.html))

Surface weather measurements were obtained from multiple sources:

1. EPA AQS
2. NOAA airport station files (<https://www.ncdc.noaa.gov/data-access/land-based-station-data>)
3. NOAA observational sites (<https://www.glerl.noaa.gov/metdata>)
4. Solar radiation: NREL (<https://www.nrel.gov/docs/fy12osti/54824.pdf>)

Upper-air data were obtained from NOAA radiosonde sites: Green Bay, WI; Lincoln, IL; Davenport, IA; Detroit, MI; and Gaylord, MI (<https://ruc.noaa.gov/raobs/>)

Lake Michigan temperature surface temperatures were obtained from NOAA (<https://coastwatch.glerl.noaa.gov/statistic/>)

## 9.2 Data Availability

Table A1. Data availability for AQ sites with high O<sub>3</sub>, or VOC or NO<sub>y</sub> measurements.

Monitor	Nitrogen oxides <sup>1</sup>	VOC	Ozone	CO	Meteorology <sup>5</sup>	Latitude	Longitude
Newport Park WI			Yes		WS/WD/T	45.2384	-86.9940
Manitowoc WI	NO NO <sub>2</sub> NO <sub>y</sub>		Yes		WS/WD/T	44.1386	-87.6161
Sheboygan Haven WI			Yes		WS/WD	43.8156	-87.7922
Sheboygan Kohler WI			Yes		WS/WD/T	43.6674	-87.7162
Harrington Beach WI			Yes		WS/WD/T/BP	43.4981	-87.8100
Horicon/Mayville WI	NO NO <sub>y</sub>	Yes <sup>3,4</sup>	Yes	Yes	WS/WD/T/RH/BP/SR	43.4661	-88.6211
Grafton WI			Yes		WS/WD/T	43.343	-87.9200
Bayside WI			Yes		WS/WD/BP	43.1818	-87.901
Milwaukee DNR SER WI	NO NO <sub>2</sub> NO <sub>y</sub>	Yes <sup>4</sup>	Yes	Yes	WS/WD/T/BP	43.0610	-87.9135
Milwaukee Health Ctr WI		Yes <sup>3,4</sup>	Yes		WS/WD/T	43.0167	-87.9333
Kenosha Water Tower			Yes		WS/WD/T	42.5958	-87.8858
Lake Geneva WI			Yes			42.5800	-88.4990
Chiwaukee Prairie WI			Yes		WS/WD/T	42.5047	-87.8093
Zion IL	NO NO <sub>2</sub> NO <sub>y</sub> <sup>2</sup>		Yes		WS/WD/T/RH	42.4676	-87.8100
Northbrook IL	NO NO <sub>2</sub> NO <sub>y</sub>	Yes <sup>4</sup>	Yes	Yes	WS/WD/T/RH/BP/SR	42.1400	-87.7992
Evanston IL			Yes			42.06205	-87.6753
Schiller Park IL	NO NO <sub>2</sub>	Yes <sup>3,4</sup>	Yes	Yes	WS/WD	41.9652	-87.8763
Jardine IL	NO NO <sub>2</sub>	Yes	Yes		WS/WD/T/BP/RH	41.8958	-87.6077
Cicero IL	NO NO <sub>2</sub>		Yes			41.8552	-87.7525
Chicago Lawndale IL	NO NO <sub>2</sub>		Yes		WS/WD	41.7514	-87.7135
S. Water Filtration Plant			Yes			41.75583	-87.5454
Whiting-Center St/HS IN		Yes	Yes			41.6814	-87.4902
Hammond IN		Yes	Yes		WS/WD/T/RH	41.6394	-87.4936
East Chicago-Marina IN		Yes		Yes		41.6535	-87.4356
Gary-IITRI IN	NO NO <sub>2</sub>	Yes <sup>4</sup>	Yes		WS/WD/T/RH/BP/SR	41.6067	-87.3047
Ogden Dunes IN		Yes	Yes		WS/WD/T <sup>6</sup>	41.6175	-87.1992
South Bend - Shields Dr IN	NO NO <sub>2</sub>		Yes		WS/WD/T	41.6967	-86.2147
Coloma MI			Yes		WS/WD/T	42.19779	-86.3097
Holland MI			Yes		WS/WD/T/SR	42.76779	-86.1486
Muskegon MI			Yes		WS/WD/T	43.27806	-86.3111

<sup>1</sup>NO<sub>2</sub> measurements are not NO<sub>2</sub>-specific (thermal conversion of NO<sub>2</sub> and unquantified additional nitrogen oxides to NO, measured by chemiluminescence with detection limits of 5 - 10 ppbv for most instruments)

<sup>2</sup>Through 2002 but also had measurements in 2017

<sup>3</sup>Total NMOC and sum of PAMS target compounds are not reported in AQS

<sup>4</sup>Includes formaldehyde

<sup>5</sup>Measurement periods vary. WS = wind speed, WD = wind direction, T = temperature, BP = barometric pressure, RH = relative humidity, SR = solar radiation (not in AQS). WI WS and WD data are scalar for 2000 – 2014 and resultant for 2014 - 2019

<sup>6</sup>Dune Acres site, ~10 km east of Ogden Dunes

## 9.3 Data Evaluation

### 9.3.1 NO<sub>2</sub> and NO<sub>x</sub>

Two issues affect the utility of NO<sub>2</sub> and NO<sub>x</sub> measurements: (1) sensitivity (high minimum detection limits, MDL) and (2) non-selectivity of NO<sub>2</sub> (unquantified positive interferents). These issues indirectly affect the utility of NO<sub>y</sub> measurements, which usually must be combined with NO<sub>x</sub> values to estimate NO<sub>z</sub> = NO<sub>y</sub> – NO<sub>x</sub>. The long-term measurement record does not permit determination of NO<sub>z</sub> as the sum of its major components, which include nitric acid (HNO<sub>3</sub>), peroxyacetylnitrate (PAN), and other oxidized nitrogen species.

Most of the NO<sub>x</sub> measurements are based on instrumentation with high (5 – 10 ppbv) MDLs (Table A2). For Manitowoc, the period with high-sensitivity NO<sub>x</sub> measurements (2000 – 2012) predates NO<sub>y</sub> measurements. Beginning June 1, 2019, species-specific NO<sub>2</sub> measurements at Manitowoc and Milwaukee SER DNR were made with a Teledyne T500U instrument by cavity attenuated phase shift spectroscopy.

Table A2. NO<sub>x</sub> instrumentation at sites that also measure NO<sub>y</sub>.

Location	Period	Instrument	NO <sub>2</sub> MDL (ppbv)	NO <sub>x</sub> MDL (ppbv)
Manitowoc	2000 – 12	TECO 42S	Not listed	0.05
Manitowoc	2013 – 19	API Model 200A/E	2.7	5
Manitowoc	June – Aug 2019	Teledyne T500U	0.04	NA
Milwaukee DNR	2000 – 12	TECO 42	1	10
Milwaukee DNR	2013 – 19	API Model 200A/E	2.7	5
Milwaukee DNR	June – Dec 2019	Teledyne T500U	0.04	NA
Zion	2000	TECO 42	1	10
Zion	2000 – 02	API Model 200	5	10
Northbrook	2000 – 13	TECO 42	1	10
Northbrook	2014	API Model 200	5	10
Northbrook	2013 – 19	TECO 42C-Y, 42i-Y	0.05	0.05
Northbrook	2015 – 16	API Model 200A/E	2.7	5
Schiller Park	2000 – 13	TECO 42	1	10
Schiller Park	2013 – 14	API Model 200	5	10
Schiller Park	2015 – 19	API Model 200A/E	2.7	5

There are no long-term measurements of true NO<sub>2</sub> with which to estimate the bias in reported NO<sub>2</sub> concentrations. However, NO<sub>2</sub> measurements from before and after the June 1, 2019 change of instrumentation at Manitowoc and Milwaukee SER DNR can be compared.

For Manitowoc, all 2019 measurements were made using the new instruments. The 2019 mean summer (June – August) NO<sub>2</sub> concentration was  $1.34 \pm 0.06$  ppbv. This value is higher than the means for 2016 through 2018, which were  $0.16 \pm 0.05$  ppbv,  $0.49 \pm 0.10$  ppbv, and  $0.90 \pm 0.06$  ppbv, respectively. However, large (>50%) numbers of negative NO<sub>2</sub> concentrations were reported in 2016 through 2018 (minima were -1.1, -1.4, and -0.2 ppbv, respectively). For 2015, the mean summer (June – August) NO<sub>2</sub> concentration was  $1.51 \pm 0.09$  ppbv and the minimum was zero. In summary, the NO<sub>2</sub> concentrations reported by the Teledyne T500U in 2019 were not lower than the means obtained in previous summers by the API Model 200A/E. The bias in the Manitowoc API Model 200A/E NO<sub>2</sub> concentrations cannot be determined more quantitatively with the available data.

For Milwaukee SER DNR, mean monthly NO<sub>2</sub> concentrations were  $7.24 \pm 0.58$  ppbv in May 2018,  $5.36 \pm 0.60$  ppbv in June 2018,  $7.52 \pm 0.59$  ppbv in May 2019, and  $6.81 \pm 0.63$  ppbv in June 2019. The May – June decrease was less in 2019 (when instruments were changed) than the 2018 May – June decrease (when no instrument change occurred), so no obvious instrumental effect is apparent (i.e., the May – June 2019 the decline is seasonal). Time series graphs revealed no obvious step changes before and after the change of instrumentation on June 1, 2019.

Comparisons of NO<sub>x</sub> (biased) and NO<sub>y</sub> indicate that afternoon NO<sub>y</sub> generally exceeds afternoon NO<sub>x</sub> by 1 to 2 ppbv (Figures A1 and A2).

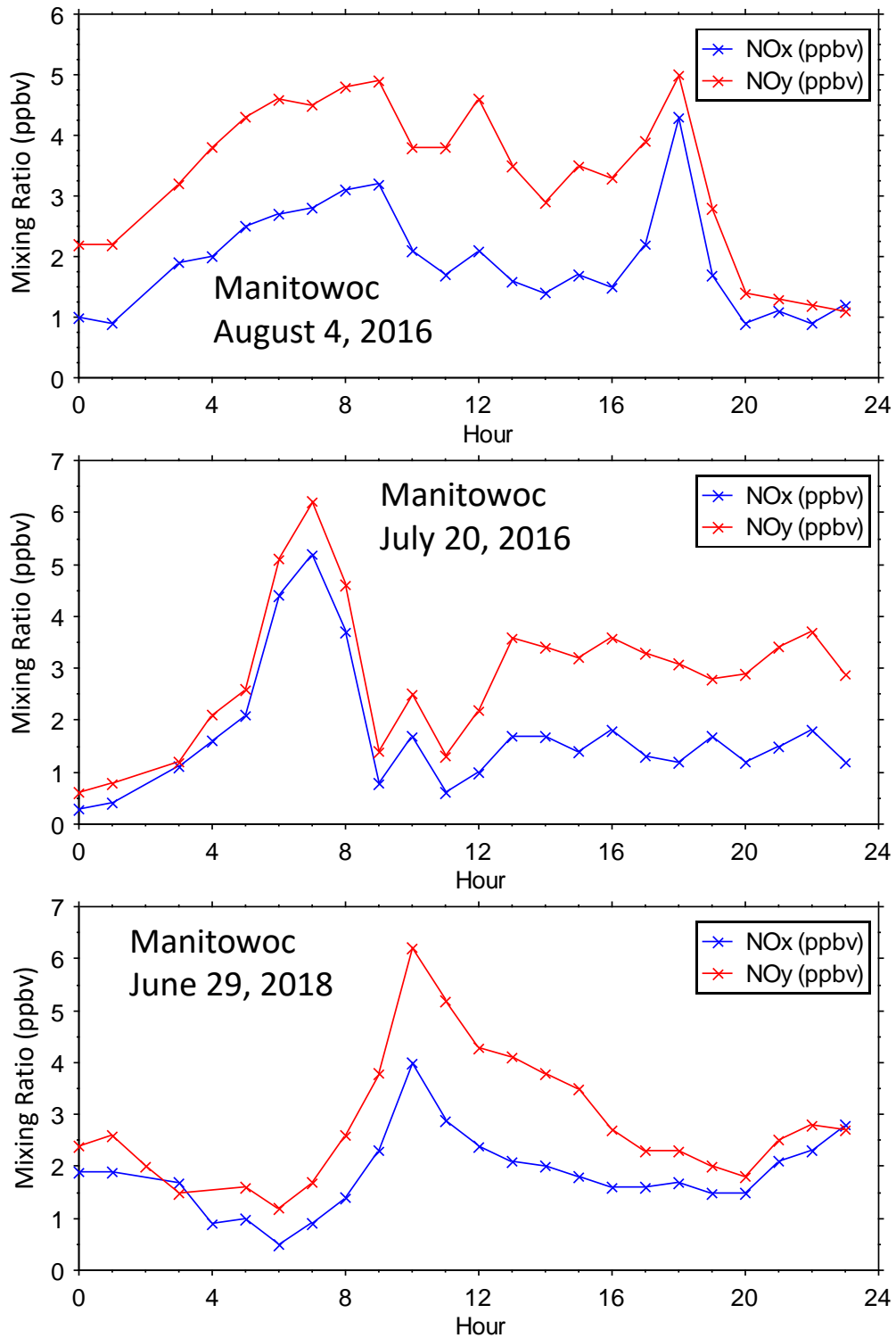


Figure A1. Example hourly NO<sub>x</sub> and NO<sub>y</sub> at Manitowoc on three high-O<sub>3</sub> days.

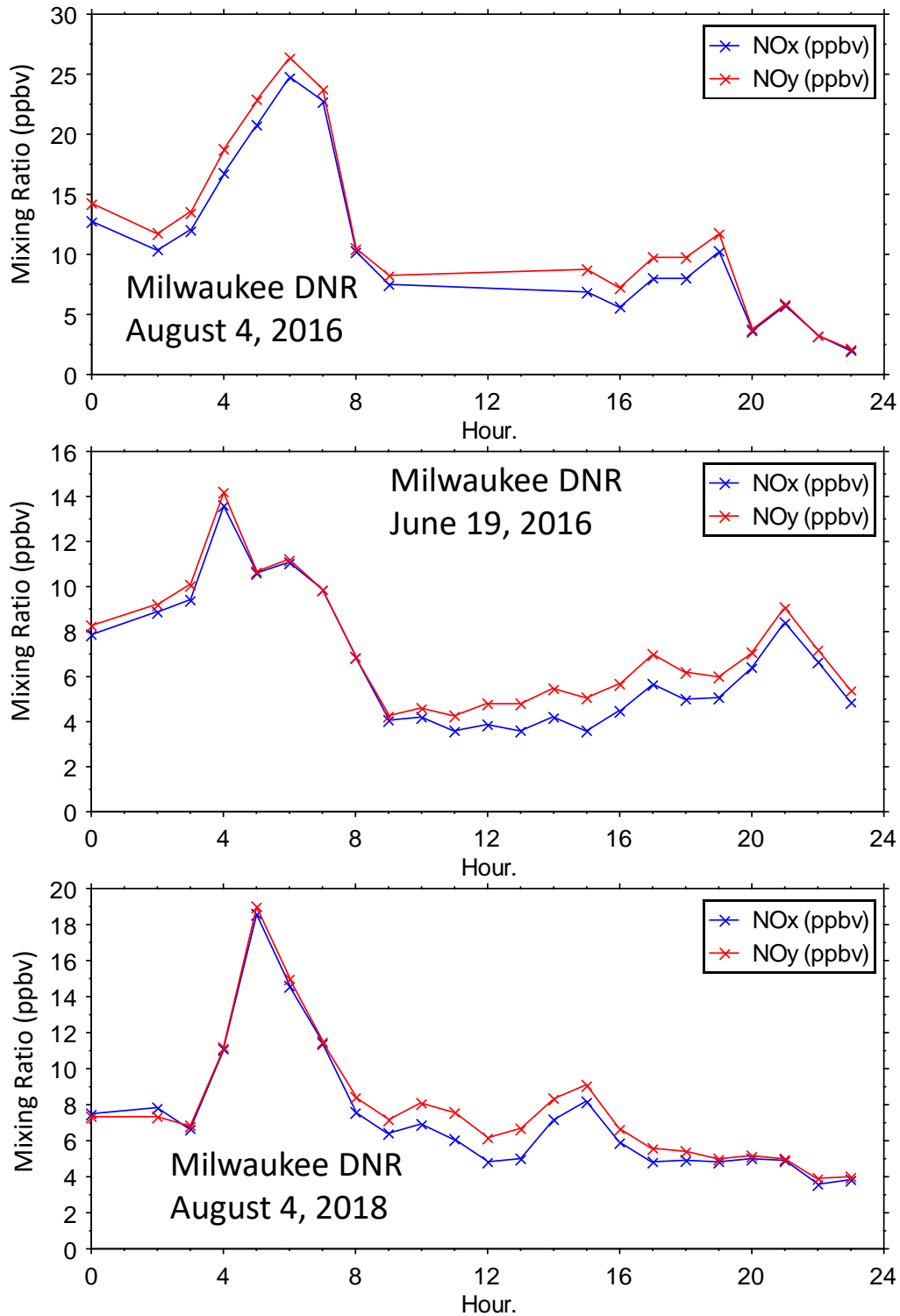


Figure A2. Example hourly NO<sub>x</sub> and NO<sub>y</sub> at Milwaukee DNR SER on three high-O<sub>3</sub> days.

### 9.3.2 Sampling Duration

Most of the NMOC data are 24-hour duration samples. Some 3-hour samples were collected at some sites, generally either once or three times per day. I paired the 11 a.m. – 2 p.m. 3-hour NMOC data with hourly NO<sub>2</sub> measurements averaged over the same three hours and compared these data with 24-hour resolution measurements (Figure A3). As shown, mid-day HCHO concentrations are higher and mid-day NO<sub>2</sub> concentrations are lower, on average, compared to corresponding 24-hour averages. As a result, mid-day HCHO/NO<sub>2</sub> is approximately twice as high as 24-hour HCHO/NO<sub>2</sub>.

### 9.3.3 Indicator Transition Ranges

The relationship of O<sub>3</sub> with HCHO/NO<sub>2</sub> varies depending on averaging times of both O<sub>3</sub> and HCHO/NO<sub>2</sub> (Figure A4). Although Figure A4 shows considerable variability, the frequency of MDA8 O<sub>3</sub> exceedances of 50 ppbv increases smoothly with daily-average HCHO/NO<sub>2</sub> up to a bin value of 0.4 (i.e., values in the range 0.4 – 0.5) (Figure A5).

Considerable day-to-day and intersite variability is also evident in plots of MDA8 O<sub>3</sub> vs. NMOC/NO<sub>x</sub> (Figure A6). Plots of NMOC vs. NO<sub>x</sub> or NO<sub>y</sub> suggest that the NMOC/NO<sub>x</sub> ratio at Milwaukee SER DNR largely reflects an emission ratio, modified somewhat by day-to-day variations (Figure A7).

Comparisons of mid-day (11 a.m. – 2 p.m.) with average ratios of O<sub>3</sub>/NO<sub>y</sub> and O<sub>3</sub>/NO<sub>z</sub> exhibit substantial variability (Figure A8). The mid-day ratios are more consistent than daily averages with the theoretical rationale that supports using them as indicators of VOC or NO<sub>x</sub> sensitivity. Mid-day ratios of O<sub>3</sub>/NO<sub>y</sub> are approximately one order of magnitude lower than corresponding ratios of O<sub>3</sub>/NO<sub>z</sub> (Figure A9). Since NO<sub>z</sub> is biased low (Section 9.3.1), ratios of O<sub>3</sub>/NO<sub>y</sub> may be more reliable than ratios of O<sub>3</sub>/NO<sub>z</sub>. The same measurement issue (high bias in NO<sub>2</sub> and NO<sub>x</sub>) yields similar ratios of O<sub>3</sub>/NO<sub>y</sub> and O<sub>3</sub>/NO<sub>x</sub>, especially for MDA8 O<sub>3</sub> exceeding 60 ppbv (Figure A9). This level of comparability is fortunate since the measurement record is more extensive for NO<sub>x</sub> than NO<sub>y</sub> (Tables A1 and A2). In contrast, mid-day ratios of O<sub>3</sub>/NO<sub>y</sub> show little relation to ratios of HCHO/NO<sub>2</sub> (Figure A9). The lack of correlation indicates that different results would be obtained when using these two ratios as indicators of VOC or NO<sub>x</sub> sensitivity, even if the expected sensitivity ranges for O<sub>3</sub>/NO<sub>y</sub> are corrected for differences from literature values.

Comparisons of MDA8 O<sub>3</sub> with mid-day (11 a.m. – 2 p.m.) ratios of O<sub>3</sub>/NO<sub>y</sub> and O<sub>3</sub>/NO<sub>x</sub>, based on both concentrations and frequency of values with MDA8 O<sub>3</sub> exceeding 50 ppbv, are shown in Figure A10. Considerable variability is evident in the concentration comparison. On a frequency of exceedance basis, Milwaukee values of O<sub>3</sub>/NO<sub>y</sub> and O<sub>3</sub>/NO<sub>x</sub> in the bins with lower limits of 7 – 11 and 9 – 13, respectively, span the highest values of MDA8 O<sub>3</sub> (Figure A10). The Milwaukee data therefore suggest a transition range of 7 – 12 for O<sub>3</sub>/NO<sub>y</sub> and 9 – 14 for O<sub>3</sub>/NO<sub>x</sub>. Higher ranges are indicated for Manitowoc (~10 – 14 and 12 – 16), which also exhibits greater variability. The ranges are approximately consistent with published transition ranges of 8 – 9 for O<sub>3</sub>/NO<sub>y</sub> (Sillman, 1995) and ~15 for O<sub>3</sub>/NO<sub>x</sub> (Tonnessen and Dennis, 2000b). Since measured NO<sub>x</sub> is biased high, the observed O<sub>3</sub>/NO<sub>x</sub> ratios may be low.

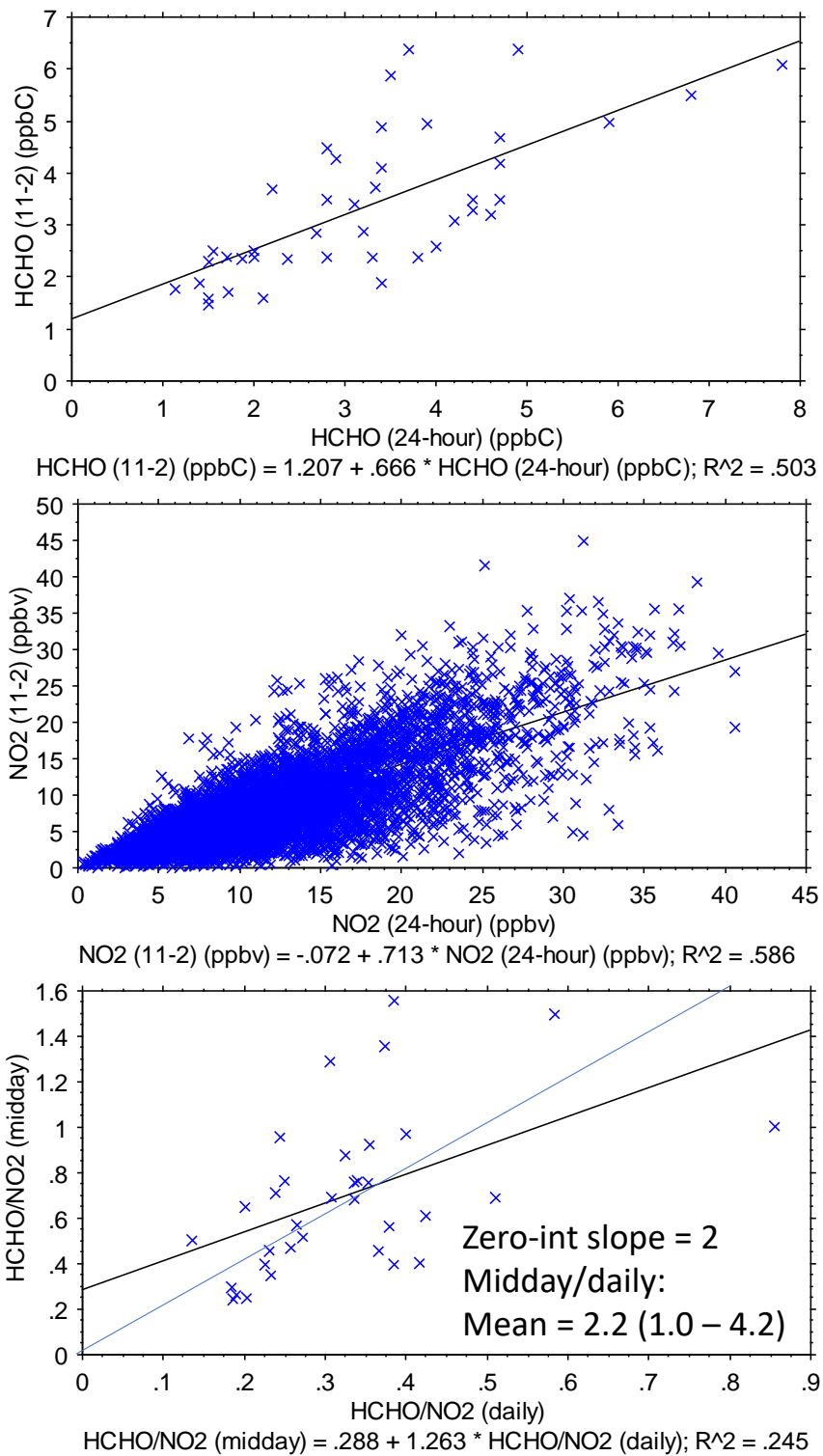


Figure A3. Comparison of Milwaukee SER DNR mid-day (11 a.m. – 2 p.m.) and 24-hour concentrations of HCHO, NO<sub>2</sub>, and HCHO/NO<sub>2</sub>.

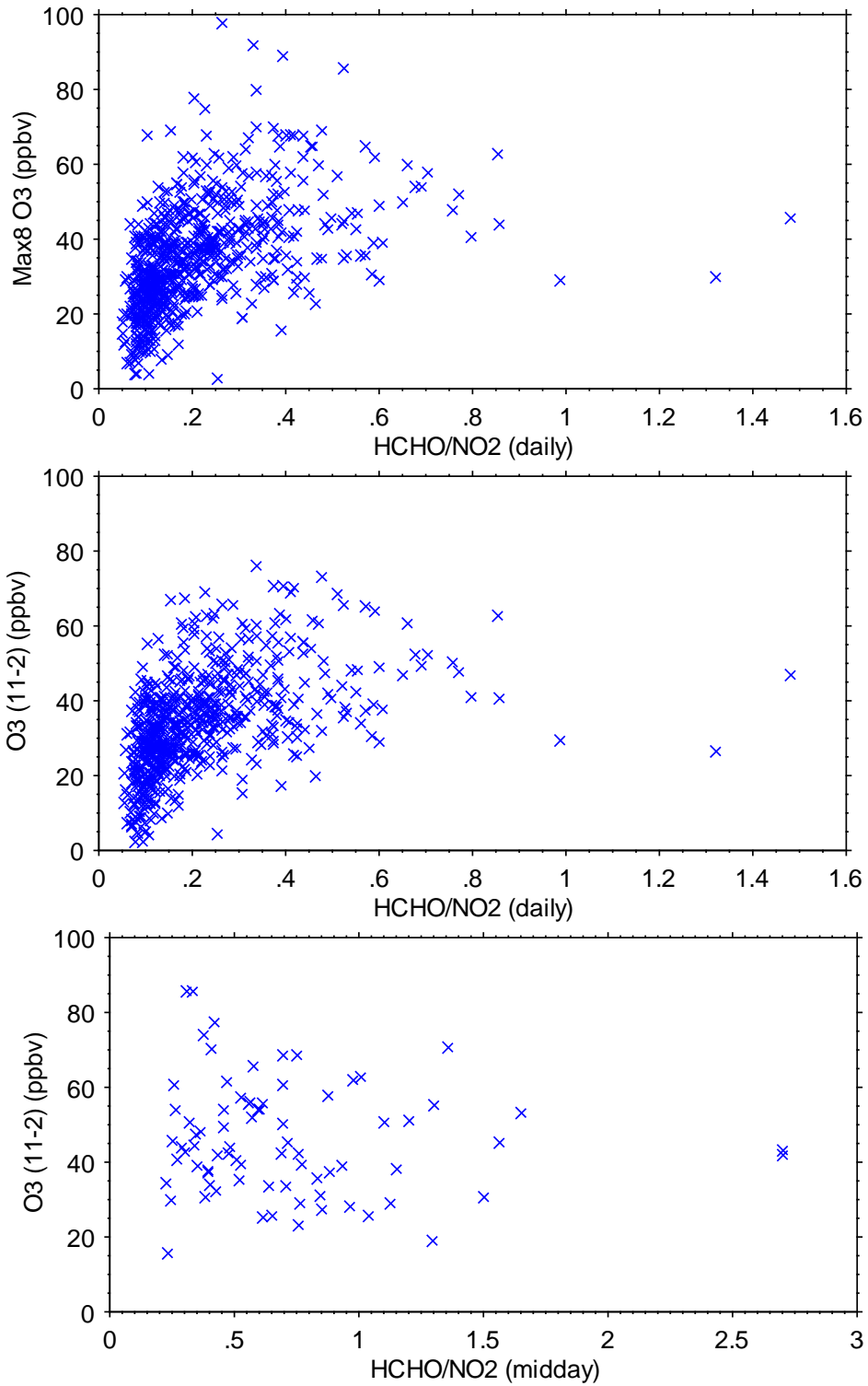


Figure A4. Milwaukee SER DNR MDA8 and 11 a.m. – 2 p.m. O<sub>3</sub> vs. 24-hour and 11 a.m. – 2 p.m. HCHO/NO<sub>2</sub>. MDA8 O<sub>3</sub> exceeds 11 a.m. – 2 p.m. on some days, generally when the starting hour of the MDA8 O<sub>3</sub> is later than 11 a.m.

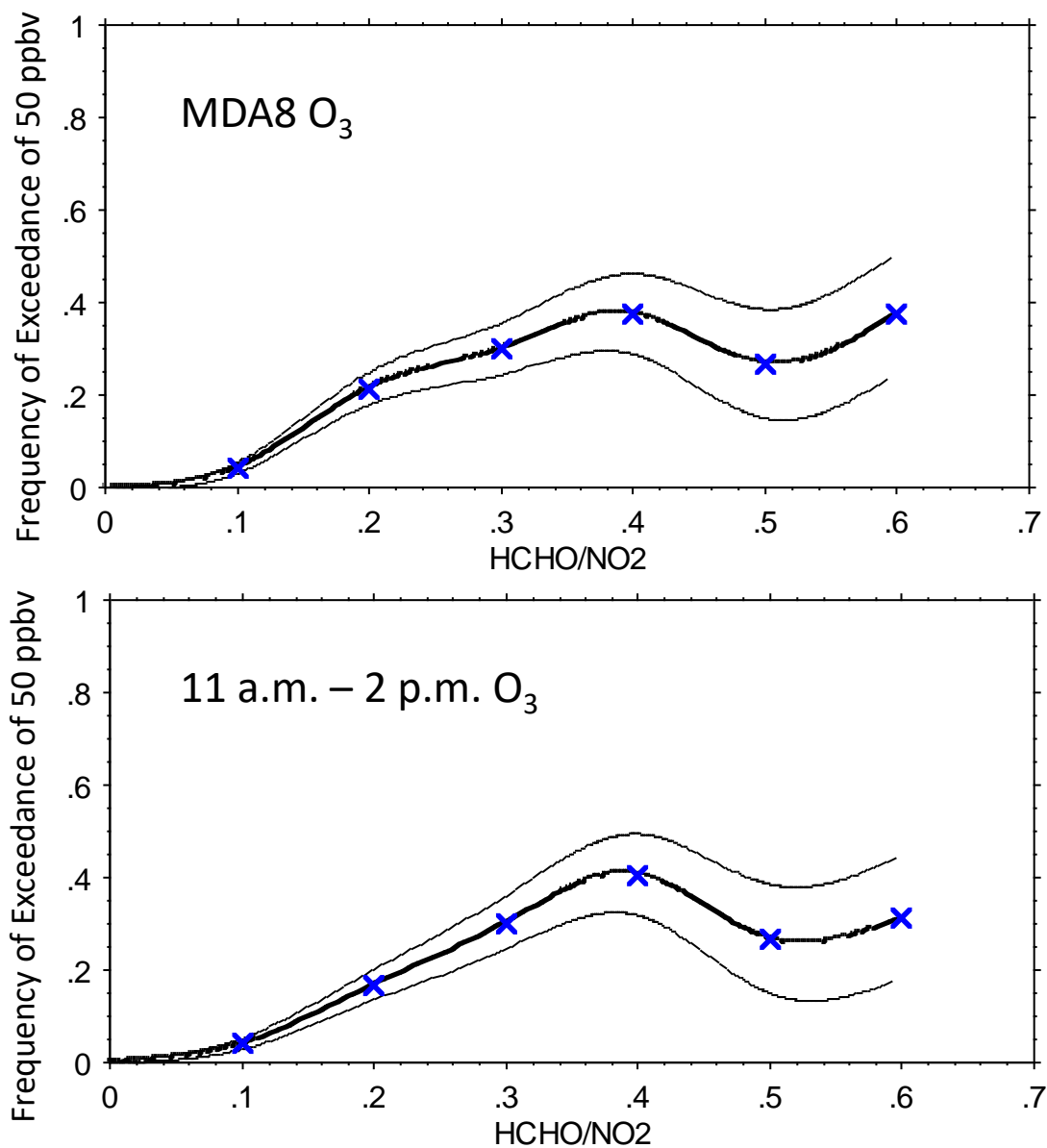


Figure A5. Frequency of exceedance of 50 ppbv for Milwaukee SER DNR MDA8 and mid-day (11 a.m. – 2 p.m.) O<sub>3</sub> versus binned HCHO/NO<sub>2</sub>. Bin intervals are 0.1 unit width except the highest interval ranges from 0.6 – 1.5 ppbC ppbv<sup>-1</sup> due to limited numbers of measurements (Figure A4). Bin-average HCHO/NO<sub>2</sub> ratios are plotted at their lower limits. Uncertainty limits indicate one standard error.

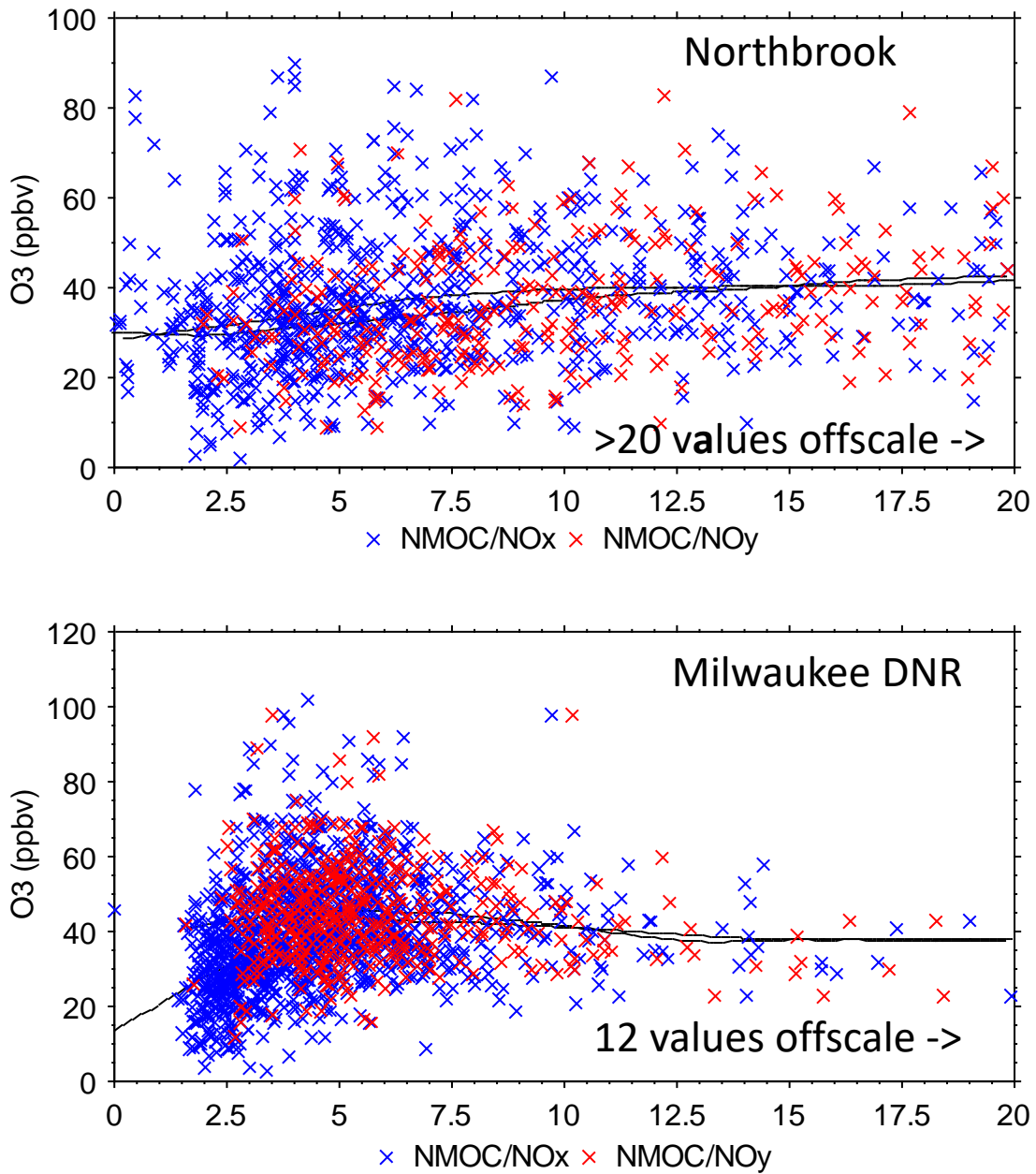


Figure A6. MDA8 O<sub>3</sub> vs. daily-average NMOC/NO<sub>x</sub> at Northbrook IL and Milwaukee SER DNR.

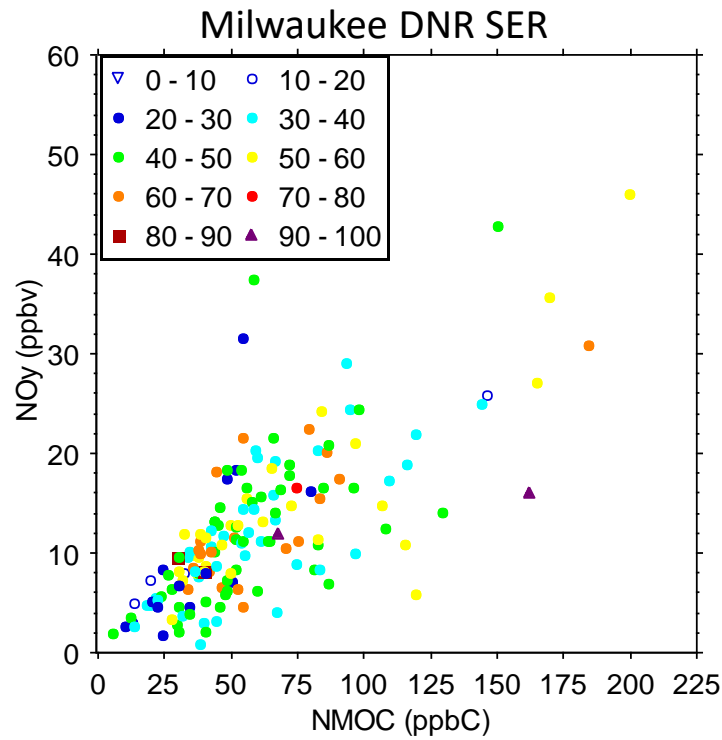
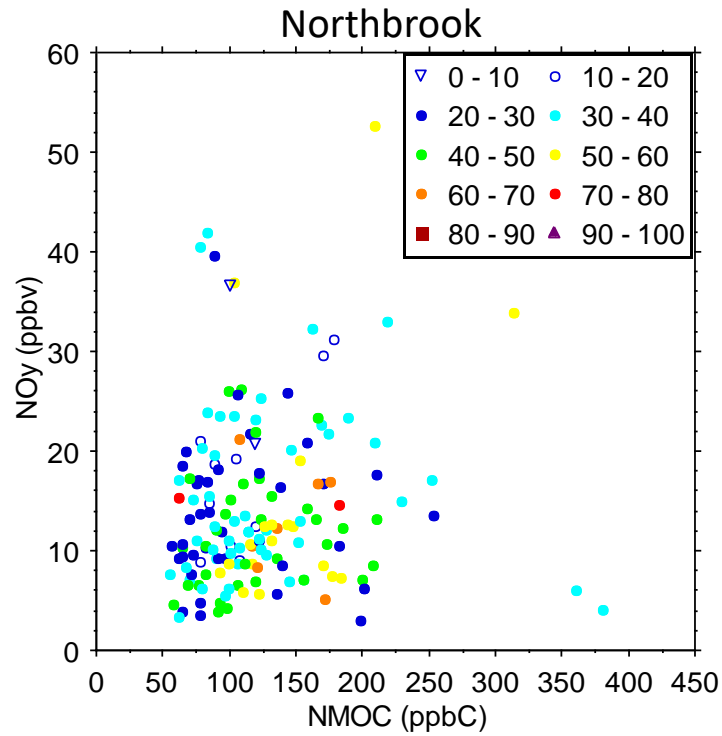


Figure A7. Daily-average NO<sub>y</sub> vs. NMOC. Symbols indicate MDA8 O<sub>3</sub> concentrations.

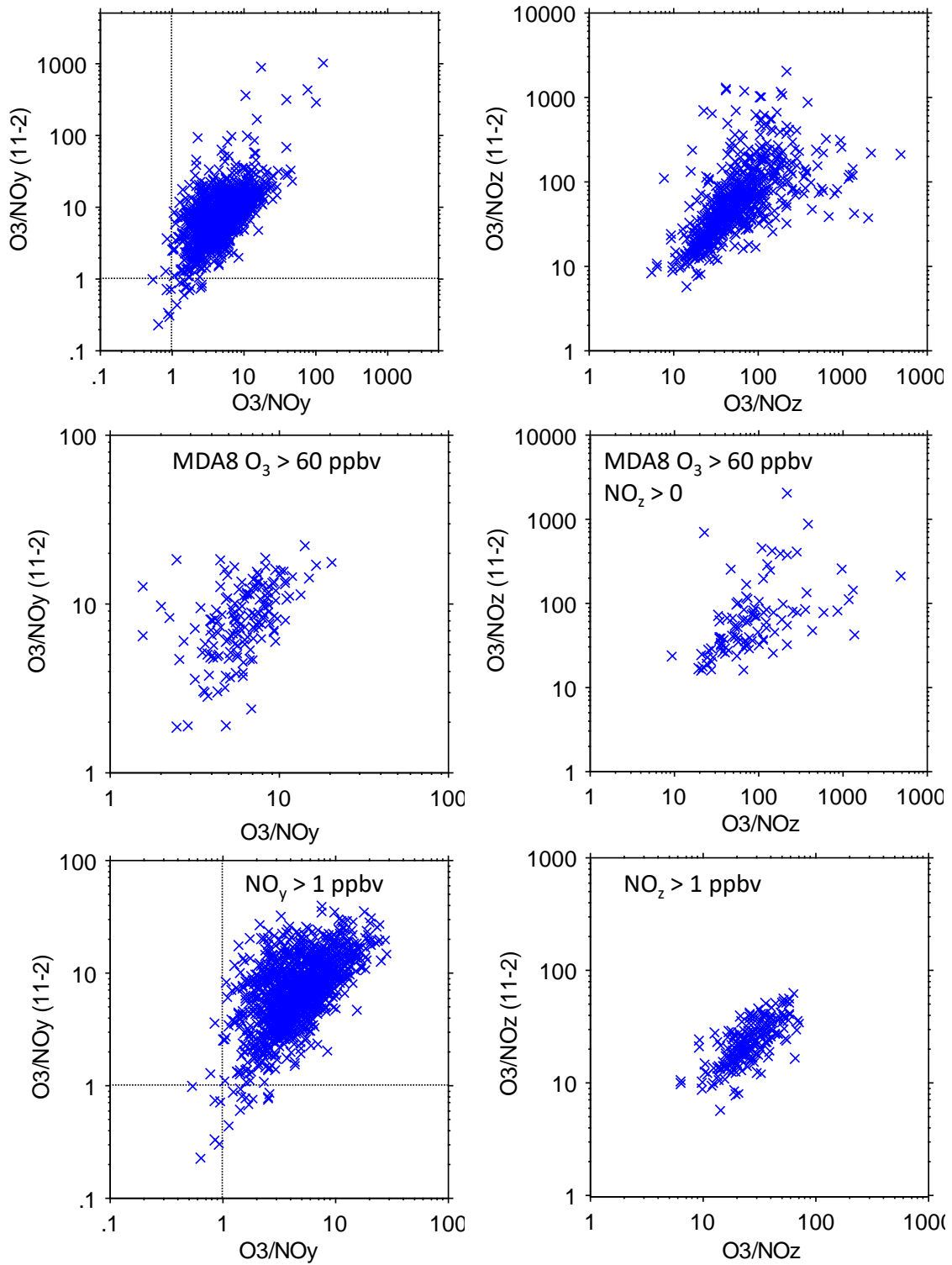


Figure A8. Comparison of Milwaukee SER DNR mid-day with daily-average ratios of O<sub>3</sub>/NO<sub>y</sub> and O<sub>3</sub>/NO<sub>z</sub>.

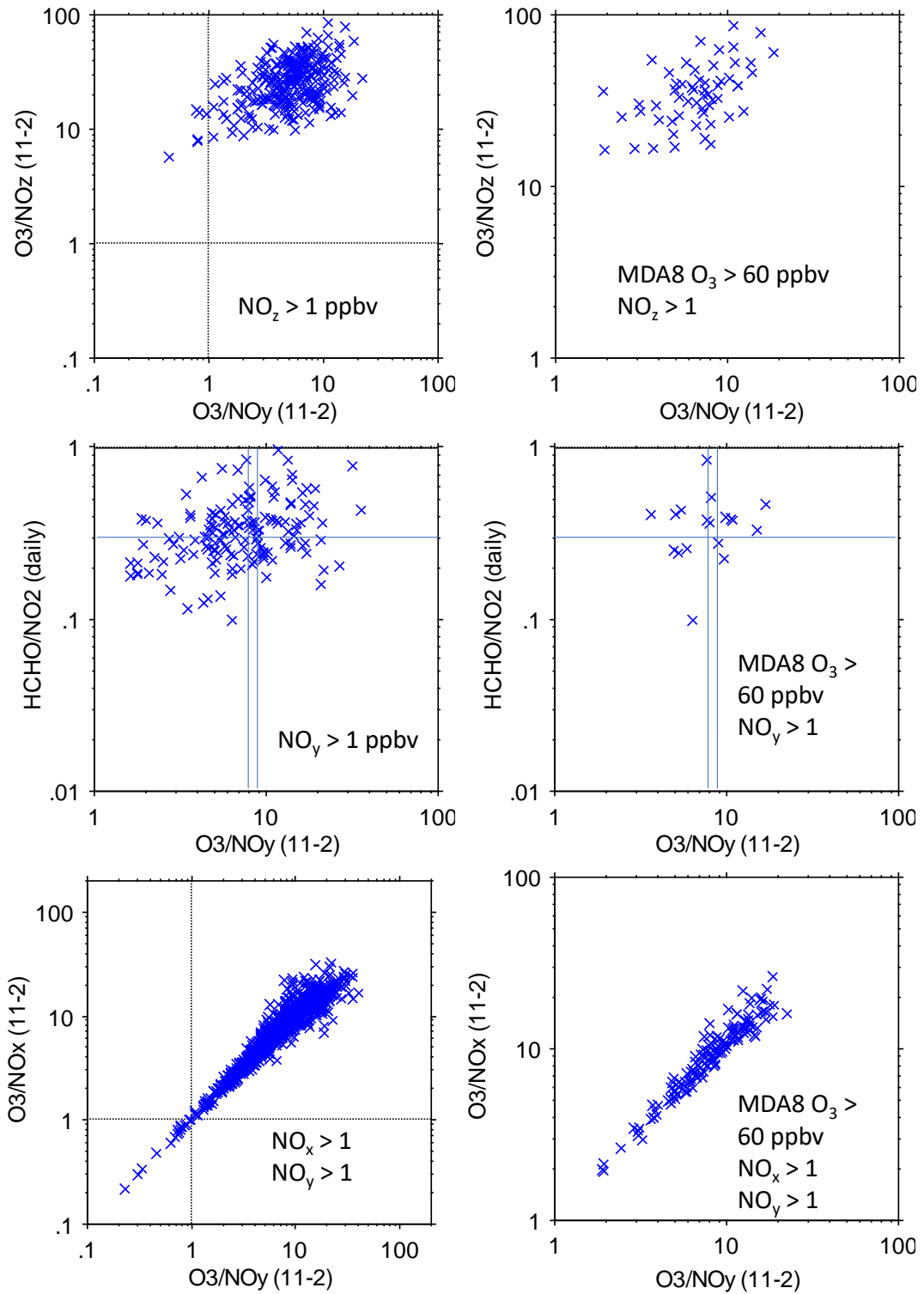


Figure A9. Comparison of Milwaukee SER DNR mid-day ratios of O<sub>3</sub>/NO<sub>y</sub>, O<sub>3</sub>/NO<sub>z</sub>, HCHO/NO<sub>y</sub> and O<sub>3</sub>/NO<sub>x</sub>.

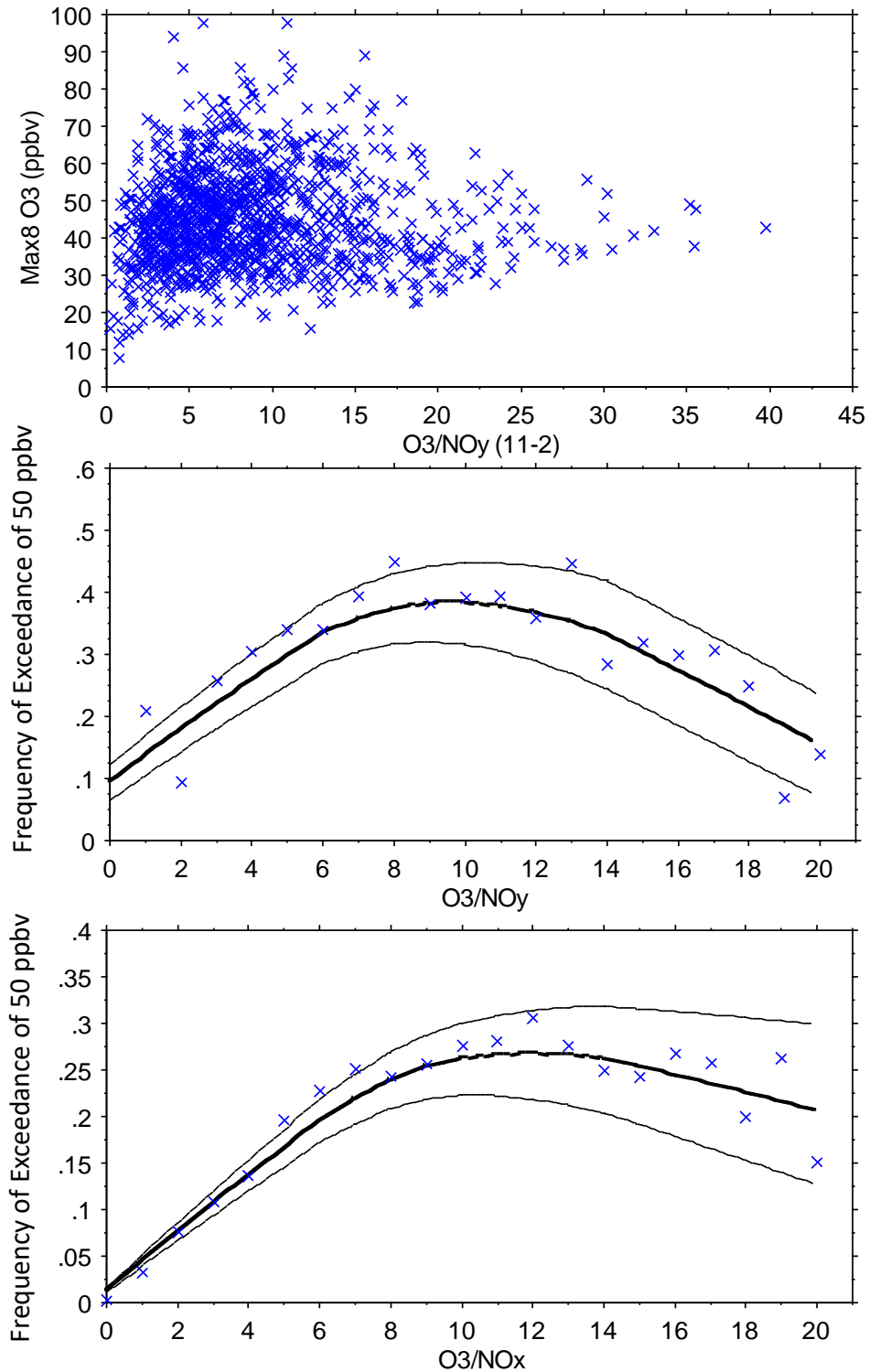


Figure A10. MDA8 O<sub>3</sub> vs. daily-average O<sub>3</sub>/NO<sub>y</sub> at Milwaukee SER DNR (top). Frequency of exceedance of 50 ppbv for Milwaukee SER DNR MDA8 O<sub>3</sub> versus binned O<sub>3</sub>/NO<sub>y</sub> and O<sub>3</sub>/NO<sub>x</sub>. Bin intervals are 1 unit wide except the highest interval ranges from 20 – 40 due to limited numbers of measurements. Bin-average ratios are plotted at their lower limits. Uncertainty limits indicate one standard error.

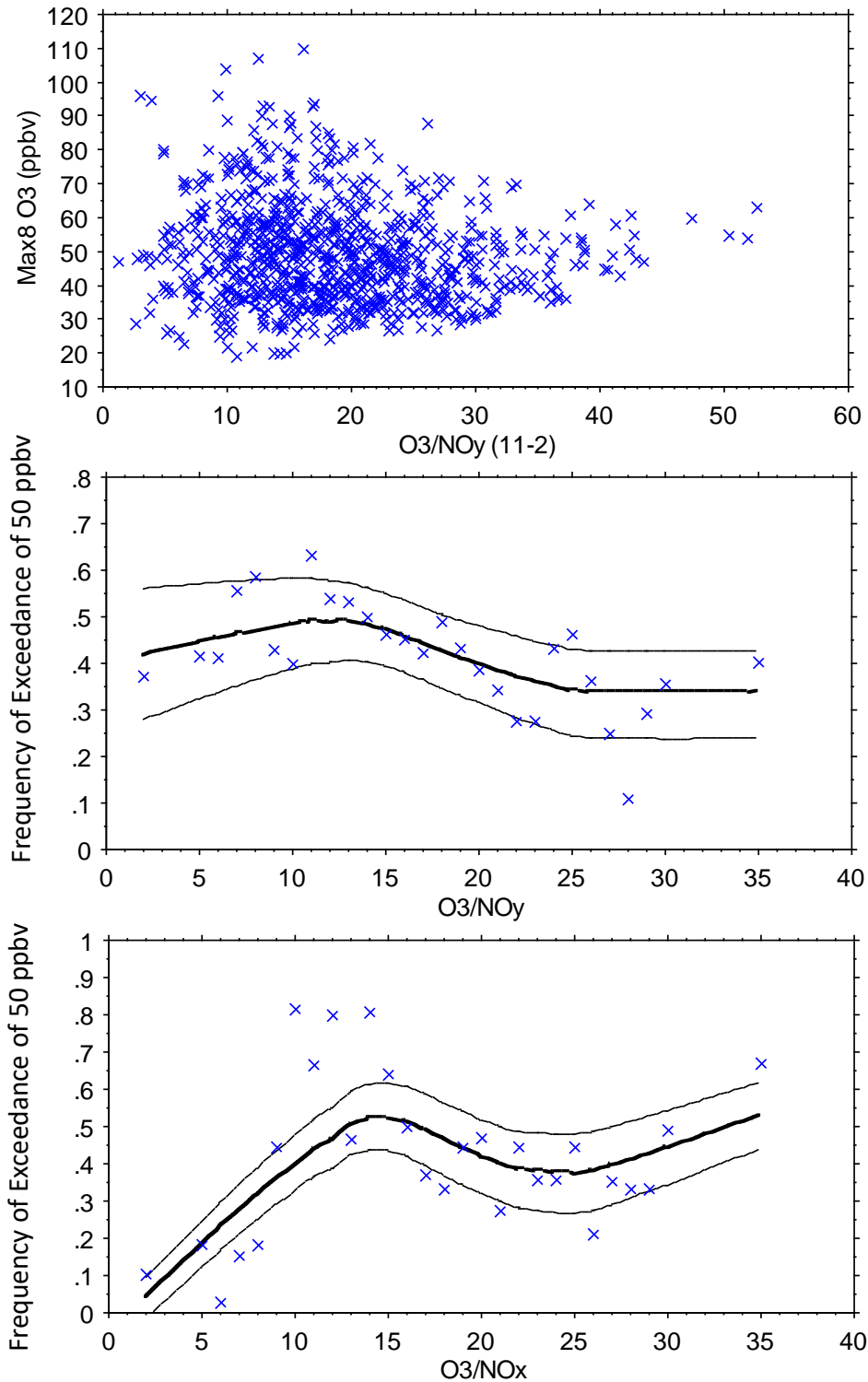


Figure A10 (continued). MDA8 O<sub>3</sub> vs. daily-average O<sub>3</sub>/NO<sub>y</sub> at Manitowoc (top). Frequency of exceedance of 50 ppbv for Manitowoc MDA8 O<sub>3</sub> versus binned O<sub>3</sub>/NO<sub>y</sub> and O<sub>3</sub>/NO<sub>x</sub>. Bin intervals are 1 unit wide except the lowest and highest intervals due to limited numbers of measurements. Bin-average ratios are plotted at their lower limits except the lowest bin (0 – 5, plotted at 2). Uncertainty limits indicate one standard error.

## 9.4 Data Summaries and Comparisons

### 9.4.1 Trends in Emissions and Ambient Concentrations

Annual emission estimates and ambient pollutant concentrations were obtained from EPA (2020e; 2020f; 2020g). Figure 1 shows annual anthropogenic emissions (including wildfires and other biomass burning sources) of CO, NO<sub>x</sub>, SO<sub>2</sub>, and VOCs in Illinois, Indiana, and Wisconsin. The discontinuity between 2001 and 2002 is attributable to EPA’s revision of its emission model for on-road mobile sources (from MOBILE6 to MOVES). Emission trends are consistent with mean annual ambient concentrations of CO, NO<sub>x</sub>, and SO<sub>2</sub>, but not with total NMOC (Figures A8 and A9). However, intersite variability is high for total NMOC and these measurements include both anthropogenic and biogenic compounds. Trends in specific anthropogenic NMOC species at individual urban monitoring locations indicate that ambient concentrations of species such as benzene and toluene declined between 1999 and 2019 by nearly a factor of two (Figures A10 and A11). Total NMOC concentrations also declined at these sites (Figure A12). For all sites, compounds, and years, the ranges of daily species concentrations exceeded the mean annual concentrations.

Multisite averages of daily species concentrations were computed using data from a set of sites selected for longevity of monitoring (Table A3). The mean annual concentrations of these multisite daily values tracked emissions, showing some variability for NMOC ( $r^2 = 0.6$ , one site only) and closer agreement ( $r^2 = 0.9$ ) for other species (Figure A13).

Table A3. Site data used for computing multisite daily species concentrations.

Site	CO	NO	NO <sub>2</sub>	SO <sub>2</sub>
Green Bay	NA	NA	NA	2000 - 2019
Milwaukee	2000 - 2007	2000,	2000,	2002 - 2019
DNR SER		2003 - 2019	2003 - 2019	
Horicon	2010 - 2019	NA	NA	NA
Mayville	2007 – 2009	NA	NA	NA
Northbrook	2007 - 2019	2000 – 16, 2011 - 19	2000 – 16, 2000 - 09	2004 – 09, 2008 - 19
Schiller	2000 - 2012	2000 - 2019	2000 - 2019	NA
Lawndale	NA	2002 - 2019	2002 - 2019	2004 - 2019
Cicero	2000 - 2012	NA	NA	NA
CTA building	2000 - 2012	NA	NA	NA
Maywood	2000 - 2012	NA	NA	NA
Gary IITRI	NA	2000 - 2019	2000 - 2019	2000 - 2019

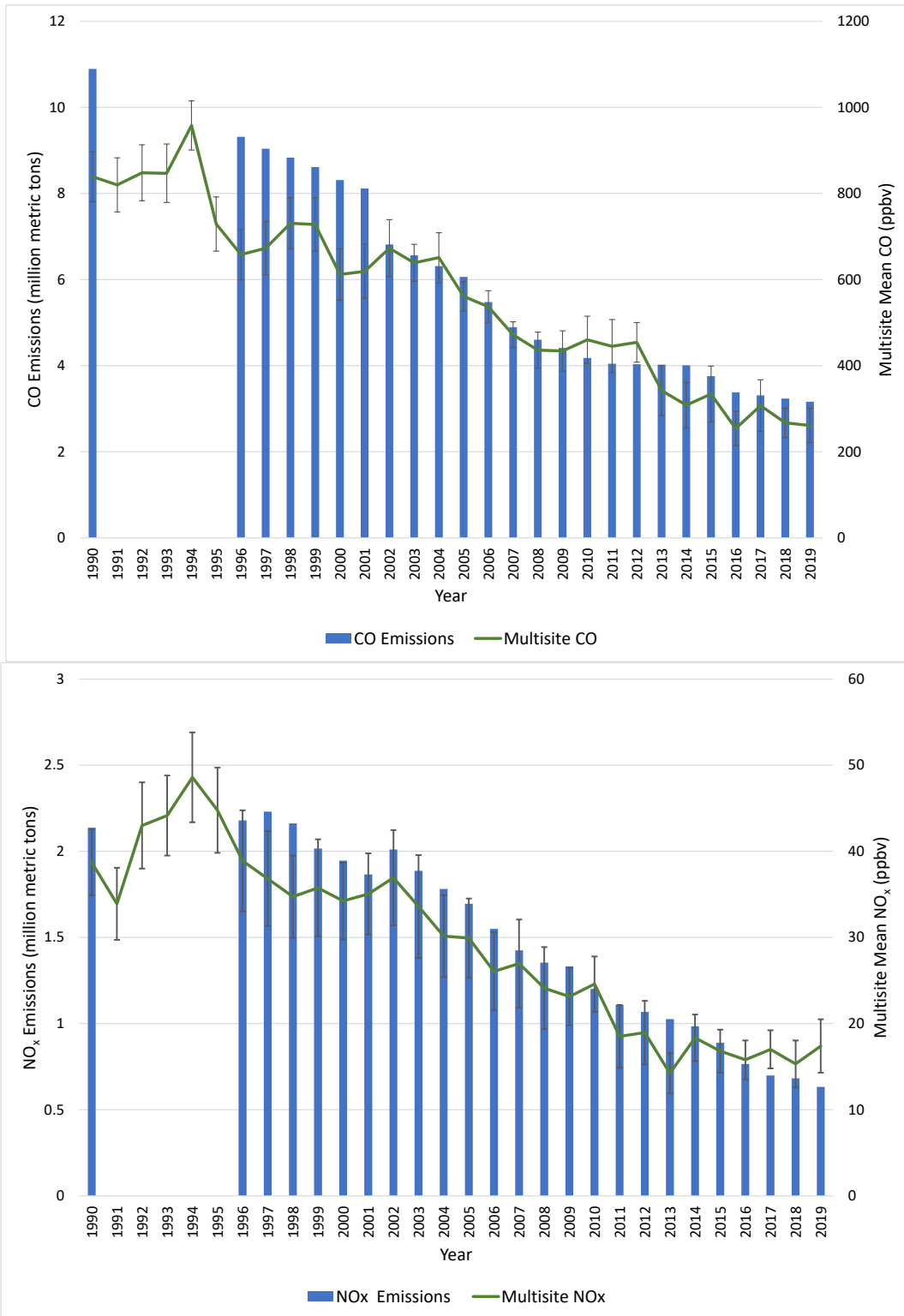


Figure A8. Comparison of trends in anthropogenic emissions and mean annual ambient concentrations of CO and NO<sub>x</sub> within IN, IL, and WI. Error bars are one standard error of the mean of the site means.

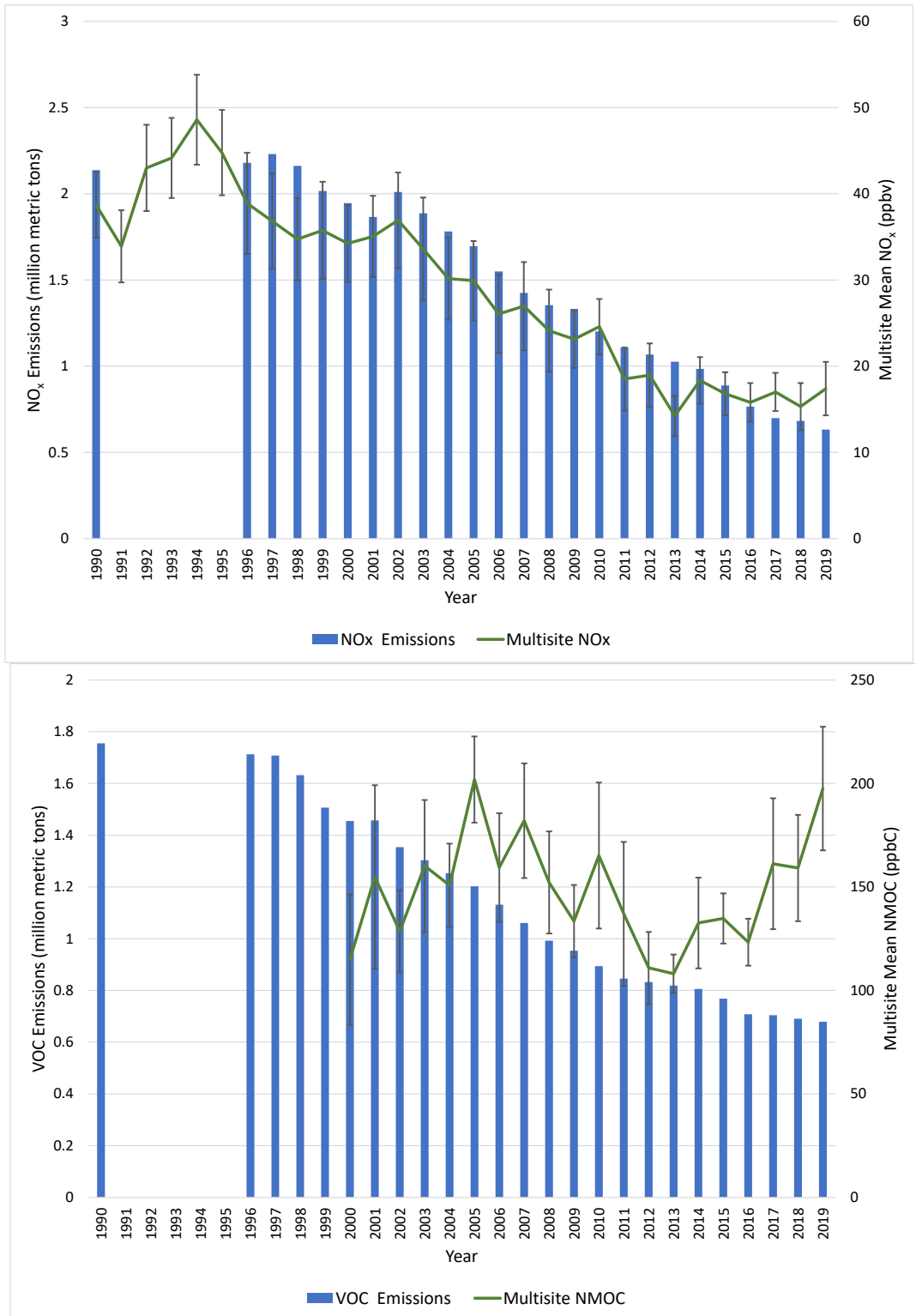


Figure A9. Comparison of trends in anthropogenic emissions and mean annual ambient concentrations of SO<sub>2</sub> and NMOC within IN, IL, and WI. Error bars are one standard error of the mean of the site means.

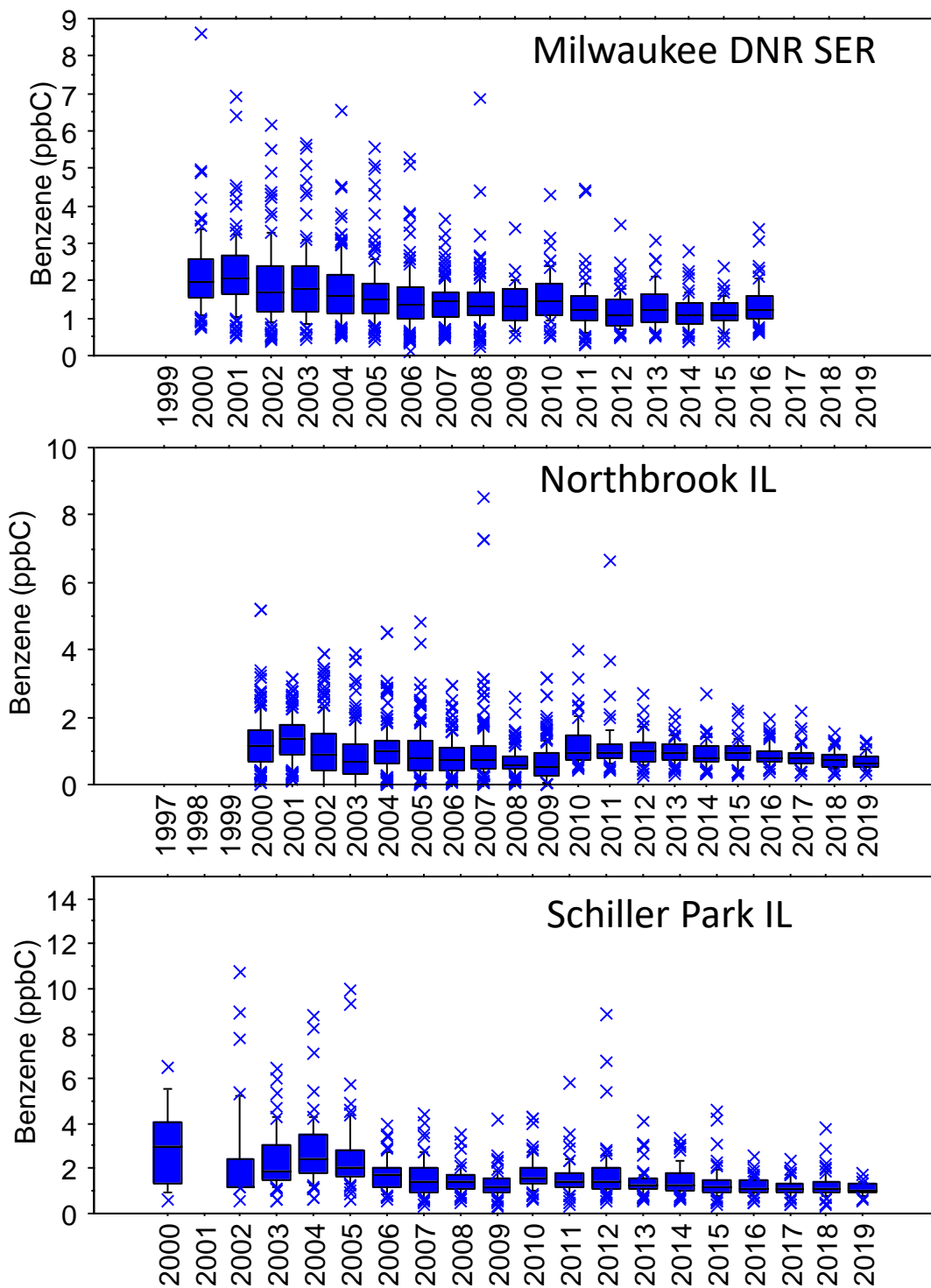


Figure A10. Statistical distributions of daily average benzene concentrations at three monitoring sites. Plots show 10<sup>th</sup>, 25<sup>th</sup>, 50<sup>th</sup>, 75<sup>th</sup>, and 90<sup>th</sup> percentiles plus values < 10<sup>th</sup> percentile or > 90<sup>th</sup> percentile. Individual values may exceed the range of the y-axis scale.

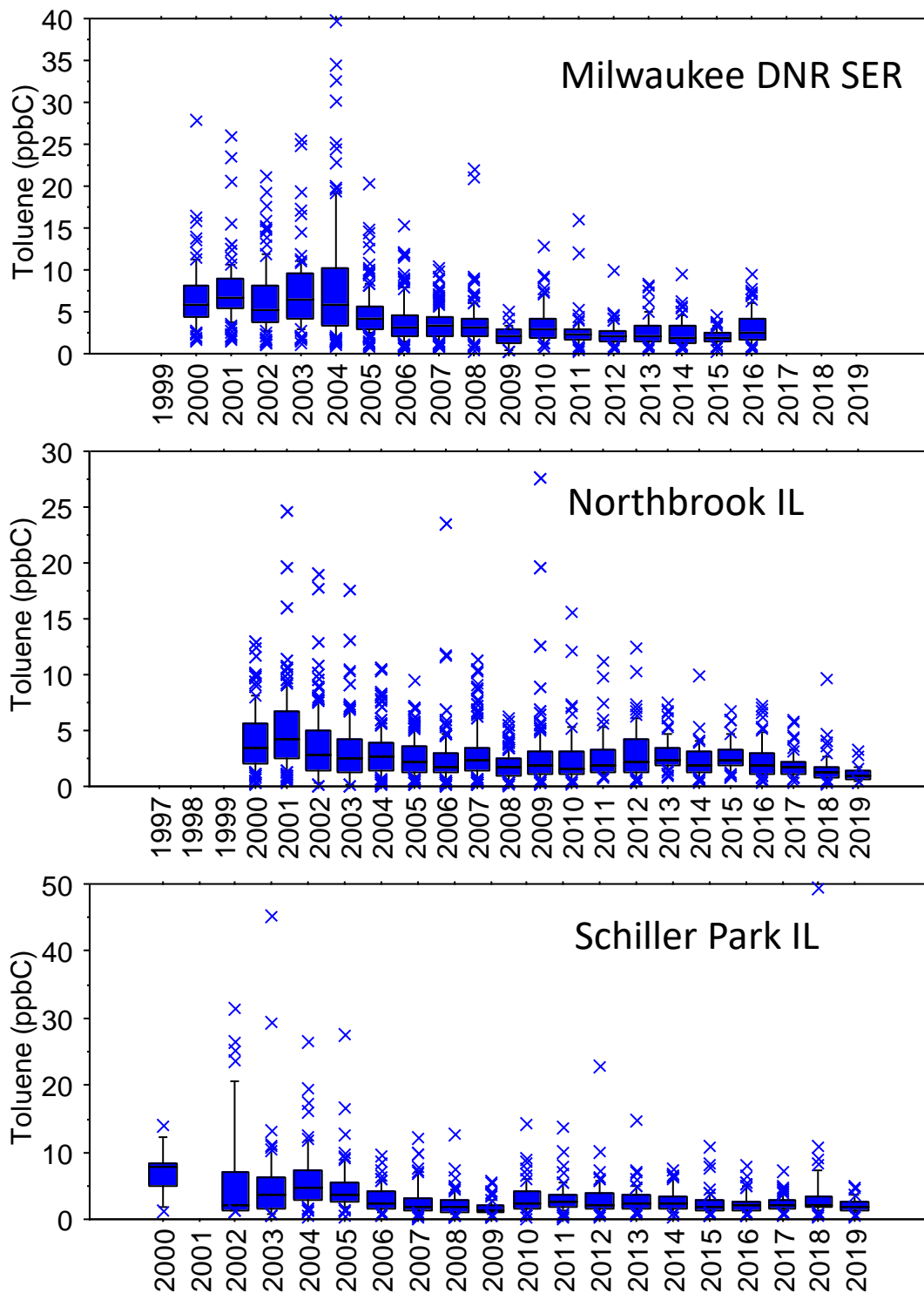


Figure A11. Statistical distributions of daily average toluene concentrations at three monitoring sites. Plots show 10<sup>th</sup>, 25<sup>th</sup>, 50<sup>th</sup>, 75<sup>th</sup>, and 90<sup>th</sup> percentiles plus values < 10<sup>th</sup> percentile or > 90<sup>th</sup> percentile. Individual values may exceed the range of the y-axis scale.

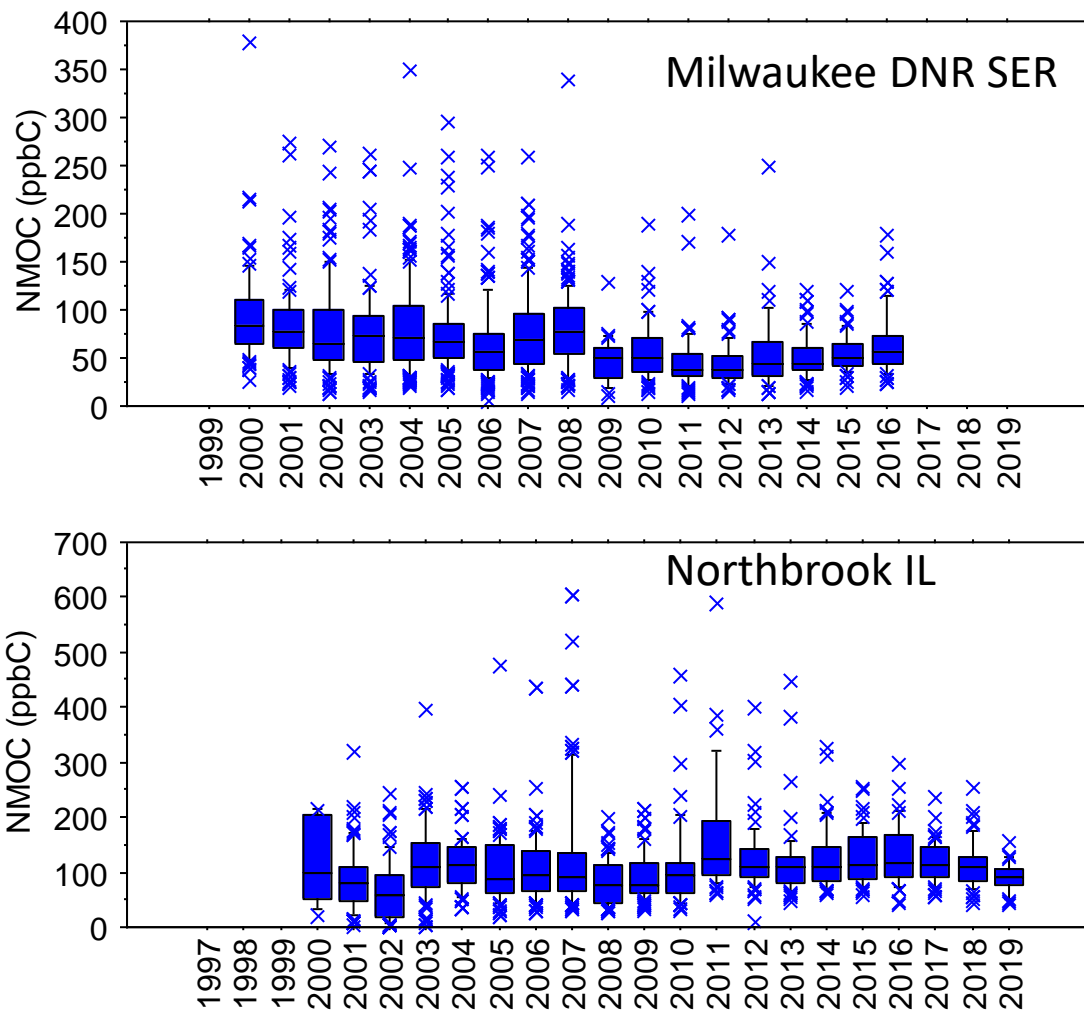
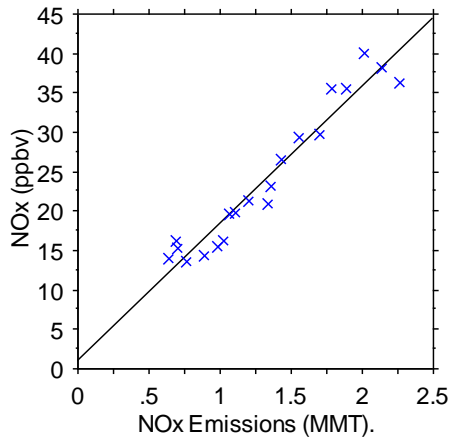
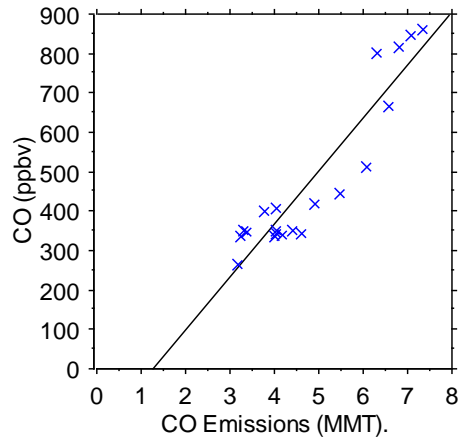


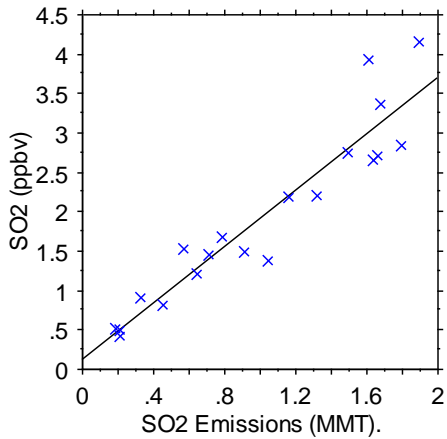
Figure A12. Statistical distributions of daily average total NMOC concentrations at two monitoring sites. Plots show 10<sup>th</sup>, 25<sup>th</sup>, 50<sup>th</sup>, 75<sup>th</sup>, and 90<sup>th</sup> percentiles plus values < 10<sup>th</sup> percentile or > 90<sup>th</sup> percentile. Individual values may exceed the range of the y-axis scale.



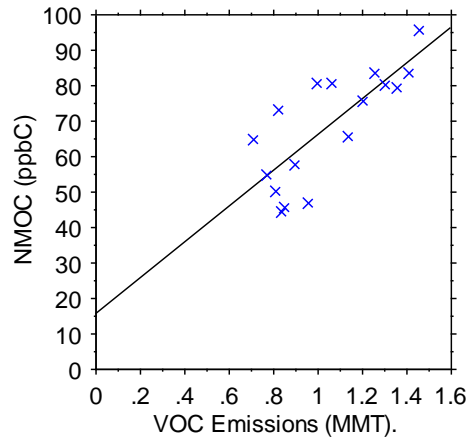
NOx (ppbv) = 1.117 + 17.393 \* NOx Emissions (MMT).;  $R^2 = .935$



CO (ppbv) = -168.668 + 133.885 \* CO Emissions (MMT).;  $R^2 = .86$



SO2 (ppbv) = .13 + 1.79 \* SO2 Emissions (MMT).;  $R^2 = .89$



NMOC (ppbC) = 15.747 + 50.522 \* VOC Emissions (MMT).;  $R^2 = .602$

Figure A13. Annual-average of daily multisite pollutant concentrations vs emissions within IL, IN, and WI. Data used in computing multisite averages are listed in Table A3. The NMOC values are from Milwaukee DNR SER.

NMOC measurements were made once every six days, generally as 24-hour samples, at a limited number of sites (Table A1). Fewer sites reported CO data (Table A1), but CO measurements were made hourly and therefore have temporal resolution that is lacking in the NMOC data. CO measurements potentially provide an indicator of mobile-source VOC emissions, since mobile-source CO emissions accounted for 78 – 90% of total anthropogenic CO emissions (including fires) in IL, IN, and WI between 2000 and 2019 (U.S. EPA, 2020e). Daily-average CO concentrations correlated with total NMOC at Milwaukee SER DNR ( $r^2 = 0.60$ ) but not at Northbrook ( $r^2 = 0.03$ ). To varying degrees, daily-average CO concentrations correlated with benzene, which is associated with mobile-source emissions:  $r^2 = 0.59$  at Milwaukee SER DNR, 0.38 at Schiller Park, 0.28 at Northbrook, and 0.08 at Horicon/Mayville. The differences among sites appear to reflect concentrations (low at Horicon/Mayville, high outliers at Schiller Park and Northbrook) and may also indicate differences in source influences.

### 9.4.2 Surface Wind

Daily-average wind directions at or near shoreline sites exhibited spatial coherence (Figure A14). Consistency was also evident in comparisons of daily-average wind direction with the direction of the fastest 2-min wind gust (reported at airport locations). Morning (6 a.m.) wind directions at the Green Bay radiosonde site were less consistent with daily-average wind directions at Sheboygan Kohler Andrae and Manitowoc.

Wind speeds exhibited greater variation among sites than wind directions did (Figure A15).

Daily-average wind directions, while useful, obscure important temporal variations (Figure A16). High-resolution (2-min) NOAA data (<https://www.glerl.noaa.gov/metdata>) are available for five sites along the southern Lake Michigan shoreline: Milwaukee, Chicago, Michigan City IN, South Haven MI, and Muskegon MI. Hourly wind direction data are available from many of the air quality sites.

### 9.4.3 Hourly Observations

Example plots of hourly species concentrations, wind speed and direction, and O<sub>3</sub> vs NO<sub>z</sub> at Manitowoc and Milwaukee SER DNR are shown in Figures A17 – A20. For these high-O<sub>3</sub> days, the day-specific slopes of O<sub>3</sub> vs. NO<sub>z</sub> are either poorly quantified ( $r^2 < 0.5$ ) or very high ( $>30$ ). As discussed previously, NO<sub>z</sub> values are biased low and subject to uncertainty (Tables A1 and A2). Slopes for Northbrook, even restricted to mid-day (e.g., 10 a.m. – 3 p.m.) hours were not statistically significant or were negative. Therefore, the slopes of O<sub>3</sub> vs. NO<sub>z</sub> regressions are not robust indicators of O<sub>3</sub> sensitivity.

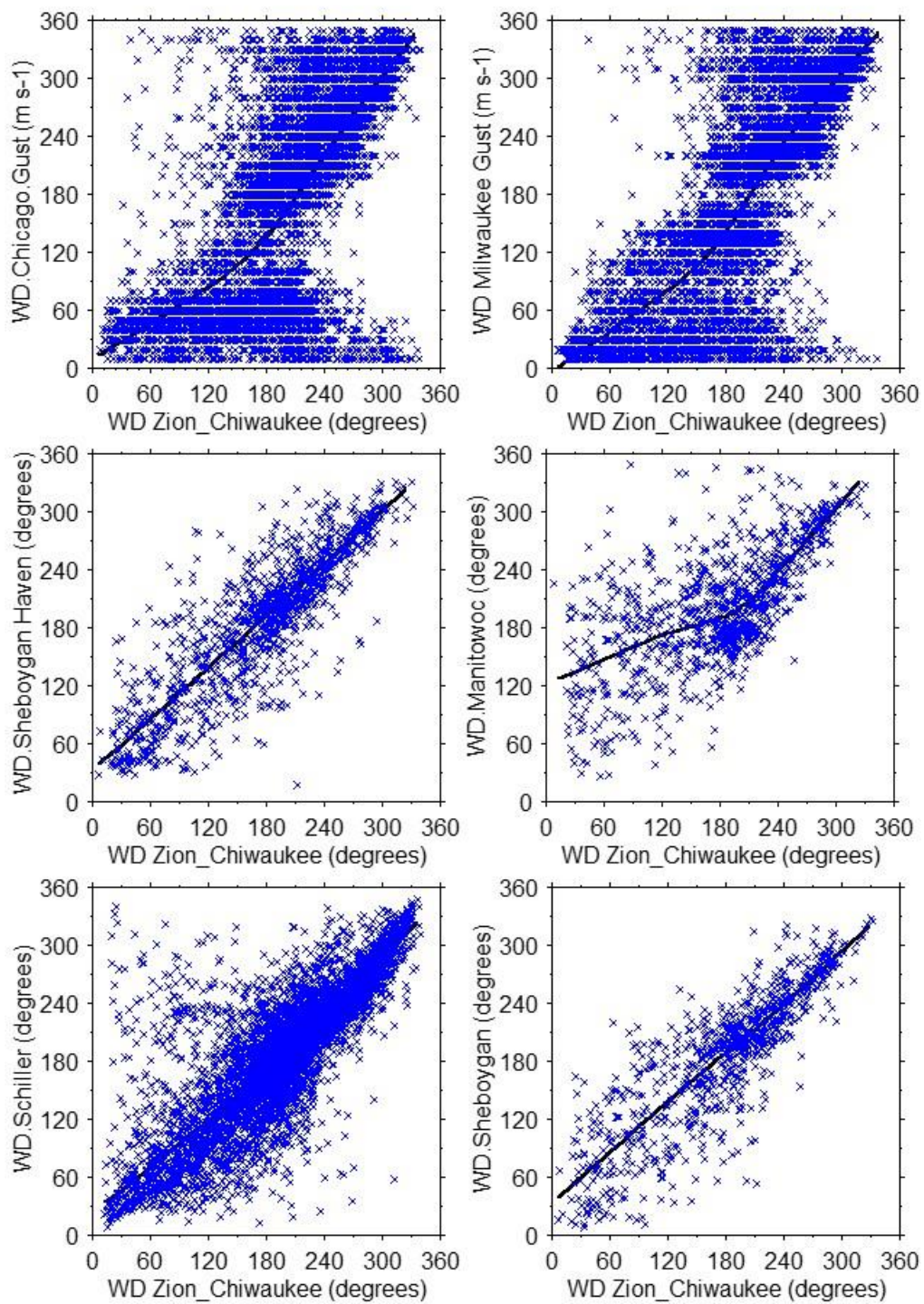


Figure A14. Comparison of wind directions.

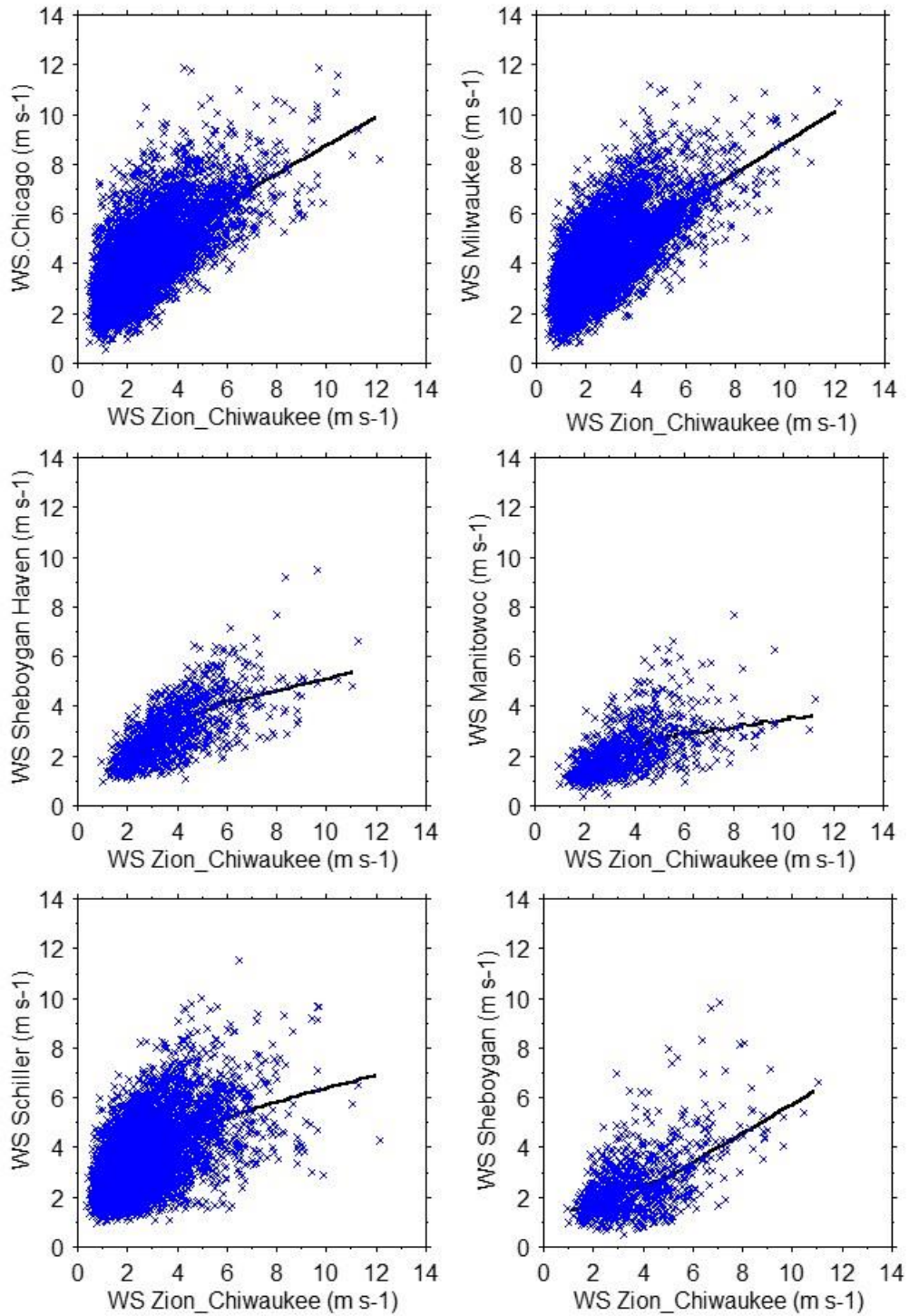


Figure A15. Comparison of wind speeds.

### Wind Direction NOAA Milwaukee 2-Min Resolution

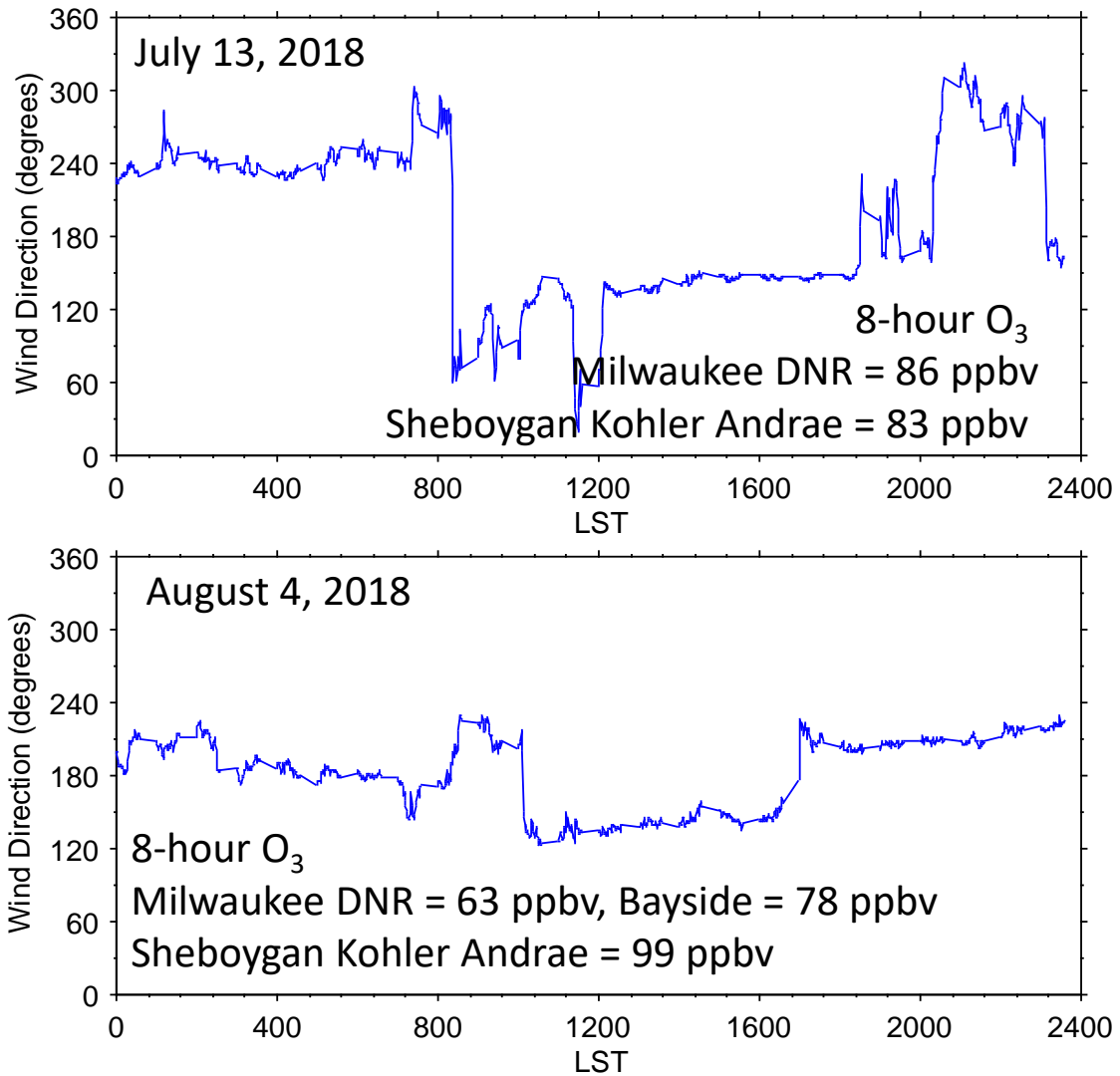


Figure A16. Time series of high-resolution (2-min) wind direction data from NOAA Milwaukee site on two dates.

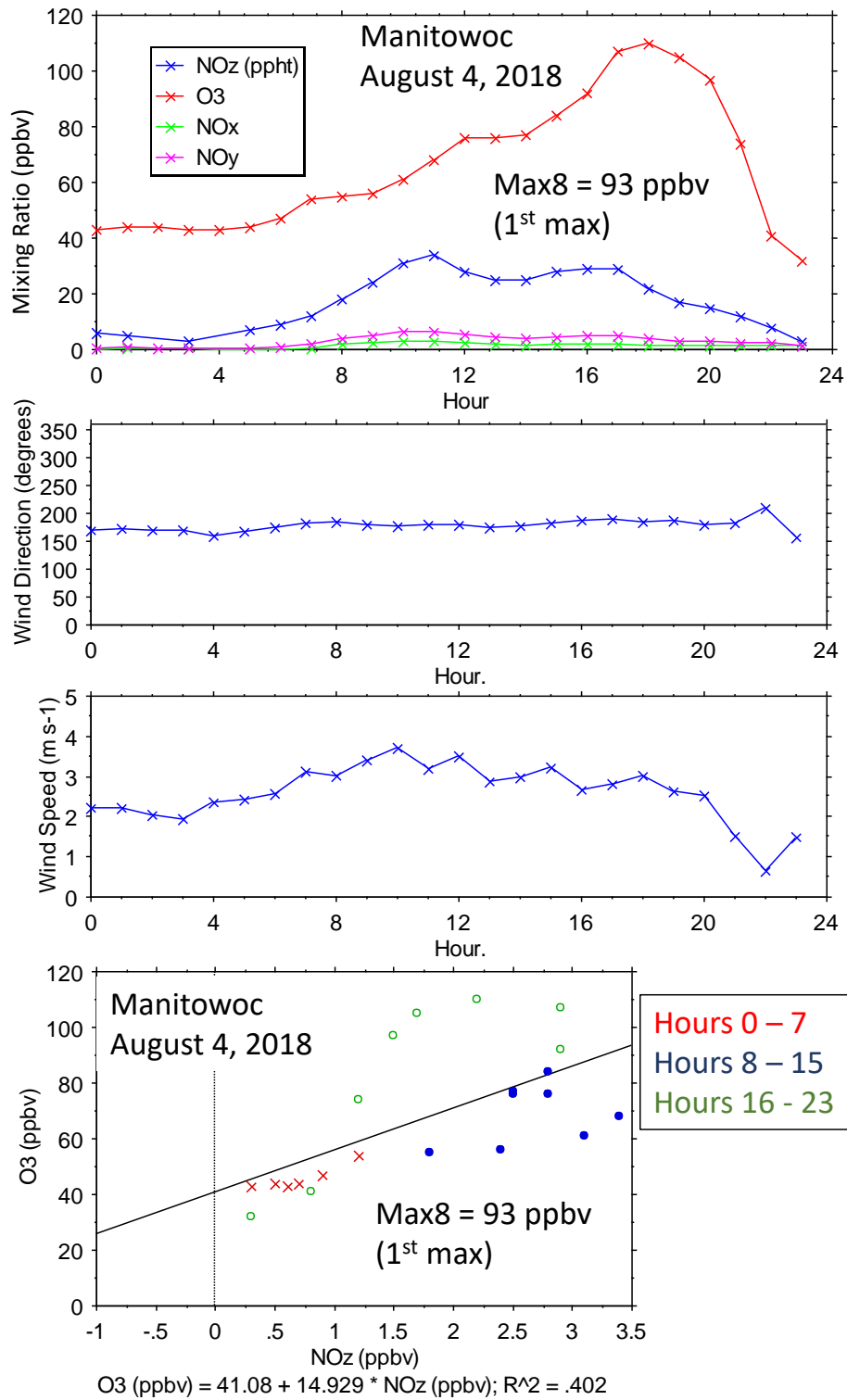


Figure A17. Hourly species concentrations, wind speed and direction, and O<sub>3</sub> vs NO<sub>z</sub> at Manitowoc on August 4, 2018.

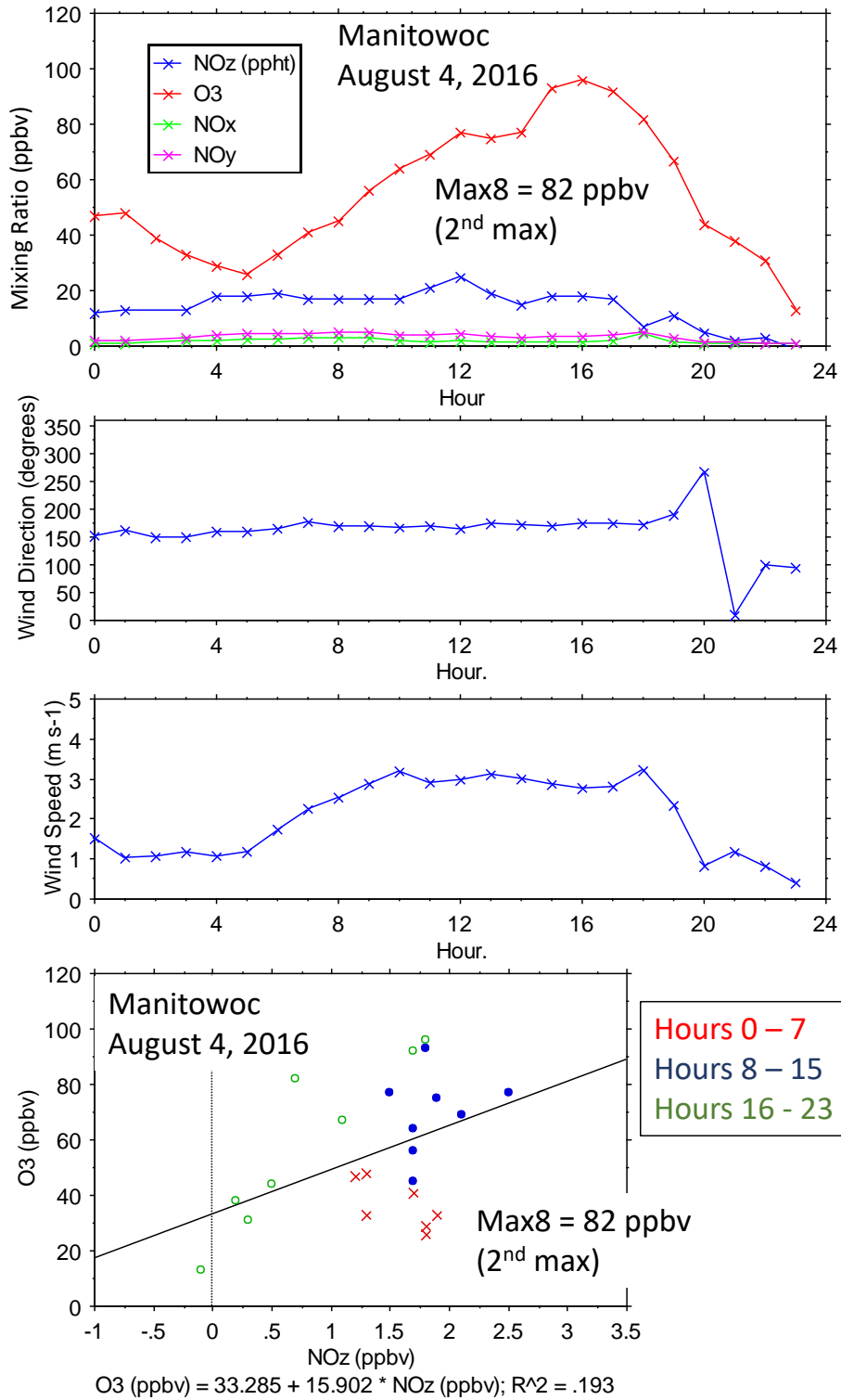


Figure A18. Hourly species concentrations, wind speed and direction, and O<sub>3</sub> vs NO<sub>z</sub> at Manitowoc on August 4, 2016.

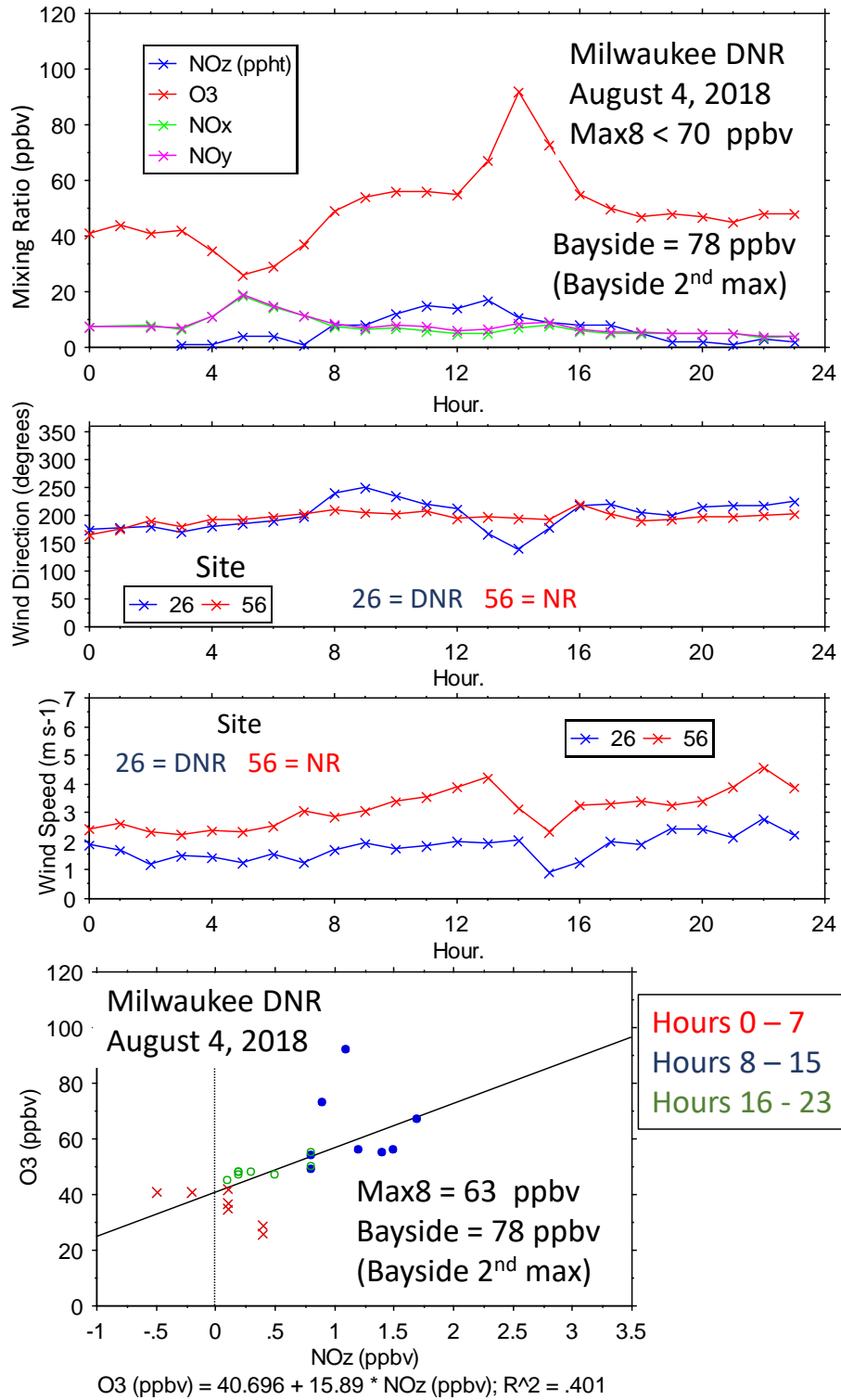


Figure A19. Hourly species concentrations, wind speed and direction, and O<sub>3</sub> vs NO<sub>z</sub> at Milwaukee SER DNR on August 4, 2018. NR = near-road site.

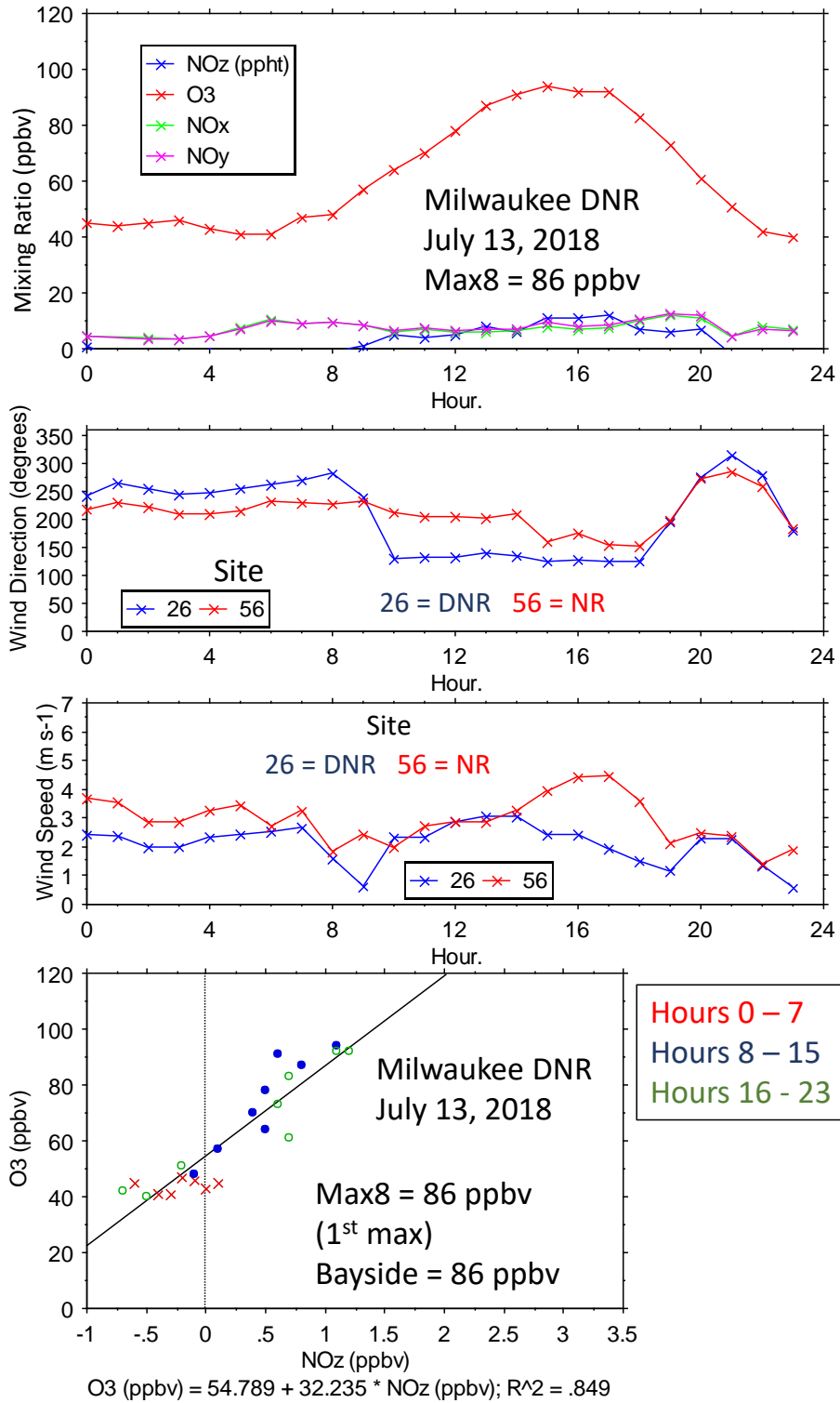


Figure A20. Hourly species concentrations, wind speed and direction, and O<sub>3</sub> vs NO<sub>z</sub> at Milwaukee SER DNR on July 13, 2018. NR = near-road site.

#### 9.4.4 Radiosonde Measurements

The sounding data provide readings from surface level to 100 mb (100 hPa) heights. Certain heights are mandatory and are therefore included in every sounding. Of these, we focused on the 850 mb (~1500 m above surface) and 500 mb (~5500 m above surface) levels. In previous studies, the 850 mb and 500 mb levels have been shown to provide useful information for relating synoptic scale weather patterns to O<sub>3</sub> exceedances.

The 500 mb height represents the approximate pressure midpoint of the atmosphere; it varies with latitude and time of year (higher when warmer). Higher than average 500 mb heights occur due to warming between the ground surface and 500 mb. Depending on where the warming occurs, higher 500 mb heights may be associated with higher 850 mb temperature, higher surface temperatures, or both. If warming occurs near the surface, upward air movement may result in lower surface pressure despite the presence of a 500 mb high pressure system. Higher than average 500 mb heights are associated with high barometric pressure, clear skies, and the presence of sinking air around the high (but rising air in the center as air masses rise on heating). An association is expected between high O<sub>3</sub> and high 500 mb heights or 850 mb temperature. Higher temperatures are known to favor photochemical reactions and O<sub>3</sub> formation. In addition, subsiding air is dry, also favoring O<sub>3</sub> formation. A blocking high can limit dispersion and subsiding air can limit vertical mixing.

The 850 mb and 500 mb heights and temperatures exhibited high correlations among radiosonde sites (Figures A21 and A22). These correlations decreased with increasing distances between sites. For example, the correlation between the 850 mb heights at Davenport and Lincoln IL was  $r = 0.973$ , between Green Bay and Gaylord MI was  $r = 0.961$ , between Gaylord and Detroit was  $r = 0.958$ , between Minneapolis and Green Bay was  $r = 0.880$ , between Minneapolis and Detroit was  $r = 0.674$ , and between Minneapolis and Wilmington OH was  $r = 0.597$ . The four locations most closely surrounding Lake Michigan (Green Bay, Gaylord, Lincoln, Detroit, Figure 3) therefore provide a good representation of synoptic-scale weather patterns affecting the study area. Computing averages from these four sites yielded nearly complete data (7302 out of 7305 days), even though individual sites were missing 73 – 274 days of specific measurements (heights were missing least often, wind speed and direction most often). Wind speed and direction were computed as vector averages of the site data.

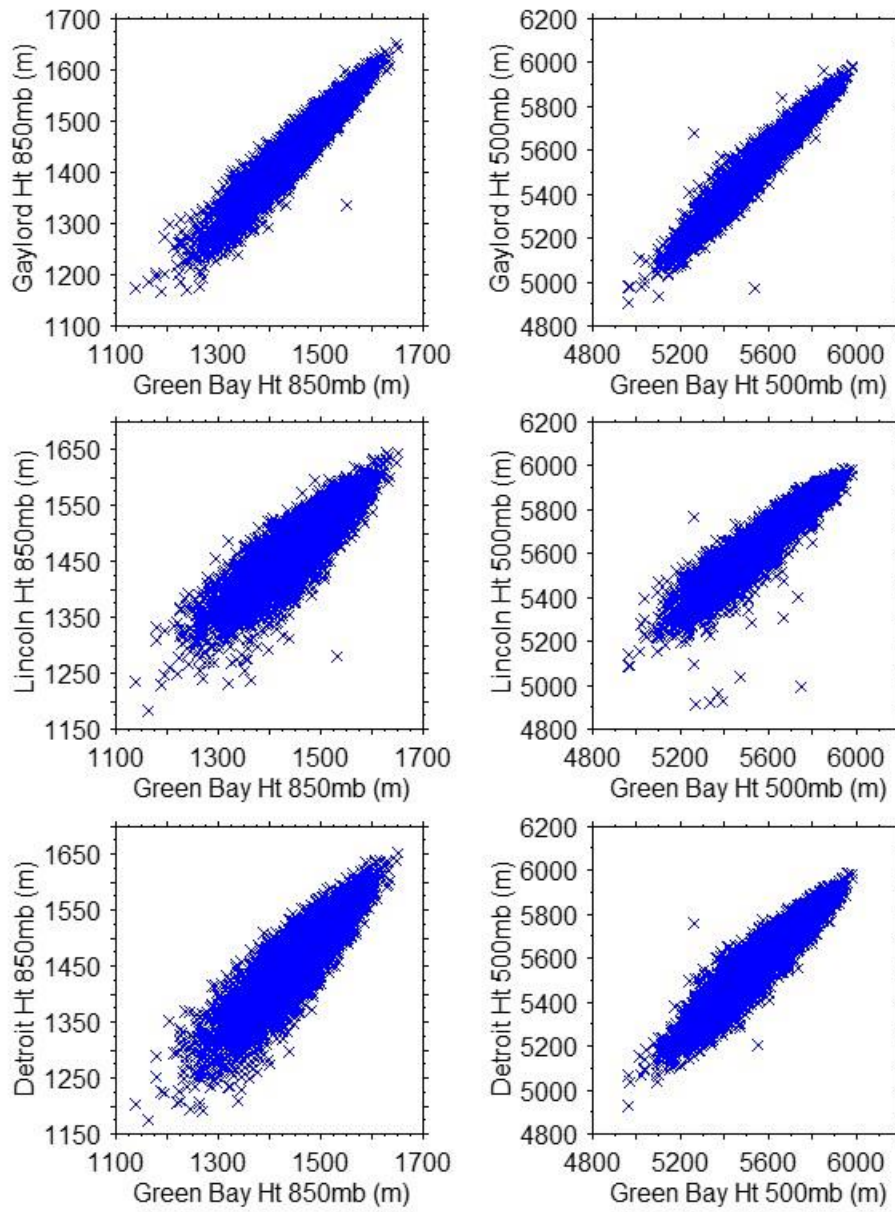


Figure A21. Comparison of 850 mb and 500 mb heights at four locations.

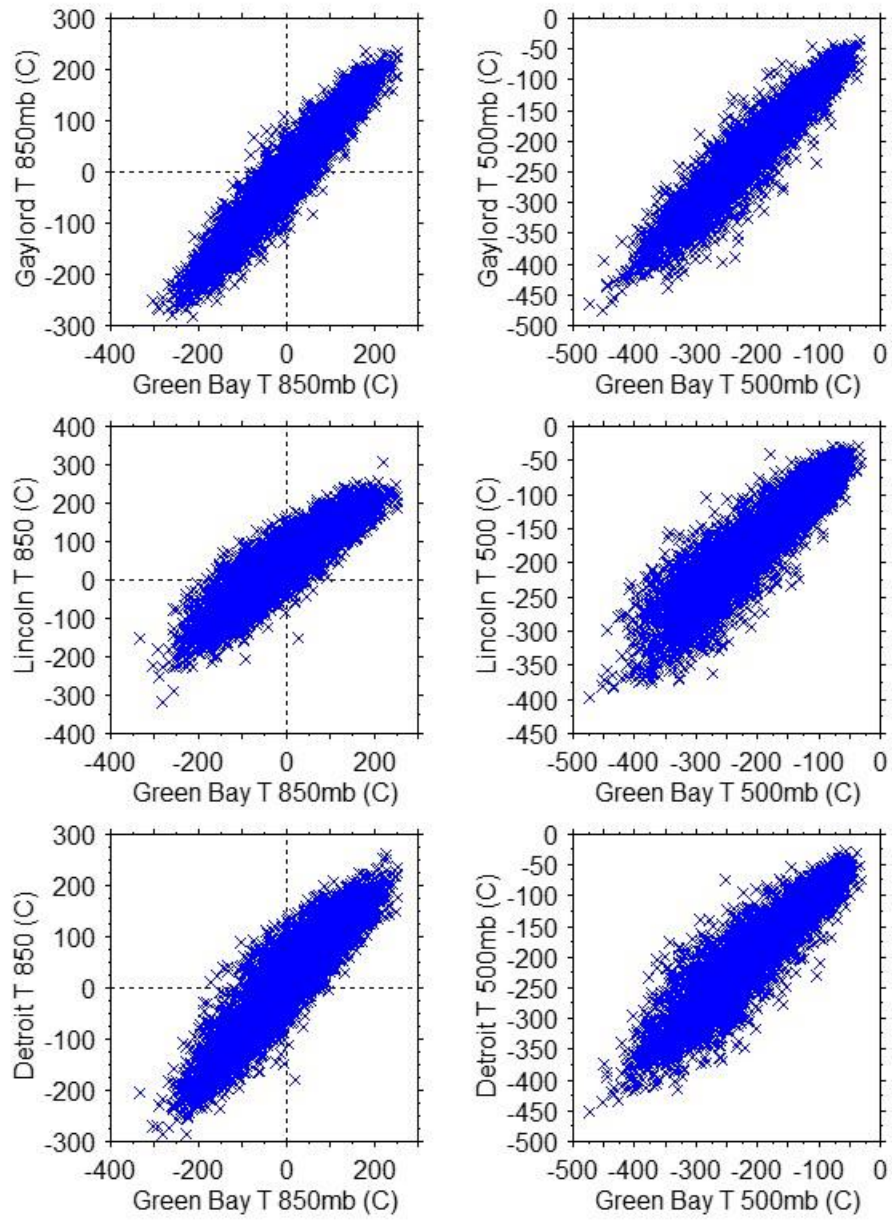


Figure A22. Comparison of 850 mb and 500 mb temperatures at four locations. Units are tenths of degrees Celsius (200 = 20°C).

#### **9.4.5 Isoprene**

Isoprene concentrations exhibited seasonality consistent with expected vegetative emissions, substantial variations among sites, and strong temperature dependence (Figure A23). Spatially-averaged isoprene concentrations decreased with increasing daily-average wind speed and increased when winds were from the southwestern quadrant (Figure A24).

The weather-related variations of isoprene concentrations are relevant to the input data used for the GAM. Isoprene, like other VOCs, was measured on samples collected once every six days. This sampling frequency limits its utility as an input variable, though it was tested (Section 5). Neither actual nor interpolated isoprene concentrations were statistically significant in the GAM. One possible explanation is that the GAM included a suite of variables (day of year, Tmax, wind speed and direction) that account for much of the variability in isoprene concentrations.

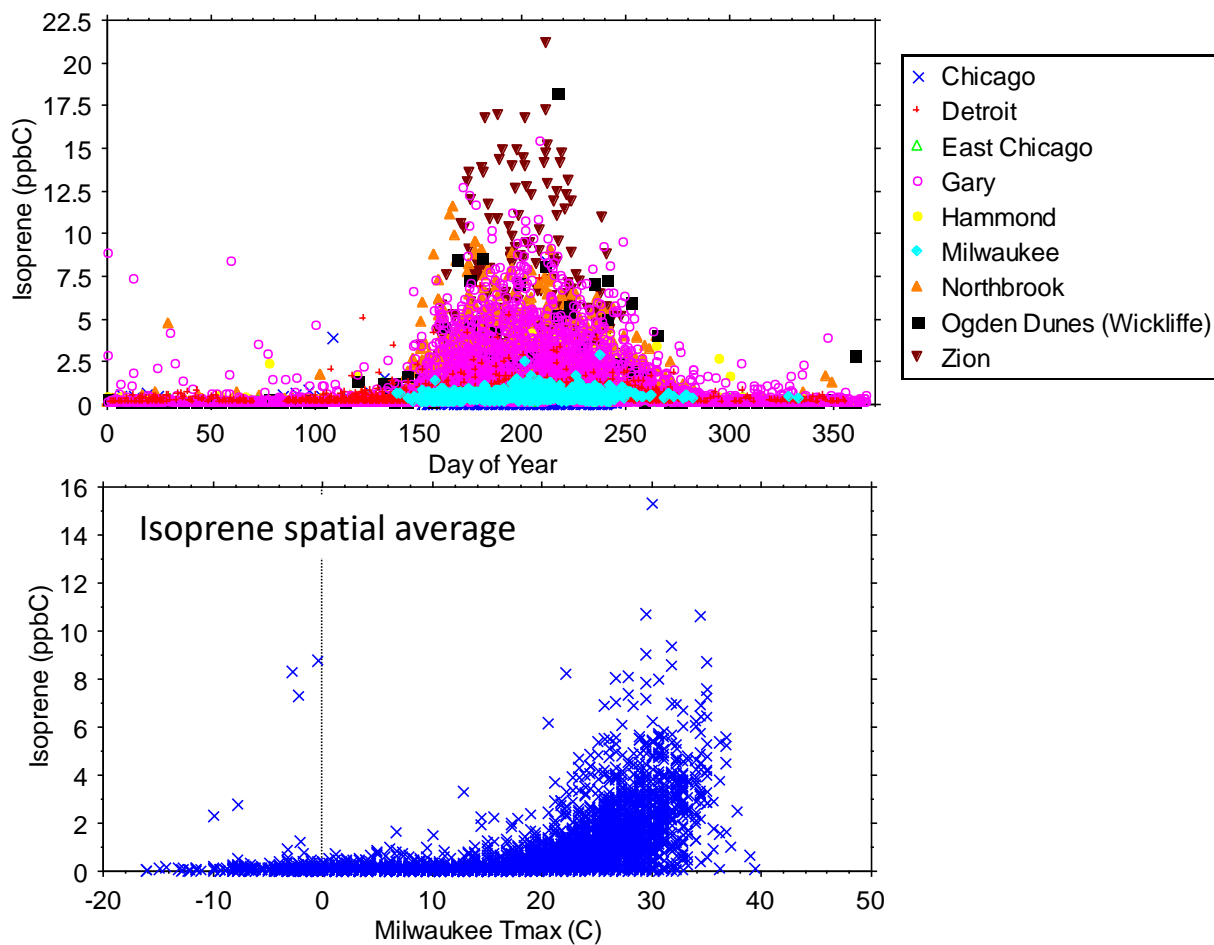
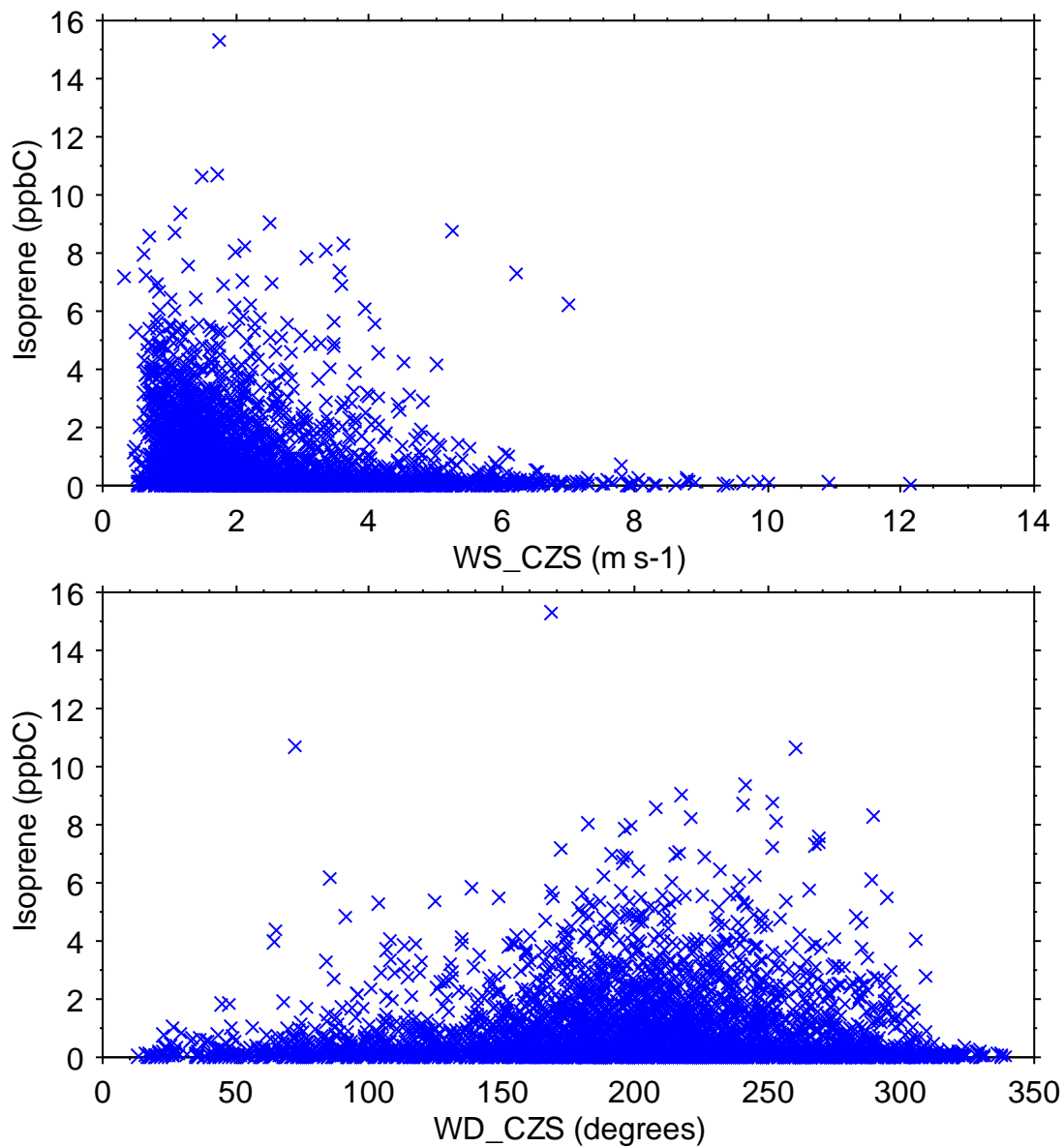


Figure A23. Spatial and temporal variations of daily-average isoprene concentrations (top). Spatially-averaged daily-average isoprene vs. Milwaukee Tmax (bottom).



CZS = Chiwaukee – Zion – Schiller

Figure A24. Spatially-averaged daily isoprene concentration vs. daily-average wind direction and wind speed (composite average of data from Chiwaukee Prairie, Zion, and Schiller Park).

#### 9.4.6 Day-of-Week Variations

Day of week variations in mean pollutant concentrations are evident at most monitoring locations. Some of these variations are documented in this section.

Statistical distributions of multisite mean concentrations of concentrations of CO, NO<sub>x</sub>, and the ratio of CO/NO<sub>x</sub> are shown by day of week in Figure A25. CO shows less reduction on weekends than NO<sub>x</sub> does, so the ratio of CO/NO<sub>x</sub> is higher on weekends. A similar effect for NMOC/NO<sub>x</sub>, if it occurred, would have implications for the efficiency of O<sub>3</sub> formation. Figure A26 shows that the weekend changes are more pronounced in summer months than otherwise.

Day-of-week variations in MDA8 O<sub>3</sub> are not pronounced and are not evident in the most recent five-year period (2015 – 2019) (Figure A27). However, day-of-week variations are evident in the ratio O<sub>3</sub>/NO<sub>x</sub> (Figure A28). These variations have not diminished and, in some cases, may have increased over time. The day-of-week variations in O<sub>3</sub>/NO<sub>x</sub> have implications for the efficiency of O<sub>3</sub> formation.

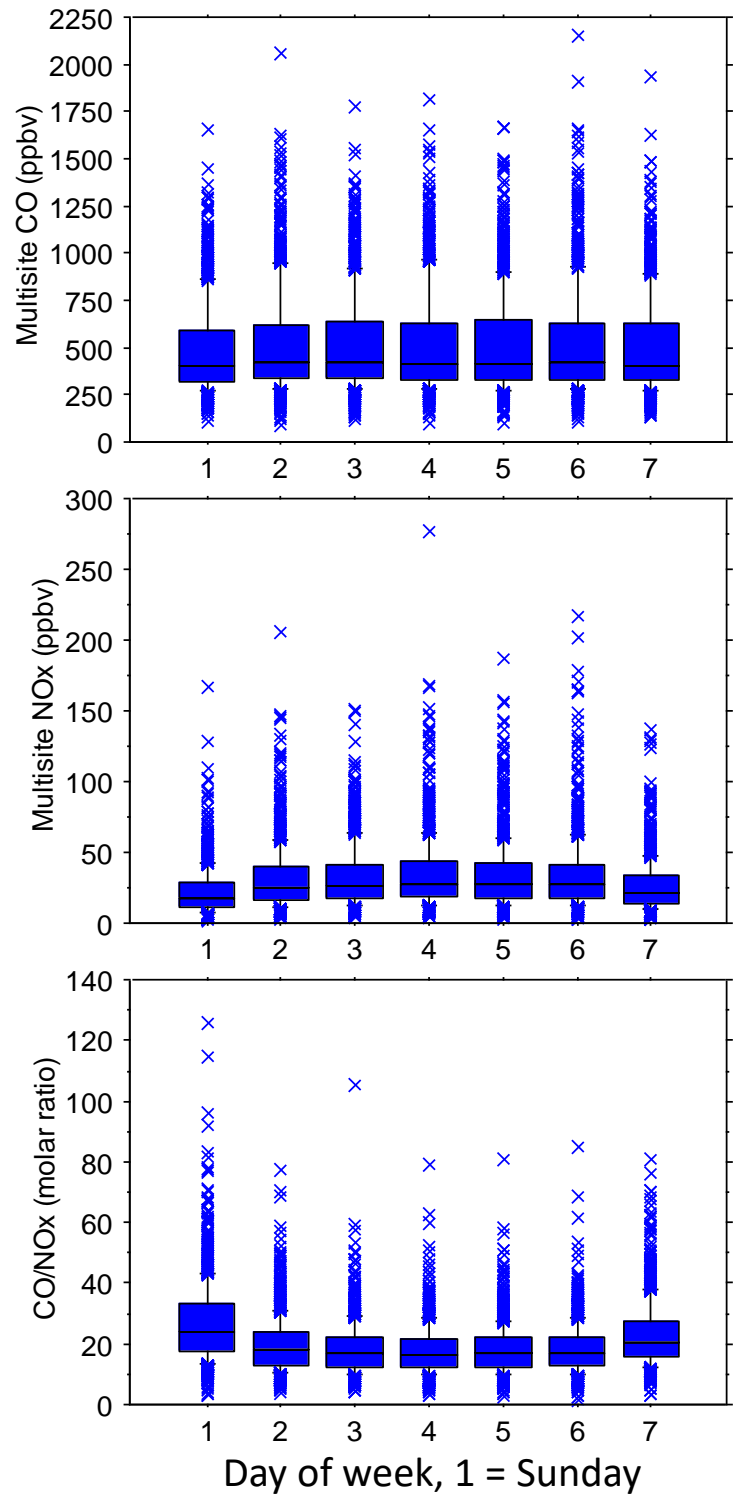


Figure A25. Statistical distributions of multisite mean concentrations of CO, NO<sub>x</sub>, and the ratio of CO/NO<sub>x</sub> by day of week.

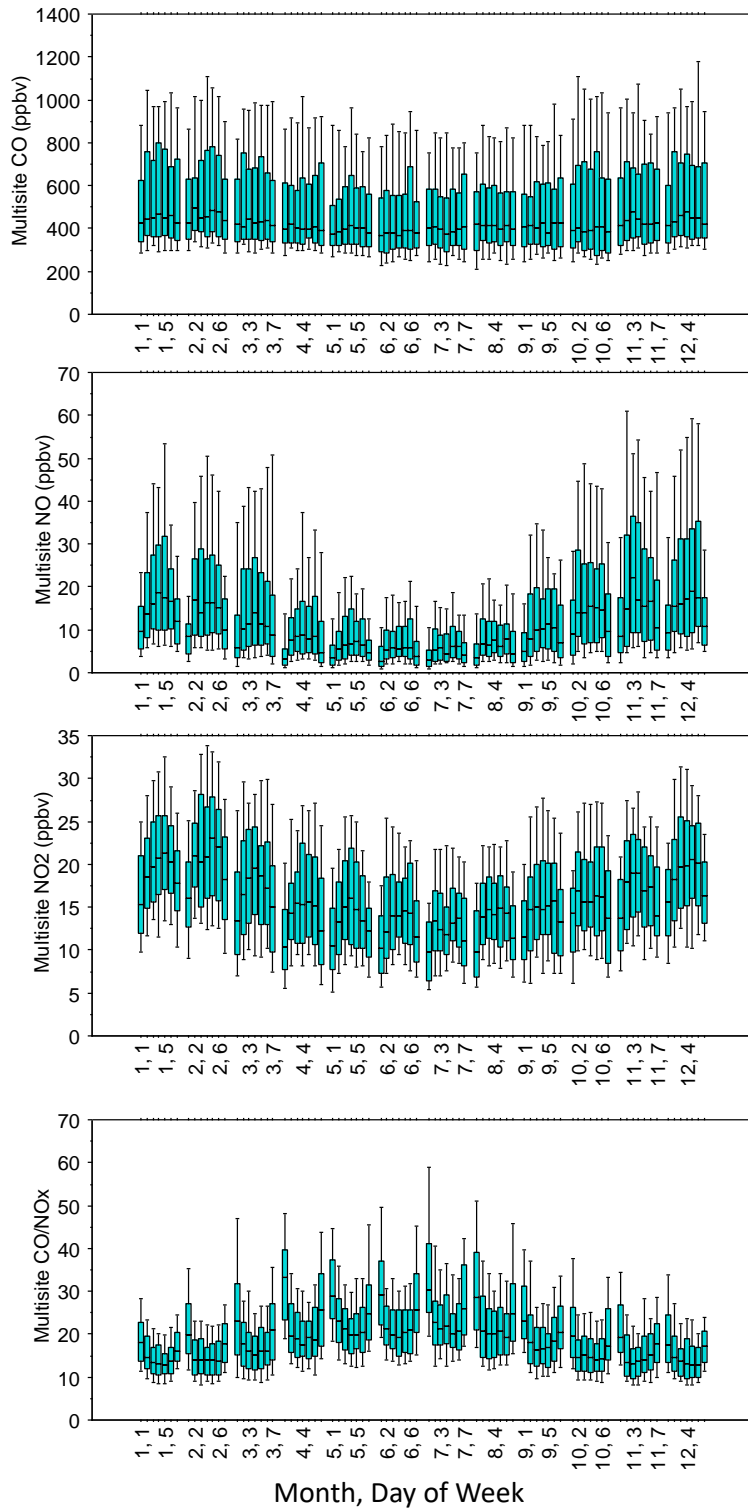


Figure A26. Statistical distributions of multisite mean concentrations of CO, NO<sub>x</sub>, and the ratio of CO/NO<sub>x</sub> by month and day of week.

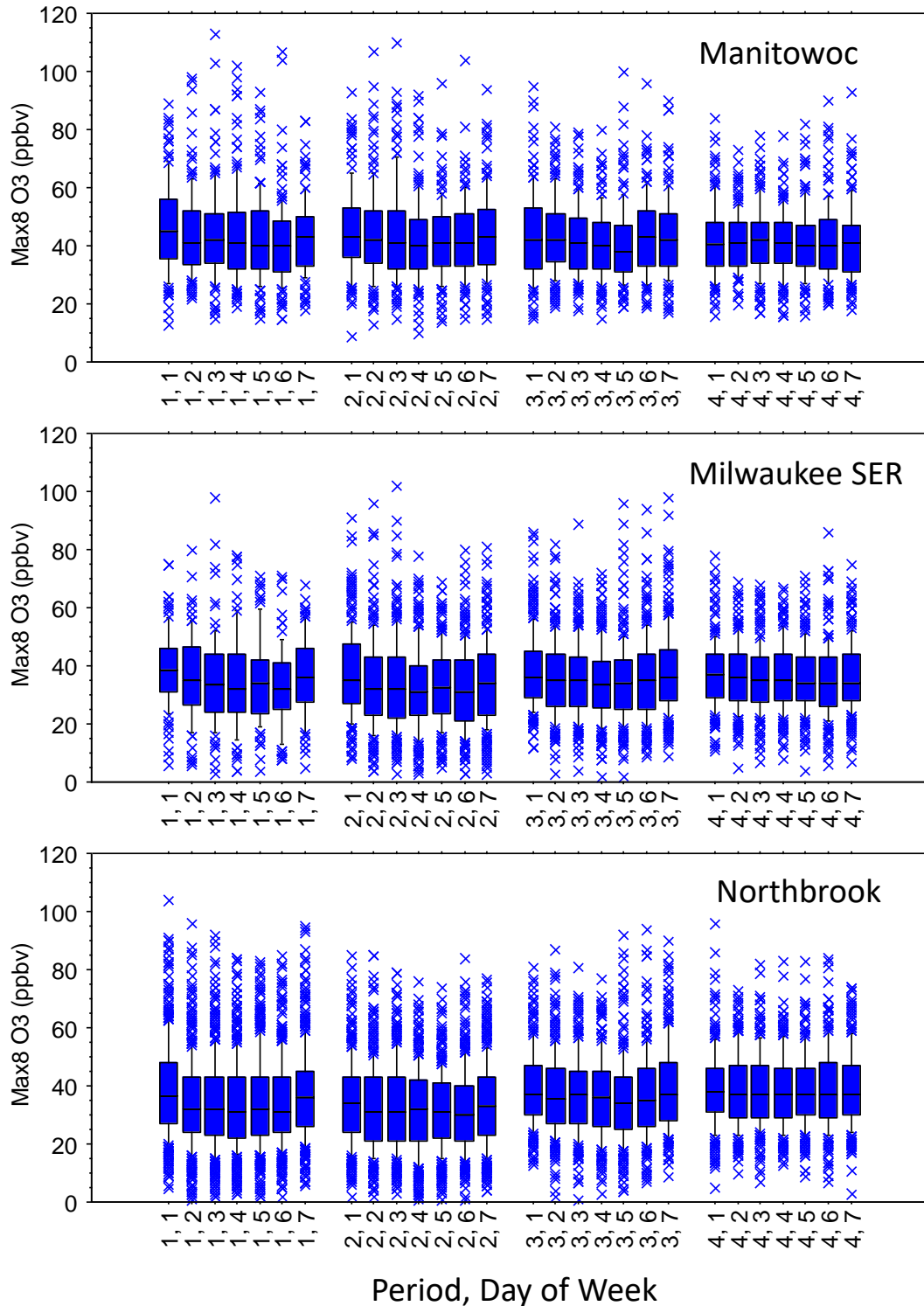


Figure A27. Statistical distributions of MDA8 O<sub>3</sub> by period and day of week. Time periods are (1) 2000 – 2004, (2) 2005 – 2009, (3) 2010 – 2014, and (4) 2015 – 2019.

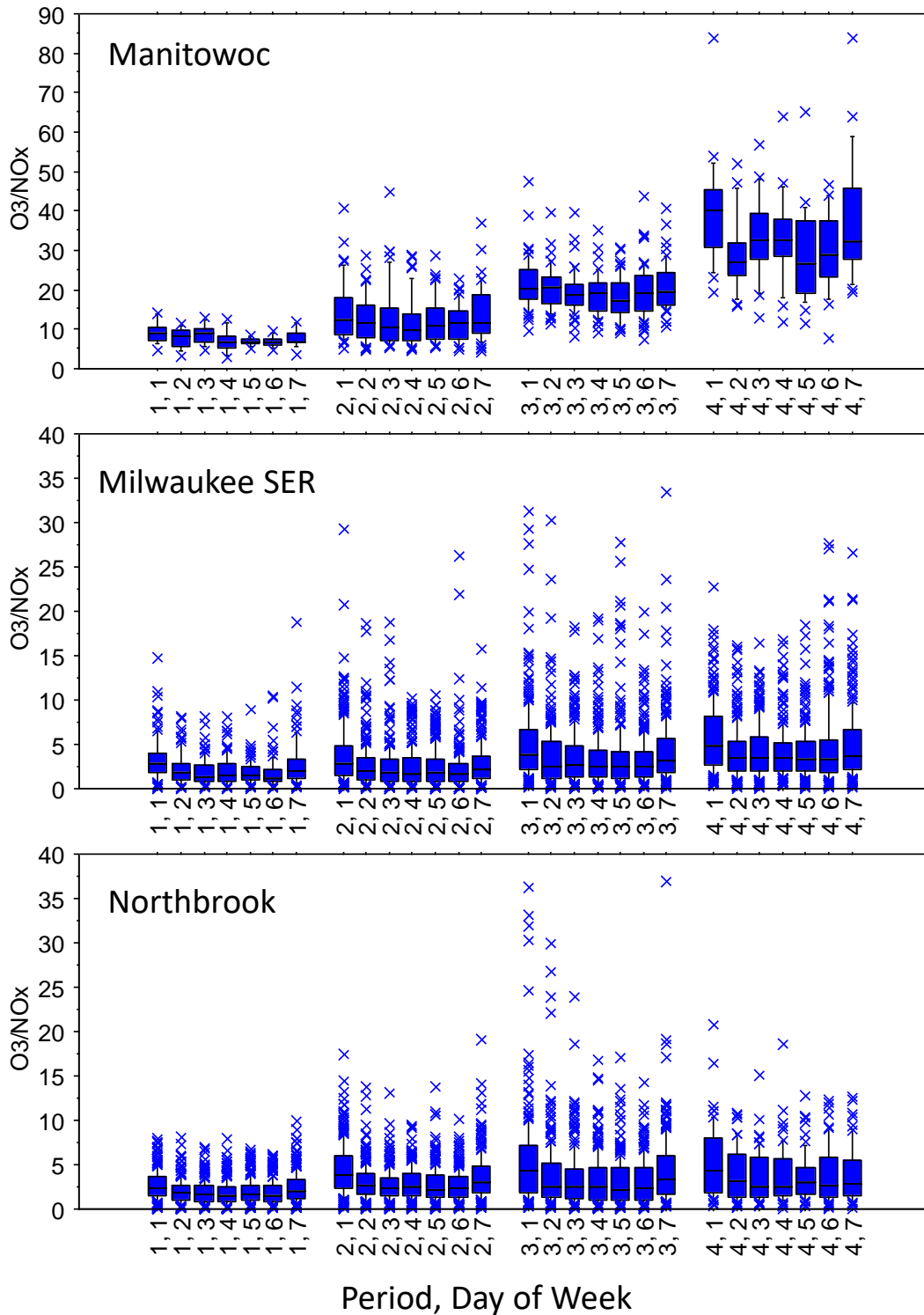


Figure A28. Statistical distributions of MDA8 O<sub>3</sub> and the ratio of O<sub>3</sub>/NO<sub>x</sub> by period and day of week. Time periods are (1) 2000 – 2004, (2) 2005 – 2009, (3) 2010 – 2014, and (4) 2015 – 2019.

### 9.4.7 VOC Reactivity

VOC OH reactivity rate coefficients were provided by WI DNR staff. I compared these reactivity rates with a data set that I had previously compiled (Blanchard et al., 2010b). For many species, the rates were the same in the two data sets because both had been developed using the same published literature values. However, the WI DNR data set also included newer rates for many species. Therefore, I used the provided rates, which covered 89 species and specified their temperature dependence. I merged the reactivity rates with site VOC data and multisite temperature data to generate daily  $k_{OH}$  reactivity for each measured species at each monitoring site. Daily species reactivities were averaged and then summed over compound classes. I also summed species reactivities to generate reactivities by classes of compounds (e.g., aromatics) by day. Five sites had sufficient measurements to prepare averages: Milwaukee SER DNR WI, Northbrook IL, Gary IITRI IN, Hammond IN, and Ogden Dunes IN. Aldehyde measurements were not reported for the last two sites (Hammond and Ogden Dunes) and were not reported at the same frequency as other compounds at Milwaukee SER DNR, Northbrook, and Gary IITRI. The number of compounds measured were 57 for Milwaukee SER DNR, 58 for Northbrook and Gary, and 56 for Hammond and Ogden Dunes. The computations were also applied to five other sites, but they reported too few species measurements (15 or 16) to provide meaningful summaries: Horicon WI, Milwaukee Health Center WI, Schiller Park IL, and East Chicago IN.

Results are summarized in Table A4. Biogenics (isoprene only) were a low (1 – 5%) fraction of the total reactivity. Aldehydes (43% formaldehyde and 3% acetaldehyde) were a large (46%) fraction of the total reactivity at Gary IITRI. Total reactivity at Hammond ( $4.379 \text{ ppb}^{-1}$ ) was much higher than at other sites ( $0.90 - 1.67 \text{ ppb}^{-1}$ ). Over half (59%) of the reactivity at Hammond was from temperature-dependent alkanes, representing much higher reactivity than at other sites ( $2.571 \text{ vs } 0.27 - 0.37 \text{ ppb}^{-1}$ ).

Table A4. Summary of VOC  $k_{OH}$  reactivity by site and class of compounds. Reactivities were computed by day for individual species and averaged. Species average reactivities were summed over species in a class. Units are  $\text{ppb}^{-1}$ . NA = not available (compounds not measured).

<b>Class</b>	<b>Milwaukee SER DNR</b>	<b>Northbrook</b>	<b>Gary IITRI</b>	<b>Hammond</b>	<b>Ogden Dunes</b>
Aromatics	0.409	0.260	0.407	0.548	0.325
Temp-Depend Alkanes	0.370	0.366	0.270	2.571	0.360
Alkenes	0.144	0.136	0.147	1.112	0.159
C1-C2 Aldehydes	0.109	0.049	0.765	NA	NA
Temp-Ind Alkanes	0.052	0.046	0.039	0.126	0.050
Biogenics	0.008	0.043	0.042	0.021	0.049
Sum	1.091	0.900	1.670	4.379	0.943
N samples	1538	2102	3140	1120	1123

#### **9.4.8 O<sub>3</sub> Trends**

Trends in O<sub>3</sub> metrics at selected sites are shown in Figures A29 through A31.

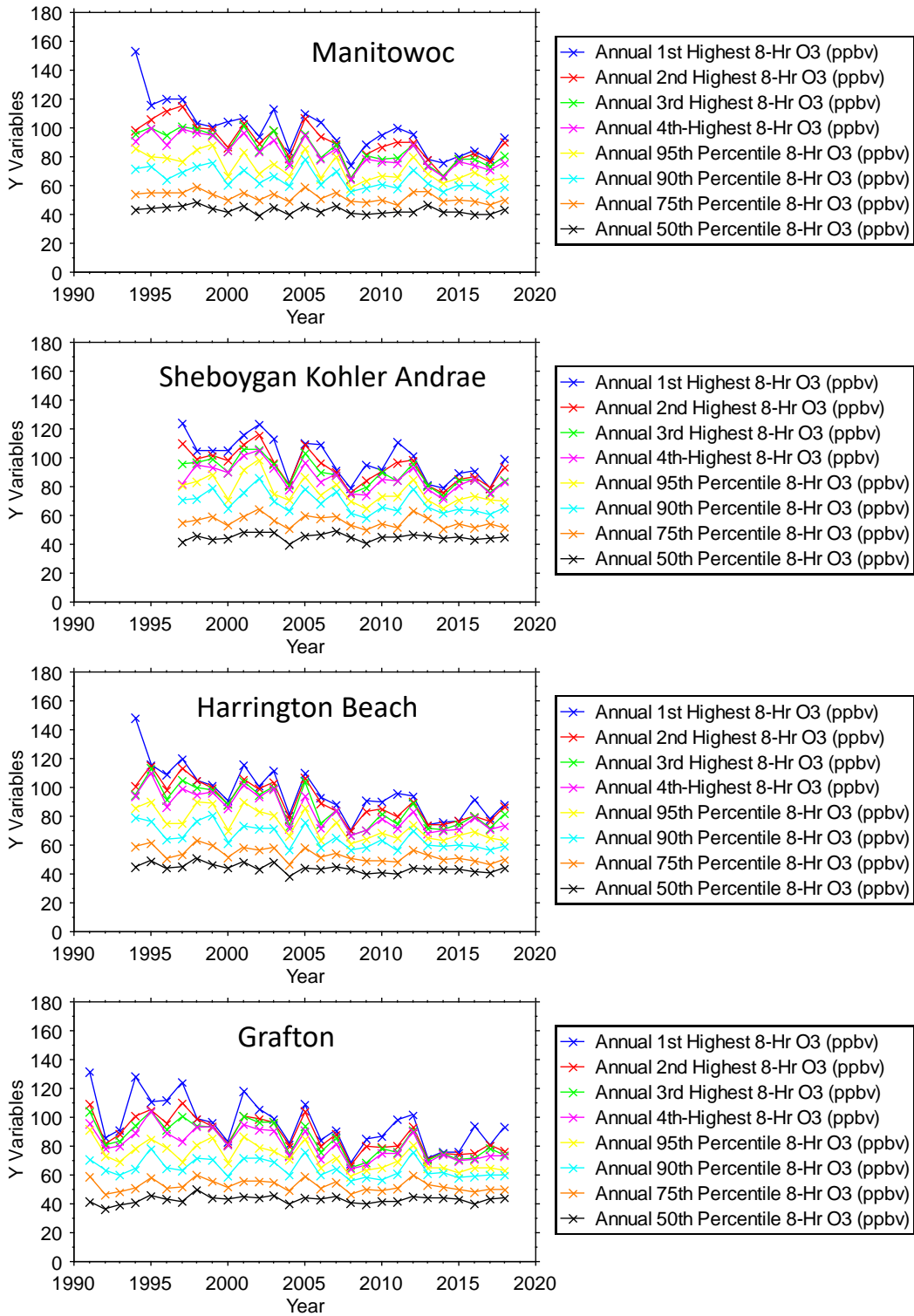


Figure A29. Trends in O<sub>3</sub> metrics at northern WI shoreline sites.

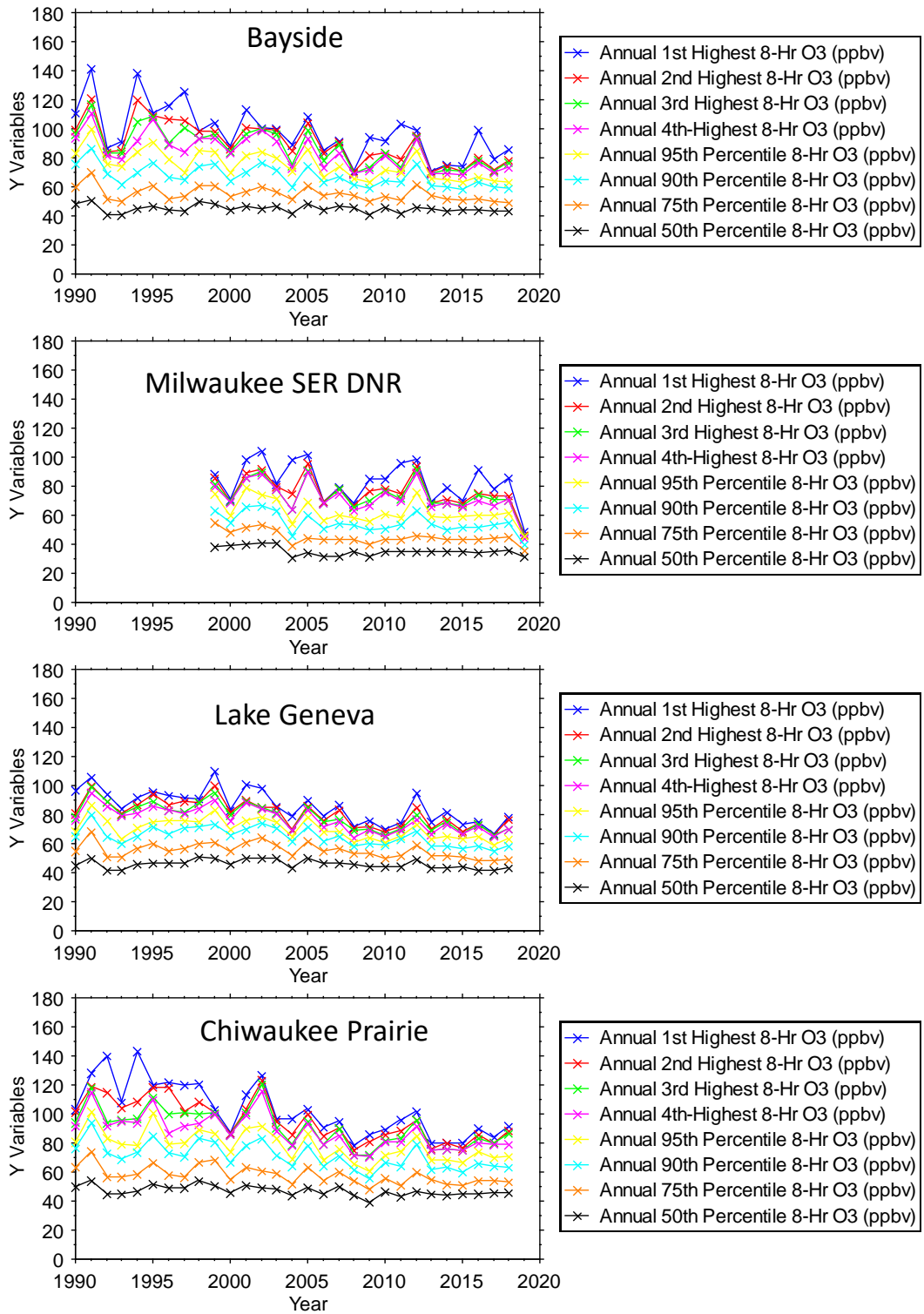


Figure A30. Trends in O<sub>3</sub> metrics at southern WI sites.

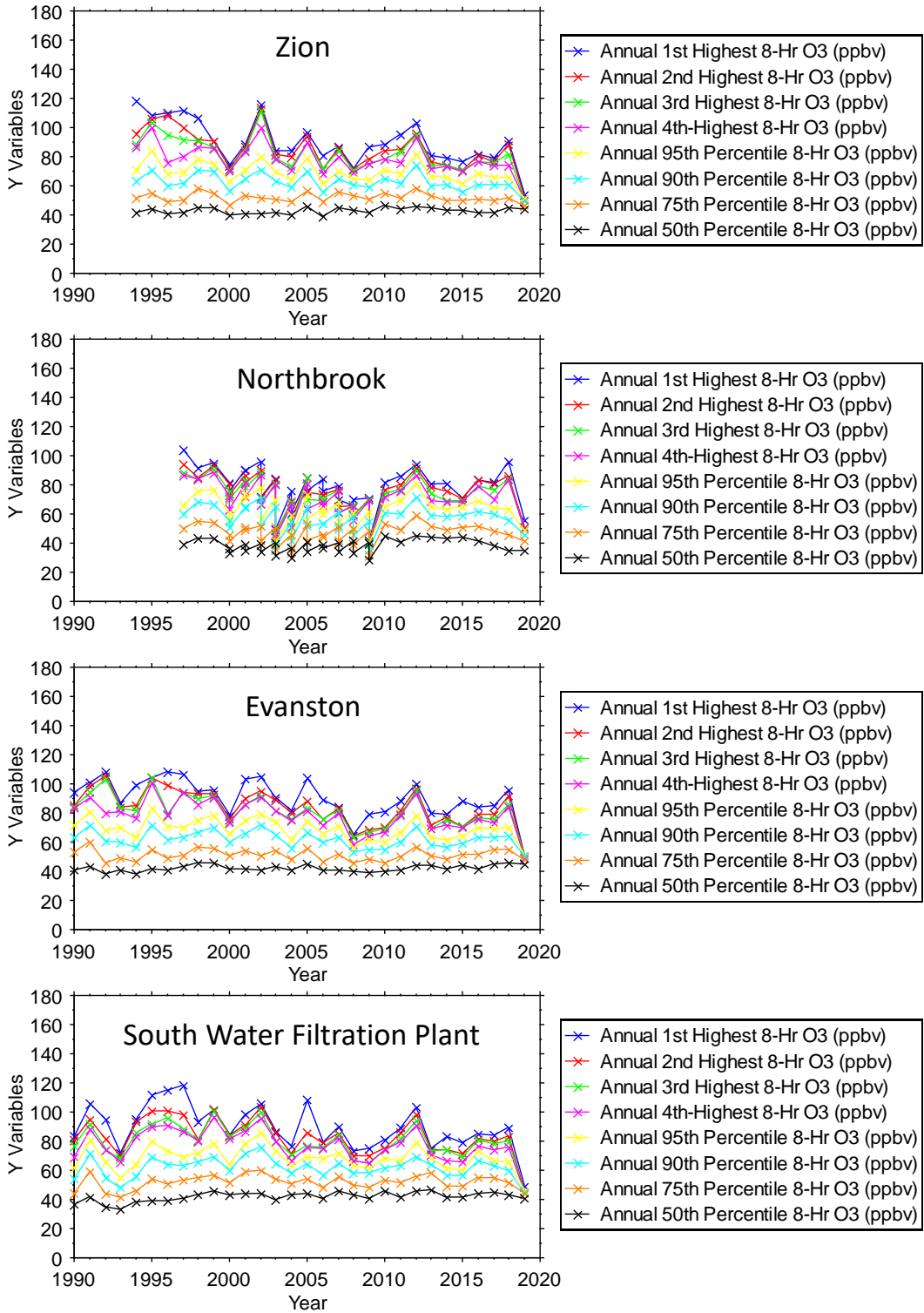


Figure A31. Trends in O<sub>3</sub> metrics at Chicago sites.

## **9.5 Supplemental GAM Model Performance and O<sub>3</sub> Sensitivity Graphs**

Supplemental graphs depicting GAM model performance and O<sub>3</sub> sensitivities are shown in this section.

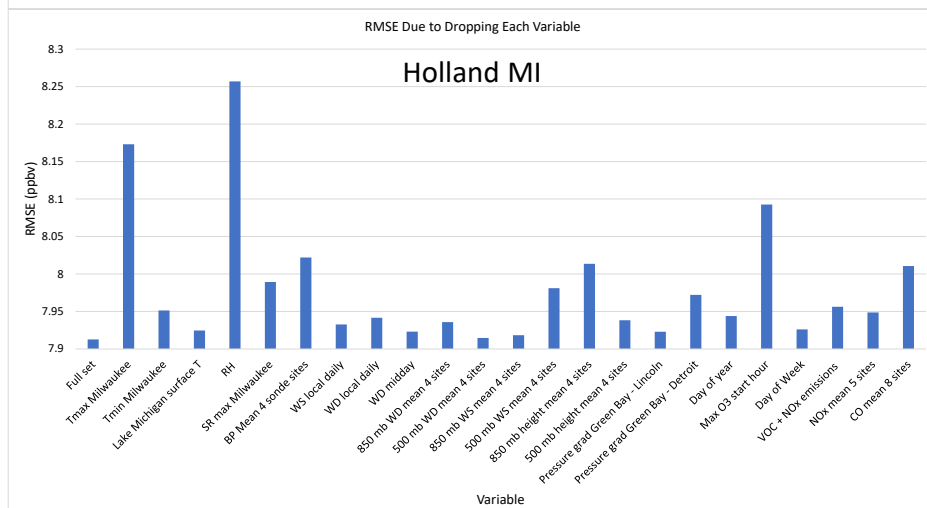
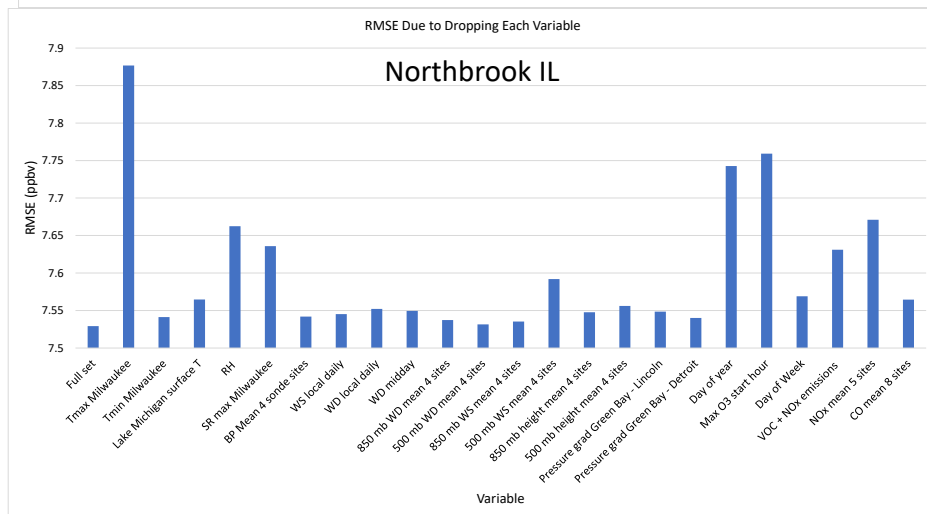
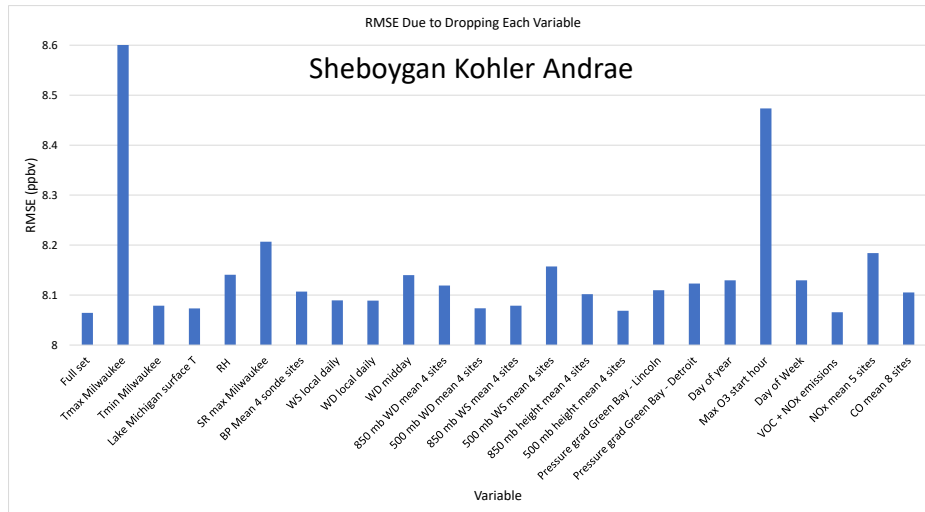


Figure A29. GAM dropterm RMSE results for two sites. Higher RMSE due to dropping a term indicates higher relative importance in the GAM.

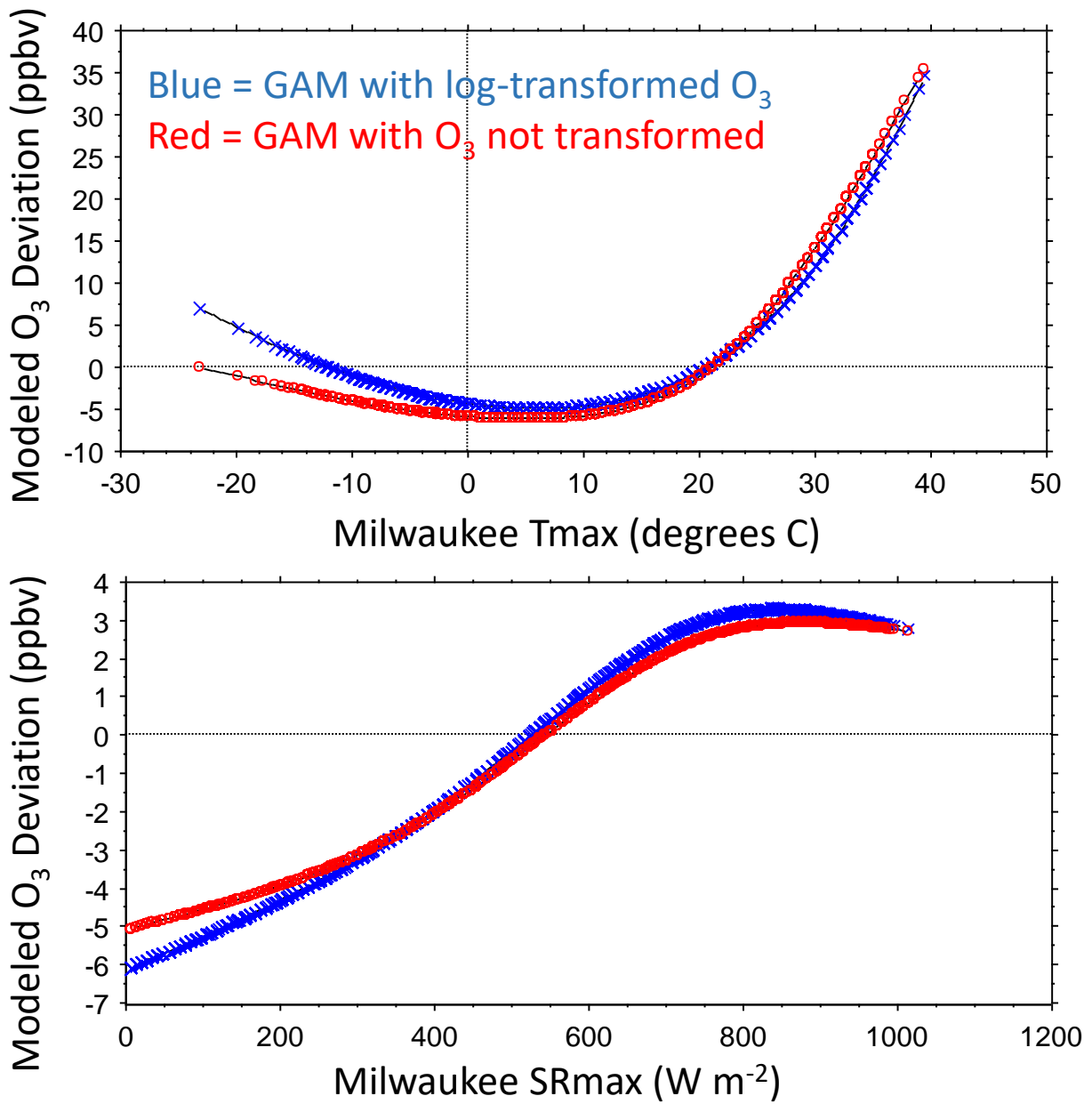


Figure A30. Comparison of modeled sensitivities of Milwaukee SER O<sub>3</sub> to predictors based on log-transformed and untransformed dependent variable in the GAM.

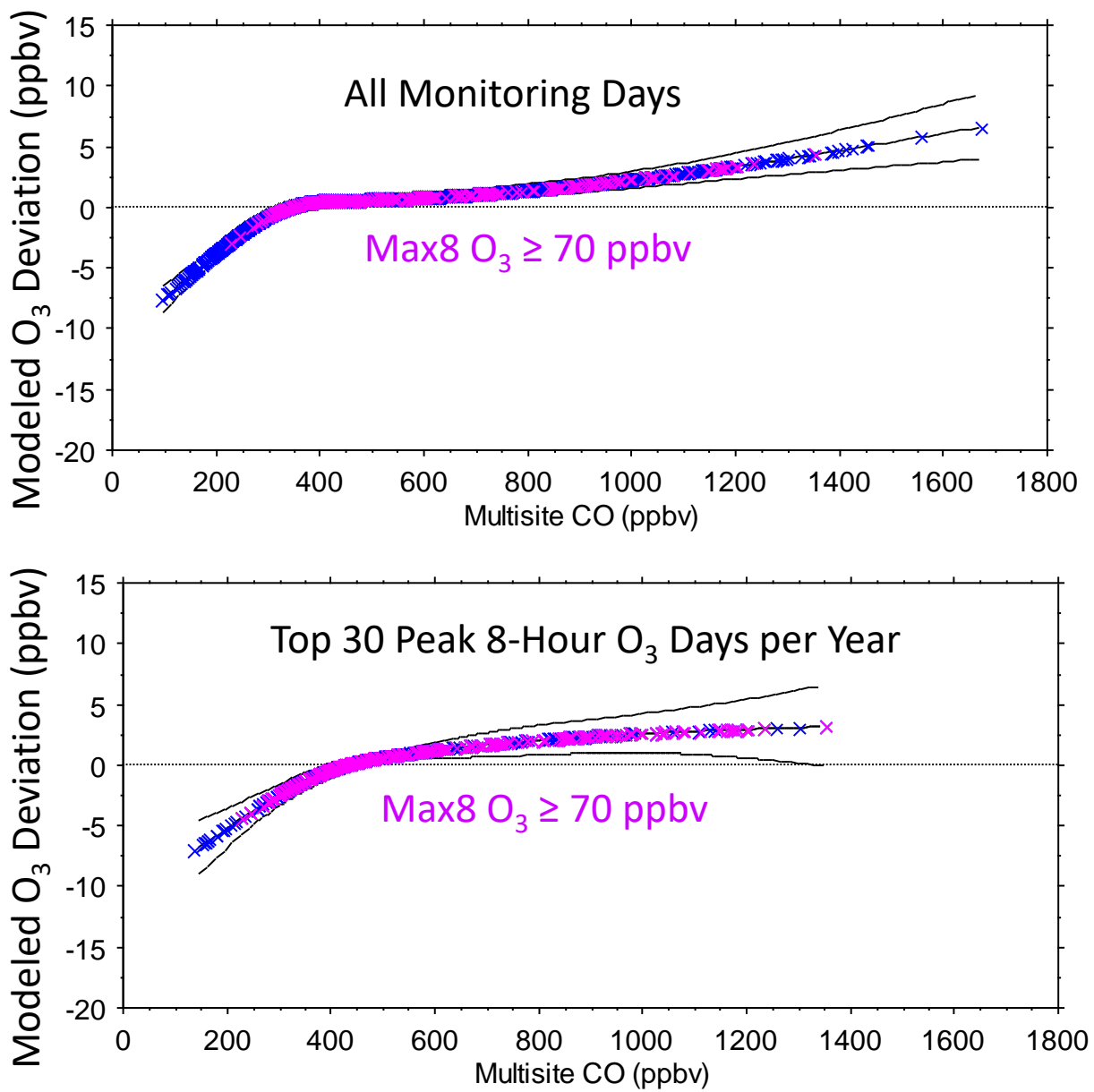


Figure A31. Comparison of modeled sensitivity of Sheboygan Kohler Andrae MDA8 O<sub>3</sub> to CO obtained by fitting the GAM to all days (top) or to a high-O<sub>3</sub> subset (bottom).

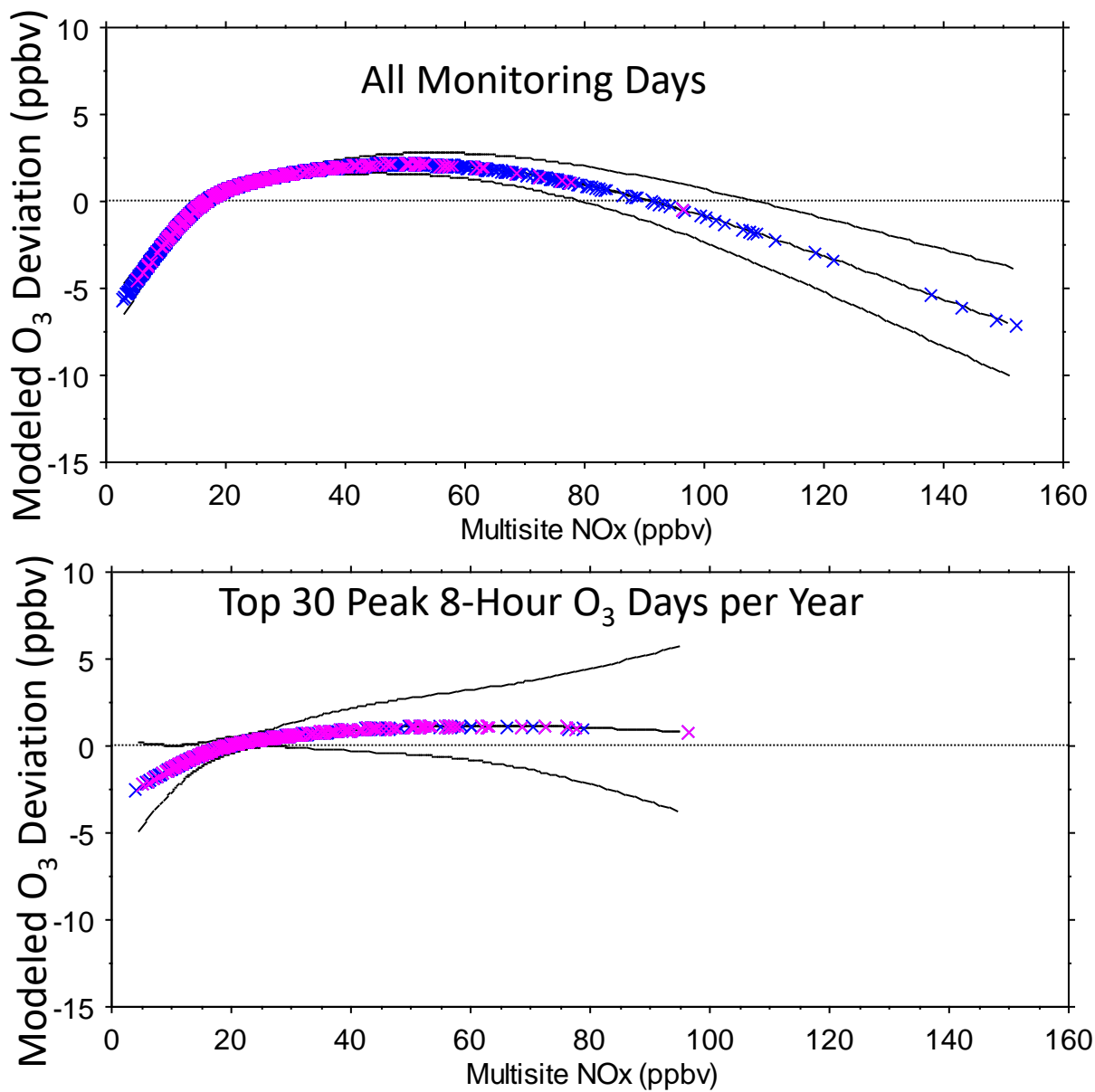


Figure A32. Comparison of modeled sensitivity of Sheboygan Kohler Andrae MDA8 O<sub>3</sub> to NO<sub>x</sub> obtained by fitting the GAM to all days (top) or to a high-O<sub>3</sub> subset (bottom).

## 9.6 Computer Programs

### 9.6.1 R Code for Reading JSON Format Files

```
#install.packages("rjson")

# Load the package required to read JSON files.
#library("rjson")

# Loop through files

for (i in 2001:2014) {

# Give the input file name to the function.
result <- fromJSON(file = paste("h:/work-
projects/LADCO/Data/Weather/WSscalar_daily_SheboyganKA",i,".json",sep=""))

# Get data component, either command works

result2 <- result[['Data']]
#altresult2 <- result$Data[]

# Extract list elements (to test code, limit to first X elements etc)
result3 <- result2

# Replace blanks with NA to ensure all list elements are the same length

result3 <- lapply(result3, function(x) {
      x[sapply(x, is.null)] <- NA
      unlist(x)
    })

# Convert JSON file to a data frame.
result4 <- as.data.frame(result3)

names(result4) = NULL

# Transpose
result5 <- t(result4)

write.csv(result5, file = paste("c:/work-
projects/ladco/data/weather/WS_SheboyganKA",i,".csv",sep=""))

tnam <- paste("WS_SheboyganKA_",i,sep="")
tval <- result5

assign(tnam,tval)

rm(list=ls(pattern="result."))

}
```

### **9.6.2 Other Programs**

The GAM program was submitted separately.